Chemoselective Chemistry: Engineering Materials and Cell Surfaces to Control Biological Interactions

Abigail Pulsipher

A dissertation submitted to the faculty of the University of North Carolina at Chapel Hill in partial fulfillment of the requirements for the degree of Doctor of Philosophy in the Department of Chemistry.

Chapel Hill
2011

Approved by,

Advisor: Professor Muhammad N. Yousaf

Chair: Professor Linda L. Spremulli

Professor Mark H. Schoenfisch

Professor Kevin M. Weeks

Professor Wei You

ABSTRACT

Abigail Pulsipher: Chemoselective Chemistry: Engineering Materials and Cell Surfaces to Control Biological Interactions
(Under the direction of Prof. Muhammad N. Yousaf)

The development of strategies to control the interface between biomolecules and a solid support is critical to a number of research areas, including drug discovery, tissue engineering, and gene microarray technology. In particular, tremendous effort has been extended toward interfacing material science with cell biology to conduct mechanistic cell adhesion, polarization, and migration studies. These investigations require the combined use of a model substrate that mimics the complex nature of the extracellular matrix and a synthetic chemical immobilization methodology to pattern biospecific, biomolecular cues for cellular recognition. Currently, self-assembled monolayers (SAMs) of alkanethiolates on gold represent the most well-studied and developed surface systems in biointerfacial science, enabling the design and implementation of complex, dynamic substrates for controlling biological interactions at the molecular level.

This research is focused on employing chemoselective chemistry to engineer materials and cell surfaces for the control of biological interactions. Thus, smart biosurfaces and materials were manipulated to investigate peptide-cell, protein-carbohydrate, and lipid-cell interactions. A library of biomolecules was designed and synthesized to include chemoselective and bio-orthogonal functional groups, ketone and oxyamine. With this coupling methodology, biomaterials and cell surfaces were successfully engineered to examine a variety of cell behaviors, such as cell-biospecific

ligand interactions, adhesion, polarization, migration, and cellular response to other cells. Chapter 1 provides an introduction to SAMs and a general discussion regarding the design and utility of dynamic SAM surfaces and for biological analyses. The use of SAMs on gold and indium tin oxide for cell adhesion studies is presented in Chapters 2 and 3, respectively. Chapter 4 demonstrates the development and application of a renewable carbohydrate microarray based on hydroquinone-terminated SAMs on gold. Hydroquinone was then incorporated with cell adhesive peptide, RGD, to survey selected carbohydrates and peptides for their combined effect on fibroblast adhesion, morphology, and migration; this data is discussed in Chapter 5. A cell-surface engineering strategy based on liposome delivery and membrane fusion to direct cell-cell contacts and generate 3D tissue-like structures is reported in Chapters 6 and 7. Finally, Chapter 8 describes my general conclusions and future research directions.

ACKNOWLEDGEMENTS

I am grateful to my advisor, Prof. Muhammad N. Yousaf, for providing guidance, support, and scientific direction during my graduate studies at UNC-CH. I will always be indebted to his invaluable training and advice. The Yousaf group members have also been instrumental in my growth as a chemist; I am appreciative to have known and worked alongside Dr. Eun-ju Lee, Dr. Wei Luo, Dr. Diana Hoover, Dr. Devin Barrett, Dr. Sungjin Park, Dr. Brian Lamb, and especially, Dr. Nathan Westcott and Dr. Debjit Dutta.

Much of my happiness and sanity is owed to my fellow chemistry graduate student roommates and rock climbing buddies. Thanks to the friendship and support of Alexis Carpenter, Jes Park, Kathryn deKrafft, Brian Matthew, Chris Gagliardi, and Andrew Stuart, the difficulties and obstacles of gradate school were manageable.

I am forever thankful to my family for their love, encouragement, and boastful attitudes toward all my life successes and failures. Dad, Mom (Harriet), Mindy, Michelle, Ben, Clay, Shanx, and the eight little ones are so wonderful; I could not have made it here without them. Finally, I want to thank Jeremy, my best friend and the love of my life. His encouraging attitude and positive future outlook have been my saving grace during graduate school. Because of Jeremy, I was able to maintain the perfect balance of grueling work and glorious play.

TABLE OF CONTENTS

LIST OF SCHEMES AND TABLES

LIST OF FIGURES

LIST OF ABBREVIATIONS

3D	Three dimensional
µCP	Microcontact printing
µFL	Microfluidic lithography
µM	Micromolar
Å	Angstrom
ACN	Acetonitrile
AcOH	Acetic acid
AFM	Atomic force microscopy
AO	Aminooxy alkane
Au	Gold
BSA	Bovine serum albumin
CBS	Calf serum albumin
$CDCl_3$	Deuterated chloroform
$CHCl_3$	Chloroform
ConA	Concanavalin A
cRGD	Cyclic-RGD
CV	Cyclic voltammetry
DAPI	4',6-diamidino-2-phenylindole
DCM	Dichloromethane
DLS	Dynamic light scattering
DMF	Dimethylformamide
D_2O	Deuterated water

DOTAP	1,2-dioleoyl-3-trimethylammonium-propane
DPN	Dip-pen nanolithography
ECM	Extracellular matrix
EG_4SH or EG_4	Tetra(ethylene glycol)-terminated alkanethiol
EtOAc	Ethyl acetate
EtOH	Ethanol
FAC	Focal adhesion complex
FACS	Fluorescence-activated cell sorting analysis
Fbs	Fibroblasts
FBS	Fetal serum albumin
Fc	Ferrocene
Fc-ONH_2	Ferrocene-oxyamine
Fn of FN	Fibronectin
FRET	Fluorescence or Fourier resonance energy transfer
g	Gram
Gal	Galactose
Glc	Glucose
HCl	Hydrochloric acid
$HClO_4$	Perchloric acid
Hex	Hexanes
hMSCs	Human mesencymal stem cells
^1H NMR	Proton nuclear magnetic resonance

H_2O	Water
HQ or H_2Q	Hydroquinone
$H_2O_3PC_{11}OH$	11-hydroxyundecyl-phosphonic acid
IR	Infrared spectroscopy
ITO	Indium tin oxide
K_d	Disassociation constant
KDa	Kilodalton
KKKTTK	Lys-Lys-Lys-Thr-Thr-Lys
L	Liter
LFM	Lateral force microscopy
Man	Mannose
MADLI-MS	Matrix-assisted laser/ desorption ionization spectroscopy
$MeOEG_4SH$	Methoxy-terminated tetra(ethylene glycol) alkanethiol
MeOD	Deuterated methanol
MeOH	Methanol
mg	Milligram
$MgSO_4$	Magnesium sulfate
mL	Milliliter
mM	Millimolar
mmol	Millimoles
MS	Mass Spectrometry
$NaHCO_3$	Sodium bicarbonate

NaOH	Sodium hydroxide
NBD-PE	egg 1,2-diphytanoyl-*sn*-glycero-3-phosphoethanolamine-N-(7-nitro-2-1,3-benzoxadiazol-4-yl) (ammonium salt)
NEXAFS	Near-edge X-ray absorption fine structure spectroscopy
nL	Nanoliter
Ox	Oxidation
OA	Oxyamine
PBS	Phosphate buffer solution
PCC	Pyridinium chlorochromate
PDMS	Poly(dimethylsiloxane)
PGs	Proteoglycans
PHSRN	Phe-His-Ser-Arg-Asn
PNA	Peanut agglutinin
POPC	egg palmitoyl-oleoyl phosphatidylcholine
POPG	egg 1-palmitoyl-2-oleoyl-phosphatidylglycerol
Q	Quinone
RAIRS	Reflectance absorption infrared spectroscopy
RGD	Arg-Gly-Asp
Red	Reduction
Rhod-PE	egg 1,2-dipalmitoyl-*sn*-glycero-3-phosphoethanolamine-N-

	(lissamine rhodamine B sulfonyl) (ammonium salt)
Rhod-ONH_2	Rhodamine-oxyamine
RNH_2	Amine
$RONH_2$	Oxyamine ligands
SAMs	Self-assembled monolayer
SEM	Scanning electron microscopy
SPR	Surface plasmon resonance spectroscopy
SSPS	Solid-phase peptide synthesis
TEM	Tunneling electron microscopy
TEM	Transmission electron microscopy
THF	Tetrahydrofuran
TIRFM	Total internal reflection fluorescence microscopy
TLC	Thin layer chromatography
TRITC	Tetramethyl rhodamine isothiocyanate
UV	Ultraviolet
XPS	X-ray photoelectron spectroscopy

CHAPTER 1

Self-Assembled Monolayers: Model Surfaces for the Analyses of Cell Adhesion and Migration

1.1 Introduction

Cells exist in a complex, dynamic, and highly evolving environment, a key component of which is the extracellular matrix (ECM).[1-6] The ECM provides structural support for the cell and also contains a host of supramolecular assemblies of proteins and glycosaminoglycans, which play a vital role in cell behavior. To undergo fundamental biological processes, cells must adhere to the underlying ECM. Upon receiving and responding to complex molecular signals, cells then migrate from the various epithelial layers to target locations, where they differentiate to form specialized cells that form various organs and tissues. As a result, cell adhesion and migration are critical to processes, such as embryogenesis,[7] normal tissue repair,[8] the immune response,[9,10] wound healing,[11,12] and angiogenesis.[13,14] Moreover, improper cell adhesion and migration have been implicated in tumor invasion in cancer cell metastasis.[15-19] Therefore, understanding the mechanisms of cell adhesion and migration will impact a broad range of research communities, including medicine and cell-based biotechnologies.

For cells to migrate *in vivo*, they must first adhere to the ECM through ligand-cell interactions.[20] While there are many proteins that facilitate this process, integrins

represent a family of cell-surface receptors that specifically mediate the attachment of a cell to another cell or to the ECM. Structurally, integrins are heterodimeric, transmembrane glycoproteins that consist of α and β subunits. There are 18 α and 9 β subunits and a total of 24 integrin heterodimers known. This chemical diversity gives rise to biological complexity, and thus, integrins have been implicated in numerous functions including cell–ECM and cell–cell adhesion, organization of actin filaments, signal transduction, cell survival, cell growth and differentiation, and unique roles in developmental processes.[21,22]

Despite this complexity, most integrins share two key interrelated functions: (1) promote the assembly and organization of the actin cytoskeleton[23,24] and (2) regulate signal transduction cascades.[25-27] Spanning the cell membrane, these protein subunits serve as a communication pathway, linking the actin cytoskeleton and intracellular cytoplasmic proteins involved in focal adhesion complexes (FAC) with the cell's dynamic extracellular environment (Figure 1.1).[28-31] There are at least 50 distinct proteins known to be involved in focal adhesions. Actin,[32] vinculin, talin, tensin, α-actinin, and filamin provide a structural role, while focal adhesion kinase,[33] integrin-linked kinase, Src-family kinase, PINCH, paxillin,[33,34] and G-proteins serve regulatory roles in signaling cascades. As mentioned, integrins serve as the link between these internal proteins and enzymes to the outside environment of the cell. Depending on the strength of the ECM interaction, integrins may be loosely connected through a meshwork of filaments at the leading edge or strongly adhered by robust actin fibers or fibrillar adhesions. These interactions affect the rate of cell motility. The short peptide sequence Arg-Gly-Asp (RGD) was identified as a binding motif in several ECM components including, fibronectin (Fn), fibrinogen, vitronectin, laminin, and some collagens.[35-37] Most of the known integrin receptors recognize the RGD sequence when binding to ECM ligands. With the advent of live-cell

imaging, the temporal distribution of integrin complexes could begin to be addressed.[38] It is now clear that various adhesive structures dynamically mature from nascent structures at the edge of the cell to the larger interior structures, such as FACs. In a migrating cell, a loss of adhesion at the trailing edge that involves a combination of regulated proteolysis of integrins and associated proteins, as well as physical tearing, occur. While previous studies have provided a great deal of information about how cells dynamically control the cytoskeleton–integrin linkages in space and time, new methodologies are required to advance our understanding of this process.

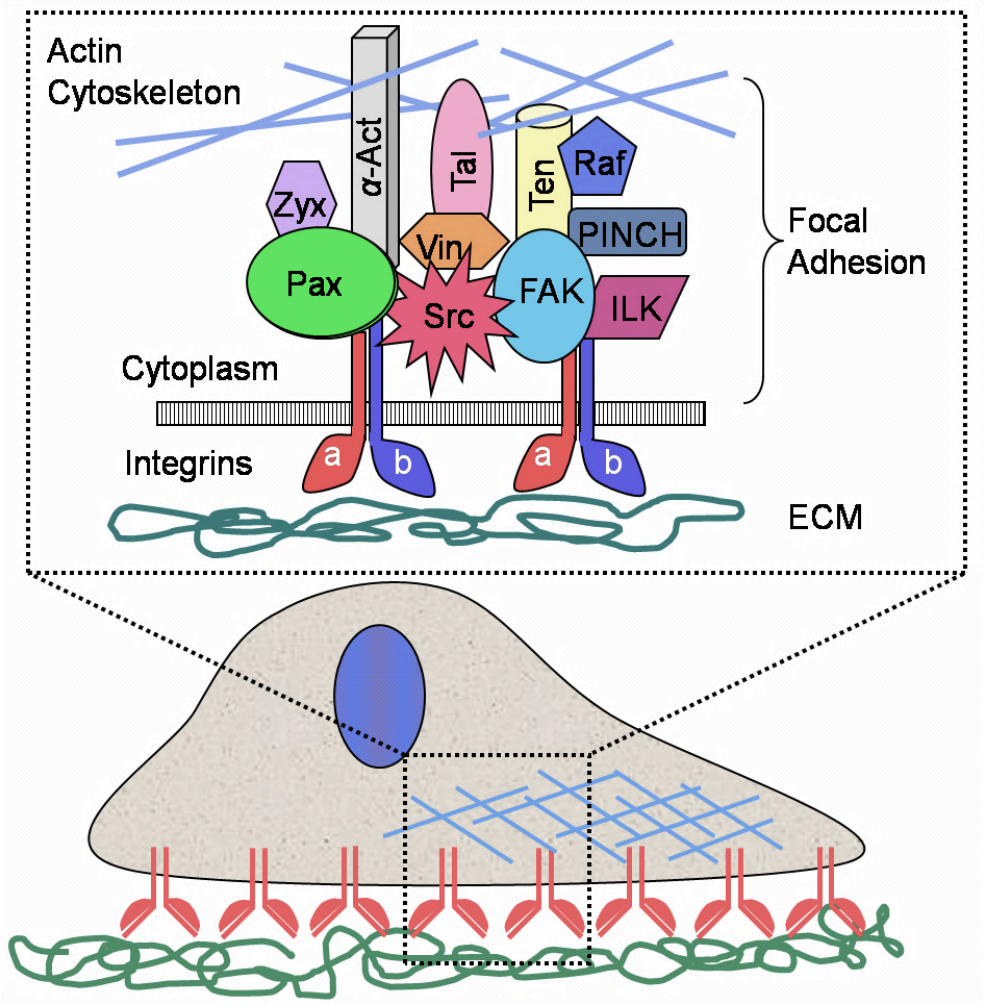

Figure 1.1 Simplified schematic of cell adhesion through integrin-mediated communication with the ECM, cytoplasmic proteins, and the actin cytoskeleton in formation of a focal adhesion complex (FAC).

In the past few years, the surface chemistry community has actively pursued the development and integration of strategies to control the interface between cells and a solid support. In doing so, tailored substrates that aim to mimic the ECM and induce cellular behavior have been generated.[39,40] Different materials have been exploited for studies in cell biology; however, self-assembled monolayers (SAMs) of alkanethiolates on gold remain the ideal, model platform due to a number of factors.[41-43] The organic coupling strategies amenable to thiol chemistry permit a vast variety of biomolecules to be tethered to the surface, as well as to be confined to selective regions so that a specific biological interaction can be observed. In addition to this system's compatibility with cell culture, the non-fouling properties of oligo(ethylene glycol)-alkanethiols enable the creation of complex, patterned mixed-SAMs. Another advantage to this model platform is the wide range of analytical and patterning techniques available to simulate and characterize cell behavior. Therefore, SAMs have been used in many biological studies including the interrogation of protein-protein, protein-cell, carbohydrate-protein, lipid-carbohydrate, and cell-cell interactions, as well as employed in the investigation of cell adhesion, polarization, and migration.[39-45] Furthermore, technologies to create dynamic SAM gradients with immobilized adhesion molecules and other chemoattractants have been developed to aid in the elucidation of the mechanism of directed migration.[46-50]

In this chapter, the design and utility of dynamic surfaces for biological analyses will be discussed. The structure, physical properties, and advantages of SAMs of alkanethiolates on gold for use as model substrates are first summarized. Specific applications of SAMs as dynamic surfaces for the analysis of cell adhesion and migration are then reported.

1.2 Self-Assembled Monolayers as Model Substrates for Bioanalyses

SAMs are highly ordered films that are formed by the spontaneous adsorption of surfactant molecules on a solid support.[41-43] One of the most well studied SAM platforms is alkanethiolates on gold. Since the first report of monolayer assembly by Nuzzo and Allara, the structure, physical properties, and potential uses of SAMs on a number of different materials have been extensively characterized. These substrates range from planar substrates (e.g., glass or silicon, single crystals, and metal films or foils) to curved nanostructures (e.g., colloids, nanorods, and nanospheres).[41-43,51] As a result, SAMs have served as a platform for many diverse applications in research areas, such as optoelectronics, environmental chemistry, biomedical engineering, and cell biology.[52-57] SAMs of alkanethiolates on gold offer numerous advantages over the other platforms (e.g., siloxanes on glass, phosphonates on metal oxides, and alkanethiolates on silver, palladium, platinum, or copper).[39-44] For reasons listed later, this system has been widely investigated as a potential model surface for biological study and will be the focus of this chapter.[58]

Long-chain alkanethiolates will rapidly and spontaneously form densely packed, well-ordered, and trans-extended monolayers on gold (111) surfaces.[41-43,58] The thiol head-group has a high affinity for transition metals and binds the gold through chemisorption, consequently displacing any adventitious materials from the surface. The sulfur atoms and in turn, the alkyl chain spacer, promote stabilization and regular packing through dipolar and van der Waals intermolecular forces, respectively. To maximize these interactions, the alkyl chains adopt the optimum distance between one another. A generic diagram representing the ideal SAM structure is displayed in figure 1.2. SAMs of alkanethiolates on gold have several attractive advantages to serve as a model substrate for biological applications. For one, the gold films can be prepared by a

number of different methods. Another benefit to using gold is its inherent conductivity, allowing for compatibility with several analytical techniques (e.g., electrochemistry, surface plasmon resonance, scanning electron microscopy, and tunneling electron microscopy) that are incompatible with other SAM systems.[41-43,58] The thiol can easily be protected to amend the other functional group at end of the alkane chain.[59] Therefore, the synthetically flexible terminal group provides the means for specific tailoring with the presentation of a variety of ligands from the surface. Similarly, there are many patterning methodologies amenable to SAMs on gold, enabling the opportunity to create complex substrates for the interrogation of biomolecular interactions. Both microcontact printing (μCP) and dip-pen nanolithography (DPN) have been used to pattern gold and form micro- and nano-feature SAMs.[60-64] Techniques such as photolithography, microfluidics, and electron-beam lithography were employed to activate a particular terminal group for the subsequent tethering of molecules with spatial control.

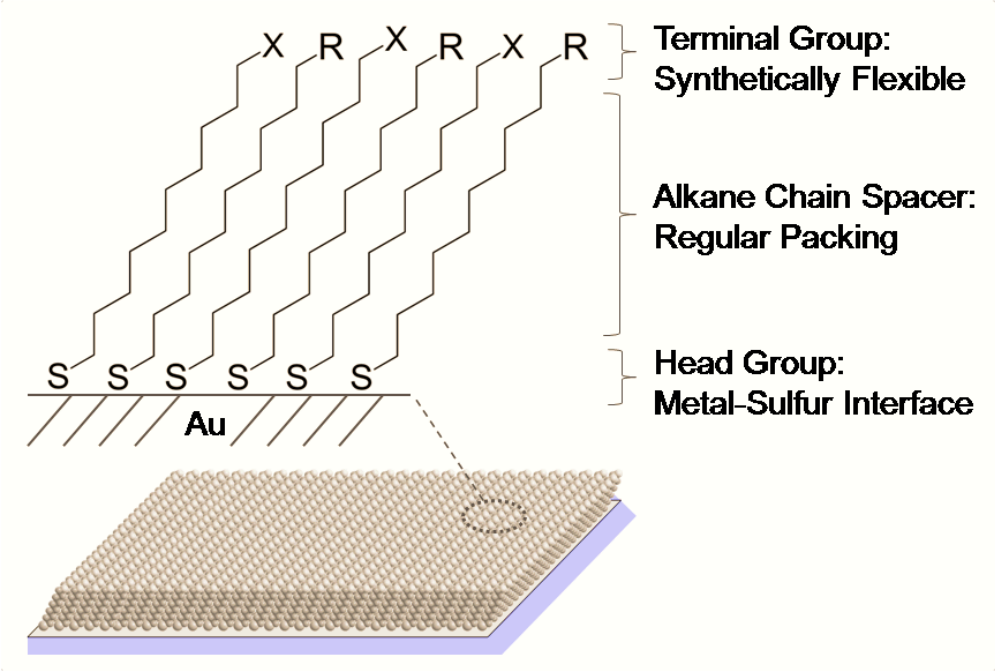

Figure 1.2 General schematic of an ideal SAM of alkanethiolates, supported on a gold surface.

Many strategies were developed to spatially control the interface between biomolecules on a solid support for a number of applications. In combination with the synthetic advantages of thiol chemistry, several patterning techniques have been adapted with SAMs on gold to enable the selective positioning and manipulation of ligands. Whitesides developed the most common method of patterning SAMs, microcontact printing (μCP).[41-43,60] This technique uses an elastomeric poly(dimethylsiloxane) (PDMS) stamp, fabricated by soft lithography, to ink and transfer hydrophobic alkanethiols onto a gold surface. The surfactant molecules instantly self assemble upon contact with the substrate, and a two-dimensional (2D) projection of the micro-features is transferred on the surface. μCP has been employed in numerous applications, including patterning SAMs for cell adhesion studies and printing functionalized biomolecules for ligand immobilization. An alternative approach uses microfluidics to form 2D SAM features on gold. This strategy, microfluidic lithography (μFL), first requires a PDMS microfluidic cassette to be sealed onto the surface[48] to create micro-channels on the SAM surface. An alkanethiol solution is then flowed through the channels, resulting in rapidly patterned SAM formation. Thus far, μFL has been employed to create dynamic SAM gradients for cell polarization, directed migration, and contiguous cell co-cultures studies. Several lithographic techniques, such as photo-, electron beam, X-ray, and dip pen nano- lithography, have been employed to pattern SAMs as well.[65-70] Although these surface manipulations require expensive or custom instrumentation, the resulting patterns are formed with high fidelity and resolution (10-30 nm) and only require extremely low sample volumes (nL).

Planar SAM systems are compatible with a number of surface characterization and spectroscopic techniques. Ellipsometry, near-edge X-ray absorption fine structure spectroscopy (NEXAFS), reflectance absorption infrared spectroscopy (RAIRS), Raman

spectroscopy, X-ray diffraction, and contact angle all have been used to elucidate physical properties about the thickness, tilt angle from the surface, and packing density of SAMs. X-ray photoelectron spectroscopy (XPS), infrared spectroscopy (IR), cyclic voltammetry (CV), and mass spectrometry (MS)[71-78] have been used to elucidate functional group transformations on the surface. Similarly, electrochemistry has been used to activate SAMs for ligand immobilization, as well as monitor the reaction and calculate ligand density. Surface plasmon resonance (SPR) has been used to monitor and calculate binding affinity between SAM-supported carbohydrates and soluble proteins on gold.[79-81] Several microscopic techniques are available to SAMs on gold to aid in the observation of cell behavior and biomolecular interactions. Atomic force microscopy (AFM) has been utilized to image adhered bacteria and cells.[63,64] Total internal reflection fluorescence microscopy (TIRFM),[82] phase contrast and fluorescence microscopy, tunneling electron microscopy (TEM), and scanning electron microscopy (SEM)[83,84] have all been used as well. Gold is compatible with cell culture and furthermore, SAMs of oligo(ethylene glycol)-alkanethiols resist nonspecific adsorption of proteins and cells.[85,86]

1.3 SAMs as Dynamic Surfaces for Cell Biology

1.3.1 Cell adhesion, polarization, and migration. Adhesion is central to cell survival, differentiation, and motility.[20] For cells to integrate and process signals to migrate *in vivo*, they must first adhere to the ECM through ligand-cell interactions. Many proteins are able to facilitate this process, however, a family of cell-surface receptors known to specifically mediate the attachment of a cell to the ECM or to another cell is integrins. Integrins are heterodimeric, transmembrane proteins that span the plasma membrane and promote the assembly and organization of the actin cytoskeleton.[23,24] Serving as a

link between a cell's extra- and intra- cellular environment, integrins also play a vital role in regulating signal transduction cascades.[25-27]

A variety of strategies have been adopted to modulate cell-integrin interactions *in vitro*, such as altering the composition, concentration, and presentation of ECM ligands. In 1989, Danilov and Juliano isolated and identified the peptide sequence, Arg-Gly-Asp (RGD) as a cell-binding motif found in several ECM proteins including fibronectin (Fn), fibrinogen, vitronectin, laminin, and some collagens.[6,25,36,37] Most of the known integrin receptors recognize the RGD sequence when binding to ECM ligands as shown in the representative diagram in figure 1.3. Due to the ease of solid-phase peptide synthesis, RGD-containing ligands have been integrated with SAM technology to promote cell adhesion and spreading, as well as to conduct studies in cell motility and co-culture and will be the basis for much of the examples listed in this chapter.[39-50]

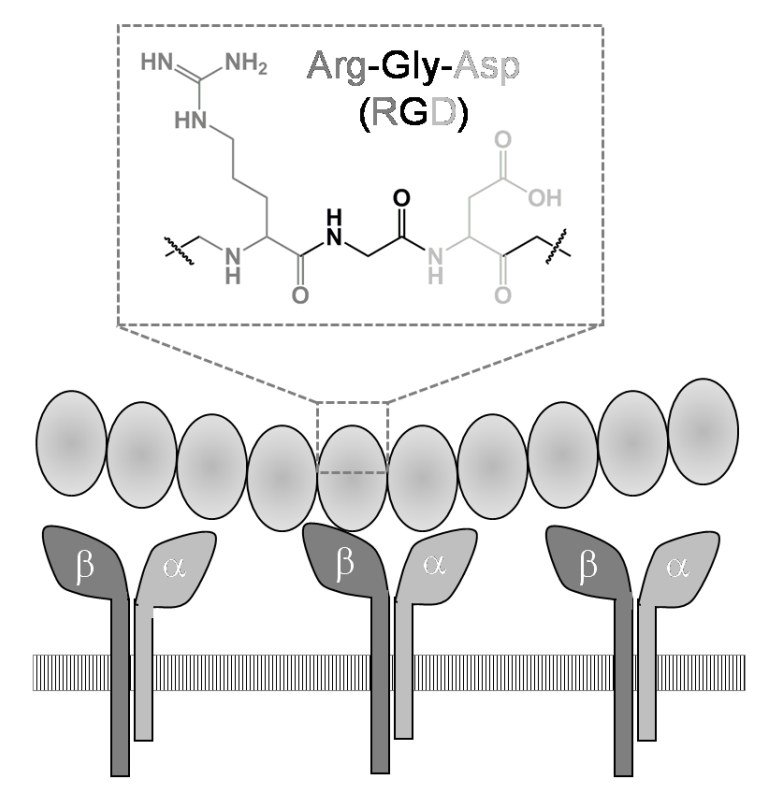

Figure 1.3 A general schematic illustrating integrin-mediated cell adhesion to ECM protein, fibronectin. The minimum peptide sequence required for cell attachment is Arg-Gly-Asp (RGD).

1.3.2 Integration of dynamic surfaces for cell adhesion. The term "dynamic surface" refers to the ability to modulate and control biological interactions and cell behavior in culture. Generally, an external stimulus, such as an electrochemical, photochemical, or biochemical signal, may be applied to turn on and off cell binding *in situ*. This platform allows for the real-time monitoring and manipulation of biological ligands to induce a particular cellular response. For the advantages listed previously, SAMs of alkanethiolates on gold have been employed in several studies to serve as model, dynamic substrates for cell biology. Moreover, the ability to create and tailor dynamic surfaces for the control of the complex cellular microenvironment has proven important for a range of scientific disciplines, such as biomedical and tissue engineering and cell biology.[39-45] Most of literature devoted to the use of SAMs of alkanethiolates on gold to research key biological problems indicates its broad applicability and proven performance to serve as a model platform for such studies.

As mentioned, RGD has been utilized throughout the SAM and surface community to promote the biospecific attachment of cells via integrin (cell-surface receptor) recognition. Liu and colleagues demonstrated that cell adhesion can be modulated by photochemical control of azobenzene SAMs on gold (Figure 1.4).[87] The authors used light to illuminate (450-490 nm) the azobenzene SAMs, which adopted the *E* configuration, presenting RGD. After 1 h of culture, cells adhered and began to spread and grow. This binding interaction was turned off by irradiating light at a lower wavelength (340-380 nm), forcing azobenzene to convert to the *Z* conformation. This configuration masked RGD, and the cells were prevented from attaching to the surface.

Extensive work has shown that through control of an electrochemical potential, a monolayer presenting electroactive molecules can undergo reversible oxidation and reduction to modulate the ability to react with other biomolecules. Therefore, cell

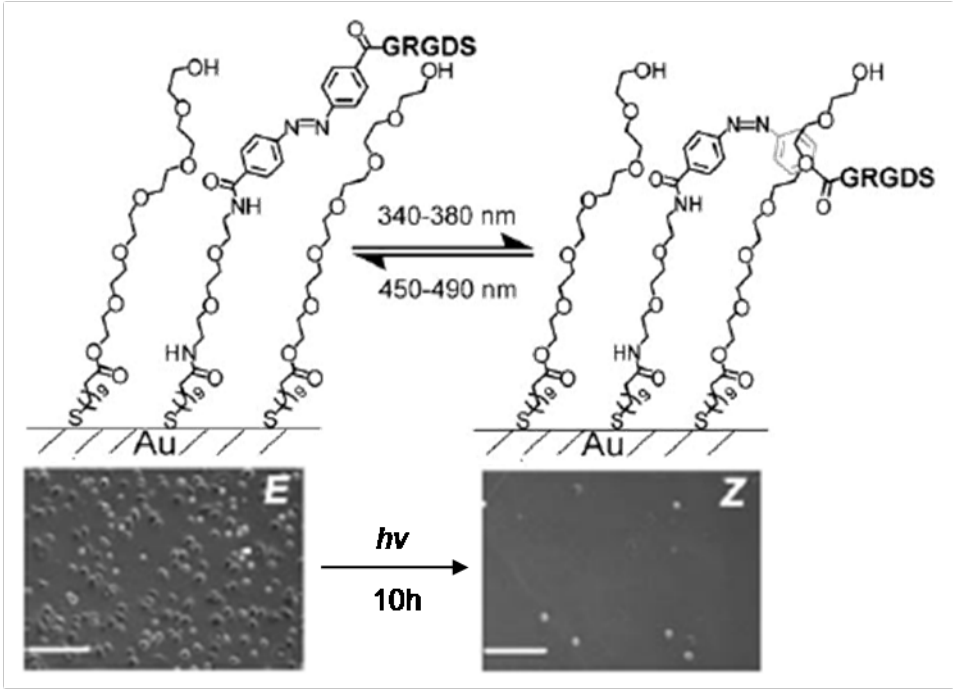

Figure 1.4 Photochemical control of azobenzene SAMs on gold to generate cell adhesive and cell resistant surfaces. RGD is accessible to cells for attachment when SAMs adopt the *E* configuration at 450-490 nm. At 340-380 nm, azobenzene converts to the *Z* conformation, masking RGD, and cell adhesion is prevented. The scale bars represent 200 μm.[87]

adhesion and migration can be actively modulated.[46-48,88-90] Mrksich and colleagues published a series of studies using electroactive-terminated SAMs to immobilize biomolecules for cell adhesion promotion.[91-93] After application of an oxidation potential, mixed SAMs terminated with penta(ethylene glycol) and hydroquinone were converted to the quinone form to permit a Diels-Alder cycloaddition of cyclopentadiene-conjugated RGD.[91] This reaction in turn allowed for the adhesion, spreading, and migration of cells *in situ*. It was shown later by the same group that the release of biotin could be controlled by electrochemical reduction of a quinone propionic ester-terminated SAM.[92,93] This stimulus interrupted the streptavidin-biotin interaction, subsequently causing cells to detach. Likewise, there have been other reports demonstrating the electrochemical release of ligands to turn off cell adhesion.[44,45,88-90] Utilizing the electroactive behavior of hydroquinone-terminated SAMs, Chan *et al.* were able to immobilize and release

oxyamine-containing RGD from selectively patterned regions for the adhesion of fibroblast cells.[88] One of the most widely used patterning techniques that can support protein- or ligand-mediated cell adhesion is μCP.[94] Generally, prefabricated elastomeric stamps are inked with a hydrophobic alkanethiol and then pressed onto a gold surface. The substrate is then immersed in a solution containing oligo(ethylene glycol)-terminated alkanethiol to backfill and render the remaining surface biologically inert. Hydrophobic alkanethiols permit the adsorption of ECM proteins, such as Fn and laminin.

In a recent publication, James and co-workers used μCP to survey the lamellipodial response and distribution of B16F10 cells to local and global geometric cues (Figure 1.5).[95] After printing a variety of differently curved shapes, inked with alkanethiol, actin and cortactin (i.e., cytoplasmic proteins that promote polymerization and rearrangement of the actin cytoskeleton) and Fn were adsorbed to promote cell adhesion. Overall conclusions of this study followed that local cell curvature influenced directed migration and polarity. Concentrated lamellipodia and protrusions were imaged at the periphery and highly curved portions of the patterns. Similarly, Xia and colleague employed μCP to create Fn nanoarrays with differently sized and spaced features to direct NIH cell, focal adhesion positioning, and Rac activation.[96] Focal adhesion sites were imaged by immunofluorescence microscopy, and were likewise, concentrated along the cell periphery. Rac was activated shortly after peripheral membrane extensions spread to new Fn islands. Another study by Luo and colleagues demonstrated μCP-induced human mesenchymal stem cell (hMSC) adhesion and differentiation on a range of different geometric shapes (Figure 1.6).[97] hMSCs were imaged at 3, 5, 10, and 14 days. After two weeks, the hMSCs that were concentrated in the middle of the patterns had differentiated into adipocytes, while the other hMSCs on the pattern's border remained undifferentiated.

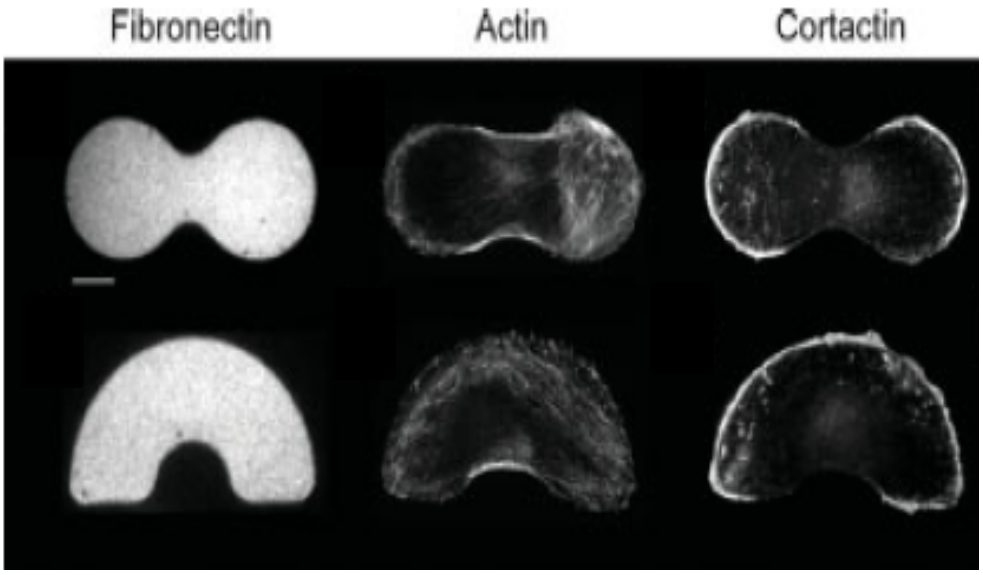

Figure 1.5 Cell cytoskeletal distribution and polarization studies in response to local and global shape curvature. B16 cells adhered to differently shaped patterns presenting Fn, actin, and cortactin and lamellipodia were polarized in individual cells, as well as in cell populations toward the perimeter. The scale bar represents 10 μm.[95]

Photodeprotection and microfluidic strategies have also proven useful for patterning cell-adhesive areas. Park *et al* reported the synthesis and application of a photodeprotection method to reveal oxyamine-terminated groups in different geometric patterns and gradients by UV irradiation (365 nm).[50] After RGD-ketone was immobilized, followed by ligand-mediated cell adhesion, phase contrast images were taken. The micrographs illustrated the formation of thin appendages of the perimeter of the pattern, as well as cell spreading within the confines of each shape. Another technique used to study cell adhesion is microfluidics. Westcott and co-workers employed this strategy to pattern and selectively convert tetra(ethylene glycol)- and hydroxyl-terminated SAMs to aldehyde groups by chemical oxidation. The aldehydes were then reacted with RGD-oxyamine and cells adhered only to the patterned regions.[98] A similar microfluidic activation methodology was used in a further study to generate biospecific microarrays for integrin recognition and cell adhesion.[84]

1.3.3 Surface microscopy techniques to study cell behavior on SAMs. There are a number of vital events that occur at the cellular plasma membrane. As a result, several microscopy techniques have been integrated with SAMs on gold to investigate these short-lived and significant events. Most of these methods have been used to image organelles and protein-cell and protein-protein interactions and calculate diffusion coefficients, affording important clues into cellular and protein dynamics.[99-10]

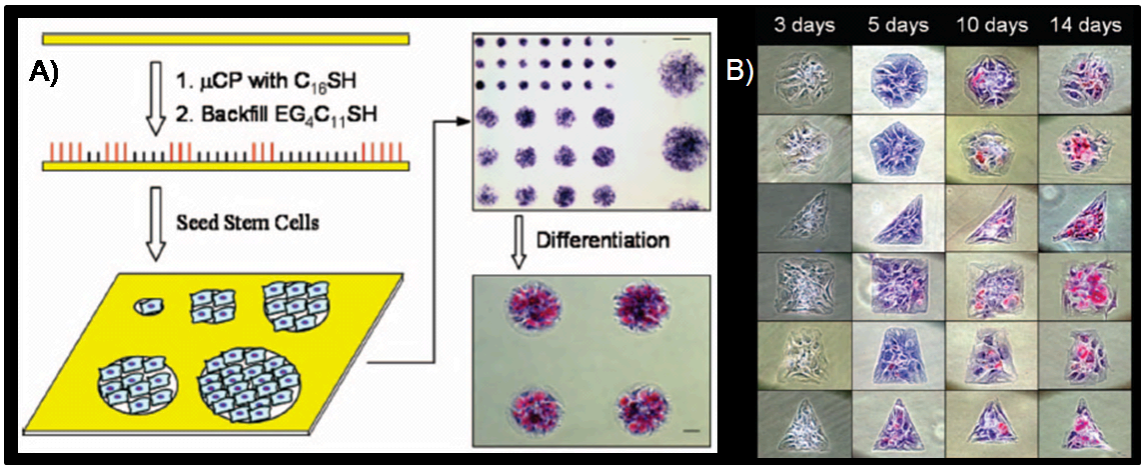

Figure 1.6 A general methodology to create patterned (A) surface arrays and (B) geometric shapes for stem cell adhesion and differentiation studies. Scale bars represent 145 (top) and 60 μm (bottom), respectively (A).[97]

In particular, fluorescence microscopy serves as a major research tool for studying cell biology.[101,102] However, gold efficiently quenches fluorescence by absorbing the low-intensity fluorescence within the cells' excitation wavelength used for live-cell imaging.[41-43] Therefore, its compatibility with SAMs on gold remains a challenge and specific measures must be addressed to overcome this technical obstacle. For example, controlling the layer of gold evaporated onto glass (≤ 10 nm) can produce optically semi-transparent substrates for immunofluorescence staining.[41-43] Another report demonstrated the application of total internal reflection fluorescence microscopy (TIRFM) to image the focal adhesion contacts between a cell and its matrix on inverted gold substrates.[82] A thin layer of gold was evaporated onto a quartz substrate, and fibroblast

cells were patterned and allowed to spread, followed by fixing, staining, and imaging for focal adhesions between the cell and its fibronectin matrix. This initial study may further be explored in order to interface TIRFM with material science for studies in cell signaling and more complex cellular behavior.

The dynamics of RhoA activation in cell protrusions was measured by a fluorescence resonance energy transfer- (FRET) based biosensor.[99] Through measuring the FRET signal intensity, it was found that RhoA activity is much higher at the periphery of the cell, relative to within the cell body. Mirkin has experienced much success with the use of an atomic force microscopy (AFM) tip to create nano-features on bare gold for the immobilization of biomolecules and cells.[104,105]

This technique termed dip-pen nanolithography (DPN) was later employed to pattern and provide lateral force images of the newly formed alkanethiol nanoarrays by Hoover *et al.*[63,64] After patterning a symmetric quinone-terminated alkanethiol array by this method, the authors patterned cells to observe the differences in focal adhesion contacts of adhered cells on linear-RGD and cyclic-RGD ligands. It is known that cells have a higher binding affinity for cyclic-RGD (nM binding affinity) and demonstrated more spreading and focal adhesion formation on arrays presenting cyclic-RGD.[106] While on linear-RGD (μM binding affinity), cells made focal contacts only in the cell periphery. The authors then investigated further into the mechanism of polarization by patterning asymmetric nanoarrays of linear-RGD (Figure 1.7).[64] After fluorescently labeling and imaging the MTOC, Golgi, and actin cytoskeleton, it was concluded that there was a distinct polarization vector formed toward the higher density regions containing the cell-adhesive peptide signal. This was indicated by the reorganization of actin cytoskeleton and positioning of the Golgi in front of the nucleus toward the higher density ligand, which is hypothesized to occur during polarization.

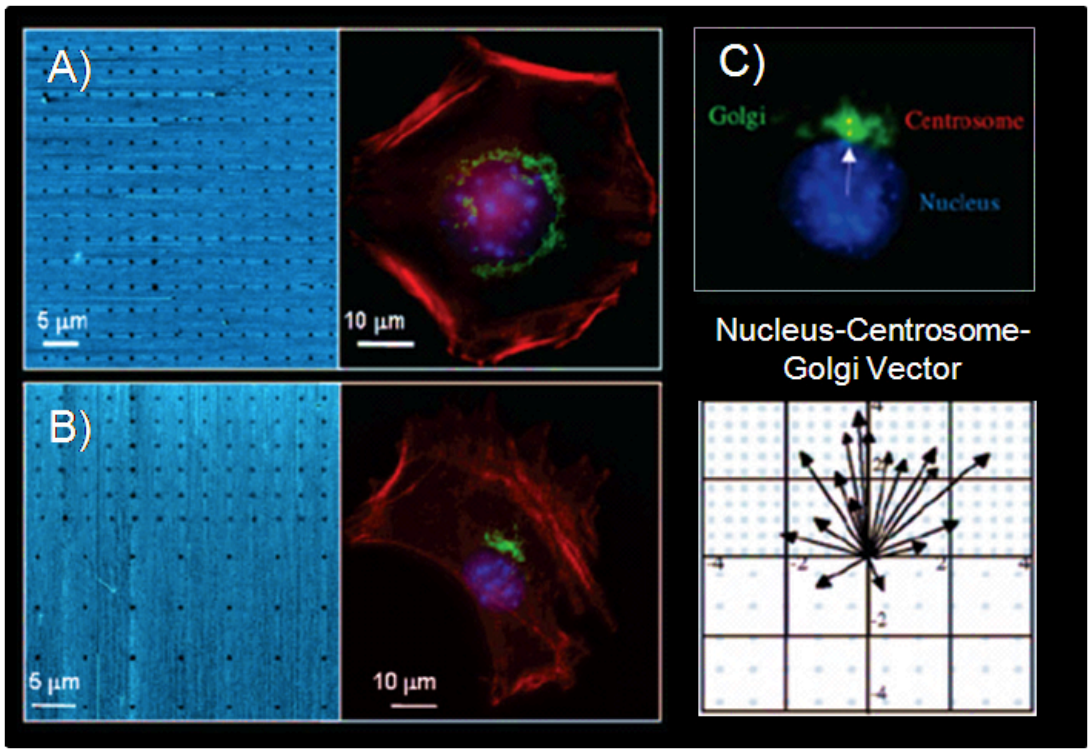

Figure 1.7 Symmetric and asymmetric electroactive nanoarrays for the study of cell adhesion and polarization. DPN was used to pattern SAM nano-spots of hydroquinone-terminated alkanethiolates for subsequent linear-RGD immobilization and cell adhesion. (A) A lateral force microscopy image of a symmetric nanoarray was taken. Cells were observed having a diffusive nucleus-centrosome-golgi vector, indicating no preferential migratory direction. (B) On asymmetric nanoarrays, cell polarity vectors orient toward higher linear-RGD density. (C) A higher magnified cell polarization vector and schematic is shown.[64]

Phase contrast microscopy has also proven to be invaluable for recording movies of cellular response to a stimulus during culture.[49,106,107] In addition to the known cell-binding domain containing RGD (10th type III domain) in Fn, a synergistic site (9th type III domain) that is necessary for obtaining maximal cell-binding activity has also been identified. As such, Yamada, Grant, and Bowditch and co-workers conducted a series of experiments to isolate the sequence of this synergistic peptide, determined to be Phe-His-Ser-Arg-Asn (PHSRN).[108-110] Although PHSRN is incapable of supporting adhesion on its own, if properly spaced from and displayed with RGD, it has been reported to enhance cell attachment and spreading. Interrogations of this relationship and its effect on cell adhesion and migration have since been adapted with SAMs of alkanethiolates

on gold. Feng *et al.* reported distinct phenotypic differences in cell lamellipodia and protrusions when cultured on surfaces of mixed monolayers presenting tri(ethylene glycol) and RGD, PHSRN, or Fn.[111] Different SAM ratios and ligand densities were tested against cell adhesion as well. In Figure 1.8, cells adhered to RGD-presenting SAMs appeared more spread out, producing focal adhesions at the end and periphery of stress fiber bundles. In contrast, cells on PHSRN, formed less stress fiber bundles and demonstrated less spreading and growth. Inhibition experiments showed that the attachment of fibroblasts to RGD-presenting SAMs could be inhibited completely by the addition of a soluble RGD peptide and partially by a soluble PHSRN peptide.

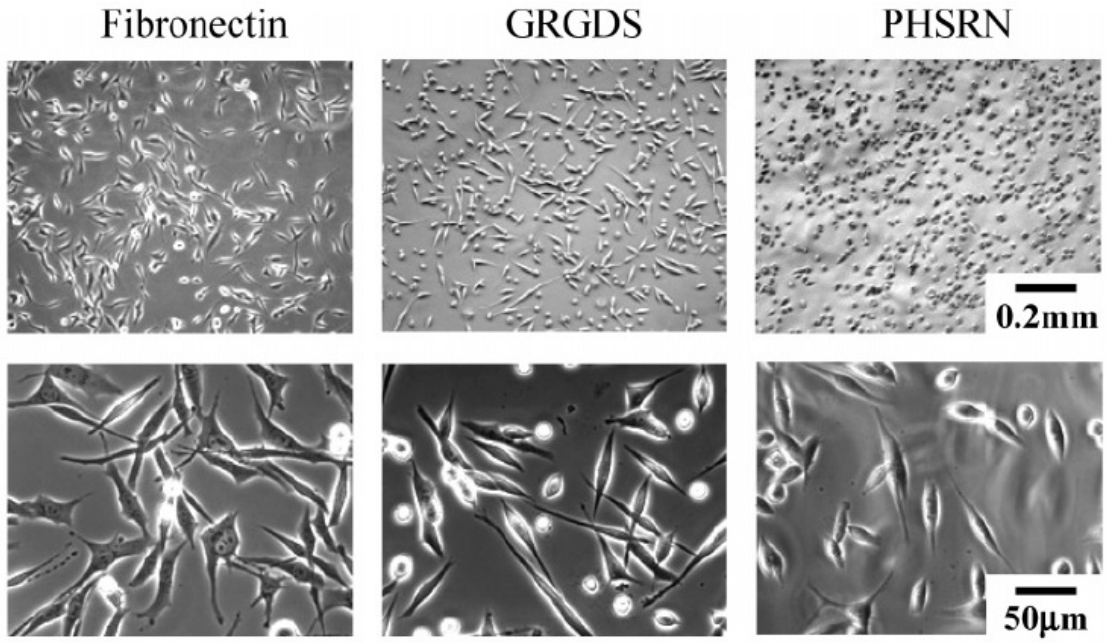

Figure 1.8 BHK cells attached to surfaces presenting fibronectin and peptides, GRGDS and PHSRN. Cells are highly spread on their natural adhesion substrate, fibronectin, as well as on GRDGS. PHSRN does not promote spreading as shown.[111]

1.3.4 SAMs for cell polarization and cell migration. After a cell adheres to another cell or the underlying matrix, it integrates signals from its surrounding environment. Once the cell receives a directional cue, it polarizes and reorients its machinery toward the direction of migration.[112-116,124] Therefore, polarization is fundamental to a number of

cellular processes. However, the mechanism is not fully understood. SAMs have been utilized to address this phenomenon. To induce cell polarization, several studies have sought to create ECM protein, other cell, or other cell-surface receptor-type molecular gradients on SAMs.[46-50]

A combined photodeprotection and electrochemical strategy was reported by Chan *et al.* in which the authors observed the effects of cell-cell and cell-matrix interactions on cell polarization and migration.[46] NVOC-protected hydroquinone-terminated SAMs were formed on gold and a photomask was placed on the surface. After light was illuminated, selective regions with different geometries were revealed. Substrates were then oxidized, followed by RGD-oxyamine immobilization and the addition of fibroblasts. Interestingly, the authors found that the adhered single cells displayed a diffusive golgi and nucleus, indicating that they were not polarized (Figure 1.9, far left). However, when two or more cells were observed on the same patterned region, the nucleus, Golgi apparatus, MTOC, and actin cytoskeleton were polarized toward the opposite direction (Figure 1.9, second to far right). This behavior was also seen on different geometries. The authors concluded that cell-cell contacts were observed cell-RGD interactions, forcing the cells to polarize away from one another.

Rather than using geometric shapes and cell-cell interactions to probe the effects of polarization, Lamb and colleagues used partially etched gold surfaces by microfluidics to determine the trajectory of cells migrating.[49] A fluorescently labeled Golgi and nucleus cell line was recorded and imaged to gain insight on the role of cell polarity on motility. They found that over a period of 12 h, the cells remained confined to the etched regions, and the Golgi was concentrated toward the leading edge of migration. After a cell was recorded migrating around a corner of the microfluidic pattern, the polarity vector (nucleus to Golgi) reoriented upon completion of a directional turn.

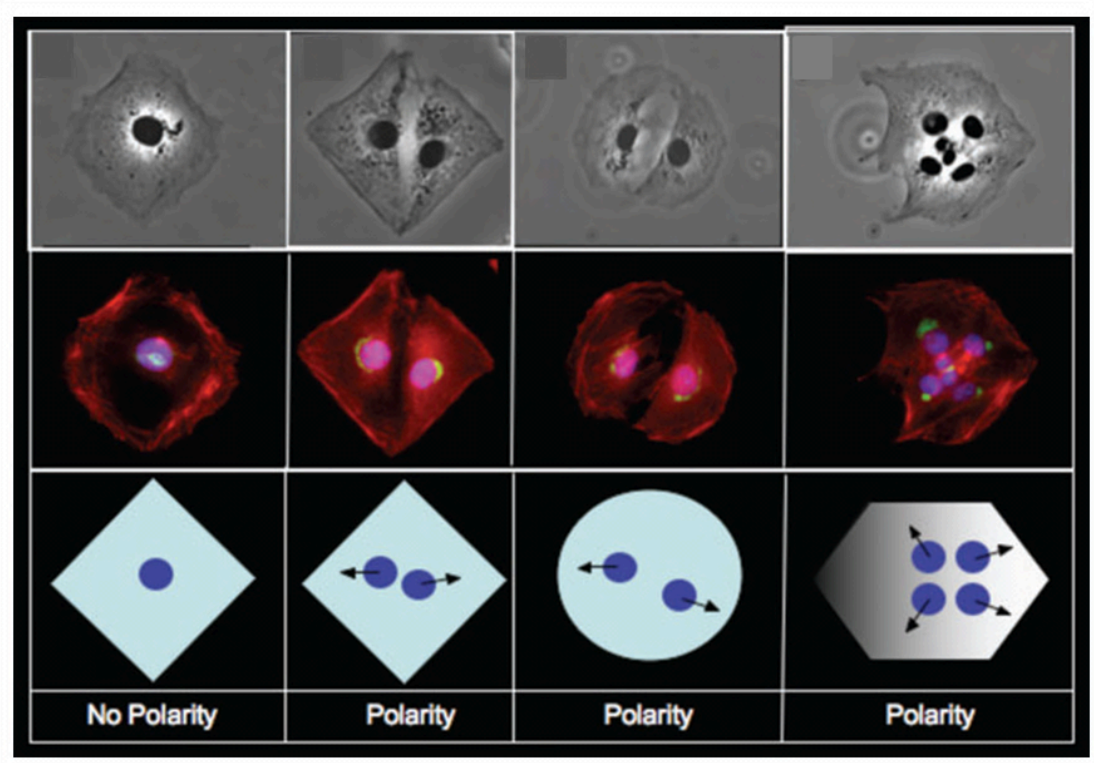

Figure 1.9 A photochemical and electroactive SAM-based strategy to study the polarization of cells on different geometries.[46]

1.3.5 Surface gradients and migration. In vivo, cell outgrowth and directional migration occur by two different methods: (1) up a concentration gradient of soluble adhesion sites (chemotaxis) or (2) surface-bound chemoattractants (haptotaxis).[117,118] These biomolecular gradients are naturally present in the ECM and are vital in the developmental stages of a cell's life and can also influence a number of disease states, such as cancer metastasis. Gradients in the form of extracellular signals, ligand- and receptor-mediated interactions cause the cell to polarize, resulting in activation and reorganization of organelles and cytoskeletal components. The polarization process then initiates a specific behavioral response. Cattaruzza and Perris created a concentration-dependent gradient of surface-bound proteoglycans (PGs) that promote polyvalent interaction of the cell with other ECM components and neighboring cells.[117] Cells migrated away from areas presenting PGs if they sensed a higher density of bound or

soluble chemoattractant nearby. This result was contrary to generated gradients displaying laminin. Similarly, McCarthy *et al.* reported that integrin receptors recognize substrate-bound laminin, promoting cell adhesion, followed by the directed migration of RN22F cells toward higher concentrations of laminin.[118] Although these studies provided invaluable information into the mechanism of directed-cell mobility, these gradients not well defined and quantitatively characterized.

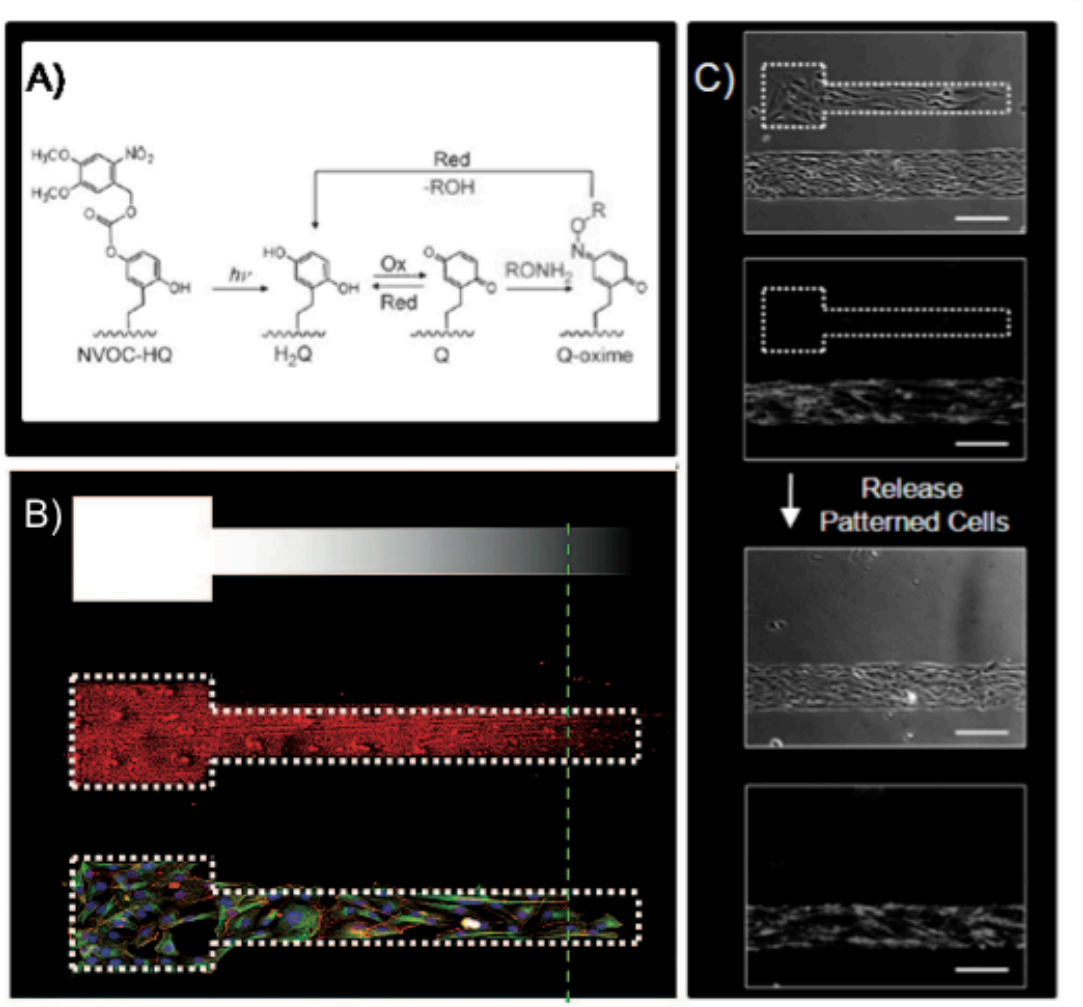

Figure 1.10 A photochemical and electroactive SAM-based strategy to generate a cell co-culture platform with spatially controlled gradient patterning. (A) A general schematic representing the activation of hydroquinone-terminated SAMs by photodeprotection of NVOC (365 nm) for subsequent tailoring of oxyamine-containing ligands is shown. (B) The photomask used to create hydroquinone-SAM gradients for cell polarization and migration studies. (C) Cell co-cultures were patterned RGD-gradients that can be released and re-adhered through an electrochemical and pH stimuli. Scale bars represent 100 μm (C).[47]

To address this issue, several experiments in generating dynamic gradients of SAMs or biomolecules with spatial and temporal control on surfaces supporting SAMs have been reported to study cell polarization and migration.[46-50] SAMs allow the precise manipulation and quantification of surface molecules. Chan and co-workers reported a photodeprotection strategy to reveal functionalized SAMs in a gradient.[47] The photomask pattern used to form the monolayer is shown in figure 1.10B. After immobilization of adhesive ligand RGD, cells were cultured on the surface in different densities. The majority of cells attached to the densest regions that contained RGD. Directed migration toward highly concentrated areas was also observed over the course of several days. The authors concluded that in high cell density on patterned gradients of substrate-bound RGD, cell-cell contacts overrode cell-matrix interactions, and directed cell migration was not observed.[47] The same group performed further experiments using μCP and photodeprotection to pattern and reveal gradients and investigate cellular behavior when co-cultured (Figure 1.10C).[48] Transfected mouse fibroblasts expressing GPF-actin were first patterned on Fn-containing patterns. As previously described, a gradient of monolayer-presenting RGD was then formed. A non-fluorescent fibroblast cell line was then cultured on and adhered to the gradient of RGD, most densely populating the higher concentrated areas of the pattern, rather than co-inhabiting the fluorescent population. Electrochemically induced release of RGD, forced detachment of the cells adhered to the gradient, leaving the population interacting with Fn attachment.

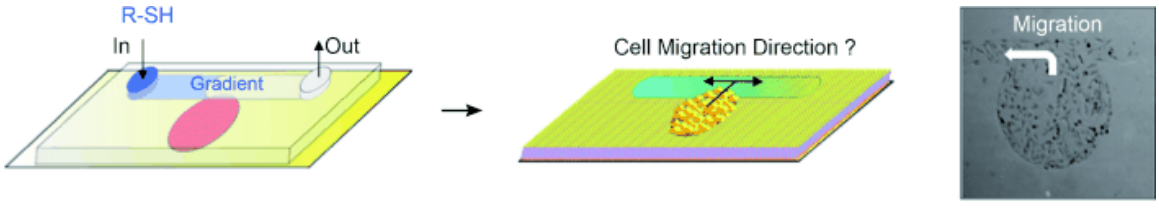

Figure 1.11 A strategy for the complete spatial control of directed cell migration using microfluidic lithography to create gradients of SAMs for studies in cell adhesion and migration.[48]

Microfluidic lithography (μFL) is another method, proven powerful in the generation of monolayer gradients. In a series of publications, Lamb and co-workers reported the fabrication and use of microfluidic cassettes to create chemoselective SAM patterns and gradients.[48,49] By controlling the capillary action and flow rate, alkanethiols could be flowed through the micro-channels to form a SAM instantly (Figure 1.11). The authors aimed to create a dynamic environment and probe the effects of ligand cues on directed-cell migration. Cells were first patterned on an island containing a hydrophobic SAM (by μCP), found in the middle of a gradient presenting a quinone-terminated SAM. RGD was then reacted on the surface, and upon immobilization, cells were seen migrating from the island toward the higher density regions containing RGD. Once there, cells adhered and grew. Microfluidics was then employed by the same group to partially etch away the SAM and gold in different patterns and test the effects of cell-migration in response to the substrate disruption. Fluorescence live-cell imaging recorded transfected Rat2 fibroblasts during migration, showing a polarized Golgi and nucleus toward the direction of movement. A current study is being conducted to examine the effects of RGD gradients on cell division. They aim to determine whether cells divide parallel or perpendicular to the gradient and if migration has an influence on when cells divide.

1.4 Outlook

SAMs offer attractive physical properties that allow fundamental studies for biointerfacial chemistry. These advantages include the synthetic flexibility in tailoring terminal functional groups and the large number of patterning techniques and analytical characterization tools compatible with SAMs, making them a model platform for a variety of applications. Complexly patterned and mixed-SAM surfaces may be generated by the combination of available ligand immobilization strategies and non-fouling properties of oligo(ethylene glycol)-alkanethiol. Due to these properties, SAMs serve as an ideal

substrate in mimicking the natural, dynamic environment of cells, and cell adhesion, polarization, and migration studies have been undertaken with great success. However, SAMs represent a 2D surface where cells are confined on a rigid matrix. Although much has been elucidated about complex biological phenomena, there still exists a gap between the data interpreted from *in vitro* experimentation and cell behavior in their native environment *in vivo.*[124-126] As such, attempts to modify planar, 2D SAM surfaces have been reported to varying degrees of success.[119] In the future, platforms combining several of the dynamic substrate aspects discussed in this chapter will be used for complete analyses cell behavior *in vivo* and in real-time. In combination with either a hydrogel matrix or 3D microfluidic scaffold, SAM chemistry may be used to incorporate spatially controlled chemotactic factors. These endeavors require a multidisciplinary effort. Overall, there has been significant progress with using SAMs of alkanethiolates on gold in conducting biological investigations. However, a few systemic disadvantages remain, including fluorescence quenching and long-term instability of the gold-thiol bond. As a result, alternate model systems (i.e., siloxanes on glass and phosphonates on metal oxides) have been explored for use in cell-based assays and biosensors.[120,121] Thus, extending some of the work to create dynamic surface chemistries on gold to other materials may provide opportunities to conduct novel investigative experiments for determining the mechanisms that regulate cell behavior.

1.5 Significance and Goals of this Research

My dissertation research is focused on the development of smart biosurfaces and materials to investigate peptide-cell, protein-carbohydrate, and lipid-cell interactions. A library of biomolecules was designed and synthesized to include chemoselective and bio-orthogonal functional groups, ketone and oxyamine. With this coupling methodology, I successfully modified biomaterials and cell surfaces to examine a variety of cell

behaviors, such as cell-biospecific ligand interactions, adhesion, polarization, migration, and cellular response to other cells.

This work comprises eight chapters. Chapter 1 provides an introduction to SAMs and a general discussion regarding the design and utility of dynamic SAM surfaces and for biological analyses. The use of SAMs on gold and indium tin oxide for cell adhesion studies is presented in Chapters 2 and 3, respectively. Chapter 4 demonstrates the development and application of a renewable carbohydrate microarray based on hydroquinone-terminated SAMs on gold. Hydroquinone was then incorporated with cell adhesive peptide, RGD, to survey selected carbohydrates and peptides for their combined effect on fibroblast adhesion, morphology, and migration; this data is discussed in Chapter 5. A cell-surface engineering strategy based on liposome delivery and membrane fusion to direct cell-cell contacts and generate 3D tissue-like structures is reported in Chapters 6 and 7. Finally, Chapter 8 describes my general conclusions and future research directions.

References

(1) de las Herra-Alarcon, C.; Farhan, T.; Osborne, V.; Huck, W.; Alexander, C. *J. Mater. Chem.* **2005**, *15*, 2089-2094.

(2) Ebara, M.; Yamato, M.; Aoyagi, T.; Kikuchi, A.; Sakai, K.; Okano, T. *Biomarcomolecules* **2004**, *5*, 505-510.

(3) Zareie, H.; Boyer, C.; Bulmus, V.; Nateghi, E.; Davis, T. *ACS Nano* **2008,** *4*, 757-765.

(4) Alberts, B.; Johnson, A.; Lewis, J.; Raff, M.; Roberts, K.; Walter, P. *Molecular Biology of the Cell;* **2002**, Garland Science: New York.

(5) Rhodes, J.; Simons, M. *J. Cell Mol. Med.* **2007**, *2,* 176-205.

(6) Danilov, Y.; Juliano R. *Exp. Cell Res.* **1989**, *182*, 186-196.

(7) Halbleib, J.; Nelso, W. *Genes & Dev.* **2006**, 20*,* 3199-3214.

(8) Hogg, N.; Landis, R. *Curr. Opin. Immunol.* **1993**, *5,* 383-390.

(9) Hogg, N. *Immunol. Today* **1992**, *13,* 113-115.

(10) Cyster, J. *Immunol. Rev.* **2001**, *194*, 48-60.

(11) Raghow, R. *FASEB J.* **1994**, *8,* 823-831.

(12) Mutsaers, S.; Bishop, J.; McGrouther, G.; Lauret, G. *Int. J. Biochem. Cell Biol.* **1997**, *29,* 5-17.

(13) Jacinto, A.; Martinez-Arias, A.; Martin, P. *Nat. Cell Biol.* **2001**, *3,* E117-E123.

(14) Sottile, J. *Biochim. Biophys. Acta* **2004**, *1654,* 13-22.

(15) Hood, J.; Cheresh, D. *Nat. Rev. Cancer* **2002**, *2,* 91-100.

(16) Bogenrieder, T.; Herlyn, M. *Oncogene* **2003**, *22,* 6524-6536.

(17) Liotta, L.; Kohn, E. *Nature* **2001**, *411*, 375-379.

(18) Keely, P.; Parise, L.; Juliano, R. *Trends Cell Biol*. **1998**, *8*, 101-106.

(19) Fidler, I. *Semin. Cancer Biol.* **2002**, *12*, 89-96.

(20) Hynes, R. *Cell* **1987**, *48*, 549-554.

(21) Tamkun, J.; DeSimone, D.; Fonda, D.; Patel, R.; Buck, C.; Horwitz, A.; Hynes, R. *Cell* **1986**, *46,* 271-282.

(22) Juliano, R.; Reddig, P.; Alahari, S.; Edin, M.; Howe, A.; Aplin, A. *Biochem. Soc. Trans.* **2004**, *32*, 443-446.

(23) Blystone, S. *Biochim. Biophys. Acta* **2004**, *1692*, 47-54.

(24) Bershadsky, A.; Balaban, N.; Geiger, B. *Annu. Rev. Cell Dev. Biol.* **2003**, *19*, 677-706.

(25) Juliano, R. *Annu. Rev. Pharmacol. Toxicol.* **2002**, *42*, 28-54.

(26) Giancotti, F.; Tarone, G. *Annu. Rev. Cell Dev. Biol.* **2003**, *19,* 173-206.

(27) Forgacs, G.; Yook, S.; Janmey, P.; Jeong, H.; Burd, C. *J. Cell Sci.* **2004**, *117*, 2769-2775.

(28) Sastry, S.; Burridge, K. *Exp. Cell Res.* **2000**, *261*, 25-36.

(29) Zaidel-Bar, R. (2004) *Biochem. Soc. Trans.* **2004**, *32*, 416-420.

(30) Zamir, E.; Geiger, B. *J. Cell Sci*. **2001**, *114*, 3577-3579.

(31) Jockusch, B.; Bubeck, P.; Giehl, K.; Kroemker, M.; Moschner, J.; Rothkegel, M.; Rudiger, M.; Schluter, K.; Stanke, G.; Winkler, J. *Annu. Rev. Cell Dev. Biol.* **1995**, *11,* 379-416.

(32) Brakebusch, C.; Fassler, R. *EMBO J*. **2003**, *22*, 2324-2333.

(33) Burridge, K. *J. Cell Biol.* **1992**, *119*, 893-903.

(34) Turner, C.; Glenney, J.; Burridge, K. (1990) *J. Cell Biol*. **1990**, *111*, 1059-1068.

(35) Danilov, Y.; Juliano, R. (1989) *Exp. Cell Res.* **1989**, *182,* 186-196.

(36) Maheshwari, G.; Brown, G.; Lauffenburger, D.; Wells, A.; Griffith, L. (2000) *J. Cell Sci.* **2000**, *113*, 1677-1686.

(37) Koo, L.; Irvine, D.; Mayes, A.; Lauffenburger, D.; Wells, A.; Griffith, L. *J. Cell Sci.* **2002**, *115*, 1423-1433.

(38) Webb, D.; Brown, C.; Horwitz, A. *Curr. Opin. Cell Biol*. **2003**, *15*, 614-620.

(39) Mendes, P. *Chem. Soc. Rev.* **2008**, *37*, 2512-2529.

(40) Wischerhoff, W.; Badi, N.; Lutz, J.-F.; Laschewsky, A. *Soft Matter* **2010**, *6*, 705-713.

(41) Ulman, A. *Chem. Rev.* **1996**, *96*, 1533-1554.

(42) Schwartz, D. *Annu. Rev. Phys. Chem.* **2001**, *52*, 107-137.

(43) Love, J.; Estroff, L.; Kriebel, K.; Nuzzo, R.; Whitesides, G. M. *Chem. Rev.* **2005**, *105*, 1103-1170.

(44) Mrksich, M. *Acta Biomater.* **2009**, 5, 832-841.

(45) Yousaf, M. N. *Curr. Opin. Chem. Biol.* **2009**, *13*, 697-704.

(46) Chan, E. W. L.; Yousaf, M. N. *Mol. Biol. Sys.* **2008**, *4*, 746-753.

(47) Lee, E.-J.; Chan, E. W. L.; Yousaf, M. N. *ChemBioChem* **2009**, *10*, 1648-1653.

(48) Lamb, B. M.; Westcott, N. P.; Yousaf, M. N. *ChemBioChem* **2008**, *9*, 2628-2632.

(49) Lamb, B. M.; Westcott, N. P., Yousaf, M. N. *ChemBioChem* **2008**, *9*, 2220-2224.

(50) Park, S.; Yousaf, M. N. *Langmuir* **2008**, *24*, 6201-6207.

(51) Nuzzo, R.; Allara, D. *J. Am. Chem. Soc.* **1983**, *105*, 4481-4483.

(52) Zhi, Z.-L. ; Laurent, N.; Turnbull, J. *ChemBioChem* **2008**, *9*, 1568-1575.

(53) Park, T.; Shuler, M. *Biotechnol. Prog.* **2003**, *19*, 243-253.

(54) Panda, S.; Sata, T.; Hampton, G.; Hogenesch, J. *Trends Cell Biol.* **2003**, *13*, 151-156.

(55) Laurent, N.; Voglmeir, J.; Wright, A.; Blackburn, J.; Wong, S.; Gaskell, S.; Flitsch, S. *ChemBioChem* **2008**, *6*, 883-887.

(56) Lahann, J.; Balcells, M.; Rodon, T.; Lee, J.; Choi, I.; Jensen, K.; Langer, R. *Langmuir* **2002**, *18*, 3632-3638.

(57) Yamato, M.; Konno, C.; Ustumi, M.; Kikuchi, A.; Okano, T. *Biomaterials* **2002**, *23*, 561-567.

(58) Schreiber, F. *J. Phys: Condens. Matter* **2004**, *16*, R881-R900.

(59) Pale-Grosdemange, C.; Simon, E.; Prime, K.; Whitesides, G. M. *J. Am. Chem. Soc.* **1991**, *113*, 12-20.

(60) Kane, R.; Takayama, S.; Ostuni, E.; Ingber, D. E.; Whitesides, G. M. *Biomaterials* **1999**, *20*, 2363-2376.

(61) Wouters, D.; Schubert, U. *Angew. Chem. Int. Ed.* **2004**, *43*, 2480-2495.

(62) Ginger, D. S.; Zhang, H.; Mirkin, C. A. *Angew. Chem. Int. Ed.* **2004**, *43*, 30-45.

(63) Hoover, D. K.; Lee, E.-J.; Yousaf, M. N. *ChemBioChem* **2007**, *8*, 1920-1923.

(64) Hoover, D. K.; Chan, E. W. L.; Yousaf, M. N. *J. Am. Chem. Soc.* **2008**, *130*, 3280-3281.

(65) Schilp, S.; Ballav, N.; Zharnikov, M. *Angew. Chem. Int. Ed.* **2008**, *47*, 6786-6789.

(66) Ballav, N.; Schilp, S.; Zharnikov, M. *Angew. Chem. Int. Ed.* **2008**, *47*, 1421-1424.

(67) Schmelmer, U.; Paul, A.; Kuller, A.; Steenackers, M.; Ulman, A.; Grunze, M.; Golzhauser, A.; Jordan, R. *Small* **2007**, *3*, 459-465.

(68) Steenackers, M.; Kuller, A.; Ballav, N.; Zharnikov, M.; Grunze, M.; Jordan, R. *Small* **2007**, *10*, 1764-1773.

(69) Klauser, R.; Huang, H.; Wang, S.; Chen, C.; Chuang, T.; Terfort, A.; Zharnikov, M. *Langmuir* **2004**, *20*, 2053-2060.

(70) Brandow, S.; Chen, M.-S.; Aggarwal, R.; Dulcey, S.; Calvert, J.; Dressick, W. *Langmuir* **1999**, *15,* 5429-5432.

(71) Laurent, N.; Voglmeir J.; Wright, A.; Blackburn, J.; Pham, N.; Wong, S.; Gaskell, S.; Flitsch, S. *ChemBioChem* **2008**, *9*, 883-887.

(72) Laurent, N.; Haddoub,R.; Voglmeir, J.; Wong, S.; Gaskell, S.; Flitsch, S. *ChemBioChem* **2008**, *9*, 2592-2596.

(73) Min, D.-H.; Su, J.; Mrksich, M. *Angew. Chem. Int. Ed.* **2004**, *43*, 5973-5977.

(74) Hu, Z.; Prunici, P.; Patzner, P.; Hess, P. *J. Phys. Chem. B.* **2006**, *110*, 14824-14831.

(75) Bae, Y.; Park, K.-W.; Oh, B.-K.; Lee, W. Choi, J.-W. *Colloid Surface A.* **2004**, *257,* 19-23.

(76) Michel, O.; Ravoo, B. *Langmuir* **2008**, *24*, 12116-12118.

(77) Kondo, M.; Nakamura, Y.; Fujii, K.; Nagata, M.; Suemori, Y.; Dewa, T.; Iida, K.; Gardiner, A.; Cogdell, R.; Nango, M. *Biomacromolecules* **2007**, *8*, 2457-2463.

(78) Kong, B.; Kim, Y.; Choi, I. *Bull Korean Chem. Soc.* **2008**, *29*, 1843-1846.

(79) Chan, E. W. L.; Yousaf, M. N. *J. Am. Chem. Soc.* **2006**, *128*, 15542-15546.

(80) Mrksich, M.; Sigal, G.; Whitesides, G. M. *Langmuir* **1995**, *11*, 4383-4385.

(81) Yonzon, C.; Jeoung, E.; Zou, S.; Schatz, G.; Mrksich, M.; Van Duyne, R. *J. Am. Chem. Soc.* **2004**, 126, 12669-12676.

(82) Hoover, D. K.; Yousaf, M. N. *Langmuir* **2009**, *25*, 2563-2566.

(83) Papadantonakis, K.; Brunschwig, B.; Lewis, N. *Langmuir* **2008**, *24*, 10543-10548.

(84) Pulsipher, A.; Yousaf, M. N. *Langmuir* **2010**, *26,* 4130-4135.

(85) Prime, K.; Whitesides, G. M. *Science* **1991**, *252*, 1164-1167.

(86) Xia, Y.; Whitesides, G. M. *Langmuir* **1997**, *13*, 2059-2067.

(87) Liu, D.; Xie, Y.; Shao, H.; Jiang, X. *Angew. Chem. Int. Ed.* **2009**, *48*, 4406-4408.

(88) Chan, E. W. L.; Park, S.; Yousaf, M. N. *Angew. Chem, Int. Ed.* **2008**, *120*, 6363-6367.

(89) Lamb, B. M.; Barrett, D. G.; Westcott, N. P.; Yousaf, M. N. *Langmuir* **2008**, *24*, 8885-8889.

(90) Horton, R.; Herne, T.; Myles, D. *J. Am. Chem. Soc.* **1997**, *119*, 12980-12981.

(91) Yousaf, M. N.; Mrksich, M. *J. Am. Chem. Soc.* **1999**, *121*, 4286-4287.

(92) Hondeland, C.; Mrksich, M. *Langmuir* **1997**, *13*, 6001-6003.

(93) Yeo, W.-S.; Hondeland, C.; Mrsich, M. *ChemBioChem* **2001,** *7*, 590-593.

(94) Whitesides, G. M.; Ostuni, E.; Takayama, S.; Jiang, X.; Ingber, D. E. *Annu. Rev. Biomed. Eng.* **2001**, *3*, 335-373.

(95) James, J.; Goluch, E. D.; Hu, H.; Liu, C.; Mrksich, M. *Cell. Motil. Cyctoskel.* **2008**, *65*, 841-852.

(96) Xia, N.; Thodeti, C.; Hunt, T.; Xu, Q.; Ho, M.; Whitesides, G. M. *FASEB J.* **2008**, *22*, 1649-1659.

(97) Luo, W.; Jones, S.; Yousaf, M.N. *Langmuir* **2008,** *24*, 12129-12133.

(98) Westcott, N.P.; Pulsipher, A.; Lamb, B. M.; Yousaf, M. N. *Langmuir* **2008**, *24*, 9237-9240.

(99) Hodgson, L.; Chan, E. W. L.; Hahn, K.; Yousaf, M .N. *J. Am. Chem. Soc.* **2007**, *129*, 9264-9265.

(100) Webb, D.; Brown, C.; Horwitz, A. *Curr. Opin. Cell Biol.* **2003**, *15*, 614-620.

(101) Steyer, J.; Almers, W. *Nat. Rev. Mol. Cell Biol.* **2001**, *2*, 268-275.

(102) Axelrod, D. *Cell Biol.* **1981**, *89*, 141-145.

(103) Mathur, A.; Truskey, G.; Reichert, W. *Biophys. J.* **2000**, *78*, 1725-1735.

(104) Demers, L.; Ginger, D.; Park, S.; Li, Z.; Chung, S.; Mirkin, C. A. *Science* **2002**, *296*, 1836-1838.

(105) Wilson, D.; Martin, R.; Hong, S.; Cronin-Golomb, M.; Mirkin, C. A. *Proc. Natl. Acad. Sci. U.S.A.* **2001**, *98*, 13660-13664.

(106) Liu, S. *Bioconjugate Chem.* **2009**, *20*, 2199-2213.

(107) Steyer, J.; Almers, W. *Nat. Rev. Mol. Cell Biol.* **2001**, *2*, 268-275.

(108) Aota, S.; Nomizu, M.; Yamada, K. *J. Biol. Chem.* **1994**, *269*, 24756-24761.

(109) Bowditch, R. *J. Biol. Chem.* **1994**, *269*, 10856-10863.

(110) Mardon, H.; Grant, K. *FEBS Lett.* **1994**, *340*, 197-201.

(111) Feng, Y.; Mrksich, M. *Biochemistry* **2004**, *43*, 15811-15821.

(112) Eaton, S.; Simons, K. *Cell* **1995**, 82, 5-8.

(113) Drubin, D.; Nelson, W. *Cell* **1996**, *84*, 335-344.

(114) Dustin, M. *Cell* **2002**, *110*, 13-18.

(115) Euteneuer, U.; Schliwa, M. J. *Cell Biol.* **1992**, *116*, 1157-1166.

(116) Yvon, A.; Walker, J.; Danowski, B.; Fagerstrom, C.; Khodjakov, A.; Wadsworth, P. *Mol. Biol. Cell* **2002**, *13*, 1871-1880.

(117) Cattaruzza, S.; Perris, R. *Matrix Biol.* **2005**, *24*, 400-417.

(118) McCarthy, J.; Palm, S.; Furcht, L. *J. Cell Biol.* **1983**, *97*, 772-777.

(119) Hoch, H.; Staples, R.; Whitehead, B.; Comeau, J.; Wolf, E. *Science* **1987**, *235*, 1659-1662.

(120) Pulsipher, A.; Westcott, N. P.; Luo, W.; Yousaf, M. N. *J. Am. Chem. Soc.* **2009**, *131*, 7626-7632.

(121) Pulsipher, A.; Westcott, N. P.; Luo, W.; Yousaf, M. N. *Adv. Mater.* **2009**, *21*, 3082-3086.

(123) Vicentes-Manzanares, M.; Webb, D. J.; Horwitz, A. R. *J. Cell Sci.* **2005**, *118*, 4917-1919.

(124) Cukierman, E.; Pankov, R.; Stevens, D. R.; Yamada, K. M. *Science*, **2001**, *294*, 1708-1712.

(125) Tibbitt, M .W.; Anseth, K. S. *Biotechnol. Bioeng.* **2009**, *103*, 655-663.

(126) Lutolf, M. P.; Hubbell, J. A. *Nat. Biotechnol*. **2005**, *23*, 47-55.

CHAPTER 2

Microfluidic Oxidative Activation: Generation of Biospecific Ligand and Cell Arrays

2.1 Introduction

The development of strategies to pattern and control the interface between biomolecules and a solid support is critical to a number of research areas, including drug discovery,[1] tissue engineering,[2,3] and gene microarray technology.[4-6] In particular, tremendous effort has been extended toward interfacing material science with cell biology to conduct mechanistic studies of cell adhesion,[7,8] polarization,[9,10] and migration.[11] These studies require the combined use of a model substrate platform and a synthetic chemical immobilization methodology to pattern biospecific, biomolecular cues for cellular recognition. Currently, self-assembled monolayers (SAMs) of alkanethiolates on gold represent one of the most well-studied and developed surface systems in biointerfacial science. In addition to several commercially available alkanethiols, thiol chemistry is compatible with a variety of functional groups, and therefore, alkanethiols are routinely synthesized to allow for the chemoselective surface coupling of ligands. Gold is also conductive, enabling compatibility with many surface spectroscopies for interfacial association characterization. Furthermore, oligo(ethylene glycol)-terminated alkanethiol SAMs enable inert surfaces where nonspecific protein adsorption and cell attachment is minimized.[12-14] Several SAM patterning techniques on

gold have been employed, such as microcontact printing (μCP)[15,16] and photo-,[17] electron beam,[18,19] X-ray,[20] and dip pen nano-[21] lithography. Although, there has been tremendous interest in generating chemoselective patterned microarrays in which most strategies have relied on multi-step synthesis of alkanethiols, complex surface manipulation, or techniques that require expensive or custom instrumentation.[22-24] μCP has been shown to be compatible with a number of hydrophobic alkanethiols; the patterning of hydrophilic alkanethiols is also possible; however, in order to do so, PDMS surface modifications must be performed for proper inking and the creation of a well-defined and uniform SAM.[25] A more inexpensive, rapid, and convergent method to immobilize ligands and cells on a chemoselective patterned array would be of great utility to the surface chemistry, biotechnology, and cell biology research communities.

In recent years, microfluidics has emerged as an important research technology for a number of applications, ranging from the development of biochemical[26-28] and environmental[29] sensors, to perform rapid high-throughput separations in addition to basic science research.[30,31] In combination with SAMs on gold, microfluidic lithography (μFL) has been utilized to create dynamic gradients for cell polarization and co-culture studies, as well as to pattern ligands for subsequent examination of cell behavior.[32-37] However, no current method exists for generating patterned, chemoselective microarrays for ligand immobilization using μFL. In addition to enabling precise control over ligand density and spatial distribution, such a strategy would provide an inexpensive and expedient platform for the high-throughput analyses of interactions between a number of biomolecular signals and their corresponding receptor.

In this chapter, we report a novel methodology that combines μFL and oxidative activation to patch pattern and chemically alter selective regions of hydroxyl-terminated SAMs on gold for subsequent chemoselective ligation. The μFL strategy is general and

can be used to pattern virtually any alkanethiol, forming a SAM within seconds and creating well-defined microfeatures.[32,33] For surface activation and chemoselective coupling, commercially available hydroxyl-terminated SAMs were selectively oxidized to aldehydes by mild microfluidic oxidation, which in turn react with oxyamine-containing ($RONH_2$) ligands to generate patterned ligand arrays. This method is inexpensive, rapid, reproducible, and may be utilized for a variety of biomolecular array studies and cell-based array assays. SAM formation, activation, ligand immobilization, and biospecific cell patterning are characterized by contact angle, cyclic voltammetry (CV), X-ray photoelectron spectroscopy (XPS), scanning electron microscopy (SEM), and fluorescence microscopy.

2.2 Materials and Methods

2.2.1 Materials. Fluorescent dyes and penicillin/streptomycin were obtained from Invitrogen (Carlsbad, CA), normal goat serum was purchased from Jackson ImmunoResearch Laboratories, Inc. (West Grove, PA), and fluorescence mounting media was obtained from Dako (Carpinteria, CA). All other chemicals and cell culture reagents were obtained from Sigma Aldrich (St. Louis, MO) and Fisher Scientific (Pittsburgh, PA). Swiss 3T3 albino mouse fibroblasts were obtained from the Tissue Culture Facility at the University of North Carolina at Chapel Hill (Chapel Hill, NC).

2.2.2 Syntheses. Tetra(ethylene glycol)-terminated alkanethiol (EG_4SH),[44] ferrocene-oxyamine (Fc-ONH_2),[36] and rhodamine-oxyamine (Rhod-ONH_2)[41] were synthesized as previously reported. Solid phase peptide synthesis of linear RGD-oxyamine peptide was performed as previously reported.[9]

*11-(2, 2, 2, 2-tetra(ethoxy))undecene (**7**):* To a solution of tetra(ethylene glycol) (8.35 g, 43.0 mmol, 5 eq.) was added 50% NaOH (1.2 mL, 43.0 mmol, 5 eq). The mixture was refluxed at 100 °C for 30 min until the color changed to brown, indicating deprotonation

to which 11-bromo-undecene (1.86 mL, 8.58 mmol) was added. The mixture was stirred for 24h and then extracted with hexanes (6 x 25 mL). The organic layers were combined, concentrated, and purified by flash chromatography (Hex/EtOAc: 1/1) to afford a pale yellow oil (1.45 g, 50 %). ^{1}H NMR (400 Hz, $CDCl_3$) δ 1.28-1.26 (s 12H, CH_2), 1.57-1.55 (t, 2H, J = 8.1 Hz, CH_2), 2.03-2.01 (m, 2H, J = 8.4 Hz, -CH_2CH=CH_2), 2.88 (s, 1H, OH), 3.44-3.41 (t, 2H, J = 12.4, -OCH_2), 3.65-3.63 (m, 2H, J = 7.8 Hz, CH_2), 3.60-6.57 (m, 14H, J = 12.0, -OCH_2CH_2O-), 4.99-4.89 (q, 2H; J = 40.4 Hz, CH_2=CH-), 5.80-5.78 (m, 1H, J = 7.9 Hz, -CH=CH_2).

11-(2-(2, 2, 2, 2-Methoxy-tetra(ethoxy))undecene (**8**): To a solution of **7** (1.45 g, 4.20 mmol), in THF (15 mL) at 0 °C was added sodium hydride (cat). The reaction was warmed to room temperature and stirred for 2 h to which iodomethane (0.78 mL, 12.6 mmol, 3 eq) was added. The mixture was stirred for 1 h, quenched with water, diluted with EtOAc, washed with $NH_4^+Cl^-$ (2 x 25 mL) and water (2 x 25 mL), dried over $MgSO_4$ and concentrated to afford a pale yellow oil (1.49 g, 99 %). ^{1}H NMR (400 Hz, $CDCl_3$) δ 1.29-1.26 (m, 12H, J = 12.2 Hz, CH_2), 1.58-1.56 (m, 2H, J = 7.9 Hz, CH_2), 2.05-2.03 (m, 2H, J = 8.0 Hz, -CH_2CH=CH_2), 3.39 (s, 3H, -OCH_3), 3.45-3.43 (t, 2H, J = 7.7 Hz, -OCH_2), 3.59-3.56 (m, 4H, J = 12.2 Hz, CH_2), 3.67-3.64 (m, 12H, J = 16.3 Hz, -OCH_2CH_2O-), 5.02-4.97 (q, 2H, J = 20.3 Hz, CH_2=CH-), 5.85-5.82 (m, 1H, J = 12.0 Hz, -CH=CH_2).

*11-(2-(2, 2, 2, 2-Methoxy-tetra(ethoxy))undecane-1-ethanethioic S-acid (**9**):* To a solution of **8** (1.68 g, 4.66 mmol) in dry toluene (15 mL) was added azobis(isobutyronitrile) (AIBN, cat.) and thioacetic acid (2.0 mL, 27.9 mmol, 6 eq) at 80 °C. The mixture was refluxed overnight (16 h). The reaction was the concentrated and purified by flash chromatography (EtOAc/Hex: 4:6) to afford a pale yellow oil (1.72 g, 81 %). ^{1}H NMR (400 Hz, $CDCl_3$) δ 1.27 (s, 12H, J = 12.2 Hz, CH_2), 1.58-1.57 (m, 4H, J = 5.6 Hz, CH_2), 2.33 (s, 3H, O=CCH_3), 2.89-2.86 (t, 2H, J = 12.3 Hz, -CH_2CH_2S-), 3.39 (s,

3H, -OCH_3), 3.47-3.45 (t, 2H, J = 7.7 Hz, -OCH_2), 3.58-3.56 (m, 4H, J = 8.1 Hz, CH_2), 3.67-3.64 (m, 12H, J = 16.3 Hz, -OCH_2CH_2O-).

*11-(2-(2, 2, 2, 2-Methoxy-tetra(ethoxy))undecane-1-thiol (**1**):* To a solution of **9** (1.41 g, 3.24 mmol) in MeOH (20 mL) was added concentrated HCl (6 mL). The mixture was refluxed overnight (16 h), concentrated, diluted with EtOAc, washed with $NH_4^+Cl^-$ (3 x 25 mL) and water (2 x 25 mL), dried over $MgSO_4$, and concentrated to afford a pale yellow oil (1.17 g, 92 %). ^{1}H NMR (400 Hz, $CDCl_3$) δ 1.41-1.27 (m, 14H, CH_2), 1.63-1.59 (m, 4H, J = 16.1 Hz, CH_2), 2.56-2.53 (t, 2H, J = 12.3 Hz, -CH_2CH_2S-), 3.39 (s, 3H, -OCH_3), 3.47-3.44 (t, 2H, J = 12.1 Hz, -OCH_2), 3.59-3.56 (m, 4H, J = 12.3 Hz, CH_2), 3.67-3.60 (m, 12H, J = 28.4 Hz, -OCH_2CH_2O-). (ESI) (*m/z*) [M + H^+]: 394.28.

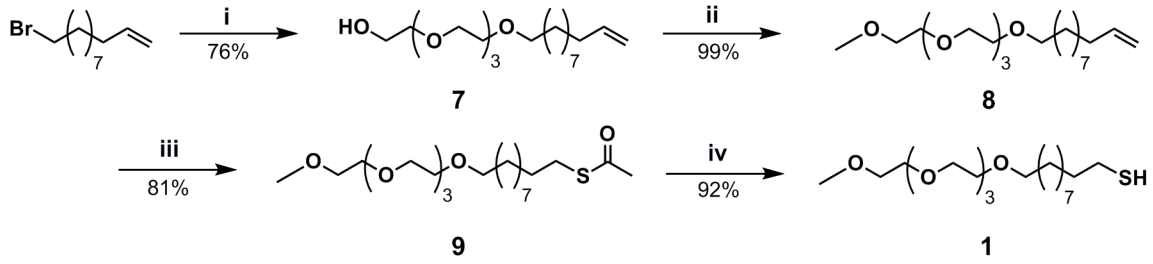

Scheme 2.1 Synthetic route to methoxy-terminated tetra(ethylene glycol) alkanethiol ($MeOEG_4SH$). Reagents and conditions. (i) Tetra(ethylene glycol) (3 eq), 50 % NaOH (3 eq), 90 °C, 24h; (ii) NaH (3 eq), 2 h, followed by methyliodide (3 eq), 30 min; (iii) thioacetic acid (6 eq), AIBN (cat.), 80 °C, 12 h; (iv) HCl, 90 °C, 12 h.

2.2.3 Microfabrication. Adobe Illustrator CS3 was used to create micropatterns, which were subsequently photo-plotted onto Mylar sheets and manufactured by Page Works (Cambridge, MA). Microfluidic cassette fabrication was carried out using soft lithography.[38,39] SU-8 50 was spin-coated onto silicon wafers (100 μm, 1500 rpm, 90 s), followed by heat curing (20 min, 90 °C). The transparency masks obtained from Page Works were then placed over the photoresist and UV light (365 nm) was irradiated, crosslinking the SU-8 patterns. The Sluggard 184 (Dow Corning) was prepared in a 3:20

curing agent:elastomer, polydimethylsiloxane (PDMS). The prepolymer was cast over the mold, degassed for 30 min, and cured for 1h at 75 °C. The PDMS was then removed from the master and access holes were made to allow fluid flow.

2.2.4 Preparation of gold-coated substrates. All thin layer metal deposition was performed using a vacuum evaporator system with a 3 kW electron beam gun (Model VE-100, Thermionics Laboratory, Inc., Port Townsend, WA). Glass slides were cleaned with Pirahna solution (**use with caution:** 1:3 (v:v) concentrated H_2SO_4 : 30 % H_2O_2) for 4 h. Substrates were then rinsed with ethanol and dried. An adhesion layer of titanium (5 nm) and a layer of gold (10-30 nm) were then thermally evaporated onto the surface. After gold evaporation, substrates were cut into pieces (2 mm^2), cleaned with ethanol, and dried before experimentation.

2.2.5 Microfluidic lithography (μFL) of SAMs. A PDMS microfluidic cassette was reversibly sealed to a bare gold surface. To pattern a SAM, a 1 mM solution of EG_4SH in ethanol was flowed through the channels for 60 s. Without removing the cassette, ethanol was flowed through the channels and suctioned to clean the surface. The substrate was then rinsed with ethanol, dried, and immersed into a 1 mM solution of methoxy-terminated alkanethiol ($MeOEG_4SH$) in ethanol for 16 h in order to backfill the remaining gold.

2.2.6 Scanning electron microscopy (SEM) characterization. After SAM patterning and backfilling, substrates were oxidized by pyridinium chlorochromate (PCC, 30 μM in ACN, 60 min). A 60 mM solution of Fc-ONH_2 in ethanol was then reacted on the surface (45°C, 20 min). Substrates were then rinsed with water and ethanol, dried, and imaged using a Hitachi S-4700 field emission scanning electron microscope (Hitachi High Technologies America, Inc., Schaumburg, Illinois).

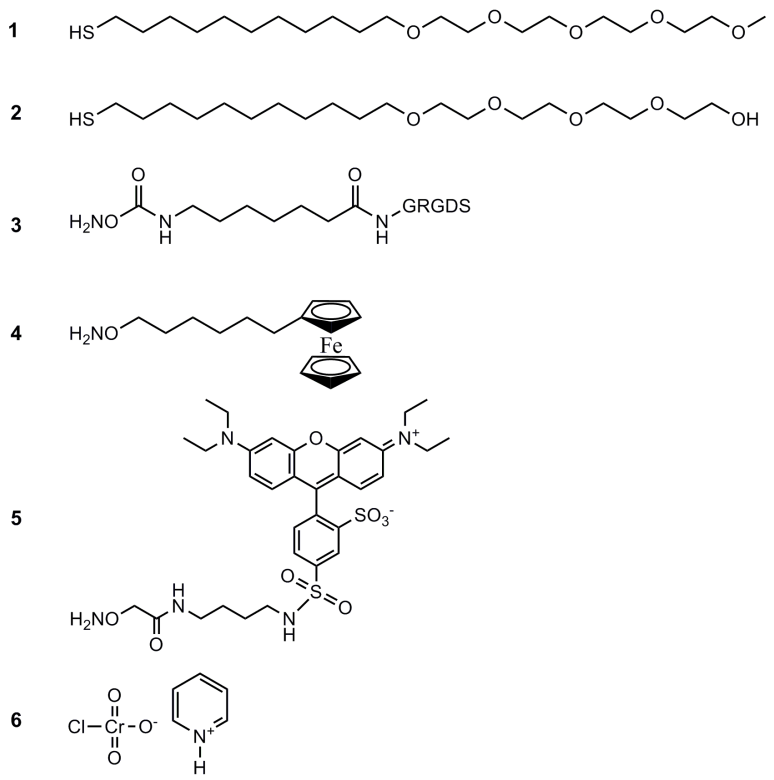

Scheme 2.2 Compounds used in this study: (1) methoxy-terminated tetra(ethylene glycol) alkanethiol ($MeOEG_4SH$); (2) tetra(ethylene glycol)-terminated alkanethiol (EG_4SH); (3) linear Arg-Gly-Asp-oxyamine (RGD-ONH_2); (4) ferrocene-oxyamine (Fc-ONH_2); (5) rhodamine-oxyamine (Rhod-ONH_2); and (6) pyridinium chlorochromate (PCC).

2.2.7 Electrochemical characterization. Fc-ONH_2 was reacted on mixed, patterned SAMs of EG_4SH and $MeOEG_4SH$ after 0 and 60 min of PCC oxidation as described above. All electrochemical experiments were performed using a Bioanalytical Systems CV-100W potentiostat. Electrochemical data was obtained in a 1 M $HClO_4$ electrolyte solution with an Ag/AgCl electrode (Bioanalytical systems) serving as the reference, the gold monolayer as the working electrode, and a Pt wire as the counter electrode. Surfaces were scanned at a rate of 100 mV/s.

2.2.8 Fluorescence microscopy. Fluorescent images were obtained on substrates prepared as described above with Rhod-ONH_2 (7 mM in H_2O, 2 h) as the immobilized ligand. The resultant patterns were imaged after ligand and SAM desorption onto scotch tape (70 °C, 20 min) by a Nikon Eclipse TE2000-E inverted microscope (Nikon USA,

Inc., Melville, NY) and a Plan Fluor 40X oil immersion objective (1.30 NA, Nikon USA). Immersion oil was purchased from Carl Zeiss MicroImaging, Inc. (Thornwood, NY) and lens paper was purchased from Fisher. Image analysis was performed using MetaMorph software (Molecular Devices, Downingtown, PA).

2.2.9 SAM array patterning. EG_4SH SAMs were patterned with μFL, as described above. After backfilling with $MeOEG_4SH$ (1 mM in EtOH, 16 h), a different microfluidic cassette was reversibly sealed to the surface, and a 30-μM solution of PCC in ACN was flowed through and left in the microchannels for 60 min. Without removing the cassette, ethanol was flowed through the channels. Then Fc-ONH_2 (SEM characterization), Rhod-ONH_2 (fluorescence imaging), or cell adhesive peptide Arg-Gly-Asp-oxyamine (RGD-ONH_2) was immobilized and characterized as mentioned previously.

2.2.10 Cell culture. Swiss Albino 3T3 mouse fibroblasts (ATCC) were cultured in Dulbecco's Modified Eagle Medium (Gibco) containing 10 % calf bovine serum and 1 % penicillin/streptomycin. With a solution of 0.05 % trypsin in 0.53 mM EDTA, cells were removed and re-suspended in serum-free medium (100,000 cells/mL). The cells were seeded to surfaces for 2 h, and after 2 h, serum-containing media was added for cell growth.

2.2.11 Cell patterning and staining. After SAM patterning and backfilling, substrates were oxidized by PCC (30 μM in ACN, 2 min). A 20-μM solution of RGD-ONH_2 in water was then reacted on the surface (3 h). Substrates were then rinsed with water and ethanol, dried, and imaged. After cell culturing, cells were seeded to surfaces for 2 h, after which serum-containing media was added for cell growth. The patterned cells were fixed with formaldehyde (3.2 % in PBS) and then permeated (PBS containing 0.1 % Triton X–100). A fluorescent dye mixture, containing phalloidin-TRITC (actin) and DAPI (nucleus) was then made in PBS containing 5 % normal goat serum and 0.1 % Triton X

–100. Cells were incubated with the dye solution for 2 h. The substrates were then secured gold-coated side down in fluorescence mounting medium (Dako, Carpinteria, CA, USA), which enhances the visualization of cells when viewed under a fluorescent microscope, on a glass coverslip.

2.2.12 Contact angle measurement. The static contact angle of bare gold and SAMs of EG_4SH, $MeOEH_4SH$, and aldehyde-terminated EG_4SH (oxidation of EG_4SH with 30 μM in ACN, 60 min) were calculated using 10 μL drops of deionized H_2O and a KSV CAM 200 instrument and software.

2.2.13 X-Ray Photoelectron Spectroscopy (XPS). Fc-ONH_2 was reacted with mixed, patterned SAMs of EG_4SH and $MeOEG_4SH$ 0 and 60 min after PCC oxidation as previously described. XPS measurements were preformed on these surfaces with a Kratos Axis Ultra DLD. A mono Al anode source was used with a specific excitation energy of 1486.6 eV and a 80 eV pass energy was used for the high-resolution scans. All binding energies are reference to the C 1s of a saturated hydrocarbon at 284.7 eV.

2.3 Results and Discussion

2.3.1 Microfluidic platform design. To generate tailored surfaces for studies of biospecific interactions, SAMs of terta(ethylene glycol)-terminated (EG_4SH, **2**) and methoxy-terminated tetra(ethylene glycol) ($MeOEG_4SH$, **1**) (Scheme 2.1) alkanethiolates were used in patterning. Both molecules are known to prevent nonspecific protein adsorption and cell attachment.[12-14] Importantly, SAMs of EG_4SH present terminal hydroxyl groups, which are capable of being oxidized to aldehydes for subsequent ligation by the mild oxidative reagent, pyridinium chlorochromate (PCC, **6**). $MeOEG_4SH$ SAMs present terminal methoxy groups, which cannot be oxidized under the same conditions. These properties serve as the key criteria for developing a strategy to generate chemoselective, patterned SAMs by μFL and oxidative activation (Figure 2.1).

To spatially control SAM formation, poly(dimethylsiloxane) (PDMS) microfluidic cassettes were created using standard soft lithography techniques.[38,39] A PDMS cassette was placed on a gold surface, and a 1-mM solution of EG_4SH in ethanol (EtOH) is flowed through the channels for 60 s, rapidly forming a SAM. The microfluidic cassette was then removed, and the remaining bare gold regions backfilled with $MeOEG_4SH$ (1 mM in EtOH, 16 h). To activate the EG_4SH surface selectively for ligand immobilization, the terminal alcohol groups were oxidized with a 30 μM-solution of PCC in acetonitrile (60 min) to produce aldehydes.[37] The newly formed aldehydes react chemoselectively with oxyamine-containing ($RONH_2$) molecules to generate a stable interfacial, covalent oxime linkage. This results in a ligand-pattern that replicates the 2D features of the microchannels.

2.3.2 Surface characterization of platform design. To verify terminal hydroxyl group conversion to aldehydes from EG_4SH SAMs, electroactive ferrocene-oxyamine (Fc-ONH_2, **4**) was immobilized to oxidized, mixed EG_4SH and $MeOEG_4SH$ (1:1) SAMs. After 60 min of PCC oxidation and reaction with Fc-ONH_2 (60 mM in EtOH, 10 min, 40 °C), cyclic voltammetry (CV) was performed. Distinct oxidation and reduction signals at 230 mV and 210 mV, respectively, were observed from the CVs, demonstrating that Fc-ONH_2 immobilization (Figure 2.2A) had occurred. The density of the ferrocene ligand bound after 60 min of PCC oxidation, was calculated by using the classic equation, $Q = nFA\Gamma$, where Q is total charge, n is moles of electron, F is Faraday's constant, A is area of the SAM electrode, and Γ is density of electroactive molecule. Complete immobilization (~100 %) was then determined to occur at 60 min, taking into account that only 50 % of the surface area was able to produce aldehydes.[36] As a control, Fc-ONH_2 was also reacted using the same conditions with unoxidized mixed SAMs, and no peak current was observed by CV. Similarly, XPS was conducted on mixed SAMs presenting

EG_4SH and $MeOEG_4SH$ before and after 60 min of reaction with PCC, followed by Fc-ONH_2 immobilization (Figure 2.3). Surfaces were scanned for nitrogen content. As shown, no signal was observed before SAM activation. However, the characteristic 1s nitrogen peak found at 398 eV, corresponding to bound Fc-ONH_2 was present on substrates subject to oxidation.

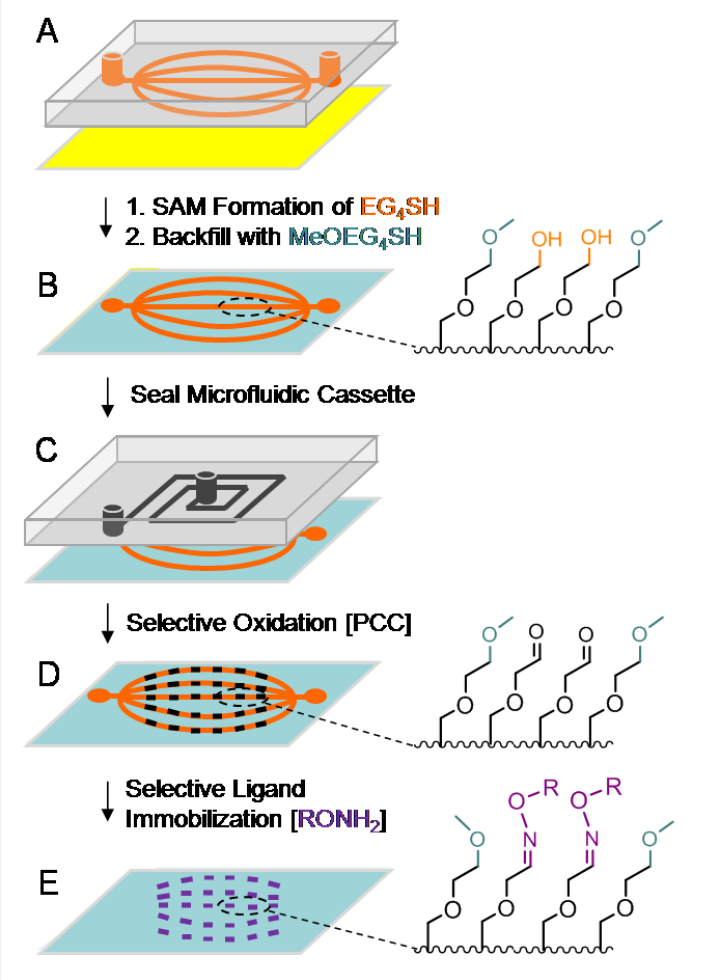

Figure 2.1 Schematic for the microfluidic generation and oxidative activation of patterned self assembled monolayers for chemoselective ligand immobilization. (A) A layer of titanium and gold were deposited onto a glass slide. (B) A PDMS microfluidic cassette was reversibly sealed to a gold substrate. (C) Microfluidic lithography (μFL) was used to rapidly pattern a SAM of tetra(ethylene glycol)-terminated alkanethiol (EG_4SH). (D) The remaining bare gold regions were then backfilled with methoxy-terminated tetra(ethylene glycol) alkanethiol ($MeOEG_4SH$). (E) The entire substrate was exposed to pyridinium chlorochromate (PCC) a mild oxidizing agent. Only regions presenting EG_4SH possessed terminal hydroxyl groups, subject to selective oxidation to aldehyde groups. The aldehydes react rapidly and chemoselectively with an oxyamine-containing ligand ($RONH_2$), resulting in a 2D-projection of tailored ligands corresponding to the original patterned microfeatures.

Static contact angle measurements of water on bare gold and various monolayers were conducted to further show that $MeOEG_4SH$ surfaces were insensitive and unreactive to PCC oxidation. The data confirmed that SAMs of EG_4SH are uniformly more hydrophilic than SAMs of $MeOEG_4SH$ (Figure 2.2B). PCC oxidation was performed on both monolayers and contact angles were compared. For EG_4SH SAMs, the angle increased from 33.7° to 45.2°, indicating aldehyde conversion. However, little to no change was observed on activated $MeOEG_4SH$ surfaces.

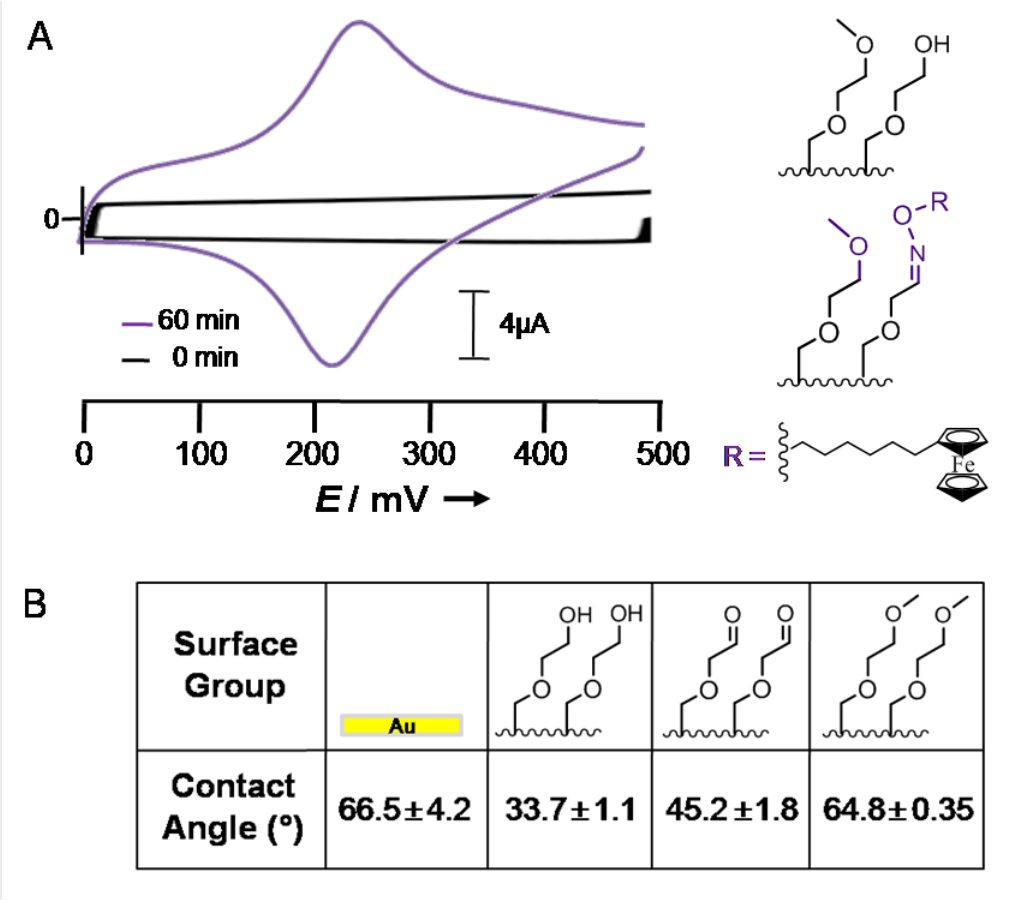

Figure 2.2 Electrochemical and contact angle characterization of EG_4SH and $MeOEG_4SH$ SAMs on gold. (A) Cyclic voltammograms (CVs) representing 0 min (black) and 60 min (purple) of oxidation with PCC on patterned EG_4SH surfaces, followed by ferrocence-oxyamine ($Fc\text{-}ONH_2$) immobilization. Ligand immobilization does not occur prior to surface oxidation, as shown by the lack of peak current in the black trace. The distinctive oxidation and reduction signals at 210 and 230 mV, respectively, displayed in the purple trace, correspond to the presence of immobilized $Fc\text{-}ONH_2$. (B) Contact angle data of SAM modifications on gold. EG_4SH tail groups are more hydrophilic than both aldehyde-terminated SAMs (formed from EG_4SH after oxidation) and $MeOEG_4SH$ SAMs.

A series of studies were performed to determine the fidelity of patterning, versatility of ligand immobilization, and to investigate whether this strategy could be extended to include biospecific ligand-mediated cell patterning. The scanning electron micrograph (SEM) in figure 2.4A indicates that line broadening did not occur, as the channel width of the micropatterned SAM replicates that of the original cassette (100 μm). A strong contrast of bound Fc-ONH_2 against $MeOEG_4SH$ background was also observed via SEM characterization. Similarly, rhodamine-oxyamine (Rhod-ONH_2, **5**) was successfully immobilized (7 mM in H_2O, 2 h) to an activated SAM and imaged by fluorescence microscopy (Figure 2.4B).

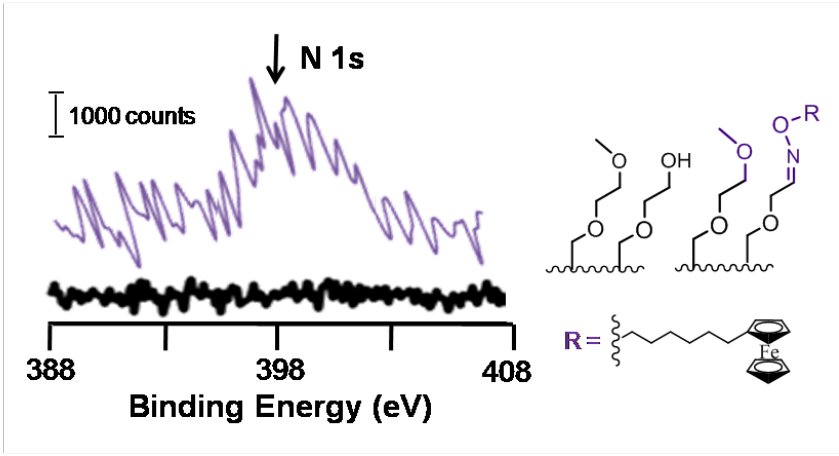

Figure 2.3. X-ray photoelectron spectroscopy (XPS) characterization of mixed EG_4SH and $MeOEG_4SH$ SAMs reacted with Fc-ONH_2 before (black) and after (purple) oxidation with PCC. Ligand immobilization does not occur prior to surface oxidation with PCC, as shown by the lack of nitrogen signal in the black trace. During oxidation, the alcohol group in EG_4SH is converted to an aldehyde, which then chemoselectively reacts with oxyamine-containing ligands ($RONH_2$). The 1s nitrogen peak found at 398 eV, corresponds to the presence of ferrocene-oxyamine immobilized to the surface, as displayed in the purple trace.

2.3.3 Biospecific cell adhesion studies. For biospecific cell adhesion studies, mixed patterned SAMs of EG_4SH and $MeOEG_4SH$ were shown to be inert to non-specific cell attachment. These substrates were oxidized by PCC (30 μM in ACN, 2 min), resulting in a low percentage of aldehyde conversion (< 5 % determined by electrochemistry). The cell adhesive peptide, Arg-Gly-Asp-oxyamine (RGD-ONH_2, **3**, 20 mM in H_2O, 3 h), was

then reacted with the newly generated aldehyde groups. The RGD peptide ligand is derived from the extracellular matrix protein, fibronectin, and is known to facilitate biospecific cell adhesion via cell-surface integrin receptors.[20] Swiss Albino 3T3 mouse fibroblasts were then seeded to surfaces presenting RGD and cultured for 4 days. As shown in figure 2.4C and 2.4D, fluorescent images of stained actin (phalloidin-TRITC) and nuclei (DAPI) show patterned fibroblasts that were confined to regions containing RGD. The ability to generate spatially controlled and biospecific ligand surfaces indicates that this general tandem microfluidic and surface activation strategy may be of broad utility for a range of biotechnological and cell adhesion and migration assays.

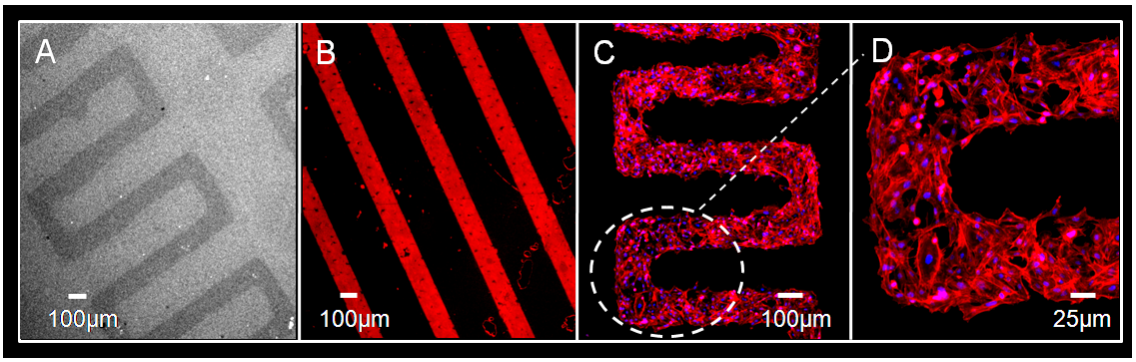

Figure 2.4 Images depicting the broad use of microfluidics to generate chemoselective patterned SAMs on gold. All surfaces were patterned with EG_4SH using μFL, followed by backfilling with $MeOEG_4SH$, oxidation of EG_4SH to aldehydes with PCC, and reaction with an oxyamine-tethered ligand. (A) A scanning electron micrograph of a patterned $EG_4SH/MeOEG_4SH$ and activated aldehyde-EG_4SH SAM presenting Fc-ONH_2. (B) A fluorescent image displaying bound rhodamine-oxyamine (Rhod-ONH_2). (C) A fluorescent micrograph showing the biospecific patterning of Swiss Albino 3T3 mouse fibroblasts on a patterned surface presenting a cell adhesive peptide, linear Arg-Gly-Asp-oxyamine (RGD-ONH_2). Cells were visualized by staining for actin (phalloidin, red) and nuclei (DAPI, blue). (D) A higher magnification of patterned cells on an activated EG_4SH and cell adhesive peptide immobilized SAM.

2.3.4 Microfluidic array patterning methodology and surface characterization. With this patterning surface chemistry strategy, we aimed to create chemoselective microarrays by activating discrete regions of EG_4SH SAMs. These complex substrates were generated by simply adding one step to the previously described patterning protocol (Figure 2.5). μFL was first performed to create a patterned SAM of EG_4SH on

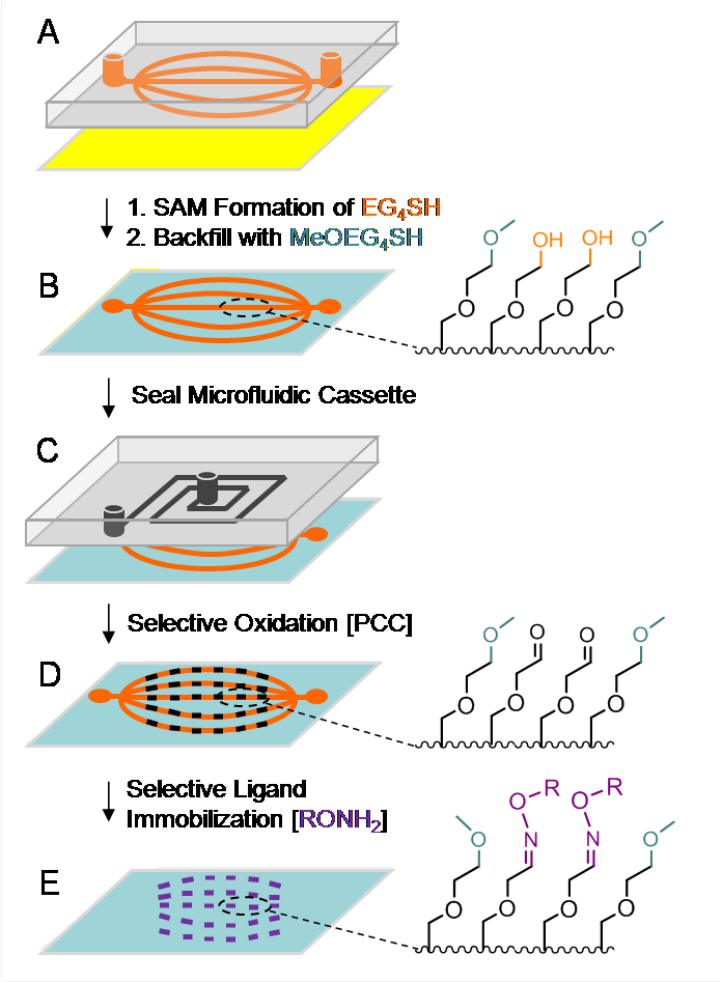

Figure 2.5 Schematic for the generation of aldehyde patch patterned arrays from EG4SH/MeOEG$_4$SH SAM surfaces by using μFL and microfluidic oxidative activation. (A) A PDMS microfluidic cassette was reversibly sealed to a gold surface. (B) A SAM of EG$_4$SH was patterned by μFL, and the substrate was then backfilled with MeOEG$_4$SH. (C) A second microfluidic cassette was then placed on the surface. (D) To generate a chemoselective, SAM microarray, the mild oxidant PCC was flowed through the channels forming aldehyde tail groups only in the regions presenting EG$_4$SH. After oxidation, three terminal functionalities are present on the surface: hydroxyl, methoxy, and aldehyde. (E) An oxyamine-containing ligand (RONH$_2$) was then reacted, chemoselectively to the patterned aldehyde groups resulting in a biospecific patterned ligand array.

gold, and the substrate was again backfilled with a solution of MeOEG$_4$SH. Rather than oxidizing the entire surface to convert all alcohol groups to aldehydes, a second PDMS microfluidic cassette was reversibly sealed to the substrate, PCC was flowed through the microchannels (30 μM in ACN, 60 min), and oxidation was performed on the selective EG$_4$SH-containing areas where the two patterns intersected. To demonstrate this patch pattern strategy with a specific example, a PDMS cassette with a globe pattern with

longitudinal stripe microfeatures was used to pattern a SAM of EG_4SH by μFL. After backfilling with $MeOEG_4SH$, a microfluidic cassette with a square spiral-shaped microfeature was placed on the surface. After mild PCC activation, three different functionalities were presented on the inert substrate: hydroxyl, methoxy, and aldehydes. The aldehyde groups were patterned by the simple overlapping of the square spiral and globe designs. Because alcohol and methoxy groups do not react with oxyamines, immobilization of oxyamine-containing ligands only occur to the patterned aldehyde regions, thereby resulting in an aldehyde microarray.

SEM and fluorescence microscopy were used to characterize the generation of patch-patterned microarrays, after Fc-ONH_2 and Rhod-ONH_2 were immobilized to the activated substrates (Figure 2.6A and 2.6B, respectively). Ligands conjugated only to the overlapping patterned areas, revealing a ligand microarray. Shown in figure 2.6A, the same bar-pattern was used to create a square-shaped microarray (100 x 100 μm). Likewise, Rhod-ONH_2 is displayed in a rectangular microarray, having used two different cassettes containing bar-patterns (200 x 300 μm). Other geometrical feature microarrays can be generated by using correctly aligned and registered PDMS microfluidic cassettes (data not shown).

2.3.5 Biospecific ligand and cell arrays for adhesion studies. By employing this strategy, biospecific ligand microarrays presenting RGD-ONH_2 were also created. Fibroblasts were seeded to these substrates and cultured for 3 days before staining and imaging. As shown in figure 2.6C, cells only adhered to regions selectively activated by microfluidic oxidation. The resulting square-microarray (300 x 300 μm) presented healthy cells, spread out along the border of intersecting patterns. This novel tandem patterning method is inexpensive, flexible, and rapid in creating chemoselective, biospecific surfaces for potential use in several biotechnology and cell based array platforms. Soft

lithography enables versatile PDMS cassette design, lending to numerous possibilities in creating different shapes and dimensions of microarrays.

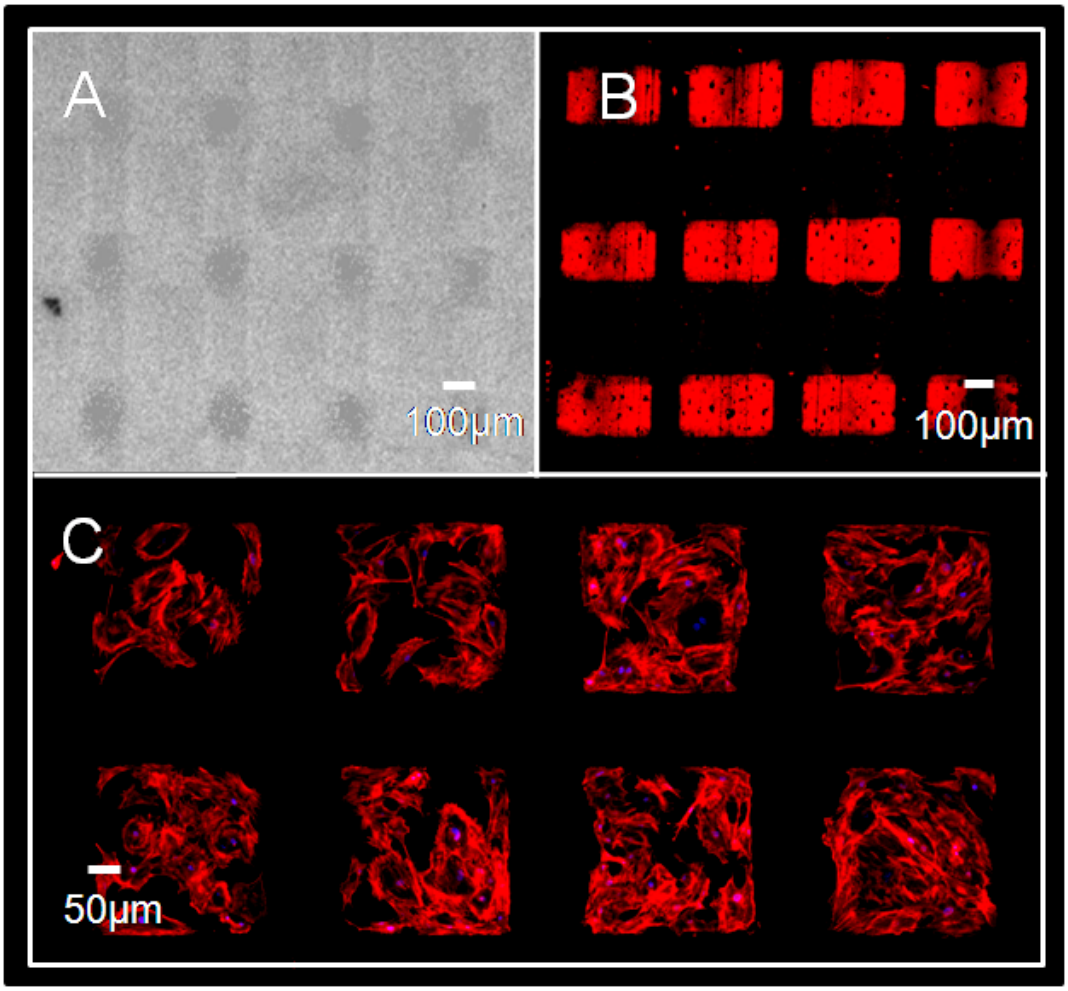

Figure 2.6 Images displaying chemoselective, patch array-patterned SAMs, generated by microfluidics. EG_4SH SAMs were patterned using μFL, followed by backfilling with $MeOEG_4SH$ and selective activation of EG_4SH by microfluidic oxidation with PCC. The newly formed aldehyde groups were then reacted with a number of oxyamine-containing ligands, resulting in a microarray. (A) A scanning electron micrograph showing a microarray of bound Fc-ONH_2 to activated SAMs. (B) A fluorescent image displaying microfeatures of immobilized Rhod-ONH_2. (C) A biospecific microarray of Swiss Albino 3T3 mouse fibroblasts bound to the cell adhesive peptide, linear RGD-ONH_2. Cells were visualized by staining for actin (phalloidin, red) and nuclei (DAPI, blue).

In summary, we have combined the use of μFL and microfluidic oxidative activation to pattern and chemically alter selective regions of SAMs in tandem on gold for subsequent chemoselective ligand immobilization. We demonstrated that PCC, a mild

oxidant, could be used to convert hydroxyl-terminated SAMs to aldehydes for subsequent ligation of a variety of oxyamine-containing molecules. This strategy is compatible with cell culture, and was employed to create a biospecific ligand platform for peptide-mediated cell adhesion arrays. By using a number of different ligands and characterization tools, we showed that the generation of both cell patterning and ligand microarray patterning is routine with this strategy.

2.4 Conclusion

Microfluidics can be used to form SAMs of alkanethiols rapidly and with precise spatial control and provide a method for SAM activation in tailoring chemoselective and biospecific surfaces. By varying microchannel widths and spacing, PDMS cassettes can be designed to create microarrays with almost any customized dimensions. Multiple channels with separate inlets and outlets can also be fabricated, allowing the delivery of multiple biomolecules to the surface for reaction with activated SAMs. Future studies utilizing this microarray technique include the precise delivery of various biomolecules, such as peptides, carbohydrates, DNA, or metabolites by microfluidics to a single surface in arrays for various high-throughput biotechnology applications in proteomics, glycomics, and transcriptomics. As an added feature, this method can be extended to incorporate a number of functionalized alkanethiols for multiple chemoselective coupling strategies. In combination with oxime conjugation, a differently functionalized SAM (e.g., Click chemistry with azide or alkyne presenting SAMs) would enable access to two orthogonal immobilization methods, widening the range of commercially available bioligands for study. This platform enables flexible, precise patterning of a broad range of biomolecules on tailored surface arrays that originated from a simple hydroxyl-terminated surface, and promises wide applicability to cell biology, surface chemistry, and biomedical engineering applications.

References

(1) Manos, P.; Pancrazio, J. J.; Coulombe, M. G.; Ma, W.; Stenger, D. A. *Neurosci. Lett.*, **1999**, *271*, 179-183.

(2) Lahann, J.; Balcells, M.; Rodon, T.; Lee, J.; Choi, I. S.; Jensen, K. F.; Langer, R. *Langmuir*, **2002**, *18*, 3632-3638.

(3) Yamato, M.; Konno, C.; Ustumi, M.; Kikuchi, A.; Okano, T. *Biomaterials*, **2002**, *23*, 561-567.

(4) Kwon, Y.; Han, Z.; Karatan, E.; Mrksich, M.; Kay, B. K. *Anal. Chem.*, **2004**, *76*, 5713-5720.

(5) Ramsey, G. *Nat. Biotechnol.*, **1998**, *16*, 40-44.

(6) Arenkov, P.; Kukhtin, A.; Gemmell, A.; Voloshchuk, S.; Mirzbekov, A. *Anal. Biochem.*, **2000**, *278*, 123-131.

(7) Langer, R.; Tirrell, D. A. *Nature*, **2004**, *428*, 487-492.

(8) Jung, D. P.; Kapur, R.; Adams, T.; Giuliano, T. A.; Mrksich, M.; Craighead, H. G.; Taylor, D. L. Crit. Rev. Biotechnol. **2001**, *21*, 111-132.

(9) Hoover, D. K.; Chan, E. W. L.; Yousaf, M. N. *J. Am. Chem. Soc.,* **2008**, *130*, 3280-3281.

(10) Jiang, X.; Bruzewicz, D. A.; Wong, A. P.; Piel, M.; Whitesides, G. M. *Proc. Nat. Acad. Sci. U.S.A.*, **2005**, *102*, 975-978.

(11) Yousaf, M. N.; Houseman, B. T.; Mrksich, M. *Angew. Chem. Int. Ed.*, **2001**, *40*, 1093-1096.

(12) Harder, P.; Grunze, M.; Dahint, R.; Whitesides, G. M.; Laibinis, P. E. *J. Phys. Chem. B*, **1998**, *102*, 426-236.

(13) Kreuzer, H. J.; Wang, R. L. C.; Grunze, M. *J. Am. Chem. Soc.*, **2003**, *125*, 8384-8389.

(14) Ostuni, E.; Chapman, R. C.; Liang, M. N.; Meluleni, G.; Pier, G.; Ingber, D. E.; Whitesides, G. M. *Langmuir*, **2001**, *17*, 6336-6343.

(15) Lahiri, J.; Ostuni, E.; Whitesides, G. M. *Langmuir*, **1999**, *15*, 2055-2060.

(16) Xia, Y.; Whitesides, G. M. *Langmuir*, **1997**, *13*, 2059-2067.

(17) Chan, E. W. L.; Yousaf, M. N. *Mol. BioSys.,* **2008**, *4*, 746-753.

(18) Ballav, N.; Schilp, S.; Zharnikov, M. *Angew. Chem. Int. Ed.,* **2008**, *47*, 1421-1424.

(19) Steenackers, M.; Kuller, A.; Ballav, N.; Zharnikov, M.; Grunze, M.; Jordan, R. *Small*, **2007**, *10*, 1764-1773.

(20) Klauser, R.; Huang, M. L.; Wang, S. C.; Chen, C. H.; Chaung, T. J.; Terfort, A.; Zharnikov, M. *Langmuir*, **2004**, *20*, 2053-2058.

(21) Hong, S.; Zhu, J.; Mirkin, C. A. *Science*, **1999**, *286*, 661-663.

(22) Eck, W.; Stadler, V.; Geyer, W.; Zharnikov, M.; Golzhauser, A.; Grunze, M. *Adv. Mater.*, **2000**, *12*, 805-809.

(23) Lawton, R. A.; Price, C. R.; Runge, C. R.; Doherty III, W. J.; Saavedra, S. S. *Colloids Surf., A*, **2004**, *253*, 213-215.

(24) Bowden, N.; Terfort, A.; Carbeck, J.; Whitesides, G. M. *Science*, **1997**, *276*, 233-235.

(25) Lee, K.-B.; Kim, D. J.; Lee, Z.-W.; Woo, S. I.; Choi, S. I. *Langmuir*, **2004**, *20*, 2531-2535.

(26) Norris, J. V.; Manning, K.; Linke, S. J.; Ferrance, J. P.; Landers, J. P.; *J. Foren. Sci.*, **2006**, *52*, 800-805.

(27) Caglar, P.; Tunce, S. A.; Malcik, N.; Landers, J. P.; Ferrance, J. P. *Anal. Bioanal. Chem.*, **2006**, *386,* 1303-1312.

(28) Yue, G. E.; Roper, M. G.; Balchunas, C.; Pulsipher, A.; Coon, J. J.; Shabanowitz, J.; Hunt, D. F.; Landers, J. P.; Ferrance, J. P. *Anal. Chim. Acta*, **2006**, *564*, 116-122.

(29) Moxom, J.; Reilly, P. T. A.; Whitten, W. B.; Ramsey, J. M. *Anal. Chem.*, **2003**, *75,* 3739-3743.

(30) Pau, S.; Whitten, W. B.; Ramsey, J. M. *Anal. Chem.*, **2007**, *79*, 68-57.

(31) Tierno, P.; Reddy, S. V.; Roper, M. G.; Jofansen, T. H.; Fischer, T. M. *J. Phys. Chem. B,* **2008**, *112*, 3833-3837.

(32) Lamb, B. M.; Westcott, N. P.; Yousaf, M. N. *ChemBioChem*, **2008**, *9*, 2628-2632.

(33) Lamb, B. M.; Barrett, D. G.; Westcott, N. P.; Yousaf, M. N. *Langmuir*, **2008**, *24*, 8885-8889.

(34) Westcott, N.P.; Yousaf, M.N. *Langmuir,* **2008**, *24*, 2261-2265.

(35) Hindler, S. J.; Connell, S. D.; Davis, M. C.; Roberts, C. J.; Tendler, S. J.; Williams, P. W. *Langmuir*, **2002**, *18*, 3151-3158.

(36) Westcott, N. P.; Pulsipher, A.; Lamb, B. M.; Yousaf, M. N. *Langmuir*, **2008**, *24*, 9237-9240.

(37) Pulsipher, A.; Westcott, N. P.; Luo, W.; Yousaf, M. N. *JACS 2009, 131, 7626-7632.*

(38) Xia, Y.; Whitesides, G. M. *Annu. Rev. Mater. Sci.*, **1998**, *28*, 153-184.

(39) Weibel, D. G.; DiLuzo, W. R.; Whitesides, G. M. *Nat. Reviews*, **2007**, *5*, 209-218.

(40) Pierschbacher, M. D.; Ruoslahti, E. *Nature*, **1984**, *309*, 30-33.

(41) Chan, E. W. L.; Yousaf, M. N. *J. Am. Chem. Soc.*, **2006**, *128*, 15542-15546.

(42) Chan, E. W. L.; Park, S.; Yousaf, M. N. *Angew. Chem. Int. Ed.* **2008**, *47*, 6267-6271.

(43) Chan, E.W.L.; Yousaf, M. N. *Angew. Chem. Int. Ed.* **2007**, *46*, 3881-3884.

(44) Pale-Grosdemange, C.; Simon, E. S.; Prime, K. L.; Whitesides, G. M. *J. Am. Chem. Soc.* **1991**, *113*, 12-20.

CHAPTER 3

Two Chemoselective Surface Chemistries via Microfluidic Oxidation: Cell Adhesion Studies on Indium Tin Oxide

3.1 Introduction

Tailoring the surface chemistry of materials to spatially control the immobilization of ligands and cells has proven to be important for a variety of basic research and biotechnological applications, ranging from molecular electronics to the design of biomaterials and drug-delivery vectors.[1-6] Self-assembled monolayers (SAMs) that are generated on a solid support represent an optimal system that can be synthetically functionalized and patterned to manipulate and study biointerfacial interactions.[7-11] To date, SAMs of alkanethiols on gold and siloxanes on glass are the most well-studied surface systems and have revolutionized SAM utilization as research tools for microarrays, biological model systems, and biosensors.[12,13] SAMs on gold are amenable to many surface-tailoring chemistry methods, and as a result, a number of thiol-containing ligands have been synthesized for various chemoselective strategies.[14,15] A significant advantage of gold is its inherent conductivity, which allows the use of routine surface spectroscopy characterization techniques to analyze surface properties and associations.[16,17] However, a number of limitations prevent the use of gold for cell biological applications. First, gold efficiently quenches fluorophore-tagged proteins and is therefore, incompatible with high-resolution live-cell fluorescence microscopy to study cell behavior in real time. Second, the relatively short lifetime of the monolayer, owing to

the weak gold–thiol bond, is unstable upon long-term exposure to ambient conditions or high temperatures.[18,19] To circumvent these problems, monolayers of siloxanes on glass have been intensely studied and utilized for cell-based assays and biosensor applications.[20,21] Not only has glass been shown to be robust, its optical transparency allows for the unimpeded observation of fluorescence.[22] However, synthetic strategies to tailor glass surfaces may prove difficult, laborious, and expensive, and characterization techniques are limited due to the lack of conductivity.

We believe indium tin oxide (ITO) combines the advantages of gold and glass. To date, ITO surfaces have been widely used in optoelectronic applications, such as organic light-emitting diodes (OLEDs), solar cells, and antistatic coatings, due to the low electrical resistance, conductive properties, and high optical transparency of ITO.[23-25] Although ITO offers attractive properties to serve as an ideal substrate for the characterization, immobilization, and control of ligands and biomolecules, tailoring the surface is difficult due to the required syntheses of molecules that are tethered with siloxane or phosphonate ligands.[26,27] Furthermore, the stability and conditions to generate a variety of SAMs are not well understood. Thus, few immobilization strategies exist to tailor ITO surfaces and a simple method to pattern ligands is not currently available.[27]

Carbonyl chemistry has proven useful on gold and glass SAMs as a chemoselective strategy for ligand immobilization. An aldehyde or ketone group on the surface reacts chemoselectively with multiple functional groups, such as amines, oxyamines, and hydrazines.[28-32] Because of the chemical versatility in the conjugation to carbonyls, it would be advantageous to design the most facile synthetic route or strategy to display a ketone or aldehyde on a surface. Generating aldehyde- or ketone-presenting SAMs on ITO requires the direct synthesis of an aldehyde- or ketone-terminated phosphonate

molecule, which has thus far not been achieved. Furthermore some terminal groups may not be compatible with siloxane or phosphonate groups, therefore rendering it impossible to generate SAMs directly. Another possible route to carbonyl chemistry on ITO surfaces is the selective conversion of a pre-installed primary-alcohol-terminated SAM to an aldehyde. This on-chip activation strategy to selectively generate aldehydes in patterns on an ITO surface would be advantageous for numerous applications in materials science and biotechnology. We have recently explored this aldehyde activation strategy on gold SAM surfaces.[9] Extending it to ITO substrates would allow a simple and expedient chemoselective immobilization methodology to tailor ITO surfaces with a variety of ligands with spatial control.

In this chapter, we report a rapid and inexpensive method to activate and generate spatially controlled aldehyde- and carboxylic acid-functionalized SAMs on ITO using microfluidic oxidation from hydroxyl-terminated SAMs on ITO. This system allows for ligand immobilization by two orthogonal strategies originating from an initial hydroxyl-terminated alkanephosphonate. Microfluidic patterning provides spatial control of the aldehydes and carboxylic acids formed by oxidation directly on the surface. Through chemoselective conjugation of oxyamine-containing ligands to aldehydes (to generate oximes) and of amine-containing ligands to carboxylic acids (to generate amides), a variety of electroactive and fluorescent molecules were immobilized. Because of the advantageous optical transparency of ITO, we are able to utilize *live-cell* high-resolution fluorescence microscopy to image fluorescent ligands and cells directly on the surface, which is not possible with the gold-SAM system. The resulting oxime and amide linkages were characterized by electrochemistry, X-ray photoelectron spectroscopy (XPS), fluorescence microscopy, contact angle and atomic force microscopy (AFM).

3.2 Materials and Methods

3.2.1 Materials. Fluorescent dyes and penicillin/streptomycin were obtained from Invitrogen (Carlsbad, CA), normal goat serum was purchased from Jackson ImmunoResearch Laboratories, Inc. (West Grove, PA), and fluorescence mounting media was obtained from Dako (Carpinteria, CA). All other chemicals and cell culture reagents were obtained from Sigma Aldrich (St. Louis, MO) and Fisher Scientific (Pittsburgh, PA). Indium tin oxide slides were purchased from Nanocs (NY, USA). Swiss Albino 3T3 mouse fibroblasts were obtained from the Tissue Culture Facility at the University of North Carolina at Chapel Hill (Chapel Hill, NC).

3.2.2 Syntheses. Ferrocene-oxyamine (**2**) was synthesized as previously reported.[9] Cell adhesive peptide, Ser-Ser-Asp-Gly-Arg-Gly-oxyamine (SSDGRG-oxyamine), was synthesized by solid-phase peptide synthesis as previously reported.[5]

*2-(11-bromoundecyloxy) tetrahydro-2H-pyran (**3**).* To a solution of **2** (4.00 g, 15.9 mmol) in THF (40 mL) was added dihydropuran (6.54 mL, 71.1 mmol) and HCl (3 drops). The reaction was stirred under inert atmosphere (N_2) for 12h and was then washed with sodium bicarbonate (3 x 25 mL) and brine (1 x 25 mL). The mixture was purified by flash chromatography (9:1 Hex:EtOAc) and concentrated to afford a colorless oil **3** (4.84 g, 91 %). ^{1}H NMR (400 Hz, $CDCl_3$) δ 4.58 (t, 1H, J = 8.1 Hz, -CH-), 3.86-3.75 (m, 2H, J = 7.9 Hz, -CH_2-), 3.52 (m, 1H, J = 8.1 Hz, -CH-), 3.41-3.38 (m, 3H, J = 7.7 Hz, -CH-, -CH_2-), 1.87-1.84 (m, 3H, J = 7.6 Hz, -CH-, -CH_2-), 1.58 (m, 1H, J = 8.4 Hz, -CH-), 1.55 (m, 6H, J = 7.6 Hz, -CH_2-), 1.43-1.40 (m, 2H, J = 7.7 Hz, -CH_2-), and 1.29 (m, 12H, J = 7.6 Hz, -CH_2-).

*diethyl 11-(tetrahydro-2H-pyran-2-yloxy)undecylphosphonate (**4**).* To a solution of **3** (3.24 g, 9.66 mmol) in neat triethylphosphite (9.85 mL, 53.1 mmol) was refluxed at 110 °C under inert atmosphere (N_2) for 12 h. The mixture was concentrated and purified by

flash chromatography Hex/EtOAc (1:1), eluted **3** with 100 % MeOH to afford a colorless oil **4** (2.98 g, 74 %). ^{1}H NMR (400 Hz, $CDCl_3$) δ 4.57 (t, 1H, J = 7.2 Hz, -CH-), 3.83-3.81, (q, 4H, J = 9.1 Hz, -CH_2-), 3.72-3.68 (m, 2H, J = 16. 4, -CH_2-), 3.48-3.39 (m, 2H, J = 7.7 Hz, -CH_2-), 1.81 (m, 1H, J = 9.2 Hz, -CH-), 1.68-1.59 (m, 3H, J = 8.3 Hz, -CH-, -CH_2-), 1.53-1.52 (m, 7H, J = 11.9 Hz, J = 7.8, -CH-, -CH_2-), and 1.32-1.30 (m, 18H, J = 7.7 Hz, -CH_2-, -CH_3).

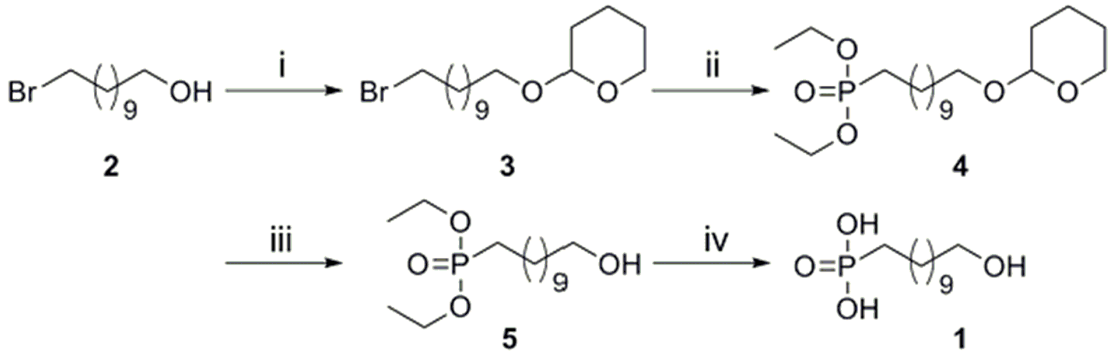

Scheme 3.1 Synthesis of 11-hydroxyundecylphosphonic acid. Reagents and conditions: (i) dihydropuran, HCl, THF, rt, 12 h, 91 %; (ii) triethylphosphite, 110°C, 12 h, 74 %; (iii) 3:1:1 AcOH:THF:H_2O, rt, 16 h, 61 %; (iv) bromotrimethylsilane, DCM, rt, 6 h, 93 %.

*diethyl 11-hydroxyundecylphosphonate (**5**).* To solution of acetic acid, water, and THF (3:1:1, 40 mL total) was added **4** (0.800 g, 2.00 mmol). The mixture was stirred under inert atmosphere (N_2) for 16 h. After completion, the mixture was concentrated, diluted with EtOAc, and washed with 0.01 M NaOH (3 x 25 mL) to afford a colorless oil **5** (0.379 g, 61 %). ^{1}H NMR (400 Hz, $CDCl_3$) δ 4.09-4.05 (q, 4H, J = 9.6 Hz, -CH_2-), 3.62-3.59 (t, 2H, J = 7.9 Hz, -CH_2-), 2.55 (s, 1H, O-H), 1.70-1.66 (m, 2H, J = 8.2 Hz, -CH_2-), 1.56-1.53 (m, 4H, J = 7.5 Hz, -CH_2-), and 1.32-1.26 (m, 18H, J = 7.1 Hz, J = 7.7 Hz, -CH_2-, -CH_3).

*11-hydroxyundecylphosphonic acid ($H_2O_3PC_{11}OH$, **1**).* To a solution of **5** (0.379 g, 0.12 mmol) in dry CH_2Cl_2 (15 mL) was added trimethylbromosilane (0.50 mL, 3.6 mmol). The mixture was stirred under inert atmosphere (N_2) for 6 h. After completion, the

mixture was concentrated and stirred with MeOH (20 mL) under N_2 for 2 h. The mixture was then concentrated to a colorless oil and recrystallized with acetone to afford a white solid **1** (0.288 g, 93 %). ^{1}H NMR (400 Hz, MeOD) δ 3.51 (t, 2H, J = 7.7 Hz, -CH_2-), 1.82-1.80 (m, 2H, J = 7.9 Hz, -CH_2-), 1.58-1.48 (m, 6H, J = 8.1, -CH_2-), and 1.30 (m, 12H, J = 7.6, -CH_2-). (ESI) (*m/z*) [M + H^+]: 252.18.

3.2.3 Microfabrication. Microfluidic cassettes were fabricated using soft lithography.[33] Patterns were achieved using masks drawn in Adobe Illustrator CS3 and photo-plotted by Page Works onto Mylar sheets. SU-8 50 (Microchip) was patterned using the manufacturer's directions to obtain 100-μm channel depth. The Sluggard 184 (Dow Corning) was prepared in a 3:20 curing agent:elastomer (PDMS). The prepolymer was cast over the mold, degassed for 30 min, and cured for 1 h at 75 °C. The PDMS was then removed from the master, and access holes were introduced to allow fluid flow.

3.2.4 Preparation of ITO and SAM formation. Indium tin oxide-coated (10 nm) slides (1" x 3" x 1.1 mm, 10 Ω/sq) were obtained from Nanocs (NY, USA). The slides were cut into 1 x 2 cm^2 pieces and sonicated in deionized water, ethanol, and acetone, each for 20 minutes. Surfaces were then rinsed with ethanol and dried. In order to form SAMs on ITO, the slides were immersed in a 1-mM solution of 11-hydroxyundecylphosphonic acid in water for at least 16 h. Once removed from solution, the surfaces were rinsed with ethanol and dried before use.

3.2.5 Electrochemical characterization. All electrochemical experiments were performed using a Bioanalytical Systems CV-100W potentiostat. Electrochemical data was obtained in a 1 M $HClO_4$ electrolyte solution with an Ag/AgCl electrode (Bioanalytical systems, West Lafayette, IN) serving as the reference, the ITO monolayer as the working electrode, and a Pt wire as the counter electrode. Surfaces were scanned

at a rate of 100 mV/s from 0 to 500 mV. All electrochemical measurements were performed in trials of four with average potentials and standard deviation reported.

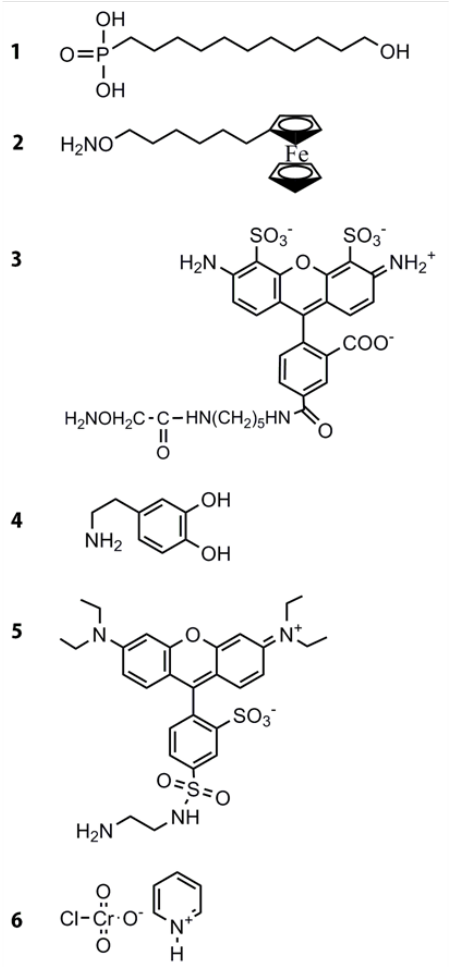

Scheme 3.2 Structures of surface groups and oxyamine- and amine-containing ligands for chemoselective immobilization to ITO activated surfaces.

3.2.6 Ferrocene-oxyamine and dopamine immobilization. Surfaces presenting SAMs of 11-hydroxyundecylphosphonic acid were oxidized using a 300-mM solution of PCC in acetonitrile for either 45 min, to generate aldehyde tail groups, or 150 min, to generate carboxylic acid tail groups. Surfaces were then rinsed with ethanol and dried before use. A 30-mM solution of ferrocene-oxyamine in ethanol was allowed to react on the aldehyde surface for 20 min at 40 °C. To immobilize dopamine, a solution of 150 mM N-hydroxysuccinimide (NHS), 150 mM dicyclohexyl carbodiimide (DCC), and 300 mM

dopamine in DMSO was prepared and allowed to react on the surface for 16 h at room temperature. Once immobilization was complete, the surfaces were rinsed with ethanol and dried before verification by cyclic voltammetry.

3.2.7 Kinetic characterization of aldehyde and acid production. The amount of immobilized ferrocene-oxyamine, corresponding to the total charge (Q) on the surface, was quantified by integrating the redox peak area observed from the CV data. The total charge was then compared to the theoretical value generated from a 100 % converted surface using $Q = nFA\Gamma$, where Q is the total charge, *n* is the number of electrons involved in the reaction (1), F is Faraday's constant, and Γ is the surface coverage in molecules per surface area. The theoretical value was calculated to be 16.1 μC cm^{-2} for a surface density of 1.66 x 10^{-10} moles cm^{-2}. Varying the reaction time with PCC controlled the density of aldehydes and ligands on the surface. After 45 min, aldehyde groups were completely converted. Similarly, oxidation times were extended from 45 to 150 min, and the amount of ferrrocene-oxyamine and dopamine immobilized was calculated by CV analysis. Each data point (0 - 150 min) was performed at least four times, and the amount of ferrocene-oxyamine immobilized was calculated as reported above. Averages and percent error were also determined. Based on the CV data, the theoretical and actual amount of ligand bound were compared and used to construct a relationship between the percent of ligand immobilized and oxidation time. Error bars were represented as the standard deviation within each time point measured. Rate profiles were fitted to pseudo-first order kinetics and determined to be 0.110 and 0.018 min^{-1} for aldehyde and acid production, respectively.

3.2.8 Patterned mixed aldehyde and carboxylic acid surfaces via microfluidic. A PDMS microfluidic cassette was reversibly placed on an ITO surface presenting an 11-hydroxyundecylphosphonic acid SAM (**1**). A 300-mM solution of PCC in acetonitrile was

flowed through the channels and allowed to react for 70 min. Without removing the cassette, the reaction was quenched, and the surface and cassette were rinsed by flowing ethanol through the channels. A solution containing 4 mM Alexa 488-oxyamine (Invitrogen), 150 mM NHS, 150 mM DCC, and 7 mM Rhodamine (Invitrogen) in DMSO was allowed to react with the surface for 3 h at 75 °C. The reaction was then quenched by submerging the surface in DMSO and was rinsed with ethanol and dried before direct imaging.

3.2.9 Dual-patterned surfaces via microfluidic oxidation. A PDMS microfluidic cassette was reversibly placed on an ITO surface presenting an 11-hydroxyundecylphosphonic acid SAM (**1**). A 300-mM solution of PCC in acetonitrile was flowed through the channels and allowed to react for 45 min to exclusively generate aldehydes. Without removing the cassette, the reaction was quenched, and flowing ethanol through the channels cleaned the surface and cassette. With the cassette still in place, a solution of 4 mM Alexa 488-oxyamine in DMSO was flowed through the channels and allowed to react for 1 h at 75 °C to generate the oxime conjugate. The reaction was quenched and the PDMS microfluidic cassette was removed. A different PDMS microfluidic cassette pattern was then reversibly sealed to the same ITO surface containing patterned Alexa 488-oxyamine and unactivated regions of 11-hydroxyundecylphosphonic acid. The immobilization procedure was repeated as described previously, with the exception of PCC oxidation for 150 min to generate only carboxylic acids followed by reaction with a solution of 150 mM NHS, 150 mM DCC, and 7 mM rhodamine in DMSO for 3 h at 75 °C to form the interfacial amide conjugate.

3.2.10 Fluorescence microscopy. After the patterning and immobilization of fluorescent ligands, ITO surfaces were imaged directly by fluorescence microscopy using a Nikon TE2000E inverted microscope. Image acquisition and processing was

carried out with Metamorph software. To show the overlay of both fluorescent dyes, images were taken of the same patterned region in separate light filters and combined into one image.

3.2.11 Cell patterning on ITO. SAMs of 11-hydroxyundecylphosphonic acid (**1**) were oxidized using a 300-mM solution of PCC in acetonitrile for 45 min. A microfluidic cassette was reversibly sealed to the surface, and a 0.1 mM solution of BSA in PBS was flowed through and left to react in the channels for 1 h. After the channels were rinsed with water and ethanol, substrates were reacted with 40 μL of a 10-mM solution of SSDGRG-oxyamine for 2 h. Surfaces were then rinsed with ethanol and dried, followed by cell seeding of Swiss Albino 3T3 fibroblasts.

3.2.12 Cell culture. Swiss Albino 3T3 fibroblasts were cultured in Dulbecco's Modified Eagle Medium (Gibco) containing 10 % calf bovine serum and 1 % penicillin/streptomycin. With a solution of 0.05 % trypsin in 0.53 mM EDTA, cells were removed and re-suspended in serum-free medium (100,000 cells/mL). The cells were seeded to surfaces for 2 h. After 2 h, serum-containing media was added to promote cell growth and division.

3.3.13 Cell staining. Swiss Albino 3T3 mouse fibroblasts were seeded on the substrates as previously mentioned, incubated for 3 d in Dulbecco's modified Eagle's medium (Sigma) with 10 % bovine calf serum and 1 % penicillin/streptomycin, and then fixed with 3.2 % formaldehyde in Dulbecco's PBS (Sigma). The cells were then permeated with PBS containing 0.1 % Triton X-100 and stained with three fluorescent dyes: 1 μL of a solution containing DAPI (1:200 PBS/DAPI; 4',6-diamidino-2-phenylindole dihydrochloride; Sigma), and 10 μL of a 10-mM solution containing phalloidin-tetramethylrhodamine B isothiocyanate (Sigma), and 2.5 μL of a 20-mM

solution containing Cy2 (cyanine, Jackson ImmunoResearch Laboratories Inc., West Grove, PA) that specifically label the nucleus, actin, and vinculin, respectively.

3.2.14 X-Ray photoelectron spectroscopy (XPS). Ferrocene-oxyamine, dopamine, and mixed, functionalized surfaces were prepared as previously described. XPS measurements were preformed on surfaces presenting the immobilized ligands mentioned, as well as bare ITO and 11-hydroxyundecylphosphonic acid SAMs with a Kratos Axis Ultra DLD. A mono Al anode source was used using a specific excitation energy of 1486.6 eV, and an 80 eV pass energy was used for high resolution scans. All binding energies were referenced to the C 1s of a saturated hydrocarbon at 284.7 eV.

3.2.15 Contact angle measurements. ITO surfaces presenting an 11-hydroxyundecylphosphonic acid SAM were oxidized with 300 mM PCC in acetonitrile, ranging from 0 to 150 min. The static contact angles of these reacted surfaces were measured using 10-μL drops of deionized H_2O using a KSV CAM 200 instrument and its corresponding software. Measurements were performed in sets of eight for alcohol-, aldehyde-, and acid-terminated surfaces. Contact angle data were averaged, and standard deviations were calculated.

3.2.16 Atomic force microscopy (AFM). Atomic force microscopy (AFM) images were obtained by using a MFP-3D Stand Alone atomic force microscope (Asylum Research, Santa Barbara, CA). Lateral force images were acquired in contact mode, using a silicon tip (0.03-0.08 N/m, MikroMasch USA, Wilsonville, OR), at a scan rate of 1 Hz, under ambient conditions. Four scans were performed on each substrate during the different stages of SAM manipulation to conclude the surface friction uniformity.

3.3 Results and Discussion

3.3.1 Microfluidic platform design. The general schematic illustrating the oxidative activation of SAMs on ITO (100 Ω/sq), with controlled generation of aldehyde and

carboxylic acid tail groups for subsequent chemoselective ligation is shown in Figure 3.1. Following SAM formation of 11-hydroxyundecylphosphonic acid ($H_2O_3PC_{11}OH$, **1**), scheme 4.1, on ITO, a polydimethylsiloxane (PDMS) microfluidic cassette (fabricated using standard soft lithographic techniques to obtain 100 μm features) was reversibly sealed to the substrate.[33-35] Pyridinium chlorochromate (PCC, **10**) (300 mM in acetonitrile) was then flowed through the microchannels and allowed to oxidize the hydroxy-terminated SAM. Dependent on the oxidative duration, surface hydroxyls could

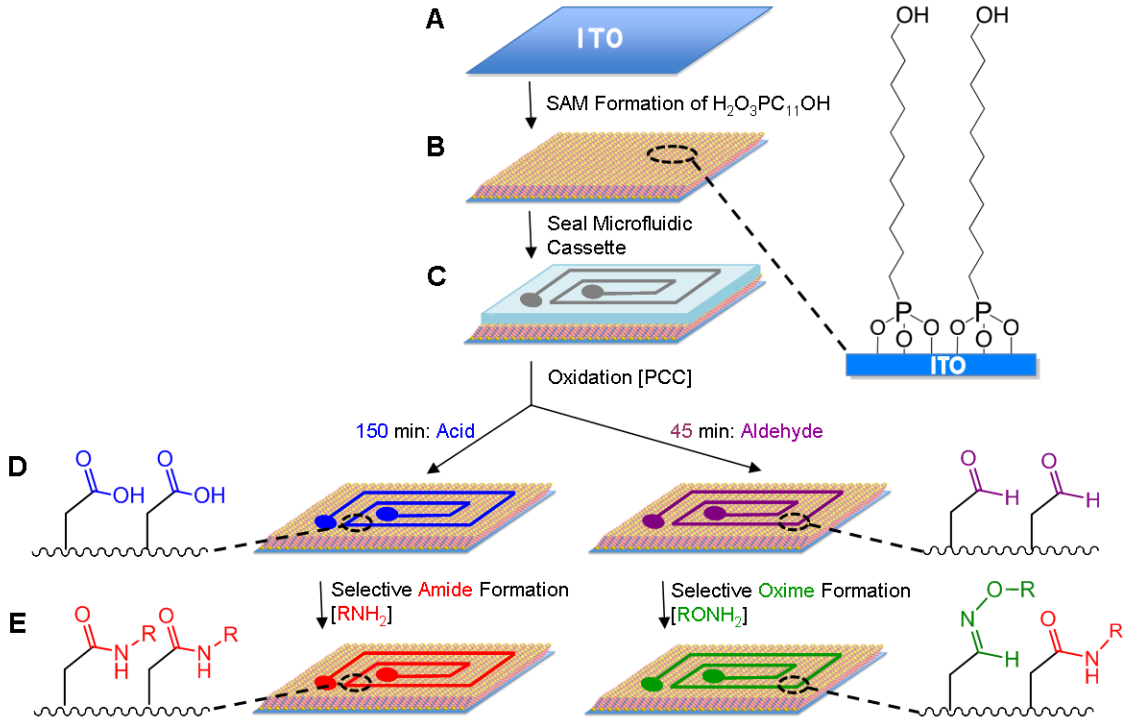

Figure 3.1 Schematic for the microfluidic oxidative activation of $H_2O_3PC_{11}OH$ SAMs on ITO with spatially controlled generation of aldehyde and carboxylic acid tail groups for subsequent chemoselective ligation. (A) An ITO substrate was sonicated in water, ethanol, and acetone. (B) To form a self-assembled monolayer, the substrate was submerged in a solution of $H_2O_3PC_{11}OH$ (1 mM) in water (16 h). (C) A microfluidic cassette was reversibly sealed to the surface, and PCC, a mild oxidant, in acetonitrile was flowed through the microchannels to convert the alcohol-terminated SAM to aldehyde (45 min) or carboxylic acid tail groups (150 min). (D) After stamp removal, the patterned microchannels represented a 2D projection of aldehydes or acids on the surface. (E) For chemoselective immobilization of ligands to aldehyde- or acid-terminated surfaces, oxyamine- ($RONH_2$) or amine- (RNH_2) containing ligand were allowed to react on the surface and immobilized only to the oxidized regions. The resulting oxime and amide conjugates represented a high fidelity 2D projection of the microchannels.

be converted to aldehydes (45 min) or carboxylic acids (150 min). After aldehyde generation, oxyamine-containing ligands were chemoselectively immobilized to the surface resulting in a covalent oxime bond. When exposed to PCC for 150 min, amide linkages were formed from reaction of acid tail groups with amine-containing ligands in the presence of N-hydroxysuccinimide (NHS) and dicyclohexyl carbodiimide (DCC). Thus, a single hydroxyl terminated SAM on ITO could be chemically altered with the same oxidant and concentration to generate two different chemical functional groups that could be independently tailored by different chemoselective ligand immobilization strategies.

3.3.2 Surface molecule characterization: Contact Angle, CV, XPS, and AFM. The uniformity of SAM formation, as well as after chemical modification was investigated by measuring the static contact angle of water on alcohol-, aldehyde-, and acid-terminated surfaces. Averages and standard deviations are reported in table 3.1. Conditions favoring aldehyde generation correspond to larger contact angles than conditions forming carboxylic acids, as well as initial $H_2O_3PC_{11}OH$ SAMs, indicating that there was a uniform increase in hydrophobicity on the surface. On ITO, carboxylic acids can be formed by the longer oxidation duration required for transforming the hydroxyl terminated SAM without monolayer desorption. A similar oxidation method was performed on gold surfaces containing SAMs of 11-mercapto-1-undecanol using PCC concentrations lower by 1000-fold, resulting solely in aldehydes. Higher concentrations or oxidizing durations longer than 70 min appeared to etch the gold and destroy the monolayer. Therefore, carboxylic acid formation is compatible with alcohol-terminated SAMs on ITO but not SAMs of alkanethiols on gold, presumably due to the greater stability of the ITO-phosphonate linkage. Milder conditions and different oxidants are currently being investigated for the gold SAM surfaces.

Surface Group	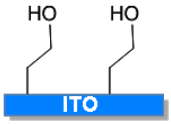	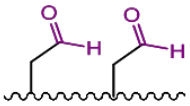	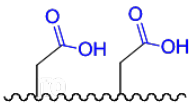
Contact Angle (°)	33.9 ± 0.40	52.9 ± 0.80	22.0 ± 2.0

Table 3.1 Contact angle measurements of hydroxy-, aldehyde-, and carboxylic acid-terminated surface-groups on ITO.

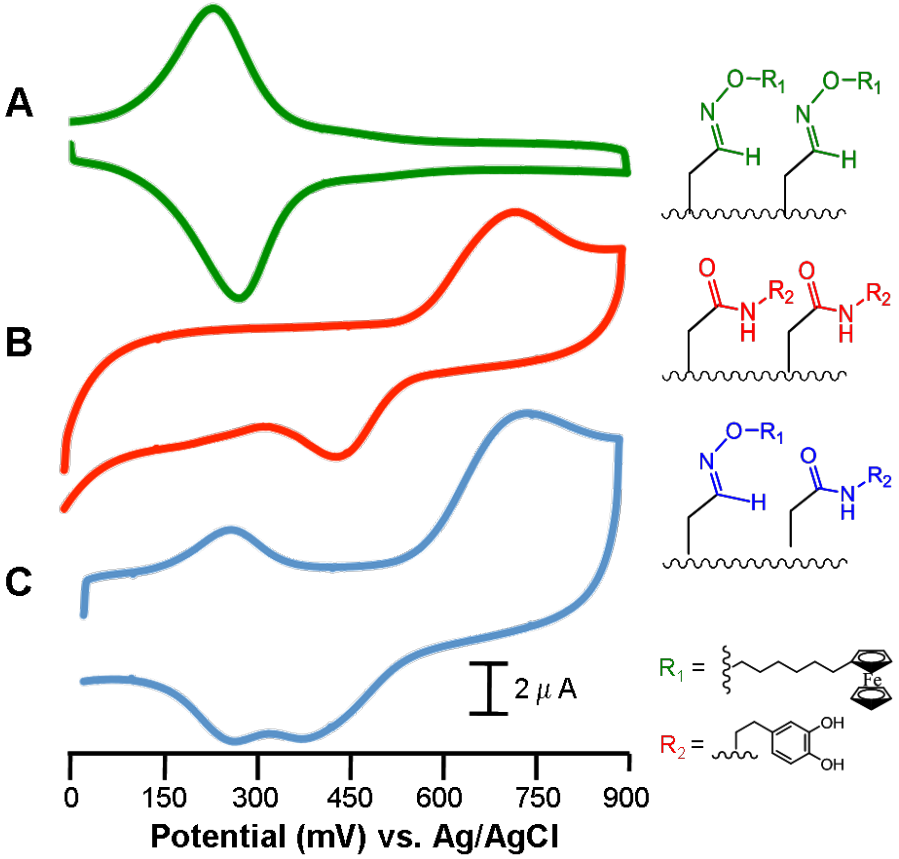

Figure 3.2 Electrochemical characterization of ferrocene-oxyamine and dopamine immobilized to surfaces presenting aldehydes and acids, or a combination of acids and aldehydes, generated on SAMs of $H_2O_3PC_{11}OH$. (A) A cyclic voltammogram of ferrocene-oxyamine (green), with distinctive redox peaks of 230 and 270 mV, chemoselectively immobilized to aldehyde tail groups generated from oxidation of $H_2O_3PC_{11}OH$ on ITO. (B) A cyclic voltammogram of dopamine (red), with distinctive redox peaks of 360 and 730 mV, chemoselectively immobilized to carboxylic acid tail groups generated from oxidation of $H_2O_3PC_{11}OH$ on ITO. (C) A mixed surface containing both electroactive ligands immobilized to a surface presenting both aldehyde and carboxylic acid tail groups after oxidation of $H_2O_3PC_{11}OH$ on ITO.

To verify that both aldehydes and acids were being generated from the same alcohol-terminated SAM on ITO, cyclic voltammetry (CV) was performed. Figure 3.2 shows CV data from surfaces that have been oxidized with conditions for aldehyde (300 mM PCC, 45 min) and acid (300 mM PCC, 150 min) generation, as well as a mixed aldehyde and acid surface (300 mM PCC, 70 min). Electroactive ferrocene-oxyamine (**6**) (30 mM in ethanol, 40 °C, 20 min) and dopamine (**8**) (300 mM in DMSO, 16 h) with NHS/DCC (150 mM) were immobilized to substrates following oxidation. Distinct redox peaks at 230 and 270 mV for ferrocene-oxyamine, and 360 and 730 mV for dopamine were observed from the resultant covalent oxime and amide linkages respectively. As a control, dopamine was immobilized to surfaces oxidized for 45 min, and ferrocene-oxyamine was reacted on substrates that had been exposed to PCC for 180 min. Redox peaks were not present when scanned, indicating that no ligand immobilization occurred.

The percentage of aldehydes generated from hydroxy-terminated surfaces as a function of oxidation duration (0-45 min) was determined by integrating the redox peak areas corresponding to the CV data following ferrocene-oxyamine immobilization. This data was easily reproduced and used to calculate the kinetic rate profile of aldehyde production, fitted to pseudo-first order kinetics. The aldehyde production rate was determined to be 0.11 min^{-1}, as described previously.[9] Similarly, the acid production rate from aldehyde surfaces was found to be 0.018 min^{-1}. Substrates were oxidized for longer durations beyond approximate complete aldehyde conversion (45-150 min), and the CV data generated after redox active ferrocene-oxyamine and dopamine immobilization was analyzed. The rate of the disappearance of aldehydes corresponds approximately with the rate of production of acids, calculated to be 0.018 min^{-1} with error as reported (Figure 3.3). Therefore, oxidation over the substrate can be controlled to generate aldehydes, acids, as well as a mixture of the two groups.

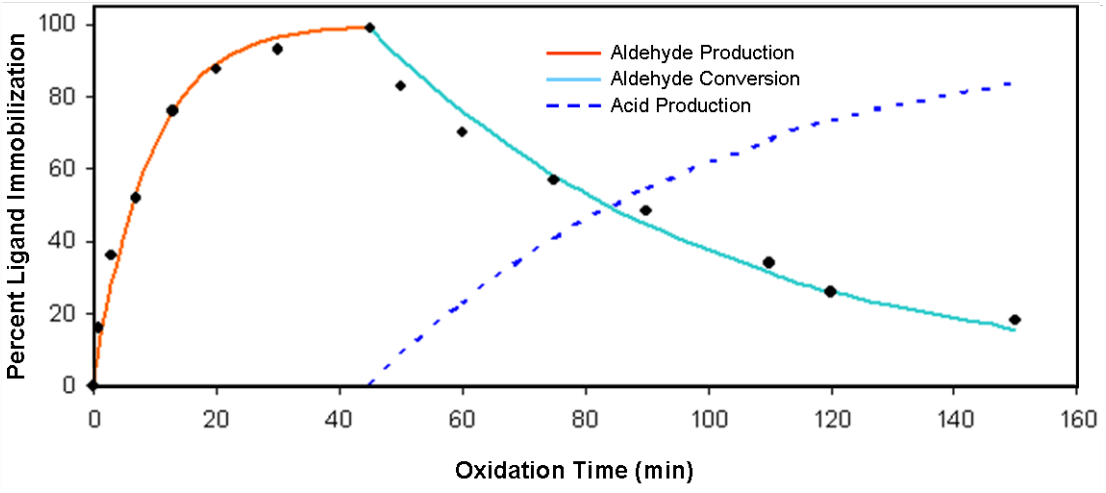

Figure 3.3 Kinetic characterization of aldehyde and acid production on ITO using redox-active ligands, ferrocene-oxyamine (for aldehyde) to generate oximes and dopamine (for carboxylic acids) to generate amides. Percent ligand immobilization versus oxidation time (300 mM PCC, ACN, 0-150 min) plot for SAMs of $H_2O_3PC_{11}OH$ with calculated pseudo-first order rates of 0.11 min^{-1} for aldehyde production (red) and 0.018 min^{-1} for aldehyde disappearance or conversion to acid (blue) and acid production (dotted blue). The acid production rate is approximately the same as the rate of disappearance of aldehydes.

X-ray photoelectron spectroscopy (XPS) was also performed to examine the amide and oxime nitrogen bound to the SAM on the surface (Figure 3.4). Hydroxy-terminated SAMs on ITO were oxidized for 45, 70, and 150 min, followed by subsequent selective immobilization of ferrocene-oxyamine and dopamine. The nitrogen 1s peak representing the oxime linkage between ferrocene-oxyamine and aldehydes was observed at 398 eV, corresponding to data as seen with gold SAMs.[9] Similarly, the nitrogen 1s peak of the amide resultant from conjugation of dopamine to acid was observed at 400 eV. This peak correlated well with the XPS data produced by dopamine immobilization to SAMs of carboxylic acid-terminated phosphonate (Fluka) on ITO. Also, substrates were oxidized for 70 min, generating mixed aldehyde and acid surfaces, followed by immobilization of ferrocene-oxyamine and dopamine ligands. Again, the nitrogen 1s peaks appeared at 398 and 400 eV, respectively, verifying that both ligands were immobilized on the same substrate. Controls including unoxidized SAMs of $H_2O_3PC_{11}OH$ on ITO, dopamine

immobilization onto surfaces that had been oxidized for 45 min, and ferrocene-oxyamine onto substrates with exposure to PCC for 180 min, showed no nitrogen present.

Atomic force microscopy (AFM) was also used to characterize SAM formation and chemical modification (Figure 3.5). Lateral force microscopy (LFM) images of bare ITO, a hydroxy-terminated SAM, a mixed aldehyde- and acid-terminated SAM after oxidation with PCC, and immobilized ferrocene-oxyamine and dopamine on ITO are shown. Without SAM formation, ITO is characteristically rough. LFM images display that there is less contrast in surface friction due to more uniformity in the chemical environment after SAM modification.

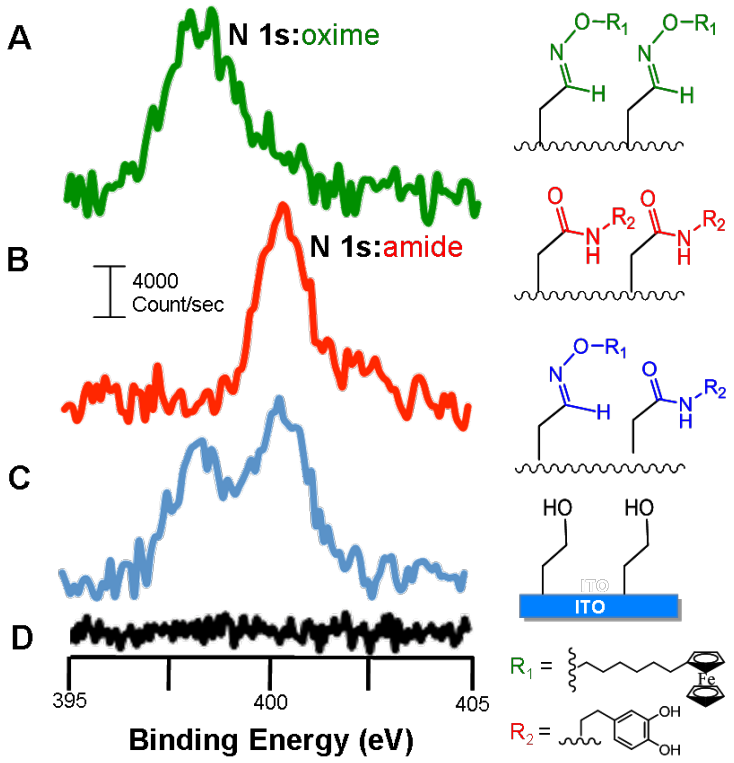

Figure 3.4 X-ray Photoelectron Spectroscopy (XPS) characterization of oxime and amide bonds on ITO. Surfaces presenting SAMs of $H_2O_3PC_{11}OH$ were oxidized to generate aldehyde or carboxylic acid tail groups for subsequent chemoselective ligation and XPS analysis. (A) The nitrogen 1s peak observed at 398 eV corresponds to the oxime nitrogen of ferrocene-oxyamine immobilized aldehyde presenting surfaces. (B) The nitrogen 1s peak observed at 400 eV corresponds to the amide nitrogen of dopamine immobilized to carboxylic acid presenting surfaces. (C) A mixed surface of ferrocene-oxyamine and dopamine ligands, showing both nitrogen peaks of oxime and amide bonds, respectively. (D) An unoxidized ITO surface presenting a SAM of $H_2O_3PC_{11}OH$ showing no nitrogen present.

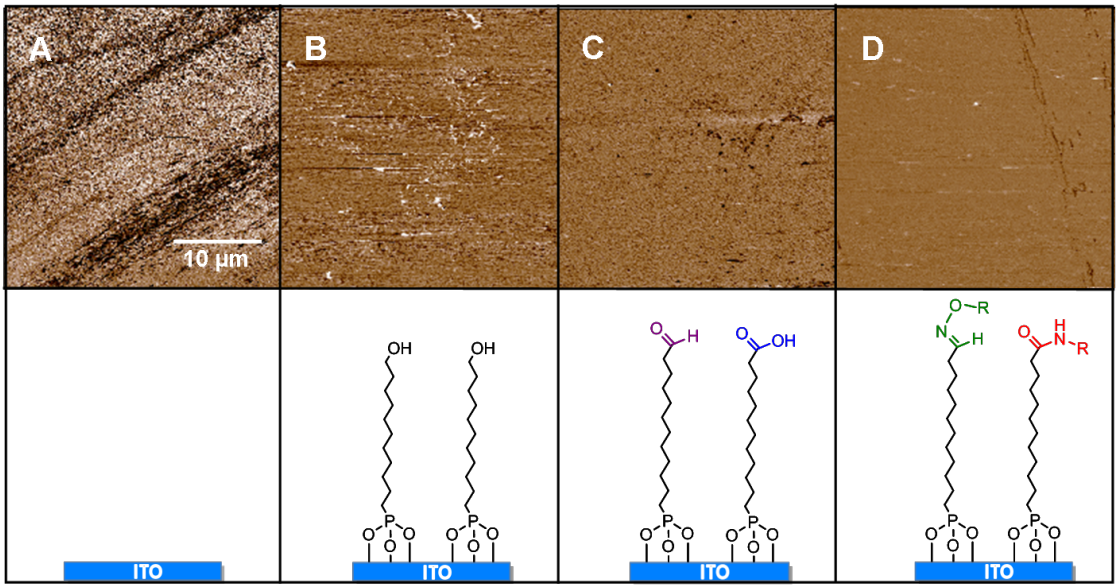

Figure 3.5 Lateral force microscopy (LFM) images of ITO. (A) Bare ITO. (B) A SAM composed of $H_2O_3PC_{11}OH$. (C) A mixed aldehyde- and acid-terminated SAM after oxidation with PCC in acetonitrile. (D) Immobilized ferrocene-oxyamine and dopamine on ITO. As shown, bare ITO is characteristically rough before SAM formation. LFM images display that there is less contrast in surface friction due to more uniformity in the chemical environment after SAM modification.

3.3.3 Fluorescence characterization of surface molecules. To exhibit the diversity in performing this dual-orthogonal strategy to spatially control the immobilization of the oxyamine- and amine-containing ligands on ITO, fluorescent compounds were patterned by microfluidics and then visualized by fluorescence microscopy (Figure 3.6). A microfluidic cassette with separate channels was reversibly sealed to an ITO surface containing SAMs of $H_2O_3PC_{11}OH$, and oxidation with PCC was carried out as previously described. Following oxidation, a mixture of Alexa 488-oxyamine (**7**) and rhodamine (**9**) were allowed to react on the surface. When imaged, the immobilized fluorescent dyes produced a 2D-projection of the microchannels, and patterns of oxime (green), amide (red), and a mixture of oxime and amide (yellow) conjugates were observed (Figure 3.6). More specifically, both carboxylic acids and aldehydes were generated with spatial control on an ITO substrate. PCC was allowed to react in the microchannels for 70 min

resulting in mixture of acids and aldehydes projected from the surface. Rhodamine (7 mM in DMSO, 3h, 75°C), followed by Alexa 488-oxyamine (4 mM in DMSO, 1h) were immobilized. In addition, a single substrate displayed in Figure 3.6 with a pattern of two dyes: Alexa 488-oxyamine (Figure 3.6A, green), rhodamine (Figure 3.6B, red), with a superimposed image showing the same mixed region (Figure 3.6C, yellow).

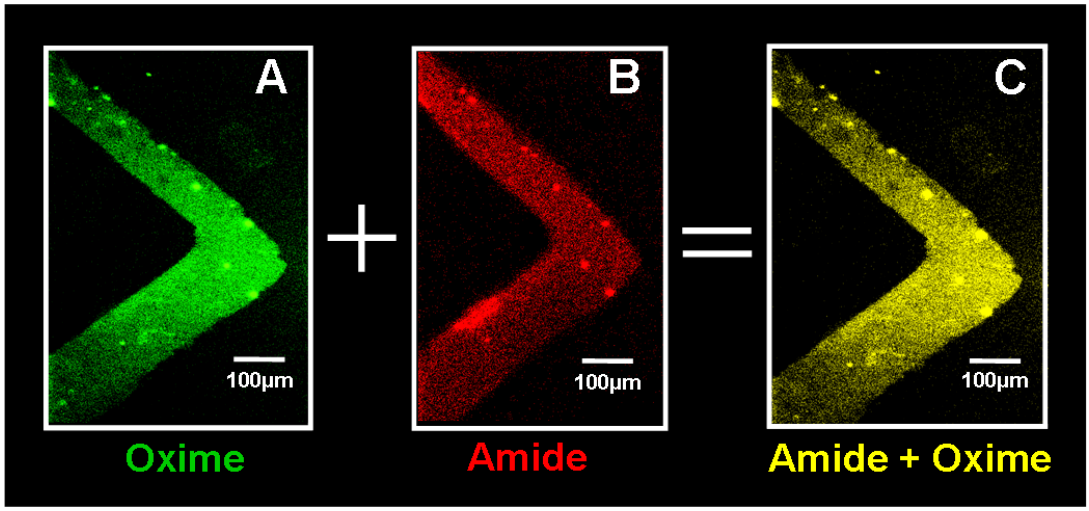

Figure 3.6 Fluorescent micrographs of a mixed aldehyde and carboxylic acid presenting surface patterned by microfluidic oxidation (PCC, 70 min) followed by chemoselective oxime and amide immobilization. Ligands were imaged directly on the surface. (A) Alexa 488-oxyamine immobilized to aldehyde surface-groups generated by microfluidic oxidation with PCC in acetonitrile is displayed. (B) Rhodamine immobilized to carboxylic acid surface-groups generated by microfluidic oxidation on the same pattern is shown. (C) A combined image of the pattern showing a mixed surface containing both oxime and amide conjugates generated by rapid and straightforward microfluidic oxidation of a hydroxy presenting ITO surface is represented.

Alternatively, spatially controlled generation of aldehydes and carboxylic acids independently is also possible by using different microfluidic cassettes for patterning ligands on the same surface (Figure 3.7). Beginning with one cassette on a SAM of $H_2P_3OC_{11}OH$, substrates were oxidized for 45 min in order to generate aldehydes, followed by immobilization of Alexa 488-oxyamine within the microchannels (4 mM in DMSO, 1h, 75 °C). The Alexa 488-oxyamine immobilized to aldehydes present, resulting in a clear projection of the pattern. After rinsing and removing the cassette, a different cassette was reversibly sealed to the surface, and PCC was left to react for 150 min in

order to generate acids for subsequent rhodamine immobilization within the channels (7 mM in DMSO, 3h, 75 °C). Rhodamine immobilized to the newly formed acids. When visualized using fluorescence microscopy, two distinct oxime (green, Figure 3.7A) and amide (red, Figure 3.7B) patterns were observed, with overlapping regions containing a mixture of both oxime and amide conjugated ligands (yellow, Figure 3.7C).

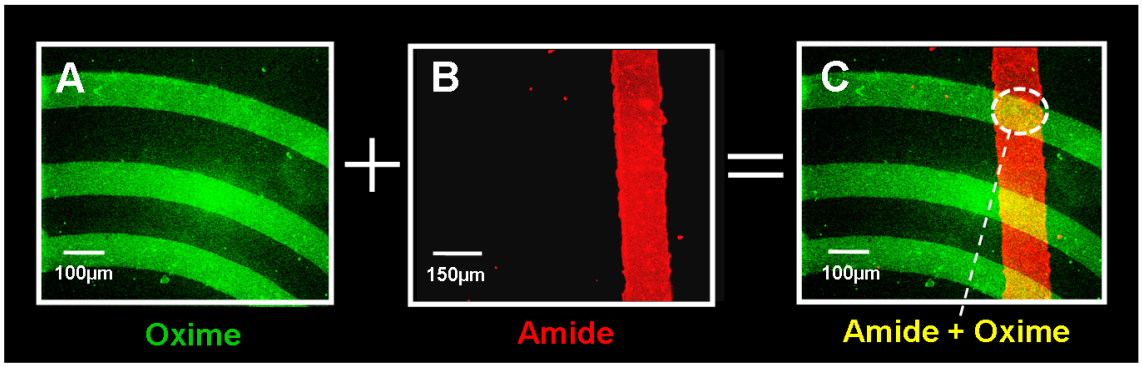

Figure 3.7 Fluorescent micrographs of patterned zones of aldehyde and carboxylic acid generated by serial microfluidic oxidation followed by chemoselective oxime and amide immobilization to ITO surfaces. (A) Immobilized Alexa 488-oxyamine after selective microfluidic oxidation conditions to generate aldehyde surface-groups in a spiral pattern. (B) Immobilized Rhodamine in a bar pattern after selective microfluidic oxidation to generate acid surface-groups in the same region. (C) A combined image of the region displaying a dual-patterned surface containing both oxime and amide conjugates, as well as the overlap upon mixing.

3.3.4 Cell adhesion studies. To demonstrate the utility of ITO for biointerfacial studies, we employed our microfluidic oxidation and immobilization methodology for biospecific cell patterning and attachment (Figure 3.8). A $H_2O_3PC_{11}OH$ surface was oxidized followed by microfluidic patterning of bovine serum albumin (BSA), which prevents cell adhesion. Next, we immobilized the cell adhesive peptide RGD-oxyamine to the remaining unpatterned aldehyde groups (**7**). The RGD peptide is the minimum peptide required to interact with cell surface integrin receptors on cells to support adhesion and migration. Swiss 3T3 fibroblast cells were seeded to the surface and allowed to grow for 3 h. The patterned surfaces remained inert to cell adhesion for over 3 days, at which point the cells were stained for the actin and nucleus and were then

imaged directly. Several controls were performed to ensure a biospecific interaction between RGD-oxyamine and cells. First, $H_2O_3PC_{11}OH$ SAMs on ITO were left unoxidized and therefore, unreactive towards soluble RGD-oxyamine. Second, oxidation was performed to generate aldehyde head-groups without the subsequent reaction of RGD-oxyamine. Cells were seeded to each surface, and no cell adhesion was observed.

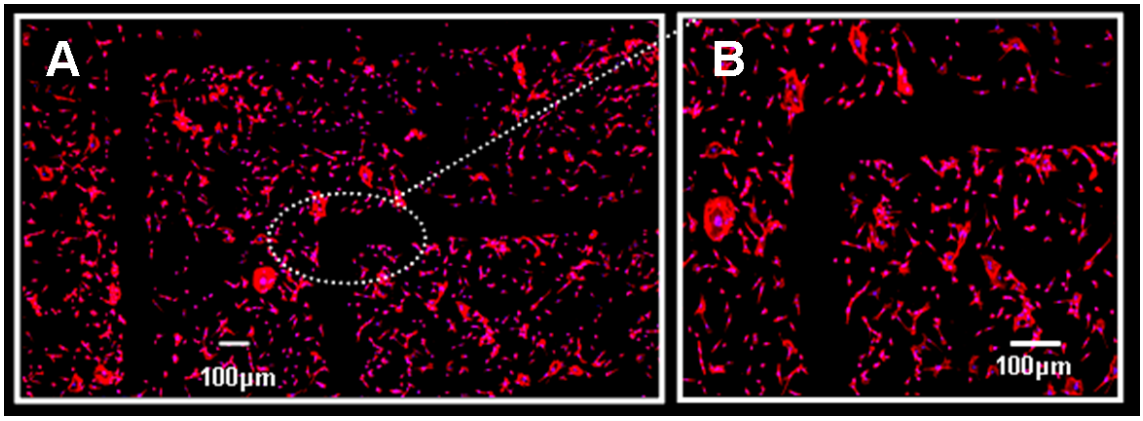

Figure 3.8 Fluorescent micrographs displaying the biospecific interaction between Swiss 3T3 fibroblast cells and an ITO surface presenting patterned RGD peptides. A SAM of $H_2O_3PC_{11}OH$ was oxidized followed by the microfluidic patterning of BSA to generate inert regions on ITO. RGD-oxyamine was immobilized to the remaining aldehyde groups present on the surface. Fibroblast cells attached, migrated, and proliferated. Cells were visualized directly on the surface, for actin (red) and nucleus (blue). The resulting images display 2D patterns of cells on ITO.

3.4 Conclusions

In this report we show the development of a new strategy to pattern ligands onto a surface. We activate a simple hydroxyl-terminated SAM surface with a rapid, inexpensive and mild microfluidic oxidation strategy to generate chemoselective and patterned ITO surfaces. This method allows the use of two orthogonal strategies for selective ligand immobilization with spatial control originating from a single SAM composition on ITO. Aldehyde and carboxylic acid surface-groups were generated by oxidation of alcohol-terminated SAMs followed by immobilization and characterization of a variety of oxyamine- and amine-containing compounds. Microfluidic patterning provides spatial control of aldehydes and acids on the surface, as well as resulting

oxime and amide conjugates, respectively. Taking advantage of the robust, conductive, and transparent nature of ITO, oxime and amide linkages were characterized by CV, XPS, AFM, and fluorescence microscopy. Having the ability to spatially control and pattern the generation of mixed aldehyde and carboxylic acid surfaces as well as distinct regions of carboxylic acids and aldehydes for subsequent immobilization of ligands would greatly benefit research fields such as cell biology and molecular electronics. This new surface patterning strategy circumvents multi-step syntheses and is applicable to tailoring a variety of other materials. Ongoing research includes exploring multiple ligand immobilization for co-culture studies, cell migration studies and for generating high-throughput ligand microarrays on Nickel and other metal-oxide surfaces.

References

(1) Hahn, M. S.; Taite, L. J.; Moon, J. J.; Rowland, M. C.; Ruffino, K. A. I.; West, J. L. *Biomaterials* **2006**, *27*, 2519-2524.

(2) Carroll, G. T.; Wang, D. N.; Turro, N. J.; Koberstein, J. T. *Langmuir* **2006**, *22*, 2899-2905.

(3) Ryan, D.; Parviz, B. A.; Linder, V.; Semetey, V.; Sia, S. K.; Su, J.; Mrksich, M.; Whitesides, G. M. *Langmuir* **2004**, *20*, 9080-9088.

(4) Herbert, C. B.; McLernon, T. L.; Hypolite, C. L.; Adams, D. N.; Pikus, L.; Huang, C. C.; Fields, G. B.; Letourneau, P. C.; Distefano, M. D.; Hu, W.-S. *Chem. Biol.* **1997**, *4*, 731-737.

(5) Hoover, D. K.; Chan, E. W. L.; Yousaf, M. N. *J. Am. Chem. Soc.* **2008**, *130*, 3280-3281.

(6) Hoover, D. K.; Lee, E.-J.; Chan, E. W. L.; Yousaf, M. N. *ChemBioChem* **2007**, *8*, 1920-1923.

(7) Park, T. H.; Shuler, M. L. *Biotechnol. Prog.* **2003**, *19*, 243-253.

(8) Panda, S.; Sato, T. K.; Hampton, G. M.; Hogenesch, J. B. *Trends Cell Biol.* **2003**, *13*, 151-156.

(9) Westcott, N. P.; Pulsipher, A.; Lamb, B. M.; Yousaf, M. N. *Langmuir* **2008**, *24*, 2261-2265.

(10) Barrett, D. G.; Yousaf, M. N. *Angew. Chem. Int. Ed.* **2007**, *46*, 7437-7439.

(11) Amatore, C.; Arbault, S.; Chen, Y.; Crozatier, C.; Lemaitre, F.; Verchier, Y. *Angew. Chem. Int. Ed.* **2006**, *45*, 4000-4003.

(12) Hodgson, L.; Chan, E. W. L.; Hahn, K. M.; Yousaf, M. N. *J. Am. Chem. Soc.* **2007**, *129*, 9264-9265.

(13) Chan, E. W. L.; Yousaf, M. N. *ChemPhysChem* **2007**, *8*, 1469-1472.

(14) Love, J. C.; Estroff, L. A.; Kriebel, J. K.; Nuzzo, R. G.; Whitesides, G. M. *Chem. Rev.* **2005**, *105*, 1103-1170.

(15) Park, S.; Yousaf, M. N. *Langmuir* **2008**, *24*, 6201-6207.

(16) Ulman, A. *Chem. Rev.* **1996**, *96*, 1533-1554.

(17) Holzl, M.; Tinazli, A.; Leitner, C.; Hahn, C. D.; Lackner, B.; Tampe, R.; Gruber, H. J. *Langmuir* **2007**, *23*, 5571-5577.

(18) Kruger, D.; Fuchs, H.; Rousseau, R.; Marx, D.; Parrinello, M. *J. Chem. Phys.* **2001**, *115*, 4776-4786.

(19) Vaughn, O. P. H.; Alavi, A.; Williams, F. J.; Lambert, R. M. *Angew. Chem. Int. Ed*. **2008**, *47*, 2422-2426.

(20) Bhatia, S. N.; Yarmush, M. L.; Toner, M. *J. Biomed. Mater. Res.* **1997**, *34*, 189-199.

(21) Crego-Calama, M.; Reinhoudt, D. N. *Adv. Mater.* **2001**, *13*, 1771-1781.

(22) Mrksich, M.; Whitesides, G. M. *Annu. Rev. Biophys. Biomol. Struct*. **1996**, *25*, 55-78.

(23) Choi, C. K.; Margraves, C. H.; Jun, S. I.; English, A. E.; Rack, P. D.; Kihm, K. D. *Sensors* **2008**, *8*, 3257-3270.

(24) Tosatti, S.; Michael, R.; Textor, M.; Spencer, N. D. *Langmuir* **2002**, *18*, 3537-3548.

(25) Gnauck, M.; Jaehne, E.; Blaettler, T.; Tosatti, S.; Textor, M.; Adler, H.-J. P. *Langmuir* **2007**, *23*, 377-381.

(26) Yanker, D. M.; Maurer, J. A. *Mol. BioSyst.* **2008**, *4*, 502-508.

(27) Cureli, M.; Li, C.; Sun, Y.; Lei, B.; Gunderson, M. A.; Thompson, M. E.; Zhou, C. *J. Am. Chem. Soc.* **2005**, *127*, 6922-6923.

(28) Yousaf, M. N.; Mrksich, M. *J. Am. Chem. Soc.* **1999**, *121*, 42864287.

(29) Chan, E. W. L.; Yousaf, M. N.; Mrksich, M. *J. Phys. Chem. A* **2000**, *104*, 9315-9320.

(30) Bunimovich, Y. L.; Ge, G.; Beverly, K. C.; Ries, R. S.; Hood, L.; Heath, J. R. *Langmuir* **2004**, *20*, 10630-10638.

(31) Chan, E. W. L.; Yousaf, M. N. *J. Am. Chem. Soc.* **2006**, *128*, 15542-15546.

(32) Luo, W.; Westcott, N. P.; Pulsipher, A.; Yousaf, M. N. *Langmuir* **2008**, *24*, 12129-12133.

(33) Xia, Y.; Whitesides, G. M. *Annu. Rev. Mater. Sci.* **1998**, *28*, 153-184.

(34) Weibel, D. G.; DiLuzo, W. R.; Whitesides, G. M. *Nat. Reviews*. **2007**, *5*, 209-218.

(35) Lahiri, J.; Ostuni, E.; Whitesides, G. M. *Langmuir*, **1999**, 15, 2055-2060.

CHAPTER 4

Renewable, Chemoselective, and Quantitative Ligand Density Microarray for Biospecific Interaction Studies

4.1 Introduction

Microarray-based technologies serve as high-throughput analytical tools for the evaluation of a variety of biomolecular interactions, provide a platform for rapid analyses and automation, and require low analyte and reagent volumes.[1-4] Such technologies have incorporated the use of functionalized self-assembled monolayers (SAMs) of alkanethiolates on gold surfaces for the preparation of DNA, peptide, and carbohydrate microarrays to conduct studies in genomics, proteomics, and glycomics, respectively.[5-8] SAMs can also be specifically tailored to present a number of derivatized ligands from the surface through covalent modification, affording a well-defined, biocompatible system.[9-11] Current chemoselective conjugation strategies include Staudinger ligation,[12,13] Click chemistry,[14] maleimide,[15] amide,[16] Diels-Alder,[17-19] and oxime chemistry.[20-23] One methodology in particular that uses electroactive, hydroquinone-terminated SAMs, has proven to be a powerful approach toward the immobilization and release of ligands.[24] This strategy enables the quantification of attached ligand amount, as well as provides the ability to monitor the reaction progression in real time and calculate kinetic rates.[25]

Carbohydrates represent the most abundant class of organic compounds that are found in living organisms and are known to mediate several biological processes,

including neural development, signal transduction, viral invasion, and cancer metastasis.[26-33] As a result, understanding carbohydrate constituent binding properties at the molecular level would impart invaluable information for basic research areas, as well as glycomics, therapeutic discovery, and diagnostics.[34] Carbohydrate microarray technologies have been designed to perform high-throughput screening of various vital events, including enzymatic glycosylation, sugar identification, and bacterial detection.[35-38] A method based on a renewable and quantitative platform that can perform similar analyses and also prove to be compatible with numerous biological systems, including carbohydrates, would greatly benefit a number of industries and tremendously reduce costs, materials, and time.

Herein, we present a renewable microarray technology to immobilize and release carbohydrates and proteins through the control of electrochemical potential and pH. Monosaccharides were synthesized to incorporate oxyamine functionality for chemoselective conjugation to the ketone in electroactive quinone-terminated SAMs on gold substrates. Sugar immobilization and release was monitored and the SAM and ligand density were precisely controlled and quantified via cyclic voltammetry. In addition to the formation of mixed quinone- and tetra(ethylene glycol)-terminated SAMs, which provide resistance to nonspecific lectin adhesion, microarray technology allows for the control over the orientation and spatial distribution of SAM molecules and ligands, criteria that are both essential for studying the biospecific interactions between molecules.[39] Different microarray densities of quinone-terminated SAMs were generated, and a number of oxyamine-containing sugars were immobilized. The resulting oxime linkages were characterized by electrochemistry, X-ray photoelectron spectroscopy, and contact angle, and lectin-carbohydrate binding interactions were observed via fluorescence microscopy. This method can be used in conjunction with the tailoring of

other biomolecules, such as DNA, peptides, and phospholipids for studies in genomics, transcriptomics, and proteomics.

4.2 Materials and Methods

4.2.1 Materials. Fluorescent lectins were obtained from Invitrogen (Carlsbad, CA); all other chemicals were obtained from Sigma Aldrich (St. Louis, MO).

4.2.2 Syntheses. Tetra(ethylene) glycol- (EG_4SH) and hydroquinone- (H_2Q) terminated alkanethiols were synthesized as previously reported.[39,42] The syntheses of oxyamine-containing monosaccharides are described below.[43,44]

*1,2,3,4,6-Penta-O-acetyl-β-D-(sugar)pyranose (**6-8**).* Typical procedure; to a solution of acetic anhydride (50 mL) was added sodium acetate (5.40 g, 66.6 mmol, 3 eq). The mixture was refluxed at 90 °C for 20 minutes to which D-sugar (4.00 g, 22.2 mmol) was added and stirred for 4 h. The mixture was then concentrated, dissolved in methanol, and recrystallized with cold water. A white solid was then filtered and dried to afford **(6)** (6.73 g, 77 %), ^{1}H NMR (400 Hz, $CDCl_3$) δ 2.01, 2.09, 2.13, 2.15, 2.18 (s, 15H, CH_3), 4.17-4.13 (dm, 3H, J = 16.4 Hz, CH, CH_2), 5.11-5.09 (dm, 1H, J = 7.8 Hz, CH), 5.34-5.33 (t, 1H, J = 4.2 Hz, CH), 5.93-5.92 (m, 1H, J = 4.3 Hz, CH), 5.72-5.70 (d, 2H, J = 8.3 Hz, CH_2); **(7)** (7.44 g, 85 %), ^{1}H NMR (400 Hz, $CDCl_3$) δ 2.01, 2.03, 2.07, 2.09, 2.13 (s, 15H, CH_3), 4.17-4.14 (m, 2H, J = 12.3 Hz, CH_2), 4.40-4.38 (dm, 1H, J = 7.7 Hz, CH), 4.71-4.69 (d, 1H, J = 8.2 Hz, CH), 5.32-5.31 (t, 1H, J = 4.4 Hz, CH), 5.37-5.36 (t, 1H, J = 4.3 Hz, CH), 5.41-4.40 (d, 1H, J = 4.1 Hz, CH); **(8)** (8.32 g, 95 %), ^{1}H NMR (400 Hz, $CDCl_3$) δ 1.99, 2.02, 2.09, 2.13, 2.16 (s, 15H, CH_3), 4.24-4.22 (m, 2H, J = 8.1 Hz, CH_2), 4.43-41 (m, 1H, J = 7.7 Hz, CH), 5.02 (s, 1H, CH), 5.34-5.33 (t, 1H, J = 4.4 Hz, CH), 5.58-5.57 (m, 1H, J = 4.0 Hz, CH), 5.66-5.65 (d, 1H, J = 4.3 Hz, CH).

*O-(2,3,4,6-tetra-O-acetyl)-β-D-(sugar)pyranosyl-bromoethyloxy (**9-11**).* Typical procedure; to a solution of **6-8** (1.00 g, 2.56 mmol, 1 eq) and $ZnCl_2$ (catalytic) in

anhydrous dichloromethane (15 mL) was added 2-bromoethanol (0.24 mL, 3.33 mmol, 1.3 eq), followed by the addition of boron trifluoride diethyl etherate (0.41 mL, 3.33 mmol, 1.3 eq) dropwise at 0 °C. The mixture was stirred under inert atmosphere (N_2) for 6h at room temperature. Upon completion, the mixture was then washed with water (2 x 50 mL), sodium bicarbonate (1M) (2 x 50 mL), concentrated, and recrystallized in hexanes to afford a white solid **9** (0.721 g, 59 %), ^{1}H NMR (400 Hz, $CDCl_3$) δ 2.01, 2.12, 2.15, 2.18 (s, 12H, CH_3), 4.10-4.06 (dm, 2H, J = 8.3 Hz, J = 16.0, CH_2), 4.17-4,14 (m, 2H, J = 12.2, CH_2), 4.41-4.39 (m, 2H, J = 7.3 Hz, CH_2), 4.76-4.74 (d, 1H, J = 8.0 Hz, CH), 5.24-5.23 (t, 1H, J = 4.3 Hz, CH), 5.42-5.41 (d, 1H, J = 4.1 Hz, CH), (ESI) (*m/z*) [M + H^+]: 454.05; **(10)** (0.93 g, 80 %), ^{1}H NMR (400 Hz, $CDCl_3$) δ 2.01, 2.03, 2.07, 2.09 (s, 12H, CH_3), 3.50-3.49, 3.53-3.51 (dm, 2H, J = 8.2 Hz, CH_2), 3.51-3.49 (m, 2H, J = 8.3 Hz, CH_2), 4.11-4.08 (m, 2H, J = 12.4 Hz, CH_2), 4.30-4.28 (dd, 2H, J = 8.2 Hz, CH_2), 4.58-4.57 (d, 1H, J = 4.1 Hz, CH), 4.99-4.98 (t, 1H, J = 4.1 Hz, CH), 5.13-5.12 (t, 1H, J = 4.3 Hz, CH), 5.21-5.20 (t, 1H, J = 4.0 Hz, CH), (ESI) (*m/z*) [M + H^+]: 454.05; **(11)** (0.81 g, 69 %), ^{1}H NMR (400 Hz, $CDCl_3$) δ 2.01, 2.07, 2.12, 2.18 (s, 12H, CH_3), 3.55-3.52 (t, 2H, J = 8.0, CH_2), 3.91-3.89, 3.87-3.85 (dm, 2H, J = 8.3 Hz; CH_2), 4.17-4.14 (m, 2H, J = 12.1 Hz, CH_2), 4.31-4.29 (m, 1H, J=8; CH), 4.89 (s, 1H; CH), 5.29-5.28 (m, 1H, J=4; CH), 5.31-5.30 (t, 1H, J = 4.3 Hz, CH), 5.34-5.33 (t, 1H, J = 4.1 Hz, CH), (ESI) (*m/z*) [M + H^+]: 454.05

*O-(2,3,4,6-tetra-O-acetyl)-β-D-(sugar)pyranosyl-ethyloxy-N-oxyphthalimide (**12-14**). Typical procedure;* to a solution of N-hydroxyphthalimide (1.07 g, 6.59 mmol, 1.5 eq) in DMF (20 mL) at 65 °C was added sodium bicarbonate (0.55 g, 6.59 mmol, 1.5 eq). The mixture was then stirred for 30 min until fully deprotonated (brown in color) to which **9-11** (2.00 g, 4.39 mmol, 1 eq) was added. The solution was stirred under inert atmosphere (N_2) for 8 hours. After completion, the mixture was diluted with dichloromethane and

washed with water (8 x 100 mL) and 1 M $NaHCO_3$ (3 x 25 mL) or until the excess N-hydroxyphthalimide was completely taken up into the aqueous layer. The organic layer was concentrated and purified by flash chromatography (Hex/EtOAc, 3.5:6.5) to afford a pale yellow oil **12** (1.80 g, 76 %). ^{1}H NMR (400 Hz, $CDCl_3$) δ 2.01, 2.07, 2.12, 2.16 (s, 12H, CH_3), 4.13-4.09 (dm, 2H, J = 8.3 Hz, J = 16.1 Hz, CH_2), 4.19-4,16 (m, 2H, J = 12.3 Hz, CH_2), 4.47-4.45 (m, 2H, J = 7.7 Hz, CH_2), 4.80-4.78 (d, 1H, J = 8.0 Hz, CH), 5.28-5.27 (t, 1H, J = 4.3 Hz, CH), 5.42-5.41 (d, 1H, J = 4.2 Hz, CH), 7.85-7.83, 7.80-7.78 (dm, 4H, J = 8.4 Hz, CH), (ESI) (*m/z*) [M + H^+]: 537.15; **(13)** (1.49 g, 63 %), ^{1}H NMR (400 Hz, $CDCl_3$) δ 2.09-2.00 (qs, 12H, CH_3), 3.78-3.76 (m, 2H, J = 8.3 Hz, CH_2), 4.04-4.02, 4.4.39-4.37 (dm, 2H, J = 8.2 Hz, CH_2), 4.09-4.06 (m, 2H, J = 12.1 Hz, CH_2), 3.50-3.48 (2xd, 2H, J=8; CH), 4.78-4.77 (d, 1H, J=4; CH), 4.97-4.95 (t, 1H, J=7; CH), 5.09-5.07 (t, 1H, J = 7.6 Hz, CH), 5.31-5.29 (t, 1H, J = 7.5 Hz, CH), 7.78-7.76 (dm, 4H, J = 8.0 Hz, 4H), (ESI) (*m/z*) [M + H^+]: 537.15; **(14)** (1.53 g, 65 %), ^{1}H NMR (400 Hz, $CDCl_3$) δ 1.89 (s, 2H, NH_2), 2.16, 2.12, 2.05, 2.00 (s, 12H, CH_3), 3.77-3.75, 3.74-3.72 (dm, 2H, J = 8.3 Hz, J = 16.1 Hz, CH_2), 4.07-4.05 (m, 2H, J = 8.3 Hz, CH_2), 2.10-2.08 (m, 2H, J = 8.0 Hz, CH_2), 4.31-4.30 (m, 1H, J = 4.3 Hz, CH), 4.87 (s, 1H, CH), 5.29-5.27 (m, 1H, J = 7.9 Hz, CH), 5.38-5.37 (d, 1H, J = 4.2 Hz, CH), 5.40-3.39 (d, 1H, J = 4.1 Hz, CH), (ESI) (*m/z*) [M + H^+]: 537.15.

*β-D-(Sugar)pyranosyl-propyloxy-N-oxyamine (**1-3**)*. Typical procedure; to a solution of **12-14** (0.912 g, 1.70 mmol) in ethanol (15 mL) was added hydrazine (0.327 mL, 10.2 mmol, 6 eq). The mixture was stirred under inert atmosphere for up 48 h. The mixture was then concentrated and purified by flash chromatography (MeOH/DCM, 3:7) to afford a white solid **15** (0.271 g, 67 %), ^{1}H NMR (400 Hz, $CDCl_3$) δ 2.23-2.21 (t, 1H, J = 7.8 Hz, CH), 3.50-3.38 (m, 3H, CH, CH_2), 3.64-3.62 (m, 3H, J = 7.8 Hz, CH_2, OH), 3.79-3.74 (m, 2H, OH), 3.83-3.79 (m, 4H, J = 16.1 Hz, CH_2, CH, OH), 3.96-3.94 (m, 1H, J = 8.2, CH),

4.30-4.28 (d, 1H, J = 7.7 Hz, CH); (ESI) (*m/z*) [M+H$^+$]: 239.10; **16** (0.213 g, 52 %), ^{1}H NMR (400 Hz, $CDCl_3$) δ 3.18-3.16 (t, 1H, J = 7.6 Hz, CH), 3.27-3.24 (t, 1H, J = 12.2 Hz, CH), 3.36-3.34 (m, 2H, J = 8.3 Hz, CH_2), 3.60-3.59, 3.57-3.56 (dd, 1H, J = 4.1, J = 16.4 Hz, CH), 3.75-3.72 (dm, 2H, J = 12.3 Hz, CH_2), 3.78-3.77 (m, 2H, J = 8.1 Hz, CH_2), 3.93-3.91 (m, 1H, J = 8.3 Hz, CH), 4.36-4.34 (d, 1H, J = 8.1 Hz, CH); (ESI) (*m/z*) [M+H$^+$]: 239.10.

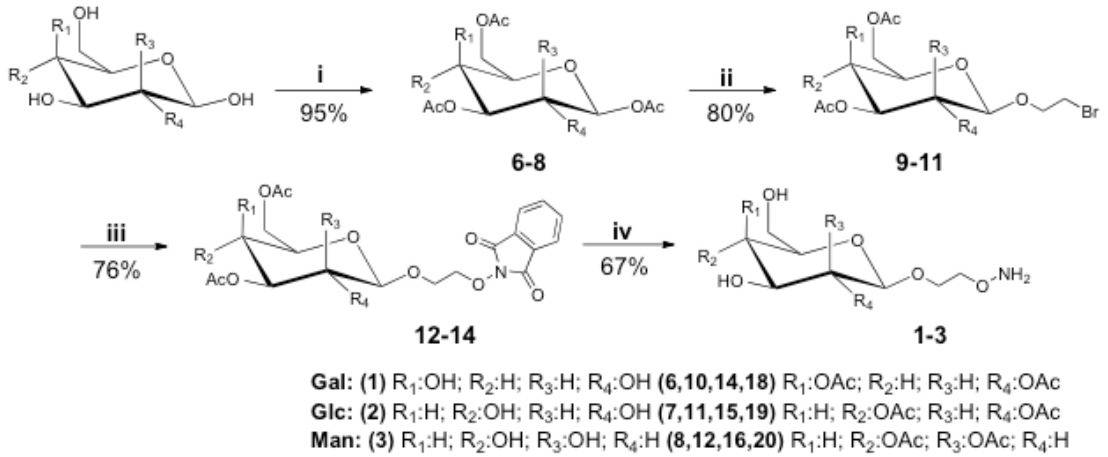

Scheme 4.1 General synthetic route to oxyamine-functionalization of carbohydrates. Reagents and conditions. (i) NaOAc (3 eq), $ZnCl_2$ (cat), Ac_2O, 90 °C, 4 h, 95 %; (ii) 2-bromethanol (1.2 eq), boron trifluoro diethyletherate (1.3 eq), $ZnCl_2$ (cat), DCM 0-25 °C, 6 h, 80 %; (iii) N-hydroxyphthalimide (1.5 eq), $NaHCO_3$ (1.5 eq), DMF, 65 °C, 8 h, 76 %; and (iv) hydrazine (6 eq), EtOH, 25 °C, 48 h, 67 %.

*4.2.3 Preparation of gold-coated substrates and monolayers***.** Glass cover slips (75 mm x 25 mm, Fisher) were immersed into a piranha solution (1:1 volume ratio of H_2SO_4 and 32% H_2O_2) for 4 h, followed by rinsing with deionized water and ethanol. Gold substrates were prepared by electron-beam deposition of titanium (5 nm) and then gold (12 nm for microarray and 50 nm for electrochemical measurements). The gold-coated slides were cut into 1 x 2 cm^2 pieces. To form SAMs on gold, the slides were immersed in an ethanolic solution containing alkanethiols (1 mM) for at least 16 h. Once removed from solution, the surfaces were rinsed with ethanol and dried before use.

4.2.4 Electrochemical immobilization and release of ligands. All electrochemical experiments were performed using a Bioanalytical Systems CV-100W potentiostat. To activate H_2Q-terminated SAMs, electrochemical experiments were performed in a 1 M $HClO_4$ electrolyte solution with an Ag/AgCl electrode (Bioanalytical systems) serving as the reference, the gold monolayer as the working electrode, and a Pt wire as the counter electrode. Surfaces were scanned at a rate of 100 mV/s. Immobilized ligands were confirmed using the same parameters. Ligands were released by applying potential for 15 min (~60 cyclic scans) in PBS buffer (pH = 7) and were characterized in similar conditions.

4.2.5 Sugar-oxyamine immobilization for electrochemical measurements. Surfaces containing mixed SAMs of H_2Q- and EG_4SH-terminated alkanethiols were electrochemically oxidized (1 M $HClO_4$, pH = 0) to generate mixed SAMs of Q- and EG_4SH-terminated groups. Surfaces were then rinsed with ethanol and dried. A 90 mM solution of sugar-oxyamine in ethanol was allowed to react on the quinone surface for 4 hours at 40 °C. Once the immobilization was complete, the surfaces were rinsed with ethanol and dried before verification by cyclic voltammetry.

4.2.6 Preparation of microarrays for density studies. Bare gold substrates (2 x 1 cm^2) were printed using a SpotBot® 2 Complete (TeleChem International, Inc., Sunnyvale, CA). Programming and printing was carried out with SpoCLeGenerator and Spot App. Software. Different densities of mixed SAMs of H_2Q- and EG_4SH-terminated alkanethiols (0, 25, 50, 75 and 100 % of H_2Q, 1 mM in EtOH) were formed in microarray patterns (12 x 12 arrays, 100 μm diameter, 300 μm spacing, 0.1 s printing time). Substrates were then backfilled with EG_4SH (1 mM in EtOH, 16 h), followed by electrochemical oxidation (1 M $HClO_4$, pH = 0) to generate corresponding mixed densities of Q- and EG_4SH-terminated groups. Surfaces were then rinsed with ethanol and dried. A 90 mM solution

of sugar-oxyamine in ethanol was allowed to react on the quinone surface for 4 h at 40 °C. Once the immobilization was complete, substrates were rinsed with ethanol and dried before cyclic voltammetry was performed.

4.2.7 Ligand density determination. The amount of sugar-oxyamine immobilized (gal, glc, and man), corresponding to the total charge (Q) on the surface, was quantified by integrating the redox peak area observed from the CV data after reaction with H_2Q-terminated SAM microarrays (different densities of 0, 25, 50, 75, and 100 % H_2Q). The total charge was then compared to the theoretical value generated from a 100% converted surface using $Q = nFA\Gamma$, where Q is the total charge, n is the number of electrons involved in the reaction (2), F is Faraday's constant, and Γ is the surface coverage in molecules per surface area. The theoretical value was calculated to be 16.1 $\mu C/cm^2$ for a surface density of 1.66×10^{-10} moles/cm^2.

4.2.8 Preparation of renewable microarrays for lectin adhesion studies. A solution of H_2Q-/EG_4SH-containing alkanethiols (1:9, 1 mM in EtOH) were transferred to a bare gold surface (2 x 1 cm^2) to form microarray features (12 x 12 arrays, 100 μm diameter, 300 μm spacing, 0.1 s printing time). Substrates were then backfilled with EG_4SH (1 mM in EtOH, 16 h), followed by electrochemical oxidation (1 M $HClO_4$, pH = 0) to generate corresponding Q-terminated SAMs. Surfaces were then rinsed with ethanol and dried before the same spotting programmed was employed to randomly print sugar-oxyamines (90 mM in ethanol). Once the immobilization was complete, substrates were rinsed with ethanol and dried before lectin adhesion (1 mg/mL, PBS, 2 h, 25 °C). After rinsed and dried with PBS, substrates were visualized by fluorescence microscopy. Ligands were released from the array by applying electrochemical potential for 15 min (~60 cyclic scans) in PBS buffer (pH = 7), and sugar-oxyamines were again transferred via random microspotting. Lectins were added and visualized in a similar.

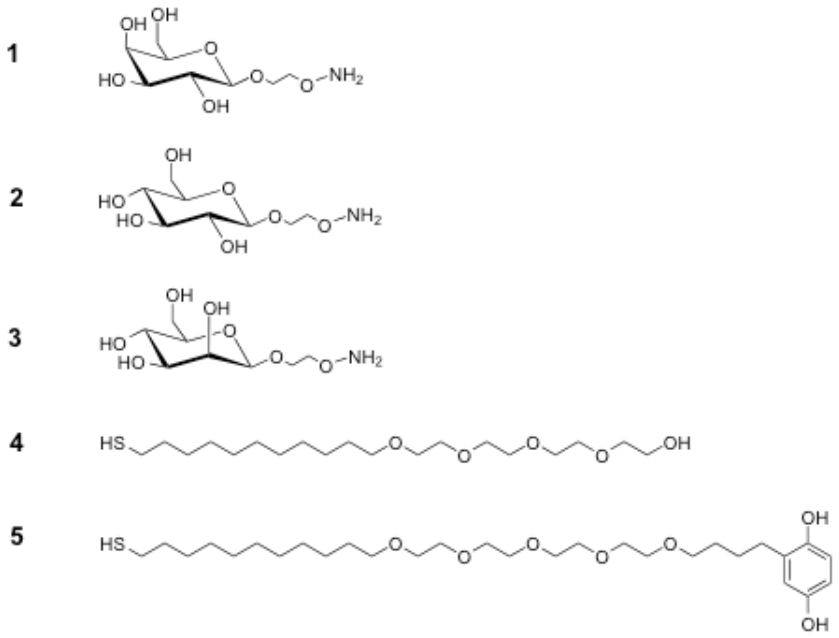

Scheme 4.2 SAM molecules and carbohydrates used in the study. (1) Galactose-oxyamine (Gal-ONH_2); (2) glucose-oxyamine (Glc-ONH_2); (3) mannose-oxyamine (Man-ONH_2); (4) tetra(ethylene glycol)-terminated alkanethiol (EG_4SH); and (5) hydroquinone-terminated alkanethiol (H_2Q).

4.2.9 Fluorescence microscopy. After fluorescence microscopy using imaged the immobilization of sugars and fluorescently labeled lectins to patterned microarrays, the substrates a Nikon TE2000E inverted microscope. Image acquisition and processing was carried out with Metamorph software.

4.2.10 X-Ray Photoelectron Spectroscopy (XPS). After immobilization of sugar-oxyamine to quinone surfaces, XPS measurements were preformed on substrates containing the immobilized ligands mentioned, as well as bare gold and quinone SAMs with a Kratos Axis Ultra DLD. A mono Al anode source was used with a specific excitation energy of 1486.6 eV and a 80 eV pass energy was used for the high-resolution scans. All binding energies are reference to the C 1s of a saturated hydrocarbon at 284.7 eV.

4.2.11 Contact angle measurements. Gold surfaces with SAMs composed of hydroquinone, quinone, and immobilized sugars were prepared. The static contact

angles of these surfaces, as well as bare gold, were measured using 10 μL drops of deionized H_2O using a KSV CAM 200 instrument and software.

Results and Discussion

4.3.1 Method development. Our interest in developing a chemoselective, renewable, and quantitative ligand density microarray for biological analyses was influenced by several factors. First, the reaction between a hydroquinone- (H_2Q, **5**, Scheme 4.2) terminated SAM and an oxyamine-containing ($RONH_2$) compound is rapid, chemoselective, and occurs at room temperature and under physiological conditions. Additionally, the oxyamine functionality is amenable to facile modification, as well as solid phase peptide synthesis (SPPS) and can be incorporated into a number of desired biomolecules.[24] Alkanethiolates, terminated with H_2Q have also been shown to rapidly form nano-patterned SAMs, granting the spatial control required for the interrogation of a specific biointerfacial interaction.[40,41] H_2Q is electroactive and can be oxidized to the corresponding quinone (Q); this molecule in turn reacts with oxyamine compounds to form stable oxime linkage. The H_2Q/Q couple and electroactive oxime product have distinct redox peaks that can be quantified through cyclic voltammetry (CV). This technique is used to monitor oxime formation and calculate reaction kinetics and ligand density. Finally, under reducing conditions and with applied potential, oxime conjugates released from the surface, regenerating the H_2Q-terminated SAM for multiple cycles of immobilization and analyses. The renewable aspect of this surface strategy is especially advantageous when only small quantities of biological ligand and receptor are available, as well as reducing the overall reagent and material consumption and waste accumulation.

The general strategy for developing a chemoselective, renewable, and quantitative, ligand density microarray for biological analyses is described in Figure 4.1. We have

chosen to use different ratios of H_2Q- and tetra(ethylene glycol)- (EG_4SH, **4**, Scheme 4.2) terminated alkanethiolates to construct our microarrays due to the non-fouling properties of EG_4SH. Alkanethiolate solutions are transferred to a bare gold substrate using an automated microarray method and the SAM microspots are rapidly formed. The remaining unpatterned surface is then backfilled with EG_4SH, oxidized to reveal Q, and biological ligands are then reversibly conjugated to the microarray. Depending on the particular biomolecule presented from the substrate, the corresponding bioassay can be performed and analyzed. The original microarray can then be regenerated for a subsequent round of immobilization, analysis, and release.

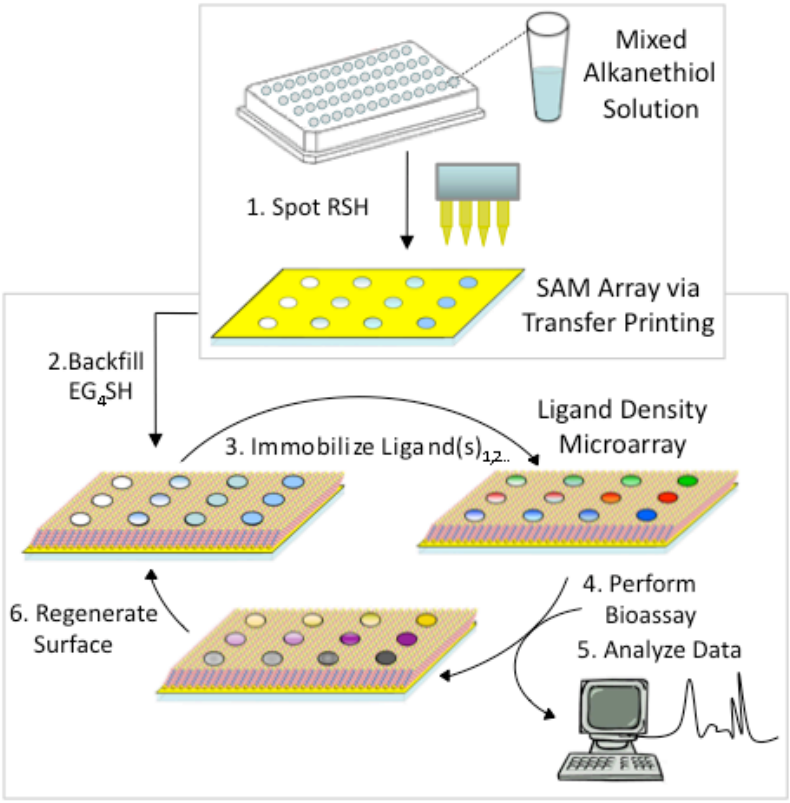

Figure 4.1 Strategy to develop a renewable and quantitative, ligand density microarray for biological analysis. (1) Different mixtures of alkanethiolates are transferred from a 96-well microplate to a bare gold substrate via automated array technology, and microspots of SAMs are formed. (2) The substrate is backfilled with tetra(ethylene glycol)-terminate alkanethiol (EG_4SH) to render the surface inert to nonspecific protein adsorption. (3) Tailored biological ligands are then immobilized to the array. (4) The corresponding bioassay is performed, (5) analyzed, and (6) the original microarray is regenerated for a subsequent cycle of ligand immobilization and analyses.

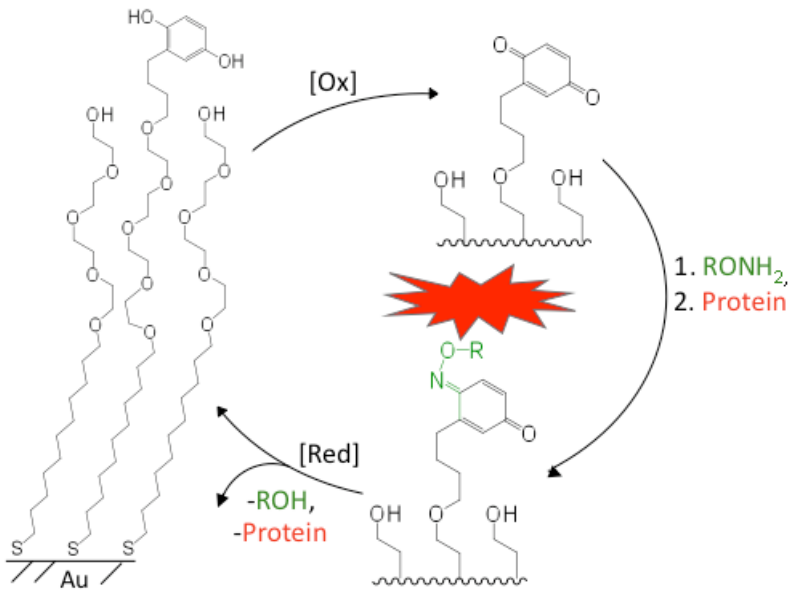

Figure 4.2 General schematic representing the reversible oxidation [Ox] and reduction [Red] of electroactive SAMs to generate renewable surfaces for the immobilization and release of ligands and proteins. H_2Q-presenting SAM microarrays are electrochemically oxidized (1 M $HClO_4$, pH = 0) to Q-terminated SAMs. The quinone reacts rapidly and chemoselectively with an oxyamine-functionalized biomolecule ($RONH_2$), followed by selective protein recognition and binding. Surfaces are then electrochemically reduced (PBS, pH = 7, 60 cyclic scans), and the bound ligand and protein are spontaneously released, regenerating the original SAM. The microarray can then be reused, continuing the cycle with [Ox], ligand and protein immobilization, [Red], and ligand release.

4.3.2 Surface chemistry. The surface chemistry and renewable nature of this microarray technology are illustrated in figures 4.1 and 4.2 and is characterized by CV in figure 4.3. Mixed SAMs of H_2Q/EG_4SH are electrochemically oxidized (1 M $HClO_4$, pH of 0, scan rate of 100 mV/s) to Q-terminated groups, which then chemoselectively react with oxyamine-functionalized compounds. In this particular study, our ligands of interest include galactose-, glucose-, and mannose-oxyamine (Gal-ONH_2, **1**; Glc-ONH_2, **2**; and Man-ONH_2, **3**, respectively, Scheme 4.1 and 4.2).[43] After the monosaccharide is covalently bound to the surface through an oxime linkage, its corresponding lectin, sugar-binding protein, is added. The protein then adheres to and interacts with its recognition signal and is able to be characterized by fluorescence microscopy. To regenerate the surface for another subsequent cycle of ligand immobilization, sugars

and lectins are released by applying a constant potential under reducing conditions (PBS, pH = 7, 60 cyclic scans, 15 min). The result consists of a reduced alcohol and renewed H_2Q-terminated SAM; this cycle may be performed again.

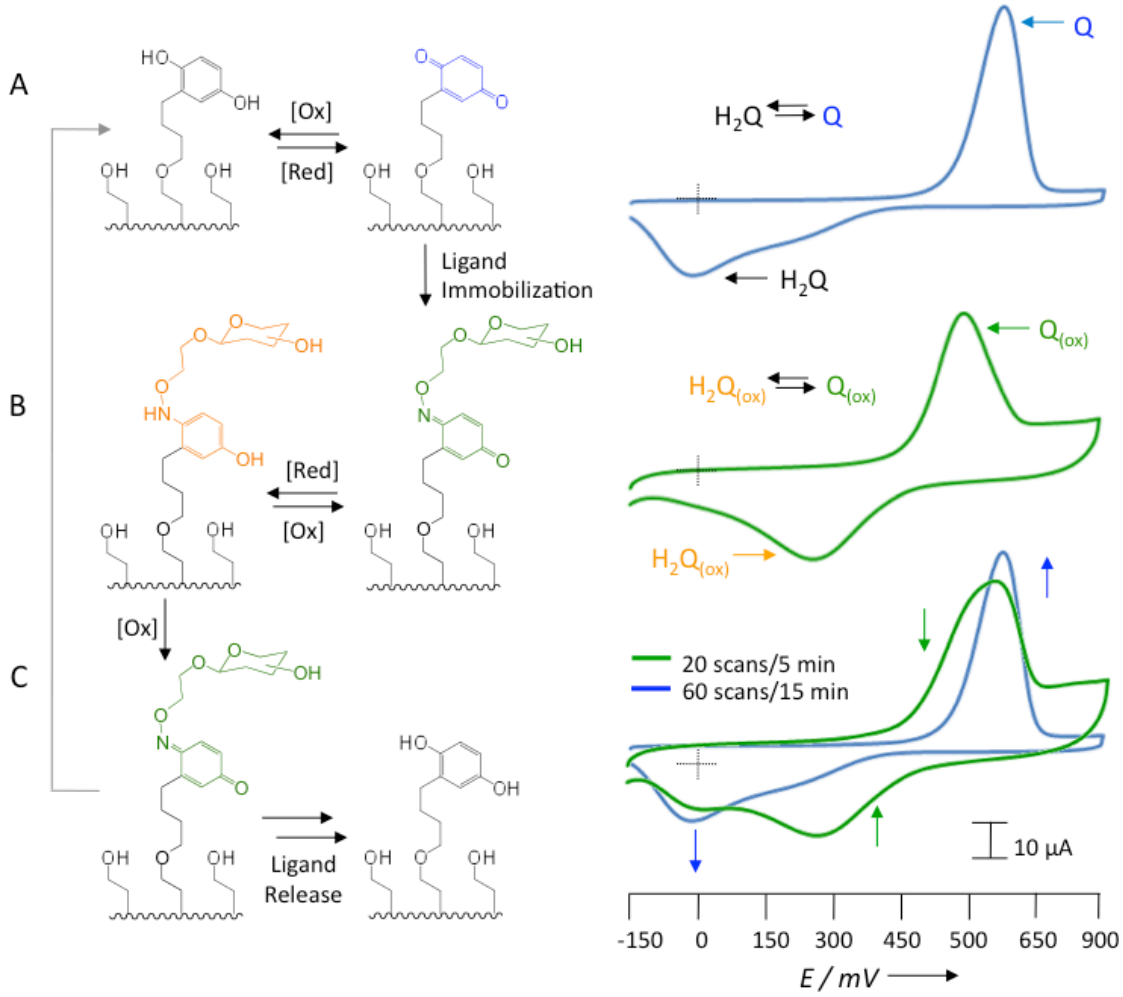

Figure 4.3 Electrochemical characterization of a renewable carbohydrate biosensor that chemoselectively immobilizes and releases oxyamine-containing sugars to and from Q-terminated SAMs on gold. (A) Cyclic voltammetry (CV) shows distinctive redox peaks (blue) of a H_2Q/Q-terminated SAM at [Q] = 630 mV and [H_2Q] = -24 mV. Once an oxyamine-containing carbohydrate is immobilized, (B) the redox peaks (green) shift to [Q_{ox}] = 610 mV and [H_2Q_{ox}] = 283 mV, indicating the presence of an oxime (ox) bond. (C) The bound carbohydrate (green) can be released by electrochemical reduction (20 scans), and the original H_2Q/Q SAM (blue, 60 scans) can be regenerated. The two blue traces in A and C show the same peaks, which correspond to H_2Q/Q before carbohydrate immobilization and after its release.

4.3.3 Electrochemical characterization: Ligand immobilization and release. As previously mentioned, CV was employed to characterize ligand immobilization and

release from Q-terminated SAMs on gold (Figure 4.3). Distinctive H_2Q/Q redox peaks were observed at -24 and 630 mV, respectively (blue trace, Figure 4.3A). Following 4 h of sugar-oxyamine conjugation (90 mM in H_2O), peaks were completely shifted to 283 and 610 mV (green trace, Figure 4.3B), indicating full oxime (H_2Q_{ox}/Q_{ox}) bond formation. It is also important to note that the sugar-Q reaction was also monitored at various time points to determine the percentage of ligand bound, as well as the approximate rate of product conversion. To release the ligand and regenerate the original H_2Q/Q-terminated SAM (blue, Figure 6.3C), potential was applied for 60 cyclic scans, or 15 min, under reducing conditions (PBS, pH = 7). Approximately one-third of the carbohydrate ligand was released following 20 scans, as shown in the green trace in figure 4.3C, with the presence of H_2Q/Q production.

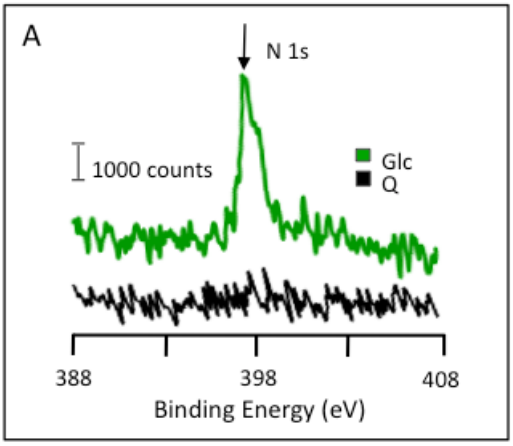

B				
Surface Group	Au			
Contact Angle (°) ± Std	59.31 ± 3.1	64.19 ± 1.2	58.69 ± 1.5	33.32 ± 1.8

Figure 4.4 X-ray photoelectron spectroscopy (XPS) and contact angle characterization of (A) Q-terminated SAMs before (black) and after reaction with glc-ONH_2 (green). The 1s nitrogen peak found at 398 eV, corresponds to the presence of an oxime linkage after reaction with glc-oxyamine. (B) Contact angle measurements of water taken on bare gold and SAMs presenting quinone-, hydroquinone-, and carbohydrate-terminated groups.

4.3.4 Surface characterization. Additional surface characterization was conducted to confirm that consistent SAMs of H_2Q/Q were being formed and that oxyamine-functionalized carbohydrates were being immobilized after reaction. The static contact angle of water (10 μL) was measured on bare gold substrates and on surfaces with SAMs of Q-, H_2Q-, and Glc-presenting groups (Figure 4.4B). There was a significant decrease in the contact angle, from 64.19° to 33.32°, for unreacted Q-terminated SAMs and Q-containing SAMs reacted with glc-ONH_2 (90 mM in H_2O, 4 h), respectively. The large difference in contact angle is accounted for in the increase of wettability and cohesive forces between the water and hydrophilic hydroxyl groups, indicating there was successful attachment of carbohydrate-oxyamine ligands. X-ray photoelectron spectroscopy (XPS) was also performed to confirm oxyamine conjugation to substrates bearing Q-terminated SAMs. The 1s nitrogen peak observed at 398 eV, corresponds to the presence of glc-ONH_2 immobilized to the surface (green trace, supporting information, Figure 4.4A), while there is no nitrogen present on substrates with Q-terminated SAMs, as shown by the black trace.

4.3.5 Molecule density quantification. Electrochemistry was also used to quantify the density of H_2Q/Q and immobilized ligands following microarray construction and conjugation, respectively. Alkanethiol solutions containing different ratios of H_2Q/EG_4SH (0:100, 25:75, 50:50, 75:25, and 100:0) were transferred to bare gold surfaces, generating highly reproducible and consistent 24 x 24 microarrays of 100 μm in diameter, SAM spots (Figure 4.5A). To determine whether the corresponding percentage of H_2Q molecules was being printed on the surface, we integrated the CV peak area to calculate the total charge and applied the relationship $Q = nFA\Gamma$ (where Q = total charge, n = number of electrons, 2 for H_2Q, F = Faraday constant, A = surface reaction

area [(spot size) x (number of spots)], and surface density of H_2Q (Γ_{H2Q}(molecules/μm^2)). The surface density can then be directly correlated to the spotting solution concentration of H_2Q by plotting $\chi_{H2Q\text{-}Surface}$ versus $\chi_{H2Q\text{-}Solution}$ (Figure 4.5C) ($\chi_{H2Q\text{-}surface}$ represents the ratio of H_2Q molecule on a mixed SAM surface, and $\chi_{H2Q\text{-}Solution}$ represents the ratio of H_2Q in the microwell solution). Following transfer, all surfaces were electrochemically oxidized, reacted with gal-, glc-, and man-ONH_2 (90 mM in MeOH, 4 h), and the oxime linkages were analyzed by CV (in triplicate for each sugar at each density, Figure 4.5B). Likewise, $\chi_{H2Q\text{-}Surface}$ can be correlated to the density of ligand bound, χ_{Ligand} (Figure 4.5D). The slope of both plots is linear, indicating that H_2Q and ligand density is in accord with the spotting solution H_2Q ratio.

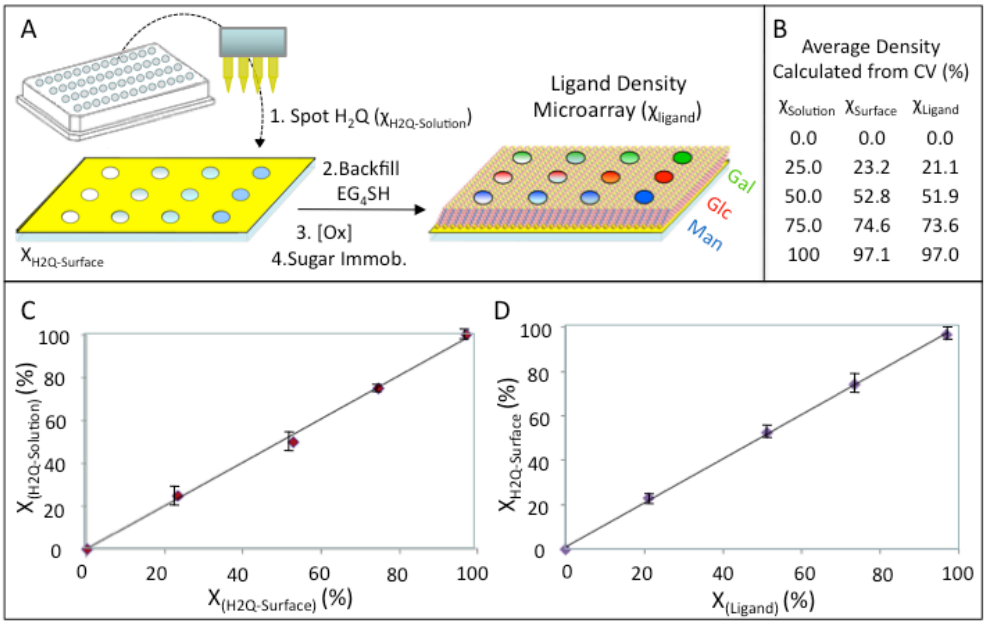

Figure 4.5 A quantitative comparison of alkanethiol solution density transferred to gold surfaces and the SAM and ligand density microarrays. (A) The general strategy to generate a ligand density microarray for carbohydrate immobilization. (B) The average density percentages calculated by integrating the redox peak area observed from the CV data and applying Q = nFAΓ. (C) A plot describing the relationship between the ratio of alkanethiol solution ($\chi_{H2Q\text{-}Solution}$) originally transferred to the surface and average-measured surface density of H_2Q molecules ($\chi_{H2Q\text{-}Solution}$). (D) The correlation between $\chi_{H2Q\text{-}Surface}$ and the density of ligand bound, χ_{Ligand}. The slope of both plots is linear, indicating that the H_2Q and ligand density within the spots on the SAM surface is in accord with the spotting solution H_2Q concentration. The averaged percentages of H_2Q and ligand on the surface, according to solution densities, 0, 25, 50, 75 and 100 %.

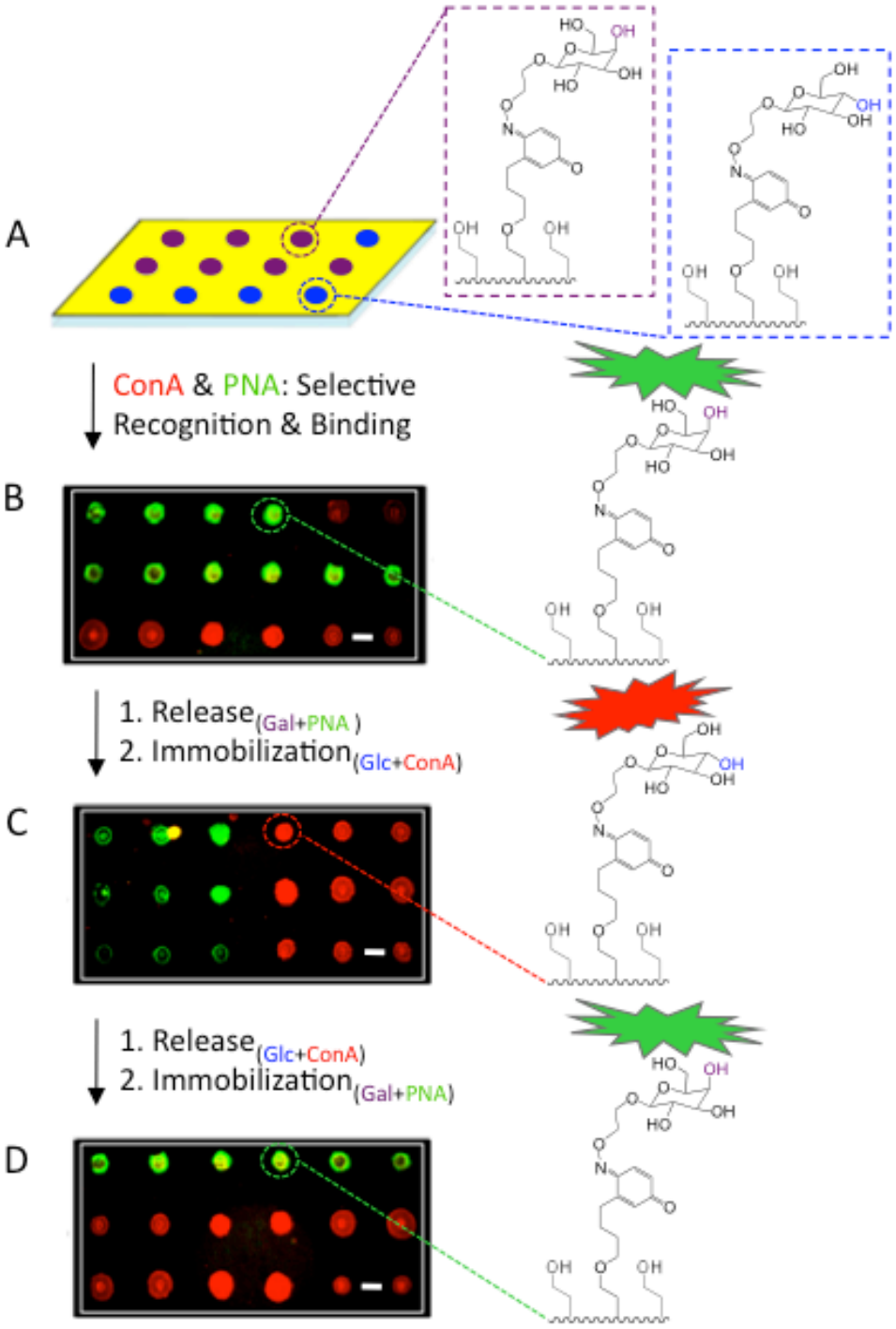

Figure 4.6 Fluorescent micrographs displaying a renewable microarray for carbohydrate immobilization and subsequent lectin recognition and adhesion. (A) A microarray of H_2Q/EG_4SH SAMs were generated using automated technology, and gal- (purple) and glc- (blue) ONH_2 were immobilized via random spotting, followed by subsequent adhesion of PNA (green) and ConA (red). (B) After electrochemical release of all ligands and regeneration of the original surface, gal and glc were again transferred randomly. (C) PNA and ConA were then added for specific carbohydrate recognition. The ligands were again released to renew the substrate, and (D) the immobilization process was performed for a third time.

4.3.6 Biospecific lectin detection. Although our renewable and quantitative ligand microarray strategy was designed for a number of biological systems, we chose to represent the biospecific interactions between carbohydrate ligands and lectins. Figure 4.6 displays three cycles of ligand immobilization and release. Automated microarray technology was utilized to generate a 24 x 24 microarray of 100 μm in diameter spot-arrays of H_2Q/Eg_4SH-containing alkanethiolates (1:9, 1 mM in EtOH) on a bare gold substrate. Glc- and gal-ONH_2 (10 μL, 90 mM in MeOH) were transferred to the microarray of SAMs at random using the same program. The surface was then backfilled with EG_4SH (1 mM in EtOH, 16 h), and a mixture containing fluorescently-conjugated concanavalin A (ConA, 1 mg/mL in H_2O, 2 h) and peanut agglutinin (PNA, 1 mg/mL in H_2O, 2 h) was allowed to bind. ConA and PNA are lectins, known to specifically recognize and bind to glucose and galactose residues, respectively. Carbohydrate ligands and lectins were then released from the substrate after 60 cyclic scans of electric potential (PBS, pH = 7, 15 min), renewing the original mixed H_2Q/EG_4SH-terminated SAM microarray, which was also determined by electrochemistry. Glc- and gal-ONH_2 were again randomly delivered to the SAM microarray, followed by reaction with ConA and PNA for two more cycles. Carbohydrate-protein binding was then analyzed by fluorescence microscopy (Figure 4.6B). As a control, lectins were added to H_2Q-presenting microarrays with no immobilized sugars, and minimal fluorescence was detected. To assure selectivity of ConA for mannose and glucose and PNA for galactose residues, carbohydrates were randomly tethered to the surface and a mixture containing both proteins was allowed to react. Images displayed color separation, with little to no overlap, indicating that the lectins were able to recognize and successfully interact with their respective adhesive signal.

4.4 Conclusions

In summary, we have developed a renewable, chemoselective, and quantitative ligand density microarray for the rapid analyses of biological interactions. Automated technology was used to transfer different mixtures of H_2Q- and EG_4SH-terminated alkanethiols to a bare gold substrate, resulting in the tailoring of SAM microspots (100 μm diameter). Following electrochemical oxidation of H_2Q to the corresponding Q, oxyamine compounds were reacted and immobilized to the microarray. A number of monosaccharides (mannose, glucose, and galactose) were synthesized to incorporate oxyamine functionality and tethered to the surface. The oxime linkages were confirmed and characterized by CV, XPS, and contact angle. By applying constant potential (15 min) under reducing conditions (PBS, pH = 7), sugar ligands were released, renewing the original H_2Q-terminated array for another round of immobilization and release. The extent of the molecule reaction, as well as its release and amount bound was monitored and quantified by CV. Fluorescently-conjugated, carbohydrate-binding proteins ConA and PNA were added to the microarray following man-, glc-, and gal-ONH_2 reaction, and substrates were visualized by fluorescence microscopy. The images displayed distinctly colored spots, corresponding to specific signal (sugar) recognition, indicating successful observation of ligand-receptor interactions on our platform. This method may be applied to a variety of scientific fields for use in biosensor technology and the generation of renewable and tailored microarrays for biospecific cell- and bacteria-based assays.

References

(1) Laurent, N.; Haddoub, R.; Flitsch, S. L. *Trends. Biotechnol.* **2008**, *26*, 328-337.

(2) Ramsey, G. *Nat. Biotechnol.* **1998**, *16*, 40-44.

(3) Perou, C. M. *Nature*, **2000**, *406*, 747-752.

(4) Laurent, N.; Haddoub, R.; Voglmeir, J.; Wong, S. C. C.; Gaskell, S. J.; Flitsch, S. L. *ChemBioChem*. **2008**, *9*, 2592-2596.

(5) Zhi, Z.-L.; Laurent, N.; Turnbull, J. E. *ChemBioChem*, **2008**, *9*, 1568-1575.

(6) Park, S.; Lee, M.-R.; Pyo, S.-J.; Shin. I. *J. Am. Chem. Soc.* **2004**, *126*, 4812-4819.

(7) Houseman, B. T.; Gawalt, E. S.; Mrksich, M. *Langmuir*, **2002**, *19*, 1522-1531.

(8) Min, D.-H.; Su, J.; Mrksich, M. *Angew. Chem. Int. Ed.* **2004**, *43*, 5973-5977.

(9) Harder, P.; Grunze, M.; Dahint, R.; Whitesides, G. M.; Laibinis, P. E. *J. Phys. Chem. B*, **1998**, *102*, 426-236.

(10) Kreuzer, H. J.; Wang, R. L. C.; Grunze, M. *J. Am. Chem. Soc.*, **2003**, *125*, 8384-8389.

(11) Ostuni, E.; Chapman, R. C.; Liang, M. N.; Meluleni, G.; Pier, G.; Ingber, D. E.; Whitesides, G. M. *Langmuir*, **2001**, *17*, 6336-6343.

(12) Watzke, A.; Kohn, M.; Wacker, R.; Schroder, S. L.; Waldmann, H. *Angew. Chem. Int. Ed.* **2006***, 45,* 1408-1412.

(13) Kohn, M.; Wacker, R.; Peters, C.; Schroder, H.; Soulere, L.; Breinbauer, R.; Niemeyer, C. M.; Waldmann, H. *Angew. Chem. Int. Ed.* **2003**, *42*, 5830-5834.

(14) Zhang, Y.; Wang, P. G. *Anal. Chem.* **2006***, 78*, 2001-2008.

(15) Houseman, B. T.; Mrksich, M. *Langmuir,* **2002***, 19,* 1522-1531.

(16) Lahiri, J.; Isaacs, L.; Whitesides, G. M. *Anal. Chem.* **1999**, *71*, 777-790.

(17) Yousaf, M. N.; Houseman, B. T.; Mrksich. M. *Angew. Chem*. **2001**, *113*, 1127-1130.

(18) Yousaf, M. N.; Houseman, B. T.; Mrksich, M. *Proc. Natl. Acad. Sci. USA*, **2001**, *98*, 5992-5996.

(19) Yousaf, M. N.; Mrksich, M. *J. Am. Chem. Soc.* **1999**, *121*, 4286-4287.

(20) Chan, E. W. L.; Yousaf, M. N. *ChemPhysChem* **2007**, *8*, 1469-1472.

(21) Park, S.; Yousaf, M. N. *Langmuir* **2008**, *24*, 6201-6207.

(22) Chan, E. W. L.; Yousaf, M. N. *J. Am. Chem. Soc.* **2006***, 128,* 15542-15546.

(23) Westcott, N. P.; Yousaf, M. N. Langmuir **2008**, 24, 2261-2265.

(24) Chan, E. W. L.; Park, S.; Yousaf, M. N. *Angew. Chem. Int. Ed.* **2008**, *47*, 6267-6271.

(25) Lee, E.-J.; Chan, E. W. L.; Yousaf, M. N. *ChemBioChem,* **2009**, *10*, 1648-1653.

(26) Zachara, N. E.; Hart, G. W. *Chem. Rev*. **2002**, *102*, 431-438.

(27) Roth, J. *Chem. Rev.* **2002**, *102,* 285-303l.

(28) Sugahara, K.; Mikami, T.; Uyama, T.; Mizuguchi, S.; Nomura, K.; Kitagawa, H. *Curr. Opin. Struct. Biol.* **2003**, *13*, 612-620.

(29) Gama, C. I.; Hsieh-Wilson, L. C. *Curr. Opin. Struct. Biol.* **2005**, *9*, 609-619.

(30) Whelan, S. A.; Hart, G. W. *Circ. Res.* **2003**, *93*, 1047-1058.

(31) Bertozzi, C. R.; Kiessling, L. L. *Science*, **2001**, *291*, 2357-2360.

(32) Osborn, H. M. I.; Evans, P. G.; Gemmell, N.; Osborn, S. J*. Pharm. Pharmacol*. **2004**, *56*, 691-702.

(33) Danishefsky, S. J.; Allen, J. R. A. *Angew. Chem. Int. Ed.* **2000**, *39*, 836-839.

(34) Hatch, D. M.; Weiss, A. A.; Kale, R. R.; Iyer, S. S. *ChemBioChem*, **2008**, *9*, 2433-2442.

(35) Houseman, B. T.; Mrksich, M. *Chem & Biol*. **2002**, *9*, 443-454.

(36) Hatch, D. M.; Weiss, A. A.; Kale, R. R.; Iyer, S. S. *ChemBioChem*, **2008**, *9*, 2433-2442.

(37) Nilsson, K. G. I.; Mandenius, C.-F. *Nature*, **1994**, *12*, 1376-1378.

(38) Laurent, N.; Voglmeir, J.; Wright, A.; Blackburn, J.; Nhan, P. T.; Wong, S. C. C.; Gaskell, S. J.; Flitsch, S. L. *ChemBioChem*, **2008**, *9*, 883-887.

(39) Pale-Grosdemange, C.; Simon, E. S.; Prime, K. L.; Whitesides, G. M. *J. Am. Chem. Soc.* **1991**, *113*, 12-20.

(40) Hoover, D. K.; Lee, E.-J.; Chan, E. W. L.; Yousaf, M. N. *ChemBioChem* **2007**, *16*, 1920-1923.

(41) Hoover, D. K.; Chan, E. W. L.; Yousaf, M. N. *J. Am. Chem. Soc.* **2008**, *130*, 3280-3281.

(42) Dillmore, W. S.; Yousaf, M. N.; Mrksich, M. *Langmuir*, **2004**, *20*, 7223-7231.

(43) Cao, S.; Tropper, F. D.; Roy, R. *Tetrahedron Lett.* **1995**, *51*, 6679-6686.

(44) Renaudet, O.; Dumy, P. *Tetrahedron Lett.* **2001**, *42*, 7575-7578.

CHAPTER 5

Dynamic Dual Ligand Extracellular Matrix: *In Situ* Modulation of Cell Behavior

5.1 Introduction

The extracellular matrix (ECM) is a highly dynamic, insoluble aggregate of collagens, proteoglycans, structural glycoproteins, and elastin, which provide structural support for and control the adhesion, growth, differentiation, metabolic state, migration, and survival of mammalian cells.[1-3] Improper cell attachment and migration have been implicated in cancer cell metastasis and other diseased states, including fibrosis.[4-7] For a cell to undergo proper migration, it must first adhere to another cell or the ECM through cell surface receptor-ligand interactions.[8] Integrins and syndecans, which are transmembrane proteins, represent the most common cell surface receptor families that facilitate cell adhesion to the ECM and transduce extra- and intracellular signals.[9-11]

Fibronectin (FN) is a predominant ECM glycoprotein that contains three homologous globular domains: type I, II, and III and has a number of interaction sites for both integrins and syndecans.[12] As such, FN plays an important role in cell adhesion, growth, migration, and differentiation and is critical to cellular processes, including embryogenesis and tissue repair.[13] A number of cell types bind FN to regions that span the 8th to 10th type III ($FNIII_{8-10}$) cell-binding domain. Arg-Gly-Asp (RGD), found in $FNIII_{10}$, was identified as the minimal cell attachment sequence via $\alpha_5\beta_1$ and $\alpha_V\beta_3$ integrins recognition.[14] A synergy site that presents Phe-His-Ser-Arg-Asn (PHSRN) was

then located in $FNIII_9$ and shown to enhance FN's association with $\alpha_5\beta_1$ integrins, mediating cell adhesion and migration.[15-18] RGD and PHSRN are presented on the same plane of FN, connected by a flexible 30-40 Å linker.[19] The spatial orientation and positioning are crucial for inducing synergistic effects on cell adhesion and migration. Furthermore, conflicting reports of whether PHSRN is alone capable of supporting cell adhesion have been a topic of debate over the last decade.[15-18]

Although $\alpha_5\beta_1$ and $\alpha_V\beta_3$ integrins serve as the primary cell surface receptors that mediate adhesion, syndecan-4, a transmembrane heparan sulfate proteoglycan (HSPG), is known to be a co-receptor for FN.[20,21] A HS-binding domain spans $FNIII_{12}$ to $FNIII_{14}$. Simultaneous interaction of syndecan-4 and $\alpha_5\beta_1$ integrin with $FNIII_{12\text{-}14}$ and $FN_{8\text{-}10}$, respectively, induces downstream signaling events, leading to the activation of focal adhesion kinase (FAK) and extracellular signal-regulated kinase (ERK) and subsequent complete cell attachment and enhanced spreading via focal adhesion complex (FAC) formation.[12,20,21] A few HS-binding mimics have been hypothesized; however, similar to the synergistic effect of RGD and PHSRN on cell adhesion, these small molecules or sequences have been reported to be less efficient in promoting cell attachment alone. Such mimics contain the sequence: B-B-B-X-X-B, where B is a basic amino acid (e.g., Arg or Lys) and X is a hydropathic amino acid (e.g., Ser, Tyr, or Thr).[22-24] Conflicting hypotheses regarding the role of HS-binding sequences on virus attachment have been reported. Kritz *et al.* reported that the Lys-Lys-Thr-Lys (KKTK) motif, found in the human adenovirus (hAd) fiber shaft, serves a minimal role in binding HSPGs, but is significant virus infection and trafficking into the nucleus.[25] In two separate works, Di Paolo *et al.*[26] and Darr *et al.*[27] demonstrated that different hAd types, which lacked the KKTK motif, were able to attach and infect hepatic cells *in vivo*. However, little is known concerning

the role of HS-binding sequences on cell adhesion and migration and its possible synergistic effects, if any, with RGD.

Due to the complex nature of the ECM, identifying all the diverse small molecules and ligand-cell surface receptor combinations that induce specific biochemical processes remains challenging.[28,29] Rather than performing *in vitro* studies with large native FN (~440 kDa), which is purified from blood plasma and tend to denature or adsorb in unnatural orientations and conformations on surfaces, researchers have sought to discover alternative approaches. As such, tremendous effort has been extended to creating model substrates that mimic the ECM using structurally well defined, decoupled biomolecules, including RGD and PHSRN.[18,30] Such surfaces enable the spatial and temporal presentation of well-defined ligands for the interrogation of biospecific ligand-cell surface receptor interactions, providing great tools for applications in cell biology, biotechnology, and tissue engineering.

Over the last decade, self-assembled monolayers (SAMs) of alkanethiolates on gold have proven to be smart, dynamic, and stimuli-responsive model surfaces for a number of cell biological investigations.[31-33] 'Dynamic' refers to the *in situ* control of cell behavior in response to an applied external stimulus. Liu *et al.* demonstrated that cells attach to the *E* isomer of RGD-conjugated azobenzene SAMs.[34] However, when UV light was irradiated, azobenzene adopted the *Z* conformation, masking RGD, and cells detached. Using a photodeprotection strategy, Lee and colleagues were able to selectively expose and conjugate SAM regions with RGD, probing cell adhesion, polarization, and migration.[35] Recently, Lamb and Yousaf reported a dynamic and switchable strategy based on electrochemically-controlled hydroquinone (HQ) SAMs, in which the affinity of RGD ligands was altered.[36] Upon the application of a specific oxidative (Ox) or reductive (Red) electrochemical potential, the HQ could be turned 'OFF' and 'ON' to reveal or hide

RGD ligands for cell attachment studies. Furthermore, in a reducing environment, HQ SAMs have been shown to release their covalently bound ligand, generating the original surface for subsequent immobilization and release cycles.[37,38] *In vivo*, ECM proteins and cell surfaces are constantly being remodeled and modified, where ligands are subject to different compositions and orientations for biomolecular recognition. Therefore, model substrates that can mimic and modulate the highly evolving ECM would serve as great analytical tools, providing insight into the mechanisms of cell adhesion and migration in real time.

Herein, we report a novel, dynamic, and redox-responsive strategy to immobilize and release ligands in the presence of cells for cell adhesion, spreading, morphology, and migration studies. Electrochemistry enables the complete quantitative control over ligand density and provides a dynamic molecular switch for the combinatorial discovery of ligand effects. Two bioothogonal coupling methodologies, Click and oxime chemistry, were incorporated and an HQ- and azide (N_3)-functionalized RGD peptide (RGD-HQ) was synthesized to modulate the ECM. Commercially available lysine-N_3 and derivatized glycine-HQ were incorporated into Ser-Ser-Asp-Gly-Arg-Gly-C_6 linker via solid-phase peptide synthesis to generate K(N_3)-C6 linker-G(HQ)GRGDSS, where the N_3 moiety is conjugated to alkyne-terminated SAMs via Click chemistry and the HQ serves as a conjugation site for a variety of oxyamine-containing ligands. Synergy peptide PHSRN, high affinity cyclic RGD (cRGD), putative HS-binding sequence KKKTTK, and monosaccharides galactose (Gal) and mannose (Man) were functionalized with oxyamine groups and surveyed for potential synergistic or antagonistic effects with cell-adhesive RGD. Fibroblasts (Fbs) were seeded to the different ECM mimics substrates, with or without RGD-HQ, and the number of attached cells, spreading area, morphologies, and migration rates were tabulated. Inhibition and competitive binding

studies were also performed in which soluble FN, cRGD, and HS were added. Chondroitinase ABC and heparinase I and II were also delivered to Fbs in culture to determine whether HS-binding KKKTTK exhibited a synergistic effect on cell adhesion and spreading. FAK protein levels were also detected and quantified. Furthermore, the ligands were released in the presence of cells, providing the dynamic component to our system, and cell adhesion, morphology, and migration rates were again examined. To our knowledge, this is the first report that uses a density-controlled, bioorthogonal, and stimuli-responsive (i.e., non-invasive electrochemical cue) model ECM to probe ligand-cell surface integrin and syndecan interactions *in situ*. The ability to switch ligands for the combinatorial screening of synergistic of antagonistic ligand effects provides a platform that would be of tremendous significance to the biosensor and biomaterials research communities.

5.2 Methods and Materials

5.2.1 Chemicals and reagents. All chemicals and reagents were of analytical grade and used without further purification. Common chemicals were obtained from Fischer Scientific (Pittsburgh, PA) or Sigma Aldrich (St. Louis, MO) unless specified. Rink amide 4-methylbenzylhydrylamine (MBHA) resin, amino acids (Fmoc-Arg(Pbf)-OH, Fmoc-Asp(OtBu)-OH, Fmoc-Gly-OH, Fmoc-Ser(tBu)-OH, Fmoc-Thr(tBu)-OH, Fmoc-Lys(Boc)-OH, and Fmoc-Lys(N_3)-OH), Boc-aminooxy acetic acid, Fmoc-ε-Ahx-OH, and HBTU were purchased from Anaspec (San Jose, CA). Antibodies anti-paxillin and anti-vinculin and Cy-2 goat anti-mouse IgG were purchased from B D Biosciences (San Jose, CA) and Jackson ImmunoResearch Laboratories, Inc. (West Grove, PA), respectively. Fluorescent dyes, DAPI and phalloidin and penicillin/streptomycin were obtained from Invitrogen (Carlsbad, CA). Fluorescence mounting medium was purchased from Dako (Carpinteria, CA). Swiss albino 3T3 mouse fibroblasts were obtained from the UNC-CH

Tissue Culture Facility (Chapel Hill, NC). Heparan sulfate, heparinase I and II, and chondroitinase ABC were obtained from Sigma Aldrich (St. Louis, MO).

5.2.2 Syntheses. Alkyne-terminated tetra(ethylene glycol) alkanethiol (alkyne-EG_4SH, **7**) was synthesized as previously reported.[39] Tetra(ethylene glycol)-terminated alkanethiol (EG_4SH, **8**) was prepared as previously described.[40] Rhodamine-oxyamine (Rhod-OA) was synthesized as previously demonstrated.[41] Galactose- and mannose-oxyamine (**5** and **6**, respectively) were also synthesized as previously reported.[38]

*1,4-bis((tetrahydro-2H-pyran-2-yl)oxy)benzene (**A**).* To a solution of hydroquinone (6.0 g, 54.5 mmol) in tetrahydrofuran (THF, 40 mL) was added 3,4-dihydropuran (20.8 mL, 245.3 mmol, 4.5 eq.) and three drops of concentrated HCl (cat.). The mixture was stirred for 16 h at room temperature. The reaction contents were then diluted with ethyl acetate (EtOAc, 20 mL) and extracted with 1 M sodium bicarbonate (3 x 25 mL) and brine (1 x 25 mL) and concentrated to afford a white solid **A**. The solid product was dried under vacuum for an additional 3 h (10.23 g, 67.4 %). ^{1}H NMR (400 MHz, $CDCl_3$, ∂): 1.58-1.67 (m, 6H, J = 36 Hz; -CH_2-), 1.85-1.88 (m, 4H, J = 12 Hz; -CH_2-), 2.00-2.03 (m, 2H, J = 8 Hz; -CH_2-), 3.60-3.62 (m, 2H, J = 8 Hz; -CH_2-), 3.96-3.98 (m, 2H, J = 8 Hz; -CH_2-), 5.32-5.34 (t, 2H, J = 7 Hz; -CH-), 7.00 (s, 4H; Ar-H).

*2,2'-((2-(6-bromohexyl)-1,4-phenylene)bis(oxy))bis(tetrahydro-2H-pyran) (**B**).* To a stirring solution of **A** (3.0 g, 10.8 mmol) in dry THF (100 mL) at 0 ºC was added tert-butyllithium (1.5 M in pentane, 10.1 mL, 13.0 mmol, 1.2 eq.) dropwise. After the base addition, a white precipitate formed. The mixture was stirred for 2 h at 0 ºC and then warmed to room temperature for 3 h. 1,6-dibromohexane (3.3 mL, 21.6 mmol, 2 eq.) was then added, and the reaction was stirred for 16 h to afford a pale yellow liquid. The mixture was then diluted with EtOAc (20 mL) and extracted with $NH_4^+Cl^-$ (2 x 25 mL), H_2O (1 x 50 mL), and brine (1 x 50 mL), dried over $MgSO_4$, and concentrated to a pale

yellow oil. Silica flash column chromatography (Hex/EtOAc/DCM, 8:1:1) was employed to purify **B** (2.4 g, 50.6 %). ^{1}H NMR (400 MHz, $CDCl_3$, ∂): 1.40-1.42, 1.46-1.47 (d x m, 4H, J = 8 Hz; -CH_2-), 1.49 (m, 8H, -CH_2-), 1.86-1.88 (m, 6H, J = 8 Hz; -CH_2-), 2.02 (m, 2H; -CH_2-), 2.60-2.62 (t, 2H, J = 8 Hz; -CH_2-), 3.41-3.44 (m, 2H, J = 12 Hz; -CH_2-), 3.61-.3.62 (m, 2H, J = 4 Hz; -CH_2-), 3.96-3.99 (m, 2H, J = 12 Hz; -CH_2-), 5.31 (s, 2H; -CH_2-), 6.85-6.87 (m, 2H, J = 8 Hz; Ar-H), 7.02-7.04 (d, 1H, J = 8 Hz; Ar-H).

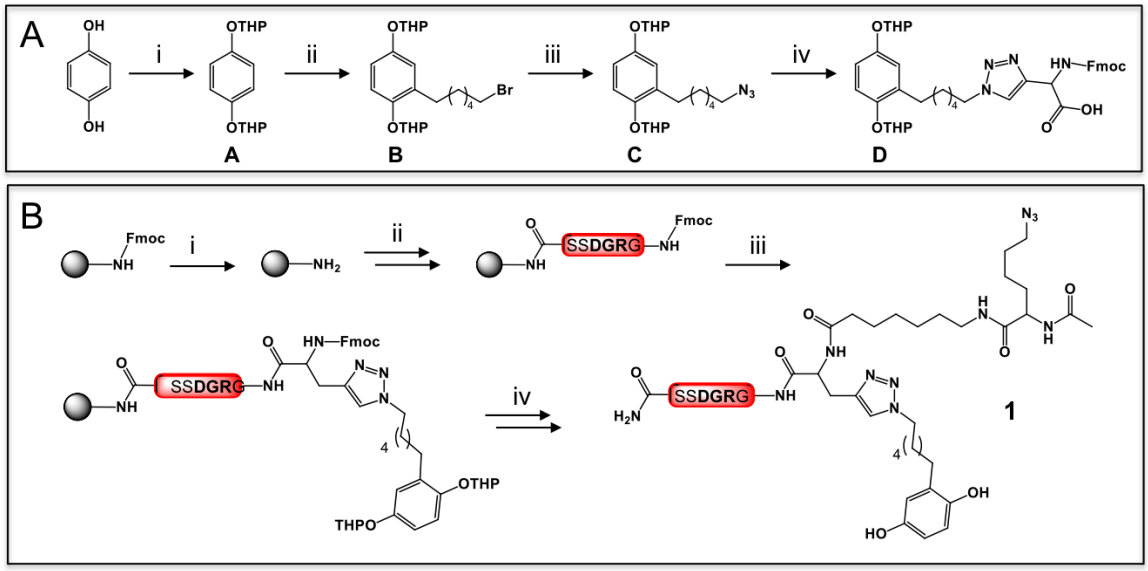

Scheme 5.1 Synthetic scheme of HQ-RGD. (A) Reagents and conditions for the solution synthesis of Fmoc-glycine-HQ. (i) DHP (4.5 eq.), HCl (cat.), THF, 16 h, 67.4 %; (ii) t-butyllithium (2 eq), 1,6-dibromohexane (2 eq), dry THF, 0 - 25 °C, 20 h, 50.6 %; (iii) NaN_3 (1.5 eq), DMF, 2 h, 80 °C; and (iv) Fmoc-propargylglycine (0.5 eq), $CuSO_4$•$5H_2O$ (1.5 eq), NaAsc (1.5 eq), DMF/H_2O/EtOH (2:1:1), 12 h, 61.1 %; (B) Reagents and conditions for the solid phase peptide synthesis of RDG-HQ using MBHA resin. (i) piperidine (20 %); (ii) repetition of DIEA (3 eq), HBTU (3 eq), Fmoc-amino acid (SSDGRG, 3 eq), DMF, then piperidine (20 %); (iii) DIEA (3 eq), HBTU (3 eq), Fmoc-Gly-HQ (3 eq), DMF, then piperidine (20 %); (iv) DIEA (3 eq), HBTU (3 eq), Fmoc-C_6-linker (3 eq), Fmoc-Lys-N_3 (3 eq), piperidine (20 %), acetic anhydride (10 %), then TFA/H_2O (9.75/0.25, 2 h), ether suspension, centrifugation (2 x 2,000 rpm, 10 min), dissolve and freeze in H_2O (10 mL), lyophilize. Overall yield: 54 mg, 65 %.

*2,2'-((2-(6-azidohexyl)-1,4-phenylene)bis(oxy))bis(tetrahydro-2H-pyran) (**C**).* To a solution of **B** (1.90 g, 4.32 mmol) in DMF at 80 ºC was added sodium azide (0.56 g, 8.64 mmol, 2 eq.). The mixture was stirred for 2 h at 80 ºC and was then cooled, diluted with DCM (20 mL), extracted with H_2O (3 x 25 mL), dried over $MgSO_4$, and concentrated to

afford pale yellow oil **C** (1.72 g, 99.9 %). No further purification was required. ^{1}H NMR (400 MHz, $CDCl_3$, ∂): 1.38-1.39 (m, 4H, J = 4 Hz; -CH_2-), 1.59-1.61 (m, 10H, J= 8 Hz; -CH_2-), 1.84-1.85 (m, 4H, J = 4 Hz; -CH_2-), 1.95-1.97 (m, 2H, J = 8 Hz; -CH_2-), 2.57-2.61 (t, 2H, J = 16 Hz; -CH_2-), 3.23-3.26 (m, 2H, J = 12 Hz; -CH_2-), 3.56-.3.61 (m, 2H, J = 16 Hz; -CH_2-), 3.86-3.96 (m, 2H, J = 40 Hz; -CH_2-), 5.28-5.30 (m, 2H, J =8 Hz; -CH_2-), 6.80-6.82 (m, 2H, J = 8 Hz; Ar-H), 6.99-7.01 (d, 1H, J = 8 Hz; Ar-H).

*2-((((9H-fluoren-9-yl)methoxy)carbonyl)amino)-3-(1-(6-(2,5-bis((tetrahydro-2H-pyran-2-yl)oxy)phenyl)hexyl)-1H-1,2,3-triazol-4-yl)propanoic acid (Fmoc-Gly(HQ), **D**).* To a solution of **C** (1.64 g, 4.51 mmol, 2 eq.) and Fmoc-propargylglycine (0.76 g, 2.26 mmol) in DMF (20 mL) EtOH (5 mL) was added a solution of $CuSO_4$•$5H_2O$ (0.85 g, 3.38 mmol, 1.5 eq.) and sodium ascorbate (0.67 g, 3.38 mmol, 1.5 eq.) in H_2O (10 mL) and EtOH (5 mL). The reaction formed a cloudy orange precipitate and was stirred for 16 h at room temperature. The mixture was diluted with DCM (30 mL) and extracted with H_2O (4 x 100 mL), stirred in a solution containing EDTA (2 x 50 mL, 10 mM in H_2O) for 10 min, dried over $MgSO_4$, and concentrated. The colorless oil was then purified via silica flash column chromatography using a gradient of MeOH/DCM (0-5 % MeOH) to afford white solid **D** (1.02 g, 61.1 %). HRMS (*m/z*): $[M]^+$ calcd. for $C_{42}H_{50}N_4O_8$, 738.36; found, 738.38. HPLC: t_r = 15.2 min, 0.1 % TFA and 5-50 % H_2O/ACN over 25 min.

5.2.3 Solid-phase peptide syntheses (SPPS). Rink amide MBHA resin (0.127 g, 0.1 mmol) was delivered to an automated glass chamber for peptide synthesis. The amino acids listed above were measured (0.30 mmol) and diluted in 5 mL of DMF (10 mL for Ser and Gly) and also delivered to peptide synthesizer chambers. The following reagents were prepared in DMF: 0.1 HBTU, 0.1 M DIEA, and 20 % piperidine. The peptide synthesizer (C S Bio Co., Peptide Synthesizer Division, Menlo Park, CA) was programmed to generate the following sequences, separately, over the course of 12 h:

resin-S-S-D-G-R-G-G(HQ)-C_6(linker)-K(N_3)-amide, (**1**); resin-S-D-G-R-G-C_6(linker)-ONH_2, (**2**); resin-N-R-S-H-P-K-C_6(linker)-ONH_2, (**3**); and resin-K-T-T-K-K-K-C_6(linker)-ONH_2, (**4**). Following elongation, the resin was washed with DMF and DCM repeated and then cleaved from the resin in an N_2-bubbling solution of H_2O/TFA (10 mL, 0.25:9.75) for 1 h. The filtrate was drained into a tube containing cold ether to form a white precipitate that was then centrifuged (2 x 2,000 rpm, 10 min), dissolved in H_2O (10 mL), and lyophilized (FreeZone 2.5, Labconco Corporation, Kansas City, MO) overnight to afford white solid **1** (54 mg, 65 %). HRMS (*m/z*) RGD-HQ: $[M]^{2+}$ calcd. for $C_{52}H_{84}N_{19}O_{16}$, 615.32; found, 616.47. HRMS (*m/z*) RGD-OA: $[M]^+$ calcd. for $C_{25}H_{46}N_{11}O_{11}$, 676.34; found, 676.31. HRMS (*m/z*) PHSRN-OA: $[M]^+$ calcd. for $C_{38}H_{67}N_{16}O_{11}$, 923.52; found, 923.56. HRMS (*m/z*) KKTTK-OA: $[M]^+$ calcd. for $C_{40}H_{79}N_{13}O_{11}$, 917.59; found, 917.46.

5.2.4 Preparation of gold-coated substrates and monolayers. Glass cover slips (75 mm x 25 mm) were immersed into a piranha solution (**use with caution:** 1:3 (v:v) concentrated H_2SO_4:30 % H_2O_2) for 4 h, followed by rinsing with deionized H_2O and EtOH. Gold substrates were prepared by electron-beam deposition (Model VE-100, Thermionics Laboratory, Inc., Port Townsend, WA) of titanium (5 nm) and then gold (12 nm for cell work and 50 nm for electrochemical measurements). The gold-coated slides were cut into 1 x 2 cm^2 pieces. To form SAMs on gold, the slides were immersed in an ethanolic solution containing the alkanethiols (1 mM of 5 % alkyne-EG_4SH for cell studies and 100 % alyne-EG_4SH for electrochemical characterization) for at least 16 h. Once removed from solution, the surfaces were rinsed with EtOH and dried with an air stream before use.

5.2.5 RGD-HQ immobilization. After monolayer formation with 1 mM of 1 % alkyne-EG_4SH/EG_4SH, a solution containing 10 mmol RGD-HQ, 15 mmol $CuSO_4 \cdot 5H_2O$, and 15

mmol NaASc (1:1:1) in H_2O and EtOH (3:1) was added as to the substrates and allowed to react for 90 min. Substrates were then rinsed with EtOH and dried with a stream of air, and RGD-HQ immobilization was confirmed by cyclic voltammetry (CV).

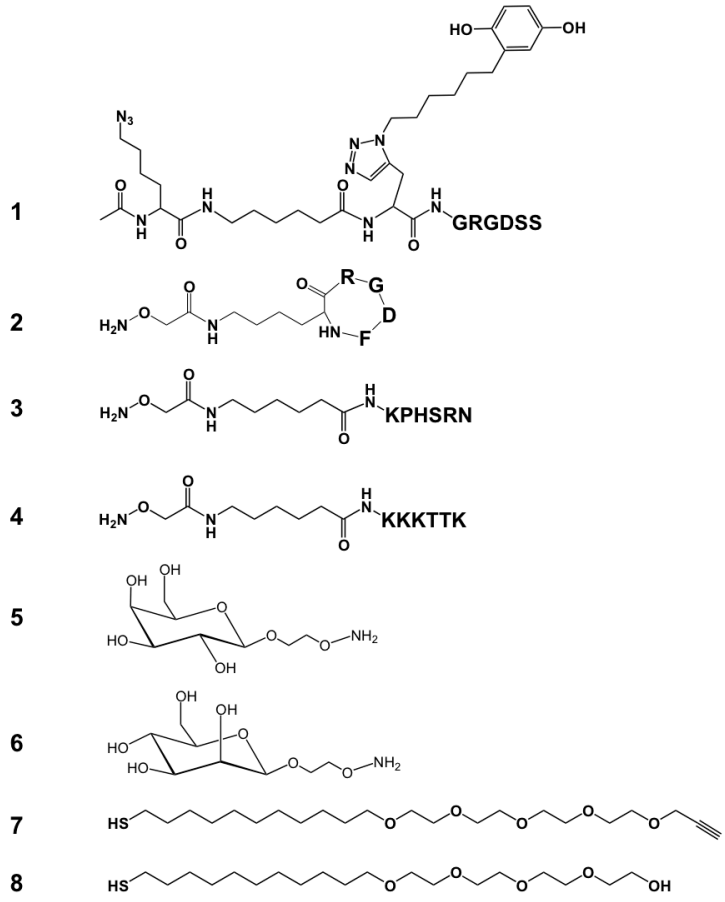

Scheme 5.2 List of molecules and surface groups used in this study. The following molecules are depicted: (1) hydroquinone- and azide-functionalized RGD, HQ-RGD; (2) cyclic RGD-functionalized oxyamine, cRGD; (3) PHSRN-functionalized oxyamine, PHSRN; (4) KKKTTK-functionalized oxyamine, KKKTTK; (5) galactose-functionalized oxyamine, Gal; (6) mannose-functionalized oxyamine, Man; (7) alkyne-terminated tetra(ethylene glycol) alkanethiol; alkyne-EG_4SH; and (8) tetra(ethylene glycol)-terminated alkanethiol; EG_4SH.

5.2.6 Electrochemical activation. Electrochemical experiments were performed using a BAS 100B/W Electrochemical Analyzer (Bioanalytical Systems, Inc., West Lafayette, IN) in a 1 M $HClO_4$ electrolyte solution with an Ag/AgCl electrode serving as the reference, the gold monolayer as the working electrode, and a Pt wire as the counter

electrode. Surfaces were scanned at a rate of 100 mV/s from -100 to 850 mV to activate "ON" (quinine form).

5.2.7 Ligand immobilization and release. Peptides and sugars were added to RGD-Q-presenting surfaces (20 mM in H_2O) and allowed to react for 90 min. Immobilized ligands were confirmed using the same electrochemical parameters listed above. The ligands were released by applying potential for 12 cyclic scans (-100 - 850 mV) in PBS buffer (pH 7) and were characterized using similar conditions.

5.2.8 Cell culture and surface seeding. Swiss albino 3T3 mouse fibroblasts were cultured in Dulbecco's Modified Eagle Medium containing 10 % calf bovine serum and 1 % penicillin/streptomycin. When passaging or seeding, a 1 mL solution of 0.05 % trypsin in 0.53 mM EDTA was employed to remove cells from the tissue culture plastic. For passaging, cells (10^5 cells/mL) were then added to a new culture flask containing fresh media and placed in the incubator (37 °C, 5 % CO_2) to grow and divide. For surface seeding, cells were re-suspended in serum free medium (10^5 cells/mL) and diluted to 10^3 cells/mL with serum-free medium. The cells were then seeded to surfaces for 2 h, and after 2 h, serum-containing media was added to promote cell growth.

5.2.9 Cell staining. After 2 h of cell growth, the cells were fixed with formaldehyde (3.2 % in PBS) and then permeated (PBS containing 0.1 % Triton X 100). Two fluorescent dye mixtures were made with the following components: 10 mmol phalloidin (1.6 μL), 10 mmol anti-paxillin or 10 mmol anti-vinculin (1 μL), and 5 % normal goat serum with 0.1 % Triton X 100 (397.4 μL) and 10 mmol phalloidin (10 μL), 10 mmol Cy-2 (1.25 μL), 1 mmol DAPI (μL), and 5 % normal goat serum with 0.1 % Triton X 100 (487.8 μL). Cells were immersed in each staining solution for 1 h. The substrates were then secured gold-coated side down in fluorescence mounting medium (Dako, Carpinteria,

CA, USA), which enhances the visualization of cells when viewed under a fluorescent microscope, on a glass coverslip.

5.2.10 Fluorescence microscopy. Fluorescent images were obtained with a Nikon Eclipse TE2000-E inverted microscope (Nikon USA, Inc., Melville, NY) and a Plan Fluor 40X oil immersion objective (1.30 NA, Nikon USA). Immersion oil was purchased from Carl Zeiss MicroImaging, Inc. (Thornwood, NY) and the lens paper was obtained from Fisher. Image analysis was performed using MetaMorph software (Molecular Devices, Downingtown, PA).

5.2.11 Cell adhesion assay. The number of adhered cells were measured 2 h after seeding on the following substrates at 2 % ligand density: ± HQ-RGD and Gal; Man; PHSRN; KKKTTK; and cRGD. Two hundred μL of cells (~10^3 cells/mL) were added to each substrate (1 cm^2), which were subsequently incubated at 37 °C and 5 % CO_2 for 2 h. Two random regions of four different substrates for each ligand combination were imaged at a 4X resolution using a Nikon Eclipse TS100 (Nikon USA, Inc., Melville, NY). The attached cells were then counted. The data are expressed as the mean of 8 replicates ± SEM.

5.2.12 Cell area determination assay. Cell areas (μm^2) were measured 2 h after seeding on the following substrates at 2 % ligand density: ± HQ-RGD and Gal; Man; PHSRN; KKKTTK; and cRGD. Two hundred μL of cells (~10^3 cells/mL) were added to each substrate (1 cm^2), which were subsequently incubated at 37 °C and 5 % CO_2 for 2 h. The cells were then fixed as previously reported, and two random cell areas from four different substrates for each ligand combination were imaged at a 20X resolution using a Nikon Eclipse TS100 (Nikon USA, Inc., Melville, NY), image analyses (Nikon Eclipse TE2000-E inverted microscope; Nikon USA, Inc., Melville, NY), MetaMorph software

(Molecular Devices, Downingtown, PA). The data are expressed as the mean of 8 replicates ± SEM.

5.2.13 Cell migration assay. Cell migration rates were determined after recording the movement of cells on the following substrates at 2 % ligand density: + HQ-RGD and Gal; Man; PHSRN; KKKTTK; and cRGD, for 18 h using image analyses (Nikon Eclipse TE2000-E inverted microscope; Nikon USA, Inc., Melville, NY) and MetaMorph software (Molecular Devices, Downingtown, PA). The data are expressed as the mean of 8 replicates ± SEM.

5.2.14 Electrochemical characterization. RGD-HQ was immobilized to alkyne-terminated SAMs (100%, 1 mM in EtOH, 16 h), as previously described. The immobilization was confirmed using a BAS 100B/W Electrochemical Analyzer (Bioanalytical Systems, Inc., West Lafayette, IN) in a 1 M $HClO_4$ electrolyte solution with an Ag/AgCl electrode serving as the reference, the gold monolayer as the working electrode, and a Pt wire as the counter electrode. Samples were scanned at a 100 mV/s ranging from -100 to 850 mV. To immobilize oxyamine-containing ligands, the substrates were activated and turned “ON” after performing a linear scan from -100 to 850 mV at 100 mV/s. After ligand immobilization, the redox reversible oxime signal was confirmed using CV with the parameters just mentioned. The ligands were then release, as described, and confirmed by CV.

5.2.15 Enzymatic adhesion assay. Fbs (~10^4/mL) were suspended in serum free-containing media and treated separately with heparinase I and heparinase II (0.025 units/mg), chondroitinase ABC (0.025 units/mg), or no enzyme (control) for 30 min at room temperature. Cell were then seeded to substrates presenting 2 % HQ-RGD and 2 % HQ-RGD + KKKTTK for 2 h after which the surfaces were fixed. Two random regions of four different substrates for each ligand combination were imaged at a 4X resolution

using a Nikon Eclipse TS100 (Nikon USA, Inc., Melville, NY). The attached cells were then counted. The data are expressed as the mean of 8 replicates ± SEM.

5.2.16 Cell detachment assay with soluble molecules. Fbs (10^4/mL) were seeded in a suspension of serum free-containing media on the following substrates at 2 % ligand density: HQ-RGD + PHSRN; KKKTTK; or cRGD, for 4 h. After 4 h, several soluble molecules, GRGDS, cGRDSF, HS, and FN (0.1 μM) were added for 1 h. The Fbs were then fixed. Two random regions of three to four different substrates for each ligand combination were imaged at a 4X resolution using a Nikon Eclipse TS100 (Nikon USA, Inc., Melville, NY). The attached cells were then counted. The data are expressed as the mean of 5-8 replicates ± SEM.

5.2.17 Focal adhesion kinase (FAK) assay. Fbs (10^6/mL) were incubated for 4 h on the following substrates at 2 % ligand density: HQ-RGD + PHSRN; KKKTTK; or cRGD. After incubation, the FAK protein levels were detected and quantified using an ELISA kit (Invitrogen, Camarillo, CA), following the manufacturer's instructions. Briefly, the cells (10^6/mL) were removed from each substrate with trypsin, centrifuged (1000 RPM, 5 min), resuspended in ice cold PBS (2 mL), centrifuged (1000 RMP, 5 min), and lysed. Then, 50 μL of the FAK detection antibody was added and incubated with 50 μL of each cell sample for 3 h at room temperature, after which the samples were aspirated and washed with PBS (4 x 2 mL). The samples were then incubated with 100 μL of HRP anti-rabbit antibody for 30 min at room temperature and then washed (4 x 2 mL PBS). One hundred μL of Stabilized Chromagen was then added for 30 min at room temperature, after which 100 μL of Stop Solution was then added to each sample. The optical densities were measured at 450 nm using a Beckman Du-640 spectrophotometer (GMI, Ramsey, MN) and compared to the standard FAK concentrations.

5.3 Results and Discussion

5.3.1 Dynamic surface design and ligand selection rationale. The development and use of smart materials that have switchable or stimuli-responsive properties have proven to be important for a number of biological studies ranging from fundamental basic cell biology research to biomedical implants and tissue engineering scaffolds.[31-33] Therefore, we aimed to modulate the dynamic extracellular matrix (ECM) with redox-responsive surfaces to survey ligands effects on cell behavior. Fibronectin (FN) is an abundant glycoprotein that promotes cell adhesion to the ECM via integrin (i.e., transmembrane, cell surface receptors) interactions. Two key peptide sequences, Arg-Gly-Asp (**1**, RGD, Scheme 5.2) and Phe-His-Ser-Arg-Asn (**3**, PHRSN, Scheme 5.2), located in $FNIII_{10}$ and $FNIII_9$, respectively, were identified as cell-binding ligands. Polymers, nanoparticles, and other biomaterials are routinely functionalized with both linear ($K_d \sim \mu M$) and cyclic (**2**, cRGD; $K_d \sim$ nM, Scheme 5.2) forms of RGD to promote integrin recognition and subsequent cell attachment.[31,42,43] PHSRN is described as a synergy ligand with RGD and interacts simultaneously with $\alpha_5\beta_1$ integrins to mediate cell adhesion and migration.[15-18] Furthermore, a heparan sulfate- (HS) binding domain, located between FNIII[12-14], was identified and promotes cell surface syndecan and integrin co-recognition and interaction. With the FN structure in mind, we hoped to reproduce the combined ligand effects of coupling PHSRN and cRGD with RGD on cell adhesion, spreading, morphology, and migration. As a new ligand, we chose to survey the combined effects of RGD and Lys-Lys-Lys-Thr-Thr-Lys (**4**, KKKTTK, Scheme 5.2), which bares four positive charges, on cell behavior. We assumed that KKKTTK would mediate electrostatic interactions with negatively charged cell surface HS proteoglycans (HSPGs), mimicking the HS-binding domain on FN and producing a synergistic effect on cell adhesion, growth, and migration.

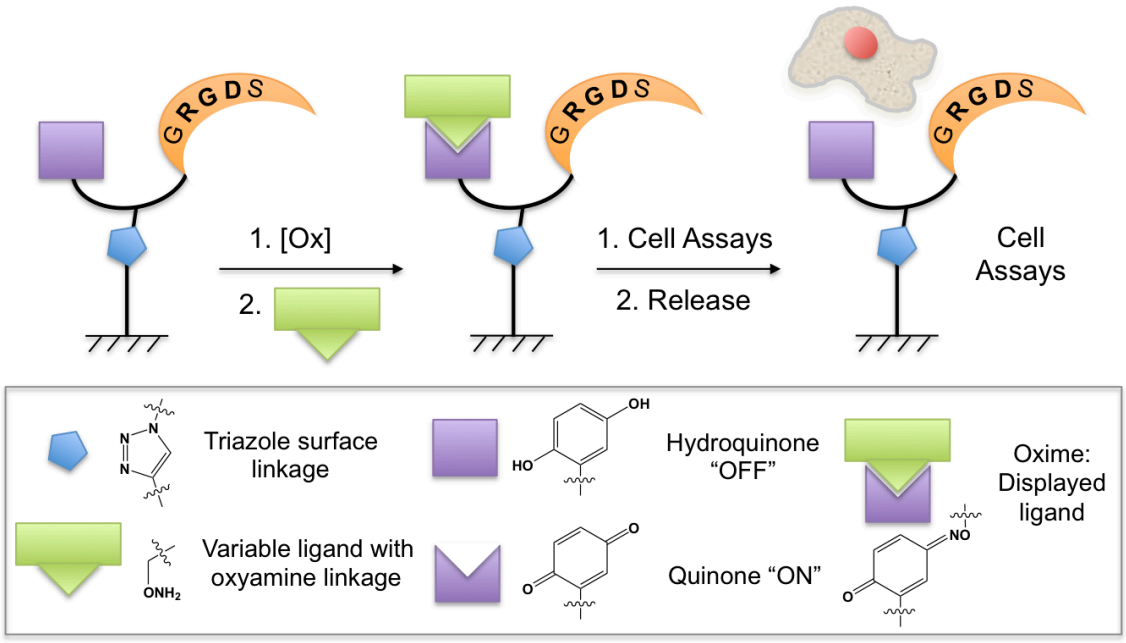

Figure 5.1 General schematic representing dynamic dual ECM ligand-presenting surfaces for the study of cell behavior. Self-assembled monolayers (SAMs) of alkyne-terminated tetra(ethylene glycol) alkanethiol (alkyne-EG_4SH) are generated on gold substrates and reacted with hydroquinone- and azide-functionalized cell adhesive peptide RGD (RGD-HQ). HQ is considered "OFF" and can be turned "ON" for oxyamine ligand conjugation by electrochemical oxidation. Biomolecules, functionalized with oxyamine (OA) groups (i.e., peptides, KKKTTK-OA, PHRSN-OA, RGD-OA, cRGD-OA, and sugars, Man-OA, Gal-OA), react and conjugate to Q-presenting surfaces under physiological conditions. Cells are cultured and observed on surfaces displaying cell adhesive RGD and variable biomolecule. *In situ* electrochemical reduction dynamically releases the variable biomolecule and cellular response to this environmental change is monitored.

We also chose to investigate the dual ligand effects of RGD with galactose (**5**, Gal, Scheme 5.2) and mannose (**6**, Man, Scheme 5.2) monosaccharides due to a few published works. Du *et al.* reported the enhancement of hepatocyte adhesion using a hybrid Gal/RGD monolayer via hepatic asialoglycoprotein receptor interactions.[44] Fibroblasts (Fbs) that express the mannose receptor, which contains a FNII domain, have been shown to exhibit specificity in binding to type I, III, and IV collagens, abundant ECM proteins, to facilitate cell-ECM adhesion.[45] Thus, we hypothesized to observe an increase in cell adhesion and spreading and a decrease in migration when presented with RGD.

The general dynamic redox-responsive surface strategy to present two ECM ligands is represented in figure 5.1. Self-assembled monolayers (SAMs) of mixed tetra(ethylene glycol) (**8**, EG_4SH, Scheme 5.2) and alkyne-terminated tetra(ethylene glycol) (**7**, alkyne-EG_4SH, Scheme 5.2) alkanethiols were formed on gold substrates in a ratio of 99:1 (1 mM total in EtOH, 16 h). Both alkanethiols are resistant to nonspecific protein adsorption and cell adhesion, which is extremely significant when conducting biospecific ligand-receptor interaction studies.[45] Here, EG_4SH (99 % density) serves as the inert background and alkyne-EG_4SH (1 % density) provides an alkyne terminal group for ligand immobilization via Click chemistry with an azide-containing RGD ligand. The molecule density was maintained at 1 % to ensure that only the specific interactions between the ligands in questions with Fb cell surface receptors occur.

The redox-responsive trigger, in a hydroquinone/quinone (HQ/Q) couple form, was built into an Fmoc-protected glycine residue (**E**, Scheme 5.1A) and was compatible with routine solid-phase peptide synthesis. **E** was incorporated into an RGD-containing peptide (**1**, RGD-HQ, Schemes 5.1 and 5.2) that was capped with an azide-functionalized lysine residue for coupling to the 1 % alkyne-EG_4SH SAMs via Click chemistry (20 mM in H_2O/EtOH (3:1), cat $CuSO_4 \bullet 5H_2O$ and NaAsc, 90 min). We have previously shown and extensively characterized the immobilization and release of oxyamine- (OA) functionalized ligands (i.e., peptides, small molecules, and carbohydrates) to and from HQ/Q SAMs on gold substrates for a number of biotechnological applications and cell behavioral studies.[36-38] As shown in figure 5.1, after RGD-HQ immobilization to alkyne-EG_4SH SAMs, the substrates are oxidized [Ox] using linear sweep voltammetry to the corresponding Q (1 M $HClO_4$, -100 to 850 mV, 100 mV/s), which then reacts rapidly and chemoselectively at room temperature and under physiological conditions (20 mM in PBS, pH of 7, 2 h) to form an oxime conjugate.

The oxime bond is stable in all pH ranges until application of a reducing potential at a pH of 7, in which the ligands are spontaneously cleaved, regenerating the original HQ-RGD-tethered SAM.[36,38] A key feature of this system is that both HQ-RGD and corresponding oxime conjugate exhibit signature redox signals that can be monitored and quantified by cyclic voltammetry (CV) in terms of ligand immobilization, release, and density, characteristics that are significant when designing a platform for biological investigation. Thus, this dual ligand ECM and combinatorial screening strategy possesses the following features: a dynamic, molecular redox-responsive trigger for immobilizing and releasing structurally well defined ligands in the presence of cells; density control over ligands; and rapid, chemoselective, and bioorthogonal coupling reactions (i.e., Huisgen cycloaddition and oxime chemistry).

5.3.2 Cell adhesion assays. Before testing our dual ligand ECM system, we first verified whether Fbs could adhere and healthily spread on substrates presenting HQ-RGD and each decoupled ligand in question (Figure 5.2A). As such, HQ-RGD and cRGD, Man, Gal, PHSRN, and KKKTTK ligands were immobilized to alkyne-EG_4SH (20 mM in H_2O/EtOH (3:1), cat $CuSO_4•5H_2O$ and NaAsc, 90 min) and HQ-terminated (20 mM in PBS, 2 h) SAMs, respectively, at a ligand density of 2 %. Fbs cells were then seeded to surfaces (~10^3/mL, 2 h), fixed, imaged, and counted after 2 h. As shown in figure 5.2A, all ligands were able to support cell adhesion to varying degrees. The data is represented as the average number of attached cells per 4x frame (8 random regions). HQ-RGD and cRGD demonstrated similar affinity for attracting Fbs when compared to the surfaces presenting Man, Gal, KKKTTK, and PHSRN, which exhibited almost a 2-fold reduction in the amount of attached Fbs. Additionally, the Fbs were more loosely adhered and adopted a rounder morphology on substrates presenting Man, Gal, KKKTTK, and PHSRN. However, when these ligands were combined with and

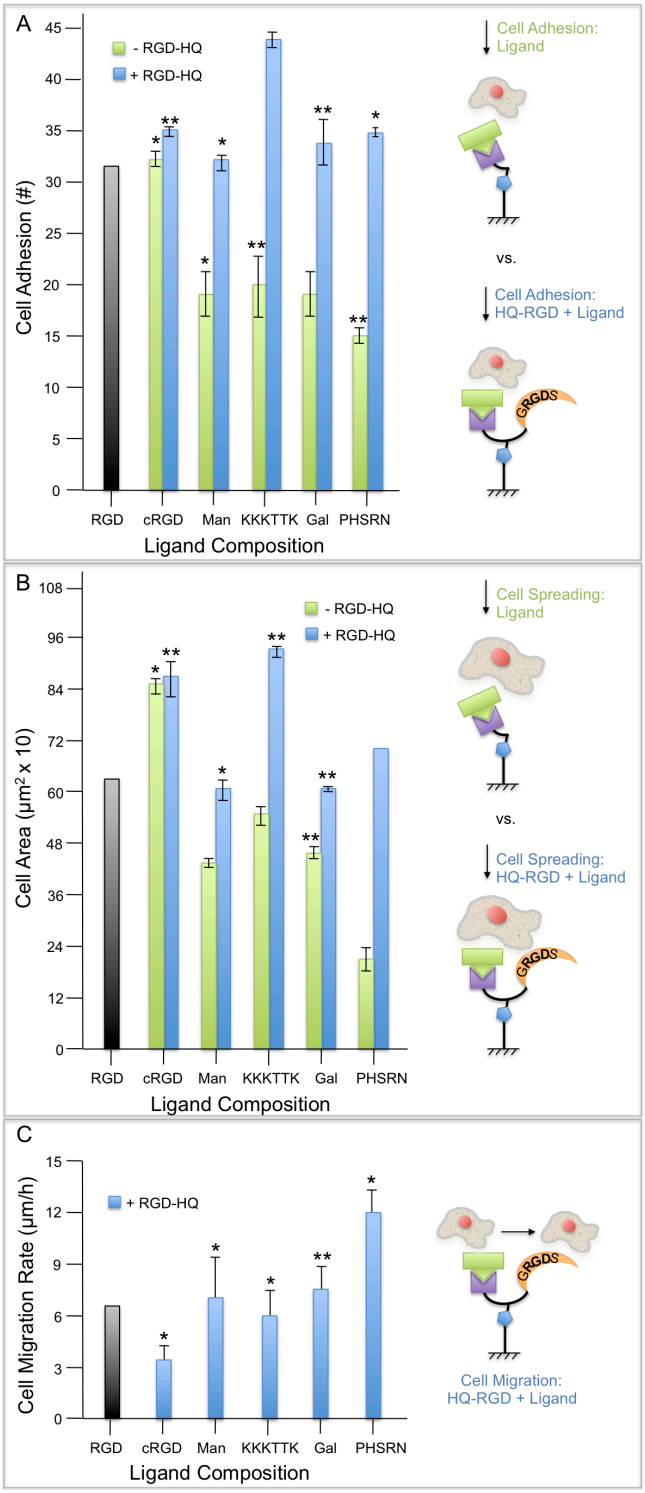

Figure 5.2 (A) Number of adhered cells, (B) cell areas, and (C) cell migration rates after 2 h of culture on the following substrates: (■) cRGD; Man; KKKTTK; Gal; or PHSRN; +RGD-HQ (■) and cRGD; Man; KKKTTK; Gal; or PHSRN. Migration rates were calculated from an 18-h period using live-cell recording and imaging software. Each bar (mean ± S.E.M.) represents an average of 8 trials (~10^3 cells/mL). Statistical analyses were performed with respect to RGD-HQ (■): * $P < 0.001$ and ** $P < 0.01$.

immobilized to SAMs with 1 % Q-RGD (2 % ligand total), the amount of cells increased significantly, approximately 2-fold, resembling the results observed with 2 % HQ-RGD. When Man and Gal were coupled to HQ-RGD, Fbs behaved similarly to when in the presence of cell adhesive RGD; similar numbers of attached cells and morphologies were observed. When PHSRN was coupled to HQ-RGD, a synergistic effect on the amount of cell adhered and over cell spreading and morphology was observed, although at surface value, the actual number of attached cells did not increase significantly from the substrates with 2 % HQ-RGD. Surprisingly, KKKTTK coupled to HQ-RGD showed a dramatic increase in the amount of attached Fbs when compared to HQ-RGD- and KKKTTK-presenting substrates, indicating a profound synergistic effect between KKKTTK and RGD on adhesion. A marked 0.5-fold increase from HQ-RGD substrates was observed on KKKTTK + HQ-RGD. Furthermore, these adhesion results were verified after investigating cell spreading and areas, morphologies, and migration rates on the same substrates.

5.3.3 Cell spreading, morphology, and migration assays. Similar immobilization and fixing conditions were employed to survey the possible synergistic or antagonistic effects of coupling cell adhesive RGD with a number of peptides and carbohydrates on cell spreading, growth, and morphology. A cell undergoes the following sequential events when adhering to the ECM or another cell: attachment, spreading, actin cytoskeleton organization, and focal adhesion (FA) formation. Cells then migrate from various epithelial layers to target locations, where they then differentiate to form specialized cells that make up different tissues and organs. FA and actin were visualized by staining for vinculin (anti-vinculin and Cy-2, green) and F-actin (phalloidin, red) after 2 h of culture on all surfaces (Figure 5.3). Cells were also observed migrating on all substrates during an 18-h period via life-cell recordings, and migration rates were calculated. As shown in

figures 5.2B and 5.3A-B, when compared to HQ-RGD, Fbs were extremely well spread on both cRGD and HQ-RGD + cRGD presenting surfaces. These results are not surprising because the RGD sequence in native FN is located on a beta turn, and thus, the cyclic form of RGD has nM affinity for integrin binding, compared to linear RGD, which has a μM binding affinity.[47] Cells exhibited a 30 % increase (HQ-RGD, 630 μm^2; cRGD, 850 μm^2; HQ-RGD + cRGD, 850 μm^2) in area from HQ-RGD with a more pronounced and intricate network of actin striations and FAs on the periphery and along the actin extensions of the main cell body (top right panel, Figure 5.3B). These morphological characteristics are common to well adhered, healthy cells, as depicted by the cells on adsorbed FN (top left panel, Figure 5.3B). Moreover, when comparing Fb migration on HQ-RGD (7.2 μm/h), cells exhibited a 2-fold decreased rate (3.1 μm/h) on HQ-RGD + cRGD, corroborating the adhesion, spreading, and morphology data (Figure 5.3C).

Synergistic effects of coupling HQ-RGD + PHSRN on Fb spreading and morphology were observed, verifying the results from the cell adhesion assay. An approximate 4-fold increase in average cell area from PHSRN (180 μm^2) to HQ-RGD + PHSRN (700 μm^2) was recorded, indicating that PHSRN, which resembles $FNIII_9$, does not alone sustain adequate attachment and growth. This result was expected due to the lower binding affinity of integrins for PHSRN.[18,30] Moreover, cells were larger on average than those on HQ-RGD alone (630 μm^2). The cell morphologies were drastically different when observing figure 5.3A and 5.3B. Cells on PHSRN alone remained small with rounded ruffling features at the cell periphery and little to no FA formations, as compared to cells on HQ-RGD. However, when coupled to HQ-RGD, cells spread but appeared to be a migratory state; the actin cytoskeleton was not fully extended and striated and FAs were not strongly pronounced. These cellular characteristics were further verified with the

migration data represented in figure 5.3C. Cells on HQ-RGD + PHSRN (11.9 μm/h), demonstrated a 66 % increase in migration rate when compared to cells on HQ-RGD (7.2 μm/h). From the live-cell imaging, the Fbs migrated quickly, extending lamellipodia in different directions to sense their surrounding environment.

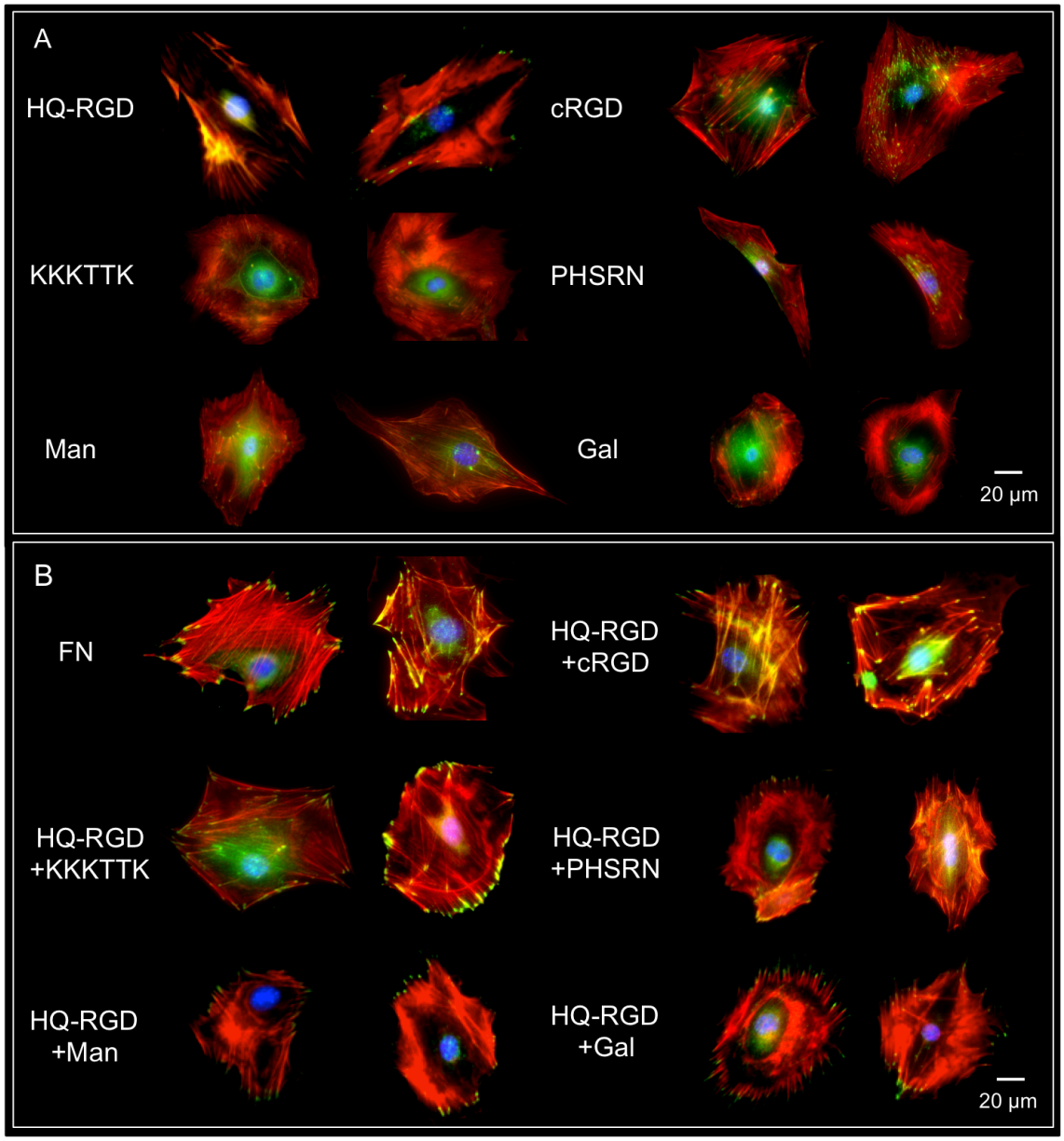

Figure 5.3 Cell morphologies after 2 h of culture on the following substrates: (A) RGD-HQ; cRGD; KKKTTK; PHSRN; Man; or Gal and (B) +RGD-HQ and cRGD; KKKTTK; PHSRN; Man; or Gal. Cells were stained for actin (red, phalloidin), nucleus (blue, DAPI), focal adhesions (FAs, green, anti-vinculin/Cy 2). Long actin extensions and striations and pronounced FAs are indicative of healthy, well spread, and strongly adhered cells.

Although marked differences were observed in the Fb spreading, areas, and morphologies on Gal and HQ-RGD + Gal (420 to 600 μm^2) and Man and HQ-RGD + Man (380 to 610 μm^2), no overall synergistic effects were observed when compared to HQ-RGD alone (630 μm^2) (Figure 5.2B). This conclusion was also apparent from the images in figure 5.3A and 5.3B. Similar to PHSRN, Fbs on Gal and Man adopted small and round shapes with no noticeable FA formations and organized actin cytoskeleton. Ruffling characteristics, typical of cells that are feeling and sensing their environment, are also observed in the bottom left and right panels of figure 5.3A. The increase in cell area after Man and Gal immobilization to Q-RGD is most likely due to the presence of cell adhesive RGD. The cells appear more spread with FA formations at the tips of spikey actin extensions. However, the cell bodies remain rounded, and the actin cytoskeleton is not well structured; it appears that these monosaccharide ligands may be partially masking the adhesive properties of RGD. When observing the migration data, the rate differences were minimal when comparing cells on HQ-RGD and HQ-RGD + Man or Gal substrates (7.2, 7.4, and 7.5 μm/h, respectively). Interestingly, Fbs migrated at approximately the same rate on both RGD and carbohydrate-presenting SAMs (Figure 5.3C).

As previously mentioned, KKKTTK weakly supported the attachment of Fbs. However, when compared to the average area of cells on HQ-RGD (630 μm^2), cells on KKKTTK alone exhibited a comparable average area of 560 μm^2. Although no defined FAs were formed on the cell peripheries (left panel, Figure 5.3A), the actin cytoskeleton appeared to be partially organized, with striations patterns and small extensions. This area may be due to the electrostatic interactions, generated from the positive lysine residues at physiological conditions and highly negatively charged cell surface. When coupled to HQ-RGD, the average cell area on KKKTTK + HQ-RGD increased by

approximately 50 % that of cells on HQ-RGD alone, indicating a synergistic effect of spreading and growth. When imaged, cells maintained a rounded, spread, dense cell body, as seen with cells on KKKTTK alone; however, the appearance of strongly pronounced FAs at the cell periphery and increased actin organization was observed (left panel, Figure 5.3B). When considering the difference in cell migration rates, Fbs on HQ-RGD + KKKTTK demonstrated a 20 % decrease from that of cells on HQ-RGD alone. The data was statistically significant ($P < 0.0001$), indicating that the presence of KKKTTK does exhibit a combined ligand effect. These significant morphological distinctions and decreased migration rate further support the synergistic effects of RGD ($FNIII_{10}$) and KKKTTK ($FNIII_{12\text{-}14}$) in promoting cell surface integrin and syndecan interactions.

5.3.4 Ligand inhibition studies on cell adhesion. Because the ligand combinations HQ-RGD + cRGD, HQ-RGD + KKKTTK, and HQ-RGD + PHSRN demonstrated an effect on Fb adhesion, several soluble molecule and enzyme inhibition studies were performed. We first surveyed the number of attached cells on HQ-RGD + cRGD, HQ-RGD + KKKTTK, and HQ-RGD + PHSRN substrates (2 %) before and after the addition of FN, cRGD, and HS (0.1 mmol in PBS). FN is a natural adhesion protein in the ECM, and we choose cRGD because integrins have a high binding (nM) affinity for the ligand. HS is a repeating disaccharide that possesses a carboxylate and varying sulfate groups. Thus, at physiological conditions, the overall net charge of HS is highly negative. We assumed that addition of soluble FN, cRGD, and HS would interfere with the binding interactions of Fbs and our dual ligand ECM substrates. In Figure 5.4A, the addition of soluble FN had significant effects on the cells that were adhered to HQ-RGD and HQ-RGD + KKKTTK; an approximate 75 % reduction of attached cells was observed. Thirty percent of the Fbs on HQ-RGD + cRGD detached from the surface after FN addition,

and only 10 % lifted from HQ-RGD + PHRSN, as expected. Therefore, RGD alone and the combination of RGD with KKKTTK or cRGD do not exhibit as strong of a synergistic effect on promoting strong cell attachment as originally anticipated. For all substrates, the addition of soluble cRGD and HS had minimal effects on Fb detachment. The high binding affinity small peptide and negatively charge oligosaccharide were not strong enough to detach the cells from the dual ligand ECM mimics, most likely due to already established cell surface integrin- and syndecan-ligand interactions. Based on the other evidence in this chapter, RGD + KKKTTK remains a good dual ligand ECM platform but is not as ideal as natural ligand FN.

We also investigated the enzymatic effects of heparinase I and II (Hep I/II) and chondroitinase ABC (chon ABC) on cleaving the HS and CS chains of PGs that are found on Fb membranes. These enzymes were incubated with Fbs at 0.025 units/mg in serum free media for 1 h, after which the cells were added to HQ-RGD and HQ-RGD + KKKTTK (2 %) for 2 h. The Fbs were then fixed, counted, and compared to the controls (-Hep I/II or -Chon ABC). Figure 5.4B presents the number of adhered cells after enzyme treatment. As shown, HQ-RGD showed little change in attracting cells to the surface with the following results: no treatment, 59; + Hep I/II, 57; and + chon ABC, 55. This could be due to the fact that only a net charge of +1 is present in the same ligand area (arginine in HQ-RGD). Therefore, cleaving the HS and CS groups from cell surfaces did not have an effect on integrin-mediated cell attachment. However, when compared to HQ-RGD + KKKTTK, Fbs experienced a 50 % decrease in adhesion after enzymatic treatment of Hep I/II and chon ABC with the following results: no treatment, 83; Hep I/II, 41; chon ABC, 53. Furthermore, the results corroborated the previous adhesion results; more cells adhered to surfaces due to the synergistic effects of HQ-RGD and KKKTTK. The inhibition in cell adhesion after Hep I/II and chon ABC treatment is most likely due to the

decreased electrostatic interactions of the negatively charged cell surface with positively charged dual ligand ECM (+5 net charge in one concentrated area), as well as less interaction with syndecan-4 surface receptors.

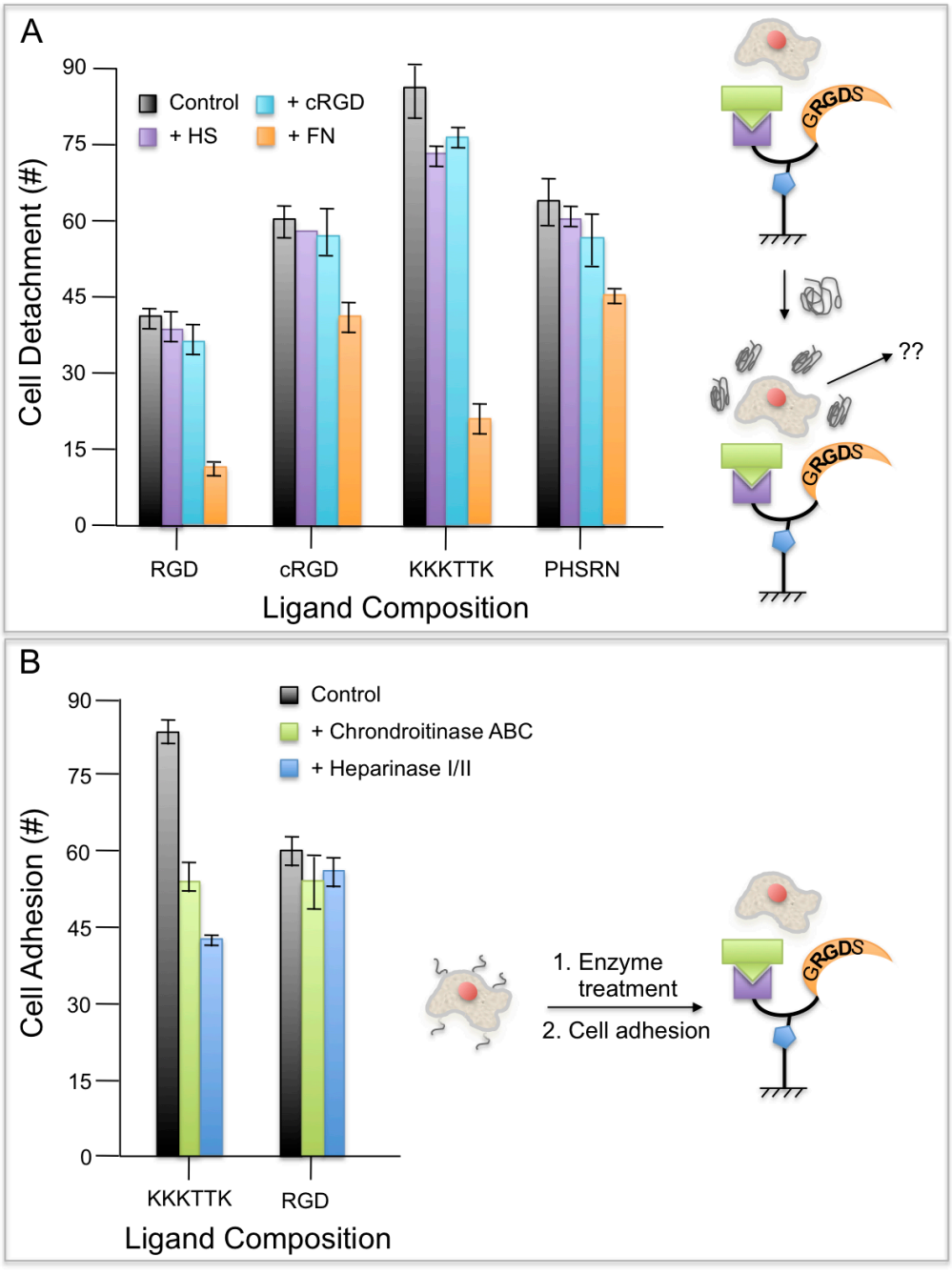

Figure 5.4 (A) Soluble competitive inhibition studies with (■) FN, (■) cRGD, and (■) HS and (B) enzymatic treatment of cells with (■) chondroitinase ABC and (■) heparinase I/II on the following substrates: HQ-RGD and HQ-RGD + cRGD, KKKTTK, or PHSRN. Each bar (mean ± S.E.M.) represents an average of 5-8 trials (~10^4 cells/mL).

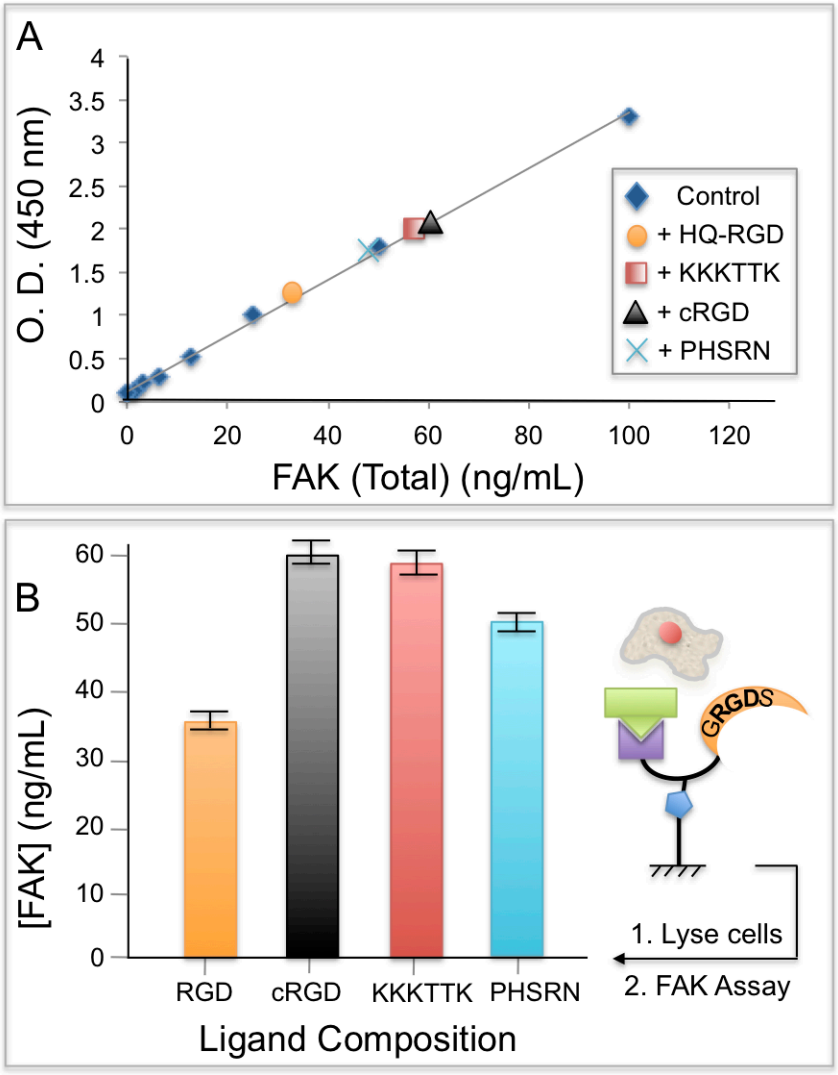

Figure 5.5 (A and B) FAK expression in cells on the following substrates: HQ-RGD and HQ-RGD + cRGD, KKKTTK, or PHSRN. Each bar (mean ± S.E.M.) represents an average of 3 trials from the same batch dilution (~10^6 cells/mL).

5.3.5 Focal adhesion kinase assay. To confirm the results inhibition and morphological assays, we detected and quantified the FAK levels in cells subject to HQ-RGD + cRGD, HQ-RGD + KKKTTK, and HQ-RGD + PHSRN substrates. FAK serves a major role in cell adhesion, spreading, differentiation, migration, division, and apoptosis. Evidence of enhanced FAC was observed in morphological data of the dual ligand ECM systems listed above. Thus, Fbs were incubated on these substrates for 4 h, and using an ELISA kit and spectrophotometry the FAK levels were quantified. The lysates of each

cell population were diluted to measure the FAK level range and generate a linear relationship between the optical density and [FAK] (Figure 5.5A). The total [FAK] was then determined according to each substrate. As shown in figure 5.5B, the decreasing total [FAK] was observed in the following order: + KKKTTK > + cRGD > HQ-RGD > + PHSRN. Therefore, the FAK assay confirmed the morphological data; more FAs were formed in the cells on + KKKTTK and + cRGD and less in the cells on + PHSRN when compared to HQ-RGD. The combined ligand effects of RGD with KKKTTK on enhancing cell adhesion and FA formation, as determined by the increased [FAK], were again verified. Thus, RGD + KKKTTK is a good dual ligand ECM mimic.

5.3.6 Dynamic modulation of cell behavior via redox-responsive ECM. The final study in this work concerned the dynamic release of immobilized ligands in the presence of cells. Fb spreading areas, migration rates, and morphologies were investigated after releasing PHSRN, Gal, Man, KKKTTK, and cRGD from separate HQ-RGD-presenting SAMs. The data is presented in figure 5.6A-C. Remarkably, after ligand release and 4-h adjusted time, the cells more or less adopted similar phenotypes (Figure 5.6C), motility (Figure 5.6B), and spreading areas (Figure 5.6A) to those of substrates that presented HQ-RGD. The Fbs that were subject to Man, Gal, and PHSRN release reorganized and extended their actin protrusions, spreading out to adopt similar sizes and migration rates. Similarly, the cells adhered to substrates in which KKKTTK and cRGD were released reorganized their actin cytoskeleton, focal adhesion assemblies, and stress fibers and contracted slightly to adapt to their new ligand stimulus, HQ-RGD. Thus, these results demonstrate the powerful nature of this surface platform in modulating the dynamic ECM environment, where ligands, proteins, and small molecules are constantly being hidden and revealed to cells.

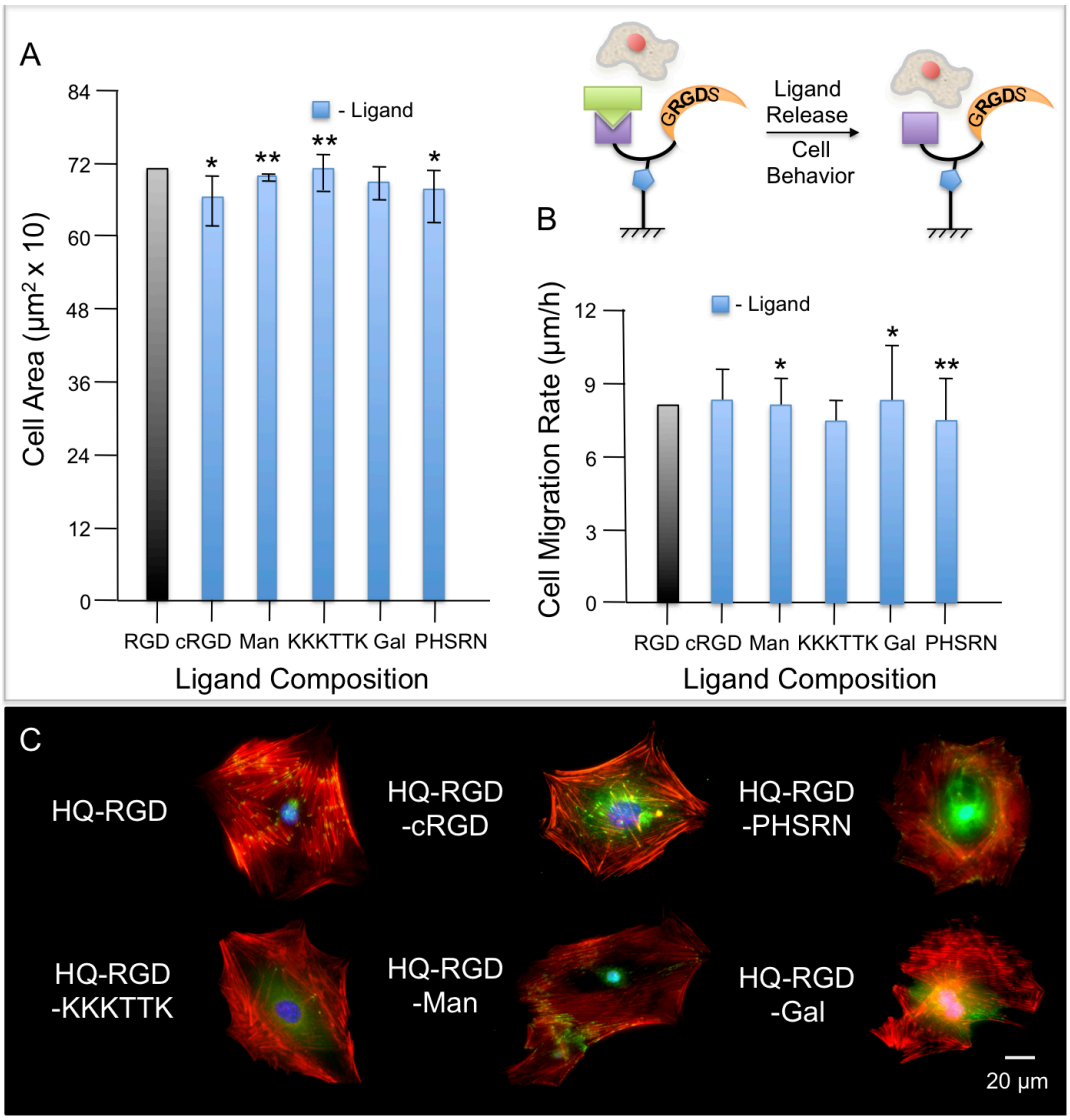

Figure 5.6 Cell behavioral responses to the dynamic release of ECM ligands. Cell (A) areas, (B) migration rates, and (C) morphologies after releasing (■) cRGD, Man, KKKTTK, Gal, or PHSRN from HQ-RGD. Fbs were cultured on the dual ECM ligand-presenting surfaces for 2 h, after which the ECM ligands were electrochemically released (PBS, pH 7, 12 cyclic scans: -100 to 850 mV, 100 mV/s) and incubated for an additional 2 h. Migration rates were calculated from an 18-h period using live-cell recording and imaging software after ligand release. Each bar (mean ± S.E.M.) represents an average of 8 trials (10^3 cells/mL). Statistical analyses were performed with respect to RGD-HQ (■): * $P < 0.001$ and ** $P < 0.01$.

5.4 Conclusions

In summary, we developed a model substrate for *in situ* cell biological studies that dynamically modulates the ECM. A library of biomolecules, Gal, Man, PHSRN, cRGD, and KKKTTK, were synthesized to bear an oxyamine group that reacts rapidly and

chemoselectively with carbonyl moieties. This reaction is also bioorthogonal and can be performed in the presence of cells without inducing any side reactions with proteins and lipids. A cell adhesive HQ-containing RGD was also synthesized and immobilized to bioinert alkyne-EG_4SH SAMs to provide the ketone (in the form of electrochemically oxidized quinone) for dual ligand display, and cell adhesion, spreading and growth, migration, and adhesion inhibition were performed. An added benefit of this platform included the redox-responsive trigger that turns the system 'ON' and 'OFF.' Such a feature allows modulation of the dynamic ECM environment, where ligands, proteins, and small molecules are constantly being hidden and revealed to cells. In surveying the synergistic or antagonistic effects of the immobilized and released ligands to and from HQ-RGD, many key results were observed. When comparing the ligands, the number of attached cells increased for all ligands when immobilized to HQ-RGD. However, HQ-RGD + KKKTTK showed a dramatic increase of 50 %, indicating a possible synergistic effect of simultaneous cell surface integrin and syndecan-4 interactions with the cell- and HS-binding domain mimics of FN. Furthermore, the formation of more FA in the morphological data were observed in the images and confirmed by the increased FAK levels from control substrates (HQ-RGD). The decreased migration rates and soluble and enzymatic inhibition assays also demonstrated that KKKTTK serves as a synergistic ECM ligand with RGD in promoting cell attachment, spreading, and division. When cRGD and PHSRN were investigated, similar results were observed to those reported previously in literature, and Man and Gal had no effect on cell adhesion, spreading, and migration. Thus, not only does this dynamic dual ligand ECM enable the immobilization and release of ligands in the presence of cells, but also provides a platform for the combinatorial screening of ligands to further probe the synergistic or antagonistic effects of cell adhesive RGD with other molecules. This surface strategy can be applied to

nanoparticles for the redox-state-dependent delivery and release of therapeutics and imaging probes *in vitro*.

References

(1) Alberts, B.; Johnson, A.; Lewis, J.; Raff, M.; Roberts, K.; Walter, P. *Molecular Biology of the Cell;* **2002**, Garland Science: New York.

(2) Rhodes, J.; Simons, M. *J. Cell Mol. Med.* **2007**, *2,* 176-205.

(3) Danilov, Y.; Juliano R. *Exp. Cell Res.* **1989**, *182*, 186-196.

(4) Williams, C. M.; Engler, A. J.; Slone, R. D.; Galante, L. L.; Schwarzbauer, J. E. *Cancer research*, **2008**, *68,* 3185-3192.

(5) Hood, J.; Cheresh, D. *Nat. Rev. Cancer* **2002**, *2,* 91-100.

(6) Bogenrieder, T.; Herlyn, M. *Oncogene* **2003**, *22,* 6524-6536.

(7) Liotta, L.; Kohn, E. *Nature* **2001**, *411*, 375-379.

(8) Hynes, R. *Cell* **1987**, *48*, 549-554.

(9) Tamkun, J.; DeSimone, D.; Fonda, D.; Patel, R.; Buck, C.; Horwitz, A.; Hynes, R. *Cell* **1986**, *46,* 271-277.

(10) Juliano, R.; Reddig, P.; Alahari, S.; Edin, M.; Howe, A.; Aplin, A. *Biochem. Soc. Trans.* **2004**, *32*, 443-446.

(11) Ginsberg, M. H.; Partridge, A.; Chattil, S. J. *Curr. Opin. Cell Dev. Biol.* **2005**, *17*, 509-516.

(12) Hynes, R. *Annu. Rev. Cell Biol.* **1985**, *1*, 67-90.

(13) Pankov, R.; Yamada, K. M. *J. Cell Sci.* **2002**, *115*, 3861-3863.

(14) Pierschbacher, M. D.; Ruoslahti, E. *Nature*, **1984**, *309*, 30-33.

(15) Aota, S.; Nomizu, M.; Yamada, K. M. *J. Biol. Chem.* **1994**, *269*, 24756-24761.

(16) Bowditch, R. D. *et al. J. Biol. Chem.* **1994**, *269*, 10856-10863.

(17) Garcia, A. J.; Schwarzbauer, J. E.; Boettiger, D *Biochemistry* **2002**, *41*, 9063-9069.

(18) Feng, Y.; Mrksich, M. *Biochemistry* **2004**, *43*, 15811-15821.

(19) Leahy, D. J.; Aukhil, I.; Erickson, H. P. *Cell* **1996**, *84*, 155-164.

(20) Ingham, K. C.; Brew, S. A.; Atha, D. H. *Biochem. J.* **1990**, *272*, 605-611.

(21) Kim, J. H.; Park, S. O.; Jang, H. J.; Jang, J. H. *Biotechnol. Lett.* **2006**, *28*, 1409-1413.

(22) Lebaron, R. G.; Athanasiou, K. A. *Tissue Eng.* **2000**, *6*, 85-103.

(23) Dee, K. C.; Anderson, T. T.; Bizios, R. *J. Biomed. Mater. Res.* **1998**, *40*, 371-377.

(24) McCarthy, J. B.; Skubitz, A. P.; Qi, Z.; Yi, X. Y.; Mickelson, D. J.; Klein, D. J.; Furcht, L. T. *J. Cell Biol.* **1990**, *110*, 777-787.

(25) Kritz, A. B. *et al*. *Mol. Ther.* **2007**, *15*, 741-749.

(26) Darr, S.; Madisch, I.; Hofmayer, S.; Rehren, F.; Heim, A. *J. Gen. Virol.* **2009**, *90*, 2849-2854.

(27) Di Paolo, N. C.; Kalyuzhniy, O.; Shayakhmetov, D. M. *J. Virol.* **2007**, *81*, 12249-12259.

(28) Buck, C. A.; Horwitz, A. F. *Annu. Rev. Cell Biol.* **1987**, *3*, 179-205.

(29) Humphries, J. D.; Byron, A.; Humphries, M. J. *J. Cell Sci.* **2006**, *119*, 3901-3903.

(30) Eisenberg, J. L.; Piper, J. L.; Mrksich, M. *Langmuir*, **2009**, *25*, 13942-13951.

(31) Pulsipher, A.; Yousaf, M. N. *ChemBioChem*, **2011**, *11*, 745-753.

(32) Mendes, P. *Chem. Soc. Rev.* **2008**, *37*, 2512-2529.

(33) Wischerhoff, W.; Badi, N.; Lutz, J.-F.; Laschewsky, A. *Soft Matter* **2010**, *6*, 705-713.

(34) Liu, D.; Xie, Y.; Shao, H.; Jiang, X. *Angew. Chem. Int. Ed.* **2009**, *48*, 4406-4408.

(35) Lee, E.-J.; Chan, E. W. L.; Yousaf, M. N. *ChemBioChem* **2009**, *10*, 1648-1653.

(36) Lamb, B. M.; Yousaf, M. N. *J. Am. Chem. Soc.* **2011**, *133*, 8870–8873.

(37) Chan, E. W. L.; Park, S.; Yousaf, M. N. *Angew. Chem, Int. Ed.* **2008**, *120*, 6363-6367.

(38) Pulsipher, A.; Yousaf, M. N. *ChemComm* **2011**, *47*, 523-525.

(39) Li, J.; Thiara, P. S.; Mrksich, M. *Langmuir*, **2007**, *23*, 11826-11835.

(40) Pale-Grosdemange, C.; Simon, E. S.; Prime, K. L.; Whitesides, G. M. *J. Am. Chem. Soc.* **1991**, *113*, 12-20.

(41) Chan, E. W. L.; Yousaf, M. N. *J. Am. Chem. Soc.* **2006**, *128*, 15542-15546.

(42) Mrksich, M. *Acta Biomaterialia*, **2009**, *5*, 832-841.

(43) Lu, J.; Shi, M.; Shoichet, M. S. *Bioconjugate*, **2009**, *20*, 87-94.

(44) Du *et al. Biomaterials*, **2006**, *27*, 5669-5680.

(45) Napper, C. E.; Drickamer, K.; Taylor, M. E. *J. Biochem.* **2006**, *395*, 579-586.

(46) Ostuni, E.; Chapman, R. C.; Liang, M. N.; Meluleni, G.; Pier, G.; Ingber, D. E.; Whitesides, G. M. *Langmuir*, **2001**, *17*, 6336-6343.

(47) Xiao, Y.; Truskey, G. A. *J. Biophys.* **1996**, *71*, 2869-2884.

CHAPTER 6

Cell-Surface Engineering via Liposome Fusion: 3D Tissue Structure Generation

6.1 Introduction

Membrane fusion processes are ubiquitous in biology and span multicellular communication, extracellular signaling, the reconstruction of damaged organelles, and integration of cells into complex tissues and organs.[1] As a result, there has been much interest in developing model systems to mimic biological membranes to investigate the mechanisms of fusion, employing various biotechnological applications. For example, cells secrete and display proteins and lipids during vesicle trafficking events that diffuse into the extracellular matrix (ECM) or become components of the cell membrane after fusion.[2] Naturally, lipid vesicles provide an ideal platform for such studies and have been widely used to examine various membrane-related processes, including fusion.[3-5] For fusion to occur, the membranes must be brought into close proximity, followed by bilayer destabilization.[6] Fusion of such lipid vesicles or liposomes can be initiated by using divalent cations, polycations,[7] positively charged amino acids,[8] and membrane-disrupting peptides.[9,10] Historically, synthetic chemical agents have also been employed to fuse vesicle membranes[11-14] through non-specific interactions. However, recent exciting efforts to improve the selectivity and control over vesicle fusion have been achieved through the use of small synthetic molecular recognition pairs.[15-16] Because vesicle fusion is a natural process and has been shown to influence the construction of cells into

multicellular organisms, much research has focused on using liposomes to deliver cargoes, reagents, nanomaterials, and therapeutic agents to cells. To our knowledge, there have been very few reports of employing liposome fusion to cell membranes as a method to deliver small chemical functional groups to tailor the cell membrane for subsequent bio-orthogonal and chemoselective ligation reactions.[17] This platform would find wide use in studying fundamental cell behavior and provide a range of new tools for tissue engineering and biomedical applications.

Cells that make up tissues and organs exist and communicate within a complex, three-dimensional (3D) environment. The spatial orientation and distribution of ECM components directly influences the manner in which cells receive, integrate, and respond to a range of input signals.[18] As such, cellular interactions with ECM molecules and/or other cells have been extensively investigated for fundamental studies in development, cell motility, differentiation, apoptosis, paracrine signaling, and applications in tissue engineering.[19,20] There has been tremendous effort toward the design and fabrication of 3D scaffolds that mimic ECM properties and induce tissue formation *in vitro*, utilizing various biomaterials, biodegradable polymers,[21] collagen,[22] and hydrogels.[23,24] Among the major challenges facing the use of these technologies for tissue engineering are the abilities to force contact between multiple cell types in 3D to control the spatial and temporal arrangement of cellular interactions and tailor and mold the biomaterial to recapitulate the 3D *in vivo* environment under laboratory constraints. Without the use of engineered scaffolds in culture, most cells are unable to form the necessary higher-order 3D structure required for the anatomical mimicry of tissue and are limited to random migration, generating two-dimensional (2D) monolayers. As a result, several approaches, including the use of dielectrophoretic forces,[25,26] laser-guided writing,[27-29] surface manipulation,[30] and a number of lithographic printing techniques[31-34] have been

integrated with 3D scaffold designs to produce multi-type cellular arrays[26,28,34] or 3D cell clusters or spheroids.[24,25,30] In a recent study, 3D aggregates consisting of multiple cell types were formed within a hydrogel matrix through DNA hybridization after cell surfaces were engineered with complementary short oligonucleotides via a metabolic labeling approach.[24] However, for some applications, the presentation of cell-surface DNA may not be stable for extended time periods in cell culture or *in vivo*.[35]

Cell-surface engineering methodologies have primarily been of interest in molecular biology. As such, biosynthetic approaches have been employed to introduce different functional groups on cell surfaces. In a previous study, an unnatural derivative of N-acetyl-mannosamine, which bears a ketone group, was converted to the corresponding sialic acid and metabolically incorporated onto cell surface oligosaccharides, resulting in the cell surface display of ketone groups.[36] However, metabolic or genetic methods may alter many of the biochemical pathways that are required for normal cell function. Thus, there is a growing demand for tools that can provide simple alternatives to the complex genetic and biosynthetic approaches. Other approaches to cell-surface engineering have also been undertaken to incorporate a functional group into a target biomolecule, such as an endogenous protein, utilizing a cell's biosynthetic machinery.[37,38] These strategies aim to produce a site that can then be covalently modified with its delivered counterpart or probe. However, most of these protein-based tags are large and bulky and become problematic when interacting with the other glycans and biomolecules on the cell suface.[39,40] Additionally, the perturbation of cellular physiology with biomolecules at the cell surface may result in the interference of significant biochemical pathways or cellular functions.[41,42] Thus, a methodology that combines cell-surface modification without the use of molecular biology techniques or biomolecules and a simple, stable bio-orthogonal conjugation bottom-up approach that is capable of directing tissue formation would

greatly benefit a range of medical applications, such as wound healing and burn treatment.

Herein, we develop and employ a novel strategy to induce specific and stable cell-cell contacts through chemoselective cell-surface engineering based on liposome delivery and fusion of bio-orthogonal functional groups to cell membranes.[17] Our liposome-cell membrane methodology was inspired by the work of Wilson *et al.*[43] and Csiszar *et al.*[44] who reported a noncovalent cell-surface engineering strategy via cationic graft copolymer adsorption and a fluorescent labeling technique via cationic and aromatic lipid fusion, respectively. Thus, we incorporated a cationic lipid to initiate membrane fusion and adsorption to the cell surface. This strategy enables the presentation of bio-orthogonal ketone and oxyamine molecules from cell surfaces for subsequent chemoselective oxime ligation. No proteins or large biomolecules are used in this strategy, and therefore, cellular physiology is not perturbed. We first characterize liposome-liposome fusion by matrix-assisted laser-desorption/ionization mass spectrometry (MALDI-MS), dynamic light scattering (DLS), Fourier resonance energy transfer (FRET), transmission electron microscopy (TEM), fluorescence-activated cell sorting (FACS), and fluorescence microscopy analyses. We then demonstrate how this method may be used in several applications including, the delivery of reagents to cell surfaces, formation of 3D spheroid assemblies of cells with controlled inter-connectivity, and patterned multi-layered cell tissues. Furthermore, 3D multi-layered stem cell and fibroblast (fb) co-cultures were generated, and differentiation was induced to form tissue-like structures of adipocytes and fbs. To our knowledge, this is the first report that utilizes tailored liposomes to modify a living cells surface through membrane fusion for subsequent bio-orthogonal tailoring to generate 3D tissue-like structures.

6.2 Materials and Methods

6.2.1 Materials and instrumentation. All chemical reagents were of analytical grade and used without further purification. Lipids egg palmitoyl-oleoyl phosphatidylcholine (POPC), egg 1-palmitoyl-2-oleoyl-phosphatidylglycerol (POPG), 1,2-dioleoyl-3-trimethylammonium-propane (DOTAP), egg 1,2-diphytanoyl-*sn*-glycero-3-phosphoethanolamine-N-(7-nitro-2-1,3-benzoxadiazol-4-yl) (ammonium salt) (NBD-PE), and egg 1,2-dipalmitoyl-*sn*-glycero-3-phosphoethanolamine-N-(lissamine rhodamine B sulfonyl) (ammonium salt) (Rhod-PE) were purchased from Avanti Polar Lipids (Alabaster, AL). Antibodies and fluorescent dyes were obtained from Invitrogen (Carlsbad, CA). FITC labeled beads were purchased from Spherotech, Inc. (Forest Lake, IL) and all other chemicals were obtained from Sigma-Aldrich or Fisher. Swiss 3T3 albino mouse fibroblasts (fbs) were obtained from the Tissue Culture Facility at the University of North Carolina (UNC).

Transmission electron microscopy images were acquired using a TF30He Polara G2 (FEI company) electron cryo microscope, operating at 300 keV. Images were recorded using a Tietz single port model 415 4k×4k CCD camera with a 15-μm pixel size. Fourier resonance energy transfer measurements were performed using a SPEX Fluorolog-3 Research T-format Spectrofluorometer with an excitation wavelength of 471 nm. Dynamic light scattering was performed using a Nikomp model 200-laser particle sizer with a 5 mW HeNe laser at an excitation wavelength of 632.8 nm and using a Wyatt DynoPro plate reader. Flow cytometry was performed using a Dako CyAn ADP (Beckman-Coulter, Brea, CA), and the data was analyzed with Summit 4.3 software. Phase contrast and fluorescent imaging was performed and processed using a Nikon TE2000-E inverted microscope and Metamorph software, respectively.

6.2.2 Syntheses. Tetra(ethylene glycol)-terminated alkanethiol (EG_4) was synthesized as previously reported.[45] Fluorescein-ketone (**7**) was synthesized as previously reported.[46] The syntheses of *O*-dodceyloxyamine (**A**) and rhod-oxyamine (**8**) are described below.

*2-(dodecyloxy)isoindoline-1,3-dione (**B**).* To a solution of N-hydroxyphthalimide (1.96 g, 12.04 mmol, 1.5 eq) and sodium bicarbonate (10.11 g, 12.04 mmol, 1.5 eq) in DMF (20 mL) at 80 °C was added 1-bromododecane (1.93 mL, 8.02 mmol). The mixture was refluxed and stirred for 12 h. The reaction was diluted with DCM and washed with H_2O (6 x 50 mL), 1 M $NaHCO_3$ (3 x 50 mL), and H_2O (2 x 50 mL), dried over $MgSO_4$, and concentrated to afford a white solid, **B** (2.66 g, 87 %). ^{1}H NMR (400 MHz, $CDCl_3$) δ 0.91 (m, 3H), 1.28 (bm, 16H), 1.47-1.49 (m, J = 9.2 Hz, 2H), 1.77-1.83 (m, J = 22.0 Hz, 2H), 4.20-4.23 (t, J = 13.6 Hz, 2H), 7.28-7.30, 7.75-7.77 (dm, J = 4.8, Hz, J = 5.6 Hz, 2H, 2H). (ESI) (*m/z*) [M + H^+]: 332.28.

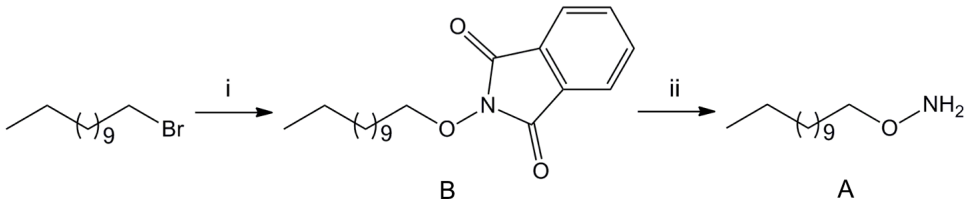

Scheme 6.1 Reagents and conditions of *O*-dodecyloxyamine. (i) N-hydroxyphthalimide (1.5 eq), $NaHCO_3$ (1.5 eq), DMF, reflux, 80 °C, 12 h; 87 % and (ii) hydrazine (6 eq), dry DCM, N_2, 12 h; 74 %.

*O-dodecyloxyamine (**A**).* To a solution of **B** (2.65 g, 8.00 mmol) in dry DCM (30 mL) under inert atmosphere (Ar) was slowly added hydrazine (1.53 mL, 48.00 mmol, 6 eq). Upon addition, a white precipitate immediately formed. The mixture was stirred for 12 h. The reaction was diluted with DCM and washed with H_2O (6 x 50 mL), dried over $MgSO_4$, and concentrated to afford a pale yellow oil, **A** (1.18 g, 74 %). ^{1}H NMR (400 MHz, $CDCl_3$) δ 0.88-0.91 (t, J = 13.6 Hz, 3H), 1.28 (s, 18H), 1.57-1.60 (m, J = 14.0 Hz, 2H), 3.65-3.69 (t, J = 13.2 Hz, 2H). (ESI) (*m/z*) [M + H^+]: 201.22.

*(N-(4-(tert-butoxycarbonylamino)butyl)sulfamoyl)-2-(6-(diethylamino)-3-(diethyliminio)-3H-xanthen-9-yl)benzenesulfonate (**C**).* To a solution of rhodamine lissamine (0.880 g, 1.53 mmol) in chloroform ($CHCl_3$, 30 mL) at room temperature (RT) was added N-BOC-1,4-diaminobutane (0.431 g, 2.29 mmol, 1.5 eq) and TEA (0.305 mL, 2.29, 1.5 eq). The mixture was stirred for 8 h and then extracted with H_2O (6 x 25 mL). The organic layers were concentrated to afford a dark purple solid **C**. H^1NMR was taken in $CDCl_3$ to confirm **C** (1.045 g, 95 %). TLC conditions for entire synthesis: $CHCl_3$:MeOH (7.5:2.5). ^{1}H NMR (400 MHz, MeOD) δ 1.09-1.07 (t, J = 8.1 Hz, 6H), 1.36-1.33 (m, J = 12.3, 15H), 1.66-1.64 (m, J = 8.6 Hz, 4H), 3.47-3.44 (m, J = 12.1, 6H), 4.20-4.18 (q, J = 7.8 Hz, 4H), 5.66 (s, 1H), 5.77 (d, 1H), 6.01 (d, 1H), 6.34-6.30 (m, J = 16.1 Hz, 2H), 7.21 (d, 1H), 7.29 (d, 1H), 7.98 (d, 1H), 8.04 (d, 1H). (ESI) (*m/z*) [M + H^+]: 716.31.

*5-(N-(4-aminobutyl)sulfamoyl)-2-(6-(diethylamino)-3-(diethyliminio)-3H-xanthen-9-yl)benzenesulfonate (**D**).* To **C** (0.600 g, 0.837 mmol) was added a solution of TFA, H_2O, and triisopropylsilane (TIPS) in a ratio of 95: 2.5: 2.5 (10 mL). The mixture was stirred at RT under N_2 for 3 h and was then extracted with $CHCl_3$ and H_2O (4 x 25 mL). The organic layers were dried and concentrated to afford a purple solid, **D** (0.45 g, 85 %). ^{1}H NMR (400 MHz, MeOD) δ 1.11-1.09 (t, J = 8.7, 6H), 1.33-1.31 (m, J = 7.4 Hz, 6H), 1.70-1.67 (m, 4H, J = 12.5, 4H), 2.63-2.62 (m, J = 4.6 Hz, 2H), 3.51-3.49 (m, J = 8.7 Hz, 6H), 4.20-4.18 (q, J = 7.8 Hz, 4H), 5.64 (s, 1H), 5.71 (d, 1H; Ar-H), 6.02 (d, 1H), 6.32-6.30 (m, J = 8.3 Hz, 2H), 7.24 (d, 1H), 7.30 (d, 1H), 7.98 (d, 1H), 8.04 (d, 1H). (ESI) (*m/z*) [M + H^+]: 628.27.

*2-(6-(diethylamino)-3-(diethyliminio)-3H-xanthen-9-yl)-5-(N-(2,2-dimethyl-4,8-dioxo-3,6-dioxa-5,9-diazatridecan-13-yl)sulfamoyl)benzenesulfonate (**E**).* To a solution containing N,N'-dicyclohexylcarbodiimide (DCC, 0.394 g, 1.91 mmol, 2 eq), N-hydroxysuccinimide (NHS, 0.220 g, 1.91 mmol 2 eq), and aminooxy acetic acid (0.356 g,

1.91 mmol, 2 eq) in DMF was stirred under N_2 for 0.5 h. **D** (0.43 g, 0.684 mmol) was then added in DMF (20 mL), followed by TEA (excess). The mixture was stirred for 4 h and then concentrated. Flash chromatography was performed using $CHCl_3$:MeOH (8:2) to elute, **E**. The product was concentrated to afford a purple solid **E** (0.32 g, 60 %). ^{1}H NMR (400 MHz, MeOD) δ 1.10-1.08 (t, J = 8.8, 6H), 1.39-1.36 (m, J = 12.3 Hz, 15H), 1.65-1.63 (m, J = 7.9, 4H), 3.08-3.06 (m, J = 8.0, 2H), 3.48-3.46 (m, J = 8.3, 6H), 4.17-4.15 (q, J = 7.7, 4H), 4.38 (s, 2H), 5.61 (s, 1H), 5.73 (d, 1H), 6.02 (d, 1H), 6.31-6.30 (m, J = 4.4, 2H), 7.24 (d, 1H), 7.32 (d, 1H), 7.96 (d, 1H), 8.09 (d, 1H). (ESI) (*m/z*) [M + H$^+$]: 801.31.

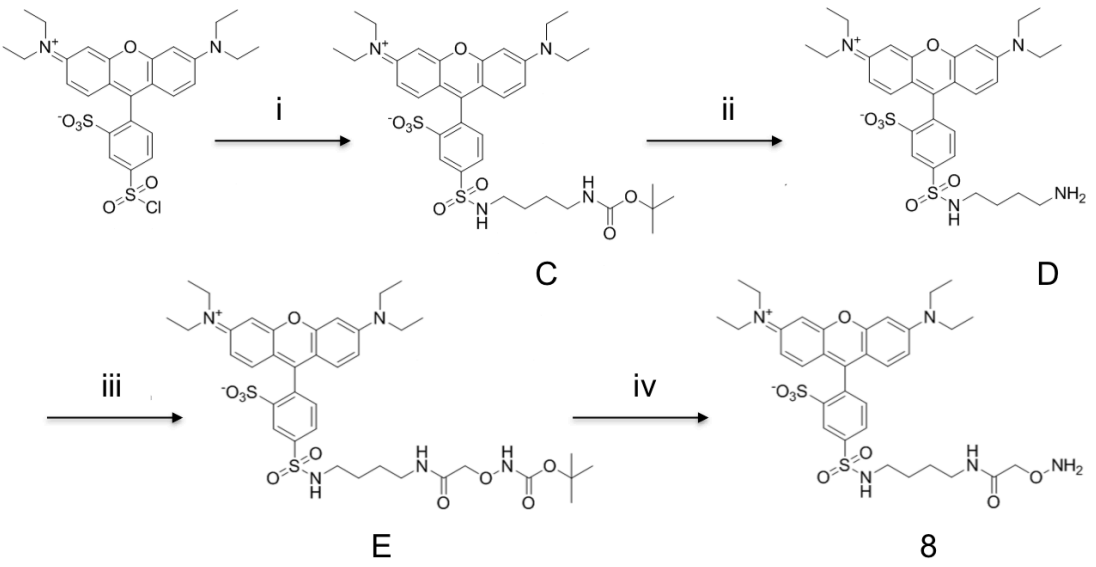

Scheme 6.2 Reagents and conditions of rhodamine-oxyamine (rhod-oxyamine). (i) N-BOC-1,4-diaminobutane (1.5 eq), TEA (1.5 eq), $CHCl_3$, N_2, 25 ºC, 8 h; 95 %, (ii) triisopropylsilane (TIPS)/H_2O/TFA (2.5 : 2.5 : 95), N_2, 25 ºC, 3 h; 85 %, (iii) N-hydroxysuccinimide (NHS, 2 eq), N,N'-dicyclohexylcarbodiimide (DCC, 2 eq), aminooxy acetic acid (2 eq), TEA (excess), DMF, N_2, 25 ºC, 4 h; 60 %, and (iv) TIPS/H_2O/TFA (2.5 : 2.5 : 95), N_2, 25 ºC, 3 h; 81 %.

*5-(N-(4-(2-(aminooxy)acetamido)butyl)sulfamoyl)-2-(6-(diethylamino)-3-(diethyliminio)-3H-xanthen-9-yl)benzenesulfonate (rhod-oxyamine, **8**).* To **E** (0.30 g, 0.374 mmol) was added a solution of TFA, H_2O, and triisopropylsilane (TIPS) in a ratio of 95: 2.5: 2.5 (10 mL). The mixture was stirred at RT under N_2 for 3 h and was then

extracted with $CHCl_3$ and H_2O (4 x 25 mL). The organic layers were dried and concentrated to afford a purple solid and flash chromatography was performed using $CHCl_3$:MeOH (8:2) to elute, **8** (0.21 g, 81 %) ^{1}H NMR (400 MHz, $CDCl_3$) δ 1.12-1.00 (t, J = 8.2, 6H), 1.42-1.40 (m, J = 7.9, 6H), 1.62-1.60 (m, J = 7.7, 4H), 3.07-3.05 (m, J = 8.0, 2H), 3.45-3.42 (m, J = 12.4, 6H), 4.11-4.09 (q, J = 8.4, 4H), 4.24 (s, 2H), 5.64 (s, 1H), 5.75 (d, 1H), 6.02 (d, 1H), 6.29-6.27 (m, J = 4; 2H), 7.28 (d, 1H), 7.31 (d, 1H), 7.92 (d, 1H), 8.05 (d, 1H). (ESI) (*m/z*) [M + H^+]: 701.28.

6.2.3 Formation of lipid vesicles. Liposome fusion studies. Dodecanone (55 µL, 10 mM in $CHCl_3$ at 5 mol %) was dissolved with egg palmitoyl-oleoyl phosphatidylcholine (POPC) (430 µL, 10 mg/mL in $CHCl_3$, at 95 mol %) and *O*-dodecyloxyamine (60 µL, 10 mM in $CHCl_3$ at 5 mol %) was mixed with POPC (410 µL, 10 mg/mL in $CHCl_3$ at 75 mol %), and egg 1-palmitoyl-2-oleoyl-phosphatidylglycerol (POPG) (92 µL, 10 mg/mL in $CHCl_3$ at 20 mol %). Both lipid sample mixtures were then concentrated under high vacuum for 4 h. The dried lipid samples were reconstituted and brought to a final volume of 3 mL in PBS buffer, pH 7.4. The contents of the vial were warmed to 50 °C and sonicated for 20 min, in a tip sonicator, until the solution became clear and large unilamellar vesicles (LUVs) containing ketone (keto-LUV, **1**) or oxyamine (oxy-LUV, **2**) groups were formed. *Fourier resonance energy transfer (FRET) fusion studies.* NBD-PE and rhod-PE were added to two separate vials at 2 mol %. The dried lipid samples were then reconstituted in 2.43 mL of PBS buffer, pH 7.4. The contents of the vial were warmed to 50˚C and sonicated for 20 min, in a tip sonicator, until the solution became clear, and LUVs containing ketone (keto-NBD-PE LUVs, **3**) or oxyamine (oxy-rhod-PE LUVs, **4**) groups were formed. *Liposome fusion to cells.* To generate ketone- and oxyamine-containing liposomes for cell fusion studies, dodecanone (55 µL, 10 mM solution in $CHCl_3$ at 5 mol %) and *O*-dododecyloxyamine (60 µL, 10 mM solution in

$CHCl_3$ at 5 mol %) were dissolved with egg-POPC (424 µL, 10 mg/mL in $CHCl_3$ at 93 mol %) and 1,2-dioleoyl-3-trimethylammonium-propane (DOTAP, 10 µL, 10 mg/mL in $CHCl_3$ at 2 mol %) in chloroform followed by concentration under high vacuum for 4 h. The dried lipid samples were then reconstituted and brought to a final volume of 3 mL in PBS buffer, pH 7.4. The contents of the vial were warmed to 50 ˚C and sonicated for 20 min, in a tip sonicator, until the solution became clear, and LUVs containing ketone (**5**) or oxyamine (**6**) groups were formed.

6.2.4 Matrix-assisted laser-desorption/ionization mass spectrometry (MALDI-MS). Preparation of gold-coated MALDI sample plates. Gold-coated MALDI sample plates (123 x 81 mm) (Applied Biosystems, Foster City, CA) were prepared by electron-beam deposition (Thermionics Laboratory Inc, Hayward, CA) of titanium (5 nm) and then gold (12 nm). To form self-assembled monolayers (SAM) of alkanethiolates on the plates, the slides were immersed in a 1-mM solution of aminooxyundecanethiol in EtOH for approximately 1 min, rinsed with EtOH and dried, and then backfilled with a 1-mM solution of mercaptoundecanol in EtOH for 1 h. Once removed from solution, the surfaces were rinsed with EtOH and dried before use. *Liposome preparation.* Keto-LUVs (**1**) were generated as previously described and were then delivered and allowed to react with the oxyamine-terminated MALDI sample plate (90 min). The plates were then washed with water (3 x 3 mL) and EtOH (2 x 3 mL) and dried before use. *MALDI Analysis.* MS analysis was carried out using an AB SCIEX TOF/TOF^{TM} 5800 System (Applied Biosystems, Foster City, CA).

6.2.5 Dynamic light scattering (DLS). Keto- (**1**) and oxy- (**2**) LUVs were generated as previously described and tested by DLS for monodispersity and uniformity. Light scattering experiments were performed using a Nikomp Model 200 Laser Particle Sizer with a 5 mW Helium-Neon Laser at an exciting wavelength of 632.8 nm. Standard

deviation determinations were made using Gaussian analysis. A Wyatt DynoPro Dynamic Scattering Plate Reader was used to collect the light scattering data.

6.2.6 Fourier resonance energy transfer (FRET). Keto- (**3**) and oxy- (**4**) LUVs containing NBD-PE and rhod-PE, respectively, were generated as previously described and tested by FRET. All fluorescence measurements were performed in a SPEX Fluorolog-3 Research T-format Spectrofluorometer. NBD fluorescence was measured at 471 nm (excitation) and 531 nm (emission), maintaining narrow excitation slits to reduce light scattering interference. To obtain FRET measurements, the NBD dye was excited at 471 nm, and the emission was scanned through 600 nm, and the emission signal for rhod-PE was observed at 578 nm. Fluorescence was followed immediately after mixing oxy-rhod-PE LUV (**4**, 3 mM in PBS, 100 μL) with keto-NBD-PE LUV (**3**, 3 mM in PBS, 100 μL) for approximately 2 h at 2 min intervals. The total lipid concentrations were adjusted to 0.2 mM, and the two LUV populations were had a 1:1 molar ratio. A constant flow of water was passed through the cuvette holder for temperature control. The temperature was maintained at 25 °C.

6.2.7 Transmission electron microscopy (TEM). Keto- (**1**) and oxy- (**2**) LUVs were made as previously described (0.2 mM in PBS, pH 7.4). The two vesicle solutions (1:1) were mixed at room temperature for 30 min. Vesicles suspended (4 μL) in buffer were applied to standard lacey carbon EM grids and prepared according to published methods.[53] The specimens were blotted from behind and then submerged into aurenyl acetate solution for staining. The hydrated specimens were then placed into a TF30He Polara G2 (FEI company) electron cryo microscope operating at 300 keV. Images were recorded using a Tietz single port model 415 4k × 4k CCD camera with a 15 micron pixel

size on the chip. Pixel sizes at the specimen level were used to calculate accurate dimensions for the specimen.

6.2.8 Cell adhesion patterning. Self-assembled monolayers (SAMs) presenting aldehyde or oxyamine and tetra(ethylene glycol) (EG_4) groups were patterned using microfluidic oxidation and microfluidic lithography, respectively.[47,48] EG_4 has been shown to passivate substrates against cell and protein adsorption.[49] Therefore, the ratio of EG_4 and aldehyde or oxyamine groups was 90:10 to ensure that fbs were only adhering to the patterned surface regions that presented 10 % oxyamine or aldehyde groups, driven via oxime conjugation. Fbs were separately cultured with keto- (**5**) or oxy- (**6**) LUVs as previously described and were then seeded (~10^2 cells/mL, 2 h) to the patterned oxyamine or aldehyde surfaces, respectively. Media that 10 % calf bovine serum (CBS) and 1 % penicillin/streptomycin was then added, and the substrates were incubated at 37 °C in 5 % CO_2 for 4 d. Cells cultured with liposomes, not containing the key functional groups, did not attach to the patterned surfaces. Substrates were then stained and imaged by fluorescence microscopy. An exposure time of 400 and 1200 ms were used to image nuclei and actin, respectively.

6.2.9 Fibroblast (Fb) culture. Swiss 3T3 albino mouse fbs and Rat2 fbs were cultured in Dulbecco's Modified Eagle Medium (Gibco) containing 10 % calf bovine serum (CBS) and 1 % penicillin/streptomycin at 37 °C in 5 % CO_2. *Delivery of functionalized liposomes to cells.* Cells were seeded onto a tissue culture plate and allowed to grow for 48 h at 37 °C in 5 % CO_2 in CBS media.

6.2.10 Cell-surface engineering. Two cell-surface engineering methods were employed to fluorescently label fbs. In this first method, a solution of oxy-LUVs (**6**, 3 mM) was incubated with a ketone-functionalized fluorescein (**7**, 0.15 mM, 1 eq, 2 h), forming

fluorescently labeled liposomes. The liposomes were then added to fbs in culture for 2 h. After fusion, the cells were washed with PBS (3 x 2 mL), trypsinized (1 mL, 5 min, 37 °C, 5 % CO_2), diluted with CBS-containing media (~10^2/mL), and seeded to a glass substrate (1 x 1 cm^2, 2 h). The cells were then imaged under a fluorescence microscope with an exposure time of 1/1200 s. In the second method, a solution of keto-LUVs (**5**, 200 μL, 0.6 mM) was added to fbs in culture for 2 h, resulting in membrane fusion and subsequent display of ketones from the cell surface (**9**). Rhod-oxyamine (**8**, 100 μL, 0.7 mM in H_2O) was then added the cells for 2 h. After oxime formation, the fbs were washed with PBS (3 x 2 mL), trypsinized (1 mL, 5 min, 37 °C, 5 % CO_2), diluted with CBS-containing media (~10^2/mL), and seeded to a glass substrate (1 x 1 cm^2, 2 h). The cells were then imaged under a fluorescence microscope with an exposure time of 1/1200 s.

6.2.11 Flow cytometry. Fluorescence-activated cell sorting (FACS) analysis was performed to quantify the approximate number of ketone and oxyamine groups at the cell surface after membrane fusion. Liposomes (**5**) were prepared as described above and were delivered to fbs in culture (3 mM in tris buffer, 400 μL added to 4 mL, 12 h). A time course assay was also conducted using FACS to determine whether the chemistry was being carried on after cell growth and division. Fbs (**9**) were reacted with hydrazine-conjugated biotin (3 mM in CBS, 1 mL added to 4 mL CBS in cell culture, 1 h) after culture with ketone-containing liposomes (**5**) for 1, 3, 5, and 7 d, followed by fluorescein-conjugated streptavidin (1 mM in CBS, 0.5 mL added to 4 mL CBS in cell culture, 1 h). A control cell population (not displaying ketone groups) was only incubated with biotin-hydrazide and streptavidin-fluorescein for 1 h each, under the same conditions. The cells were then centrifuged (5 min, 1000 rpm), resuspended in RPMI (without phenol red),

centrifuged (5 min, 1000 rpm), and resuspended in RPMI (~10^7 cells/2 mL). Fluorescence measurements were calibrated using RCP-5-30 beads (~10^7 beads/mL, Spherotech, Inc., Lake Forest, IL) of known fluorescein equivalent molecule density.[50] Fluorescent intensities based on number of cells counted were compared to the standard bead and control cells lacking fluorescent molecule conjugation and approximate numbers of fluorescent compound bound to the surface was calculated. Flow cytometry was performed using a Dako CyAn ADP (Beckman-Coulter, Brea, CA), and data was analyzed with Summit 4.3 software.

6.2.12 3D spheroid generation. Keto- (**5**) and oxy-LUVs (**6**) were added to two separate fb populations in culture for (3 mM in tris buffer, 400 μL added to 4 mL, 12 h), resulting in fusion and display of ketones and oxyamines from the cell surface. Oxyamine-presenting Rat2 fb (**11**) contained an m-cherry label (nucleus) for enhanced visualization, while the ketone-presenting Swiss 3T3 albino mouse fb (**9**) contained no fluorescent label. These two cell populations were then trypsinized and mixed together (~20^4 cells/mL, 4 mL total) in serum containing (10 % CBS, pH of 7.4) media in a 10 mL-flask and incubated at 37 °C and 5 % CO_2 for 3 h. After mixing, the cells were seeded on a glass surface (~20^4 cells/mL, 1 mL) and visualized under a Nikon TE2000-E inverted microscope or by scanning electron microscopy. Image acquisition and processing was performed using Metamorph software. An exposure time of 75 ms was used to image all spheroids.

6.2.13 Scanning electron microscopy (SEM) of 3D spheroids. Spheroids were assembled in solution (reaction for 3 h as described above), delivered to a glass slide (~20^4 cells/mL, 1 mL, 0.8 x 0.8 cm^2), and then fixed with 10 % formalin in PBS for 15 min. The substrate was then washed with water (15 min), and cells were then dehydrated stepwise in 30, 50, 70, 90, and 100 % ethanolic solutions for 15 min each.

After critical point drying and sputtering 2 nm of gold, the sample was ready for imaging using a Hitachi S-4700 field emission scanning electron microscope (Hitachi High Technologies America, Inc., Schaumburg, Illinois).

6.2.14 Human mesenchymal stem (hMSC) cell culture. hMSCs and basic, growth, and differentiation media were obtained from Lonza (Basel, Switzerland). hMSCs were cultured in Dulbecco's Modified Eagle Medium (Gibco) containing 10 % fetal bovine serum (FBS) and 1 % penicillin/streptomycin at 37°C in 5 % CO_2. Culturing with induction medium as described in the Lonza protocol induced Adipogenic differentiation.

6.2.15 Immunohistochemistry. After the growth of 3D tissue-like structures and co-culture with Swiss 3T3 albino mouse fb, surfaces were fixed with formaldehyde (4 % in PBS, 30 min). Substrates were then immersed in a solution containing water and 60 % isopropyl alcohol (3-5 min), followed by staining with Oil Red O (5 min) and Harris Hemotoxylin (1 min). Substrates were visualized by phase contrast microscopy using a Nikon TE2000-E inverted microscope. Image acquisition and processing was performed using Metamorph software. An exposure time of 75 ms was used to image all HMSCs.

6.2.16 Directed 3D tissue-like multi-layers. Ketone-functionalized fbs (**9**) were seeded (~10^4 cells/mL) to microcontact printed patterned surfaces (1 mM hexadecanethiol in EtOH, printed on gold for 5 s, backfilled with 1 mM EG_4 in EtOH, 16 h) that presented fibronectin (10 mg/mL, 2 h). The cells were allowed to grow for 3 d (37 ºC in 5 % CO_2).[29] Oxyamine-functionalized fbs (**10**) (~10^4 cells/mL) were then seeded to surfaces for 2 h, followed by addition of serum-containing (10 % CBS) media to promote cell growth. The cells were cultured for 3 more d before imaging. After generation, substrates were fixed, stained, and imaged by confocal microscopy as described below.

6.2.17 Cell staining for imaging. Cells were fixed with formaldehyde (4 % in PBS) and permeated (PBS containing 0.1 % Triton X 100). A fluorescent dye mixture,

containing phalloidin-TRITC (actin) and DAPI (nucleus) was then made in PBS containing 5 % normal goat serum and 0.1 % Triton X 100. Cells were incubated with the dye solution for 2 h. The substrates were then secured in fluorescence mounting medium (Dako, Carpinteria, CA, USA), which enhances the visualization of cells when viewed under a fluorescent microscope on a glass cover slip. An exposure time of 400 and 1200 ms were used to image nuclei and actin, respectively.

6.2.18 Confocal microscopy. Cell clusters and tissue formation were visualized with a Nikon Eclipse TE2000-E inverted microscope (Nikon USA, Inc., Melville, NY). The data were recorded using Leica software and a spectral confocal microscope (LeicaMicrosystems, Bannockburn, IL). An average of 84 image scans were used to generate the 3D reconstructions with Volocity software.

6.2.19 3D Co-culture spheroid and multi-layer generation. Spheroids: Keto- (**5**) and oxy-LUVs (**6**) were generated as previously reported and were added to hMSCs and fbs (3 mM in tris buffer, pH of 7.4, 400 μL added to 4 mL, 12 h), respectively, and were cultured, resulting in fusion and display of ketones (**12**) and oxyamines (**10**) from the cell surface. These two cell populations were then trypsinized and mixed together in serum containing (10 % FBS, pH of 7.4) media in a 10 mL flask and incubated at 37 °C and 5 % CO_2 for 1, 2, 3, and 5 h. After mixing for the allotted time, cells were seeded onto a glass surface and visualized under a Nikon TE2000-E inverted microscope under the brightfield setting (75 ms exposure time). Controls were also performed where hMSCs displaying ketone groups were co-cultured with fbs (not displaying oxyamine groups) for each of the corresponding time points, 1, 2, 3, and 5 h, seeded onto glass, and imaged under the brightfield setting (75 ms). Image acquisition and processing was performed using Metamorph software. *Multi-layers:* Keto- (**5**) and oxy-LUVs (**6**) were added to

hMSC and fbs (3 mM in tris buffer, 400 μL added to 4 mL, 12 h), respectively, and were cultured, resulting in fusion and display of ketones and oxyamines from the cell surface. hMSCs (**12**) displaying ketone groups were trypsinized and cultured on glass slides (10^5 cells/mL) and allowed to grow for 2 d. Fbs presenting oxyamines (**10**) were then trypsinized and added (10^5 cells/mL) to the hMSCs. These cells were co-cultured in media (10 % FCS) for 3, 5, and 7 d, resulting in the formation of 3D multi-layered, tissue-like structures of hMSCs and fbs.

6.2.20 Cell viability assay. Cell viability of 3D spheroid and multi-layered tissue-like structures was assessed using a trypan blue viability assay (Hyclone, Fisher Sci, Pittsburgh, PA). Fb spheroid and multi-layer structures were prepared as previously described. A solution of 0.4 % trypan blue in PBS was made and diluted in CBS (1:1) containing the spheroids (1, 3, and 5 h after mixing, 10^4 cells/mL) in solution and multi-layer cell sheets (3, 5, and 7 d after a second fb population was added, 10^5 cells/mL) on a glass slide. Trypan blue was allowed to react with the cells for 2 min, at which time spheroids and surfaces were imaged and false colored with blue for enhanced visualization using a Nikon TE2000-E inverted microscope. As a control, cells were cultured for 7 d to generate a multilayer and were then fixed as mentioned above. Trypan blue was allowed to react for 2 min, and cells were imaged. For phase contrast and fluorescent imaging, exposure times of 75 and 400 ms were used, respectively.

6.3 Results and Discussion

Vesicle fusion was directed through the use of molecular recognition and chemoselective ligation toward the goal of rewiring cell adhesion to generate 3D multi-layers of cells. Using liposomes as the simplest model of a cell, we first demonstrated and extensively characterized the parameters for chemoselectively driven liposome fusion. Vesicles were tailored with ketones (dodecanone) or oxyamines (*O*-

dodecyloxyamine, **A**) (Scheme 6.1). The resulting two populations of vesicles were used to study liposome adhesion or fusion to one another via oxime conjugation (Figure 6.2). This system was then integrated with mammalian cells in culture to fuse liposomes to cell membranes for applications in small molecule delivery and cell-surface engineering (Figure 6.3 and 6.4). Furthermore, we used this membrane modification strategy to direct the assembly of 3D spheroid clusters and tissue-like structures by culturing two cell populations functionalized with oxyamine- and ketone-containing groups (Figure 6.6-9, 6.11, and 6.12). Because this method is general, bio-orthogonal, chemically stable (oxime bond), non-invasive, and non-cytotoxic, patterned multi-layered tissue-like structures of different geometric shapes could also be fabricated without the use of 3D scaffolds to confine the cell populations.

6.3.1 Fusion methodology. In previous studies, we have shown how chemoselective oxime chemistry can be used to present biospecific ligands from supported, model fluid lipid bilayer membranes, for subsequent recognition of protein receptors.[51] Using this oxime ligation strategy, we generated a number of large unilamellar vesicles (LUVs) that present ketone or oxyamine functional groups and employed them in liposome-liposome fusion, and liposome-cell fusion studies. For liposome-liposome fusion analyses that include matrix-assisted laser-desorption/ionization mass spectrometry (MADLI-MS), dynamic light scattering (DLS), Fourier resonance energy transfer (FRET), and transmission electron microscopy (TEM), dodecanone and *O*-dodecyloxyamine molecules were incorporated, separately, into neutral, egg palmitoyl-oleoyl phosphatidylcholine (POPC) at a ratio of 5:95 to form keto-LUVs (**1**) and oxy-LUVs (**2**), respectively (Figure 6.1A and 6.1B). Dodecanone molecules were mixed with POPC and fluorescence donor, egg 1,2-diphytanoyl-*sn*-glycero-3-phosphoethanolamine-N-(7-nitro-2-1,3-benzoxadiazol-4-yl) (NBD-PE) at a ratio of 5:93:2 to form keto-NBD-PE-LUVs (**3**),

while dodecyloxyamine molecules were incorporated into POPC, negatively charged, egg 1-palmitoyl-2-oleoyl-phosphatidylglycerol (POPG), and fluorescence acceptor, egg 1,2-dipalmitoyl-*sn*-glycero-3-phosphoethanolamine-N-(lissamine rhodamine B sulfonyl) (rhod-PE) at a ratio of 5:73:20:2 to form oxy-rhod-PE-LUVs (**4**). These chemoselectively tailored liposomes (**3** and **4**) were used to conduct Fourier resonance energy transfer (FRET) studies (Figure 6.1C). Finally, liposomes that contained dodecanone, POPC, and cationic lipid, 1,2-dioleoyl-3-trimethylammonium-propane (DOTAP) (5:93:2, **5**) and liposomes that composed of dodecyloxyamine, POPC, and DOTAP (5:93:2, **6**) were generated to investigate liposome-cell fusion processes (Figure 6.1D). Cationic lipid, DOTAP, was incorporated to induce membrane fusion.[44,52] Our general fusion methodology is described in figure 6.1A. Two liposome populations (**1** & **2**, **3** & **4**, or **5** & **6**) were mixed, resulting in liposome docking, adhesion, and finally fusion due to the formation of stable, interfacial oxime bonds. Depending on the application, liposomes to each other, forming larger liposomal structures or to cell surfaces, demonstrating non-invasive, cell-surface engineering. Mixing **1** and **2** resulted in a gradual increase in size over a period of 2 h, followed by no change in size (Figure 6.2D). In a control reaction, LUVs not presenting ketones were reacted with LUVs containing oxyamines (**1**). Likewise, LUVs containing ketone groups (**2**) were mixed with LUVs that did not display oxyamines. For both of these control experiments, no size change was observed over time. This result strongly supports the idea that liposome adhesion and fusion are driven by chemoselective oxime bond formation between the ketone- and oxyamine-alkanes.

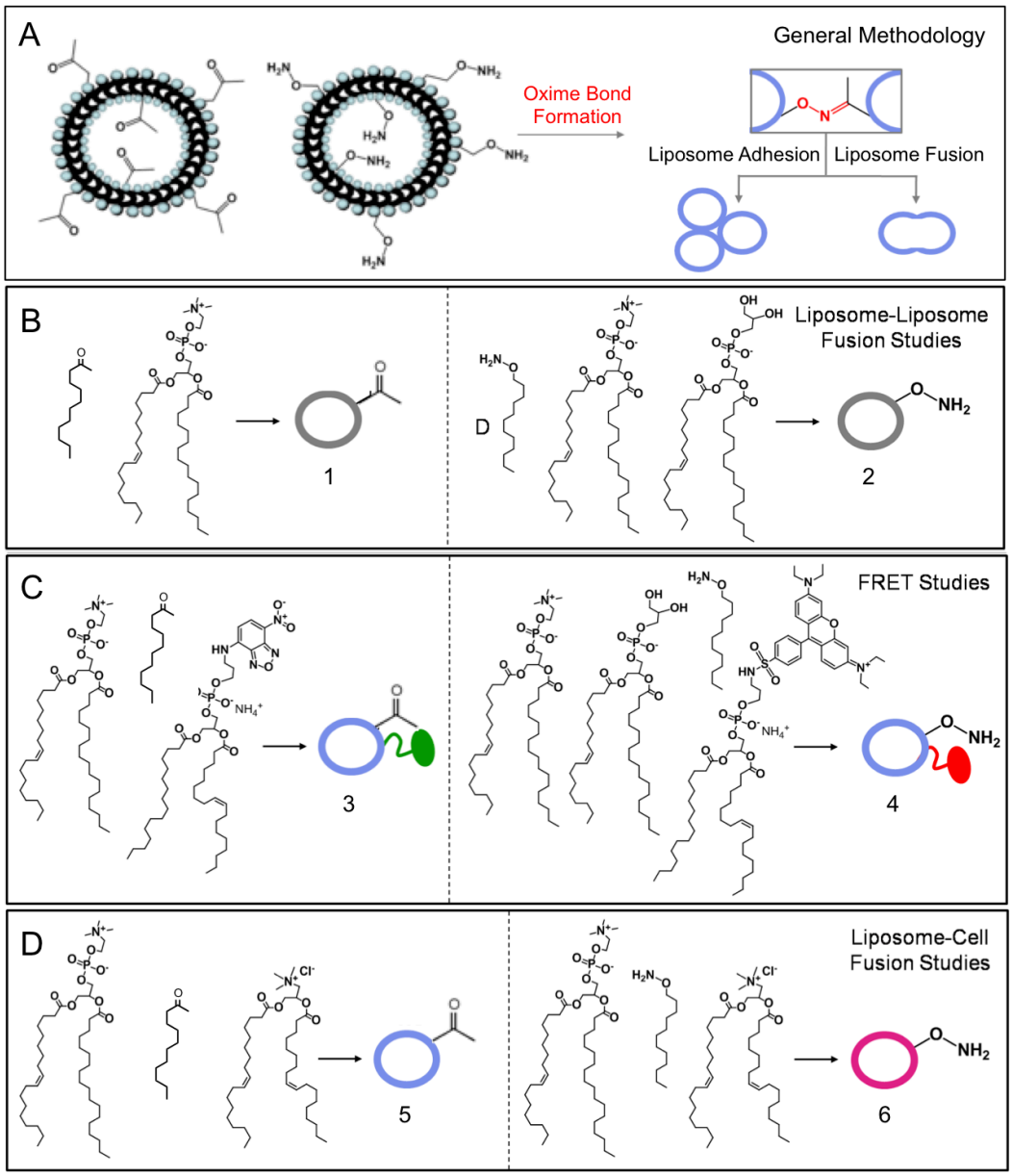

Figure 6.1 General schematic and corresponding lipid components for the formation of fused and adhered liposomes based on chemoselective oxime conjugation. (A) When mixed, ketone- and oxyamine-tethered liposomes react chemoselectively to form an interfacial, covalent oxime linkage, resulting in liposome docking and adhesion. Docked liposomes either fuse or form multi-adherent structures. (B) Dodecanone molecules were incorporated into neutral, POPC at a ratio of 5:95 to form keto-LUVs (**1**), while *O*-dodecyloxyamine molecules were incorporated into POPC and negatively charged, POPG at a ratio of 5:75:20 to form oxy-LUVs (**2**). These liposomes were used for liposome-liposome fusion studies. (C) Dodecanone molecules were incorporated into POPC and fluorescence donor, NBD-PE at a ratio of 5:93:2 to form keto-NBD-PE LUVs (**3**). *O*-Dodecyloxyamine molecules were incorporated into POPC, POPG, and fluorescence acceptor, rhod-PE at a ratio of 5:73:20:2 to form oxy-rhod-PE LUVs (**4**). These liposomes were used for FRET studies. (D) Dodecanone molecules were incorporated into POPC and positively charged, DOTAP at a ratio of 5:97:2 to form ketone-presenting liposomes (**5**). *O*-Dodecyloxyamine molecules were incorporated into POPC and DOTAP at a ratio of 5:93:2 to form oxyamine-presenting liposomes (**6**). These liposomes were used for cell-liposome fusion studies.

6.3.2 MALDI-MS characterization. Oxime conjugation, after keto-LUV (**1**) fusion, was confirmed by MALDI-MS analysis. SAMs of aminooxyundecanethiol were formed on a gold-coated sample plate.[57] A solution containing keto-LUVs (**1**) was then allowed to fuse and react with the surface for 90 min, followed by MALDI-MS examination. A mass of 387 units was detected, confirming successful oxime conjugation, resulting from liposome fusion on the surface (Figure 6.2A).

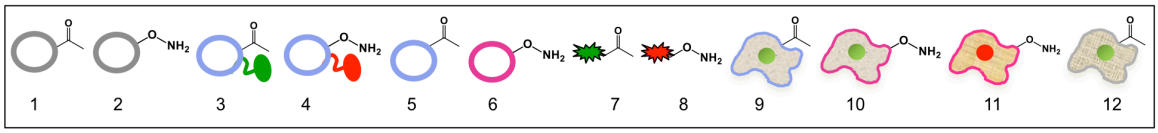

Scheme 6.3 List of liposomes, molecules, and cells used in this study: (**1**) keto-LUV; (**2**) oxy-LUV; (**3**) keto-NBD-PE LUV; (**4**) oxy-rhod-PE LUV; (**5**) ketone-functionalized liposomes; (**6**) oxyamine-functionalized liposomes; (**7**) fluorescein-ketone; (**8**) rhod-oxyamine; (**9**) ketone-functionalized fbs; (**10**) oxyamine-functionalized fbs; (**11**) oxyamine-functionalized m-cherry labeled rat2 fbs; and (**12**) ketone-functionalized human mesenchymal stem cells (hMSCs).

6.3.3 TEM. Structural insight into the formation of different adhered and fused liposomes was observed through TEM (Figure 6.2B).[53] Vesicles of different sizes and shapes result after 2 h of liposome mixing (keto-LUV, **1** and oxy-LUV, **2**). The liposome size gradually increased with time, which is consistent with the data collected from other sizing experiments (e.g., DLS). Upon reaction, the following three structures were observed: multi-adherent liposomes that were not fused, partially fused liposomes, and completely fused, large uni- and multi-lamellar liposomes (Figure 6.2B).

6.3.4 DLS. DLS was performed upon mixing liposomes (**1** and **2**) to monitor vesicle size change as a function of time. Increases in vesicle size were observed due to aggregation, adhesion, or fusion (blue trace, Figure 6.2D). Saturation was reached ~80 min after mixing with a liposomal size of 220 nm. Without the presence of ketone and oxyamine functional groups, the LUV size remains constant (red trace, Figure 6.2D).

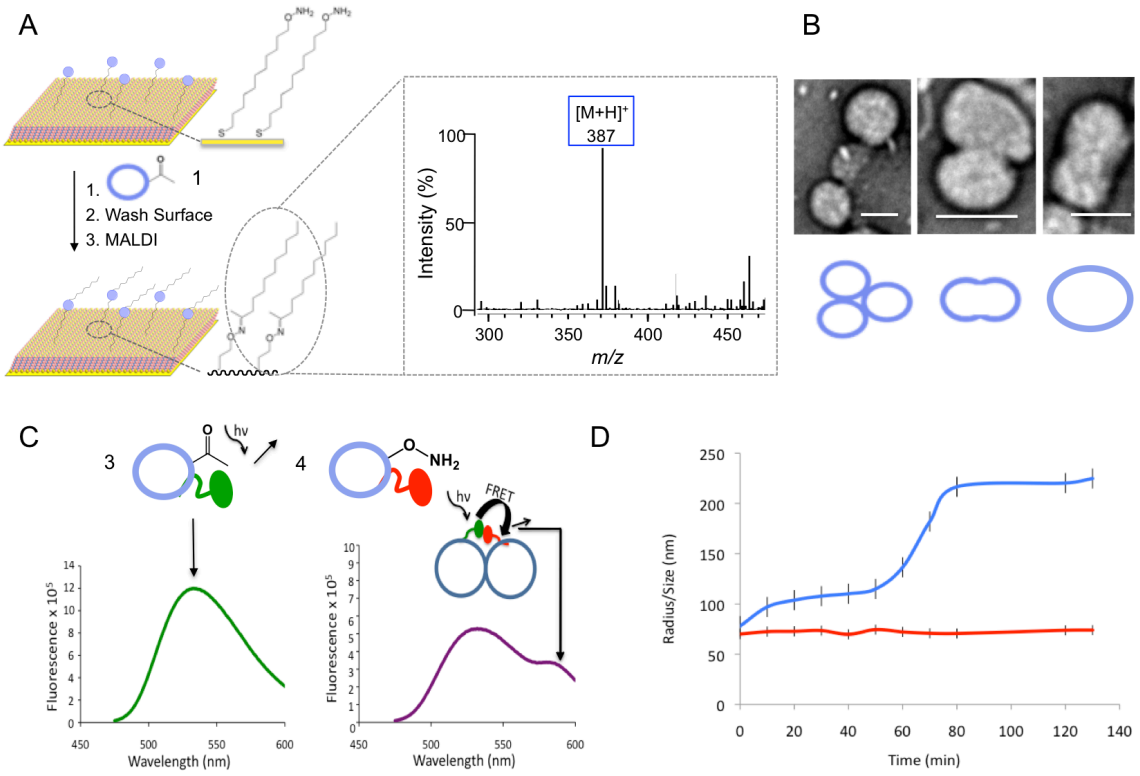

Figure 6.2 Liposome-liposome fusion characterization. (A) Mass spectrometry (MS) data representing the oxime ligation of keto-LUVs to self-assembled monolayers (SAMs) of oxyamine-terminated alkanethiol on a gold surface is displayed. Matrix-assisted laser desorption/ionization (MALDI) was performed after keto-LUVs were delivered to the surface, and a mass of 387 units was detected, confirming oxime conjugation. (B) Structural analyses using transmission electron microscopy (TEM), representing the adhesion and fusion of keto- (**1**) and oxy- (**2**) LUVs over time. The following images are shown from left to right: multi-adherent liposomes that are not fused; partially fused liposomes; and a single, large liposome after complete fusion. The scale bars represent 60 nm. (C) Fourier resonance energy transfer (FRET) analysis of liposome adhesion and fusion was monitored over 2 h. Fluorescence emission of keto-NBD-PE/PC LUVs (**3**), excited at 460 nm, was observed by scanning 475-600 nm (green trace). Fluorescence emission of keto-NBD-PE/PC LUVs (**3**) mixed with oxy-rhod-PE/PC/POPG LUVs (**4**) is represented (purple trace). A new FRET emission peak is observed at 578 nm showing mixed liposome adhesion. (D) Dynamic light scattering (DLS) was performed upon mixing liposomes (**1** and **2**) to monitor vesicle size change as a function of time. Increases in vesicle size were observed due to aggregation, adhesion, or fusion (blue trace). Liposome saturation was reached ~80 min after mixing. Without the presence of ketone and oxyamine functional groups, the LUV size remains constant (red trace).

6.3.5 FRET. Figure 6.2C shows a liposome fusion assay involving FRET characterization. A lipid-bound FRET pair, NBD-PE (donor) and rhod-PE (acceptor), were incorporated at 2 mol % concentration during liposome generation to produce keto-NBD-PE LUVs (**3**) and oxy-rhod-PE LUVs (**4**), respectively. Hypothetically, fusion of

these vesicles should result in a gradual decrease in the donor emission peak and an increase in acceptor emission peak[52] due to the close proximity of these dyes. As shown, vesicle mixing resulted in this FRET fusion signature. Fusion was observed immediately upon mixing **3** and **4**, slowing within 2 h to a stable population, which is similar to earlier sizing results. An emission peak was not observed for the acceptor rhodamine dye when performing control experiments that tested the energy transfer with an LUV that did not contain oxyamines. Similar results were observed when LUVs that did not contain ketones or oxyamines were mixed. This data further supports that liposome aggregation and fusion is based on chemoselective oxime bond formation.

6.3.6 Cell-surface engineering. Chemical approaches to engineer cell surfaces have emerged as powerful tools for a variety of biomedical and biotechnological applications, including tissue engineering, drug delivery, and cell-based therapies.[37] Several metabolic and genetic approaches to display small molecular recognition pairs at cell surfaces for further covalent modification have been achieved through Click chemistry[54] and Staudinger ligation.[55] However, such strategies may alter cellular physiology and interfere with normal biochemical pathways.[56] In this report, we use oxime chemistry to tailor and fluorescently label cell surfaces via a novel liposome fusion strategy. As mentioned, cationic lipid, DOTAP, was incorporated within keto- and oxy-LUVs to initiate electrostatic destabilization and subsequent fusion to the cell membrane.[44] As such, the minimum DOTAP concentration required to facilitate liposome-cell fusion was determined to be 2 % through fluorescence labeling optimization. Keto-LUVs were generated using DOTAP and POPC concentrations that ranged from 0.5 % to 5 % and 90 % to 94.5 %, respectively, while maintaining a 5-% ketone concentration. These liposomes were incubated with fibroblasts (fbs) for 4 h, conjugated with an oxyamine-tethered rhodamine (rhod-oxyamine, **8**) (0.7 mM, 2 h), and the cell fluorescence

intensities were then compared. From 2 % to 5 % DOTAP, the intensities were almost identical, indicating that 2 % DOTAP is sufficient to initiate fusion.

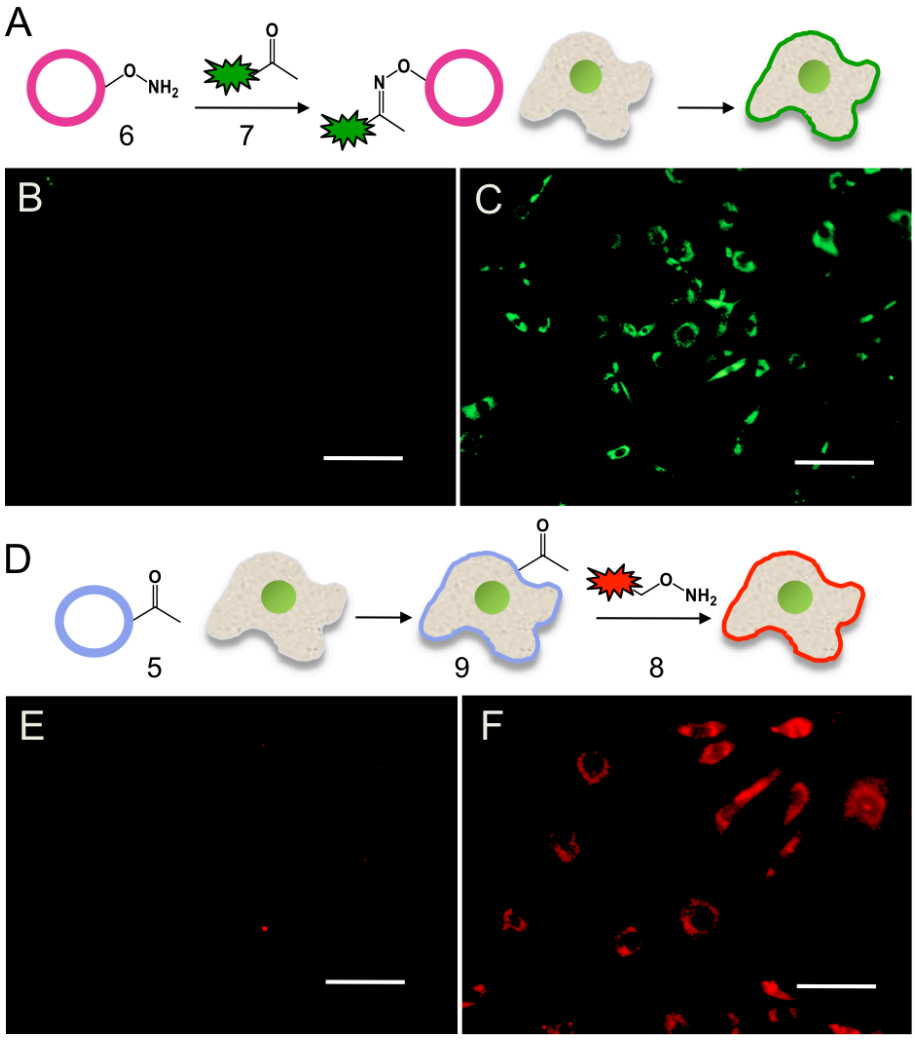

Figure 6.3 (Top) Schematic describing the delivery and subsequent fusion of fluorescent liposomes to cell surfaces with corresponding brightfield and fluorescent images. (A) Oxy-LUVs (**6**, 3 mM) were reacted with fluorescein-ketone (**7**, 0.15 mM, 2 h) to generate green fluorescent liposomes. The fluorescent liposomes were then added to fbs in culture, resulting in the fluorescent labeling of cells after liposome fusion to the cell membrane. Micrographs show (B) control cells where liposomes not containing oxyamine groups were incubated with fluorescein-ketone and added to fbs in culture for 2 h. and (C) green fluorescently labeled cells after oxyamine-functionalized liposomes were incubated with fluorescein-ketone and delivered to fbs (2 h). (Bottom) General schematic and images for cell-surface tailoring using liposome fusion and chemoselective oxime chemistry. (D) Keto-LUVs (**5**, 3 mM) were added and fused with the cells to display these groups from the cell surface (**9**). Addition of rhod-oxyamine (**8**, 0.7 mM in H_2O, 2 min) resulted in chemoselective oxime formation and red fluorescent labeling of the cells. Images display (E) control fbs where liposomes not displaying ketones were fused to the membrane (2 h) and rhod-oxyamine was added and no fluorescence was observed and (F) fluorescently labeled cells after ketone-functionalized liposomes were fused to fbs (2 h) and cells were -incubated with rhod-oxyamine. Scale bars for b and c and d and e represent 50 and 30 μm, respectively.

Given this optimized lipid ratio (POPC/ketone or oxyamine/DOTAP at 93:5:2), two cell-surface engineering methods were employed to fluorescently label fbs. Similar to our optimization experiments, a solution of keto-LUVs (**5**, 200 μL, 0.6 mM) was added to fbs in culture for 2 h, resulting in membrane fusion and subsequent display of ketones from the cell surface (**9**) (Figure 6.3D). Rhod-oxyamine (**8**, 100 μL, 0.7 mM in H_2O) was then added the cells for 2 h. After oxime formation, the fbs were washed with PBS, trypsinized, diluted with CBS-containing media (~10^2/mL), seeded to a glass substrate, and imaged under a fluorescent microscope. As observed in figure 6.3F, the conjugation of rhod-oxyamine with ketone-presenting fbs resulted in the red fluorescence labeling of cells. When the control fbs (i.e., no ketone groups present) were reacted with rhod-oxyamine (**8**) and then imaged, no fluorescence was observed (Figure 6.3E). To demonstrate the flexibility of this liposome-based surface labeling strategy, we modified fb surfaces to present a ketone-functionalized fluorescein dye (**7**) after oxy-LUV-ketone-fluorescein conjugation and subsequent membrane fusion (Figure 6.3A). A solution of oxy-LUVs (**6**, 3 mM) was incubated with a ketone-functionalized fluorescein (**7**, 0.15 mM, 1 eq, 2 h), generating fluorescently labeled liposomes. The liposomes were then added to fbs in culture for 2 h. After fusion, the cells were washed with PBS, trypsinized, diluted with CBS-containing media (~10^2/mL), seeded to a glass substrate, and imaged under a fluorescent microscope. Figure 6.3C presents green fluorescently labeled fbs after fusion with fluorescein-functionalized LUVs. When liposomes, not containing oxyamine groups were incubated with fluorescein-ketone and added to fbs in culture for 2 h, no fluorescence was observed (Figure 6.3B). Thus, our control images indicated that reaction and labeling do not occur without the proper oxime recognition pair (Figure 6.3B and 6.3E). Furthermore, under these conditions, we observed no changes in cell behavior upon liposome fusion to cells. This is a very important feature for future *in vivo*

applications. Thus, by combining liposome fusion and oxime chemistry, we were able to tailor the cell surface with either ketone groups or oxyamine groups, which may act as chemoselective cell-surface receptors for a range of small molecules, ligands, biomolecules, and nanoparticles.

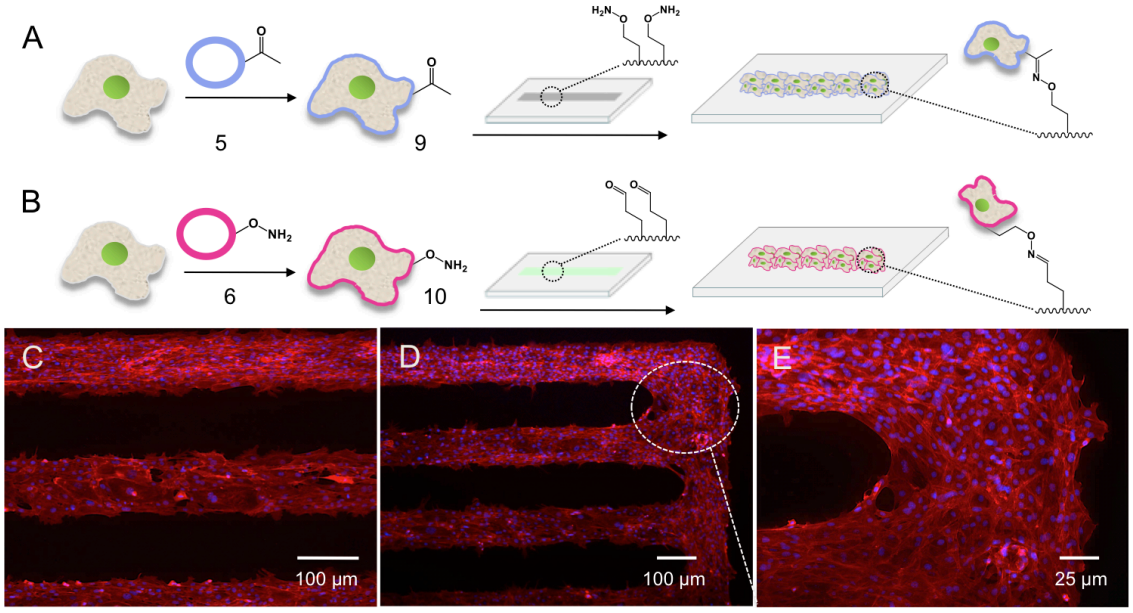

Figure 6.4 Schematics and fluorescent micrographs of rewired cells adhered to patterned self-assembled monolayers (SAMs) of alkanethiolates on gold substrates. (A and B) Keto- (**5**) and oxy-LUVs (**6**, 3 mM, 4 h) were cultured with separate fb populations, producing ketone- and oxyamine-presenting fbs (**9** and **10**, respectively). These cells were then seeded (~10^2 per mL, 2 h) to patterned, oxyamine- and aldehyde-terminated SAMs (10 %), respectively, and allowed to adhere through stable oxime conjugation. The unpatterned surface regions present tetra(ethylene glycol), which resists cell and protein adsorption. The cells then grew and proliferated only filling out the oxyamine- and aldehyde-tethered surface regions, respectively. (C) A fluorescent micrograph of patterned ketone-fbs (**9**), adhered to an oxyamine-terminated SAM is shown. (D and E) Fluorescent micrographs of patterned oxyamine-fbs (**10**), adhered to an aldehyde-terminated SAM are demonstrated. Cells were stained with DAPI (blue, nucleus) and phalloidin (red, actin).

6.3.7 Rewiring cell adhesion. The ability to adhere cells to a variety of materials through a simple bio-orthogonal approach that does not rely on proteins or complex ligands enables novel ways to manipulate cells and modify biomaterials for a range of biotechnological and tissue engineering applications. Therefore, we extended our liposome fusion strategy to rewire cells to adhere to materials presenting bio-orthogonal, complementary synthetic ligands (Figure 6.4). Two cell populations were cultured

separately with ketone- (**5**) or oxyamine- (**6**) containing liposomes and were then seeded on patterned surfaces displaying either oxyamine or aldehyde groups, respectively. Employing previously developed self-assembled monolayer (SAM) technologies, surfaces were patterned via a microfluidics to present either 10 % oxyamine[48] or aldehyde[47] and 90 % tetra(ethylene)glycol (EG_4) functional groups (Figure 6.4A and 6.4B, respectively*)*. The remaining, unpatterned regions were back-filled to present EG_4 terminal groups, which are known to resist non-specific protein adsorption and cell attachment.[49] Upon seeding cells presenting ketone (**9**) or oxyamine (**10**) groups to the complementary surfaces, an interfacial oxime reaction occurred and cells adhered, spread, and proliferated in the patterned regions (Figure 6.4C-E). However, untreated cells and cells cultured with liposomes, not containing the key functional groups, did not attach to the surface. This strategy allows for a bottom-up, bio-orthogonal synthetic approach to rewire how cells adhere to materials and does not require genetic manipulations of cells.

6.3.8 Flow cytometry. After conducting the above liposome-cell fusion characterization experiments, we hypothesized that cell proliferation of the liposome-fused cells carries unreacted ketone or oxyamine groups on the cell membranes. This hypothesis was further supported by flow cytometry in conducting FACS analyses (Figure 6.5). Ketone-functionalized cells (**5**) were reacted with hydrazide-conjugated biotin (3 mM in CBS, 1 h), followed by fluorescein-tethered streptavidin (1 mM in CBS, 1 h), and the fluorescence intensity was compared to a bead of known fluorescein density and control cells (without ketone groups) (Figure 6.5A and 6.5B).[50] The approximate number of ketone and oxyamine molecules displayed from the cell surface after membrane fusion (12 h), as well as throughout cell growth and division (3, 5, and 7 days in culture) was then tabulated. FACS showed that approximately, 9800 ketone or

oxyamine molecules were imbedded into the cell surface after 12 hours of liposome incubation (Figure 6.5C). Further culturing these cells indicated a decrease in available molecules from 3, 5, and 7 days with 7300, 2100, and 800 molecules per cell, respectively (Figure 6.5C and 6.5D). Fluorescence was still detected, although not as intense, after 7 days of cell culture, indicating that ketone and oxyamine groups were carried through cell division. The control cells (i.e., no ketone groups present) that were incubated with hydrazide-biotin and fluorescein-tethered streptavidin demonstrated little to no fluorescence.

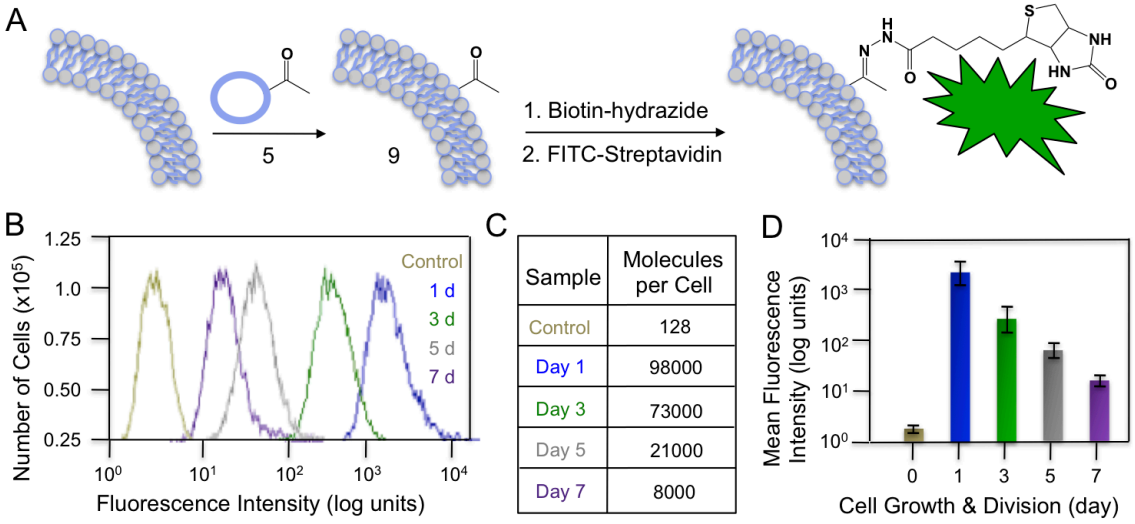

Sample	Molecules per Cell
Control	128
Day 1	98000
Day 3	73000
Day 5	21000
Day 7	8000

Figure 6.5 The determination of ketone molecules per cell by flow cytomtery is shown. (A) Fbs were cultured with (**5**) or without (control) ketone-containing liposomes for 1, 3, 5, and 7 days. The fbs (**9**) were then reacted with hydrazide-conjugated biotin, followed by fluorescein-labeled streptavidin. Fbs were then tested against a standard bead (~10^7 beads/mL) with known fluorescein molecule density. Approximately 10^5 cells were counted for all samples. Samples were run in triplicate, and the mean fluorescence intensity values are displayed ± RSD. (B) FACS data relating the number of cells counted (~10^5) as a function of fluorescence intensity are shown and labeled as control (without ketone) and days 1, 3, 5, and 7 (with ketone). Fluorescence was observed for all ketone-displaying populations with a decrease from 1 to 7 days, indicating that the ketone group is carried through cell growth and division. (C) The number of fluorescein molecules was calculated by comparing the relative mean intensity to a standard bead with known fluorescein molecule density. The numbers of ketone molecules per cell, as well as the control are listed, showing a decrease in density on the cell surface over time. (D) The relationship between the mean fluorescence intensity and the number of days incubated with ketone-containing liposomes is shown. As cells grow and divide over the course of 7 days, the ketone is carried through.

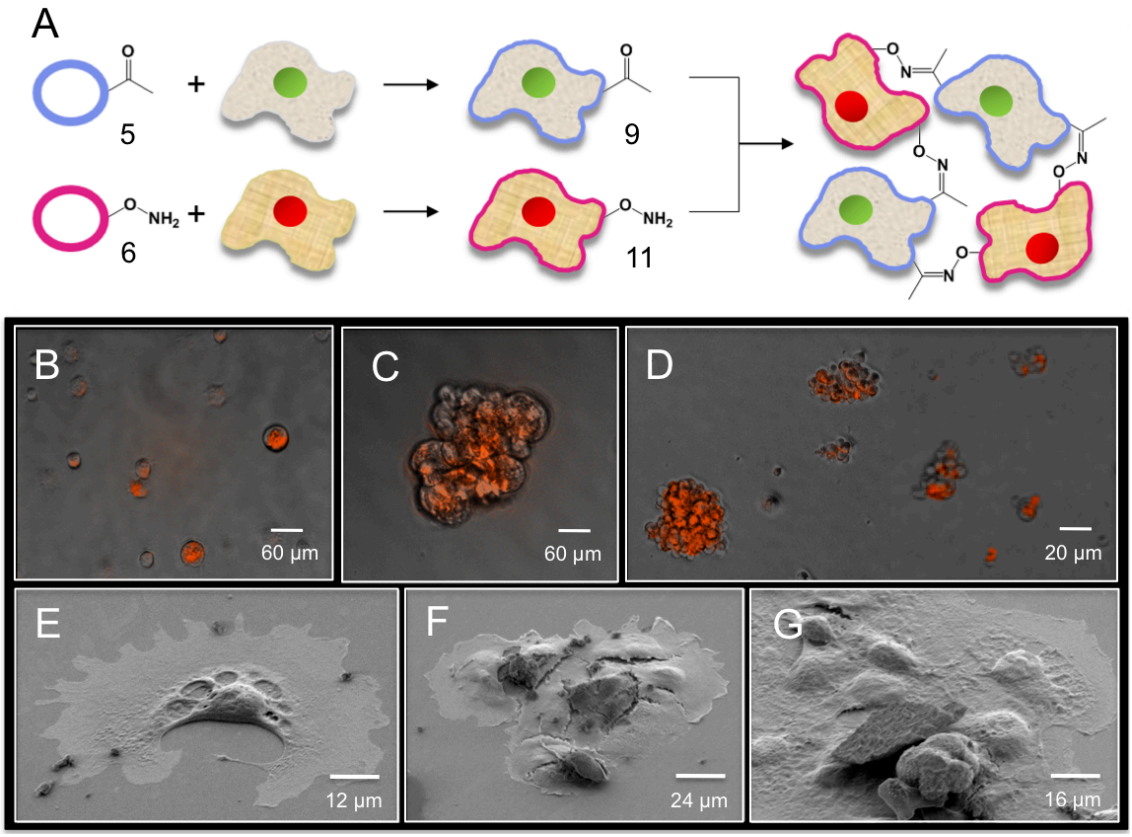

Figure 6.6 Fluorescent, phase contrast, and scanning electron micrographs (SEM) describing 3D spheroid formation via liposome fusion and chemoselective cell-surface tailoring. Two fb populations were cultured separately with ketone- (**5**) or oxyamine- (**6**) containing liposomes, resulting in membrane fusion and subsequent tethering of ketones and oxyamines from the cell surface. The oxyamine-tethered rat2 fbs (**11**) contained a fluorescent m-cherry nuclear label. The ketone-presenting Swiss albino 3T3 fbs (**9**) were not fluorescently labeled. (A) Two fb populations were cultured separately with ketone- (**5**) or oxyamine- (**6**) containing liposomes. Due to the presence of a positively charged liposome, fusion occurred, producing ketone- (**9**) and oxyamine- (**11**) tethered fbs. Upon mixing these cell populations, clustering and tissue-like formation, based on chemoselective oxime conjugation, occurred. (B) Control experiments (overlay image) demonstrate no spheroid formation for cells that did not contain either ketone or oxyamine groups. (C and D) However, when two cell populations displaying ketone (**5**) and oxyamine (**6**) recognition groups are mixed, interconnected spheroid assemblies form (overlay images). (E-G) Representative SEM images of (E) control cells and (E and F) spheroid assemblies, as described above, are displayed. For all spheroid assemblies depicted, cell populations were mixed and cultured together for 3 h before imaging at ~10^4 cells/mL.

6.3.9 3D spheroid assembly. The ability to generate multicellular connected tissues of multiple cell types *in vitro* is crucial for studying the complex interplay of cells in a range of organs *in vivo* and for developing strategies for synthetic tissue transplantation. With varying successes, a number of current strategies to generate 3D cell connections

rely on forcing mixed cell populations into complex microfabricated wells or vessels. Therefore, we extended this liposome fusion, oxime-based strategy to generate 3D spheroid assemblies of interconnected cells using two different cell-type populations (Figure 6.6). The oxyamine-presenting rat2 fbs (**11**) contained a nuclear m-cherry fluorescent label so that the cell clustering to non-fluorescent ketone-tethered cells (**9**) could be easily observed. During a 3-hour period of mixed-culturing (~10^4 cells/mL) in solution, cells formed spheroid structures due to the presence of complementary recognition groups (Figure 6.6C and 6.6D). Furthermore, when oxyamine-presenting fbs (**9**) were cultured with control fbs (i.e., cells not functionalized with ketone groups), spheroid assembly did not occur (Figure 6.6B). Studies were also performed to test whether spheroid size and cell composition could be controlled (Figure 6.7). Ketone-presenting hMSCs (**12**) were co-cultured with oxyamine-functionalized fbs (**10**) for 1, 2, 3, and 5 h. After 1 h, clusters comprised only with a few cells were observed. As the co-culturing duration was increased, larger spheroid structures were observed. Notably, control experiments were performed simultaneously to ensure that spheroid generation was being directed through chemoselective oxime conjugation. Shown as insets in figure 6.7A-D, tissue structure formation did not occur without the proper complementary pair displayed from cell surfaces, regardless of the mixing duration (1-5 h). Thus, size and composition of 3D cell assemblies in solution could be controlled, showing great promise for applications in stem cell transplantation and regenerative medicine.

Spheroid formation was also characterized by scanning electron microscopy (SEM) (Figure 6.6E-G). Cells functionalized with oxyamine (**10**) and ketone (**9**) groups were able to generate clusters when mixed in solution, as displayed in figure 6.6F and 6.6G. However, spheroid assemblies were not observed when ketone-presenting fbs were reacted with non-functionalized cells; fbs spread out on the surface, migrated, but

remained alone (Figure 6.6E). Notably, cells were able to form stable, interconnected 3D structures in solution simply upon mixing two tailored cell populations. Currently, methods to generate these structures require the support of a 3D hydrogel matrix and/or assisted assembly through an external stimulus.[22,24-26,30]

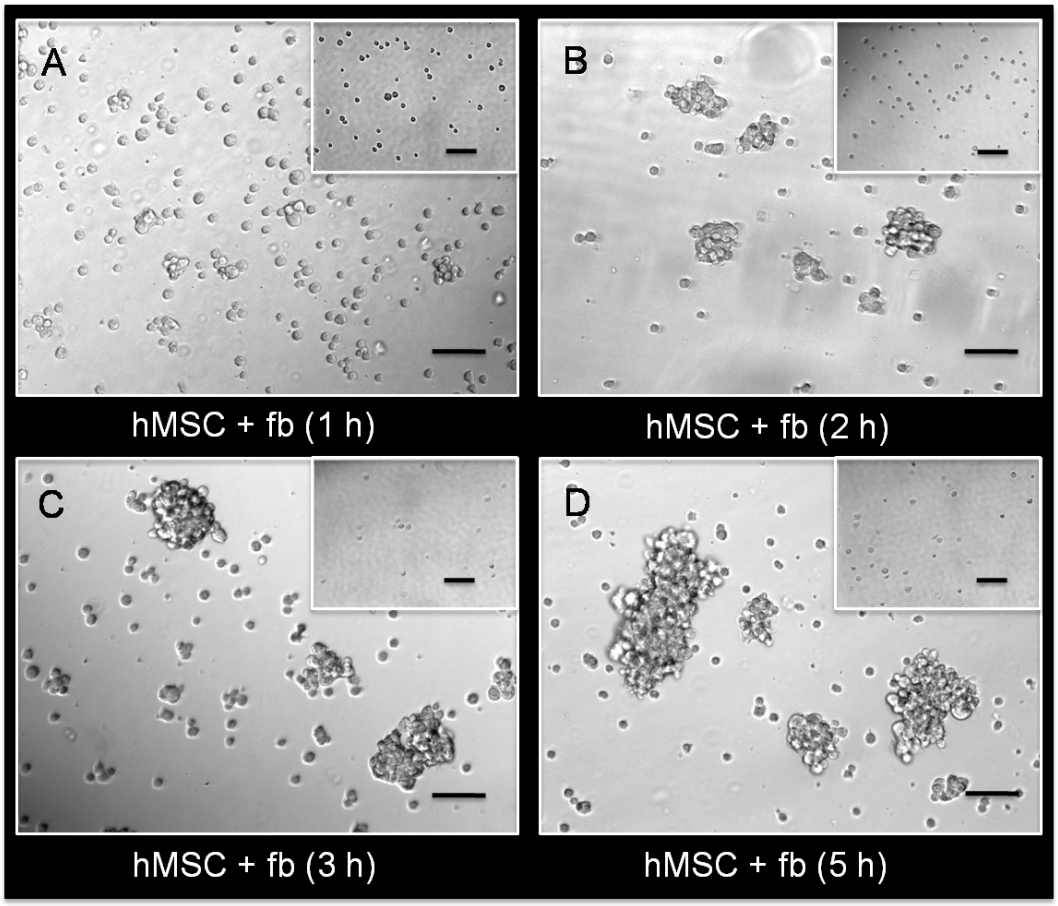

Figure 6.7 Phase contrast images representing control of spheroid size and composition. Human Mesencymal stem cells (hMSCs) were cultured with ketone-containing liposomes (12 h), resulting in fusion and display of ketone groups from the cell surface (**12**). Similarly, fbs were cultured with oxyamine-functionalized liposomes (**10**). The two populations were mixed together (10^4 cells/mL, 1:1), allowed to react for (A) 1, (B) 2, (C) 3, and (D) 5 h, pipetted onto glass substrates, and were imaged by phase contrast microscopy. As shown, the spheroids continued to grow in size as mixing duration increases. Scale bars represent 60 μm. The insets represent control experiments where ketone-functionalized hMSCs (**12**) were co-cultured with fbs (not displaying oxyamine groups) for each of the corresponding time points (A) 1, (B) 2, (C) 3, and (D) 5 h, and no spheroid assembly occurs. Scale bars for all inset images represent 300 μm.

6.3.10 3D multi-layered tissues. In addition to forming small, 3D cell clusters or spheroid structures in solution, this strategy may be employed to direct larger, dense 3D

tissue-like networks on a surface with geometric control. We used full substrates (Figure 6.8, 6.9, and 6.12), as well as surfaces that were patterned with cell adhesive and non-adhesive regions to generate multi-layered sheets and patterned tissue structures (Figure 6.11), respectively.[57] Ketone- (**5**) and oxyamine- (**6**) tailored liposomes were cultured with separate fb populations, resulting in membrane fusion and subsequent presentation of chemoselective sites for oxime conjugation from the surface (**9** and **10**, respectively) (Figure 6.8A). Culturing these groups on a solid support (~10^5 cells/mL) and in a layer-by-layer deposition manner gave rise to multi-layered, tissue-like cell sheets, which were characterized by confocal microscopy, as shown in figure 6.8E and 6.8F. Fbs naturally form a single monolayer once they become contact-inhibited. However, we have successfully induced fb-fb clustering though oxime-mediated, cell-surface engineering based on liposome fusion.

To ensure that oxime chemistry was aiding in the formation of 3D tissue-like structures, several control experiments were performed. Cells that did not present ketone or oxyamine functionality were seeded onto separate surfaces. A second cell population presenting oxyamine (**10**) or ketone (**9**) groups from the cell surface was added, resulting in the formation of only a 2D monolayer of cells (Figure 6.8B and 6.8C). Similarly, two different cell populations that were tethered with oxyamine (**10**) groups were mixed together, and only a 2D monolayer was generated after 4 days of culture. The same results were observed after culturing two different ketone-functionalized cell populations (**9**) for 4 days. These results further support our hypothesis that multi-layered cell interconnectivity is driven by complementary, oxime chemistry. We also extended this strategy toward the generation of 3D multi-layered co-cultures with hMSCs and fbs (Figure 6.9). Ketone-functionalized hMSCs (**12**) were first cultured on a substrate (~10^5 cells/mL), and stem cells were allowed to spread out and grow for 2 days.

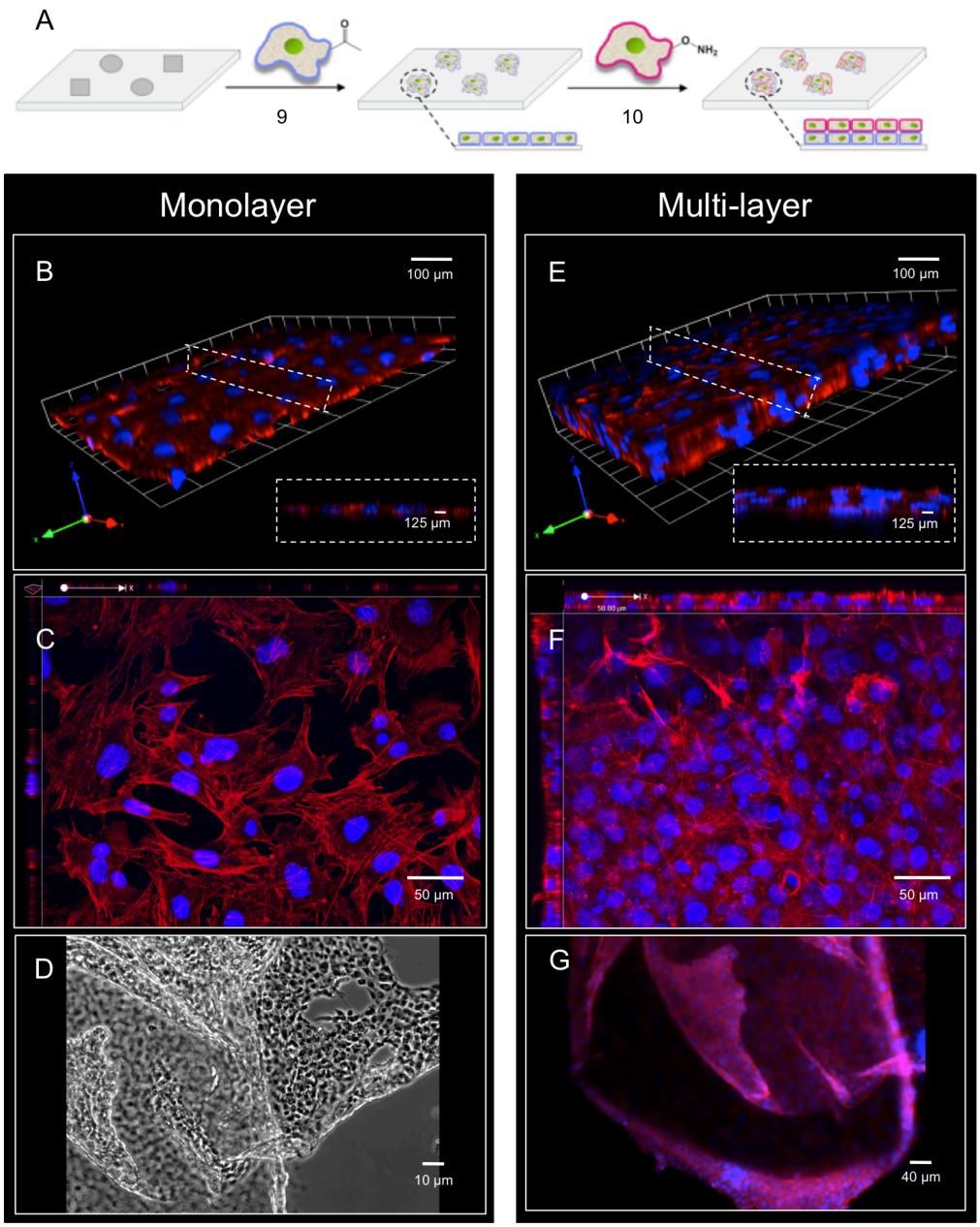

Figure 6.8 General schematic and images of oxime-mediated, 3D tissue-like structure formation with controlled interconnectivity. (A) Ketone- (**5**) and oxyamine- (**6**) containing liposomes were added to two separate fb populations, resulting in membrane fusion and subsequent presentation of the ketone (**9**) and oxyamine (**10**) groups from cell surfaces. By culturing these cells on substrates, alternating cell population seeding layer-by-layer, gave rise to multi-layered, tissue-like cell sheets through stable oxime chemistry. (B) A 3D reconstruction and (C) confocal micrograph showing only a monolayer of cells after oxyamine-presenting cells (**10**) were cultured with adhered non-functionalized cells. (E) A 3D reconstruction and (F) confocal micrograph of multiple cell layers after oxyamine-presenting cells (**10**) were added to substrates presenting ketone-containing cells (**9**). (D and G) Intact, 3D multi-layered cell sheets can be removed from the surface by gentle agitation as displayed by brightfield and fluorescent images. The insets in B and E show a z-plane cross-section that indicates the thickness of the cell layers. Cells were stained with DAPI (blue, nucleus) and phalloidin (red, actin).

Oxyamine-presenting fbs (**10**) were then added (~10^5 cells/mL) and co-cultured for an additional 2 days. As shown by the confocal images in figure 6.9B and 6.9C, 3D multi-layered cell sheets (4 layers) were formed. The proper controls were conducted; without the oxime pair, only a 2D monolayer of stem cells and fbs was formed (Figure 6.9A).

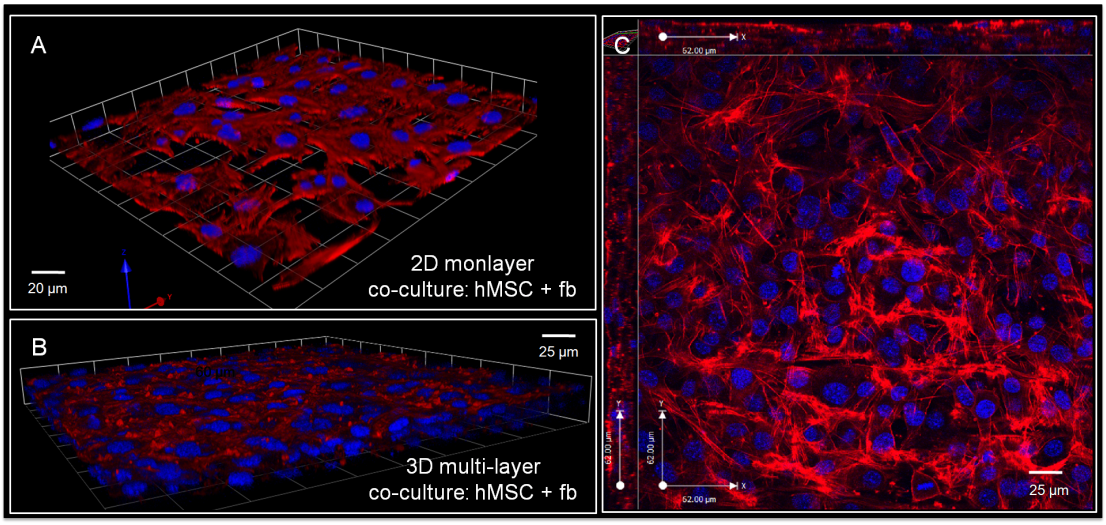

Figure 6.9 Confocal images representing images of oxime-mediated, 3D tissue-like structure formation with hMSC/fb co-cultures. Separate hMSC and fb populations were functionalized with ketone- and oxyamine-containing liposomes, respectively, resulting in membrane fusion and subsequent presentation of the ketone (**12**) and oxyamine (**10**) groups from cell surfaces. By culturing these cells on substrates, alternating cell population seeding layer-by-layer, gave rise to multi-layered, tissue-like cell sheets through stable oxime chemistry. (A) A 2D reconstruction image showing only a monolayer of cells after ketone-tethered hMSCs (**12**) were co-cultured with non-functionalized fbs. (B) A 3D reconstruction and (C) confocal micrograph displaying 3D multiple cell layers after oxyamine-presenting fbs (**10**) were added to hMSCs presenting ketone groups (**12**). Cells were stained with DAPI (blue, nucleus) and phalloidin (red, actin).

6.3.11 3D tissue release and cell viability. During multi-layer culture, it was possible to control the release of the tissues from the surface with gentle agitation (Figure 6.8D and 6.8G). The ability to release tissue after surface-supported growth *in vitro* shows great potential for applications in tissue engineering and cellular transplantation. Cell viability was also tested for 3D spheroid and multi-layered structures of fbs and hMSC/fb co-cultures using the trypan blue assay (Figure 6.10).[50] After spheroid (1, 2, 3, and 5 hours of mixing in solution) and multi-layer (3, 5, and 7 days on a surface) formation,

cells were incubated with trypan blue (0.4 %, 2 min). Viability was 100 % for all cells in the spheroid assemblies (1-5 hours) and multi-layer structure at day 3. After 5 and 7 days of multi-layer generation, cells showed an approximate viability of 91 % and 84 %, respectively. The blue intensity (fluorescence false colored for enhanced visualization) was compared to a control cell population by linescan analysis (Figure 6.10G). The control cells were cultured for 7 days to generate 3D multi-layers and were then fixed. Trypan blue was allowed to react for 2 min, followed by imaging and quantification. Overall, the viability of cells in conducting membrane fusion to generate 3D tissue-like structures in solution and on a solid support is high. Therefore, this method may be very useful for applications in tissue engineering and stem cell transplantation.

6.3.12 3D tissue patches with geometrical control. We further demonstrated spatial control by generating a number of 3D multi-cellular micropatterns. Microcontact printing[57] was used to produce a variety of patterns and geometries on a gold substrate. Employing SAM and microfabrication technologies, hexadecanethiol (1 mM in EtOH) was printed on a gold surface. The surface was then backfilled with EG_4 (1 mM in EtOH, 16 h) to render the remaining regions inert to nonspecific protein absorption. Fibronectin, a cell-adhesive protein was then added (10 mg/mL in CBS, 2 h), adhering only to the hydrophobic, patterned areas. As shown by the confocal image in figure 6.11A, only a 2D, circular cell pattern arises after ketone-presenting fbs (**9**) were cultured with fbs, not functionalized with oxyamine molecules. However, when liposome fusion occurs to display complementary ketone and oxyamine groups from cell surfaces (**9** and **10**, respectively), multi-layered 3D cell patterns were formed (Figure 6.11B-D). Circular, bar, and square circular tissue-like structures are depicted in figure 6.1B-D. The ability to generate 3D tissues with controlled geometry would find great use in tissue transplantation, in which specifically tailored patches are required.

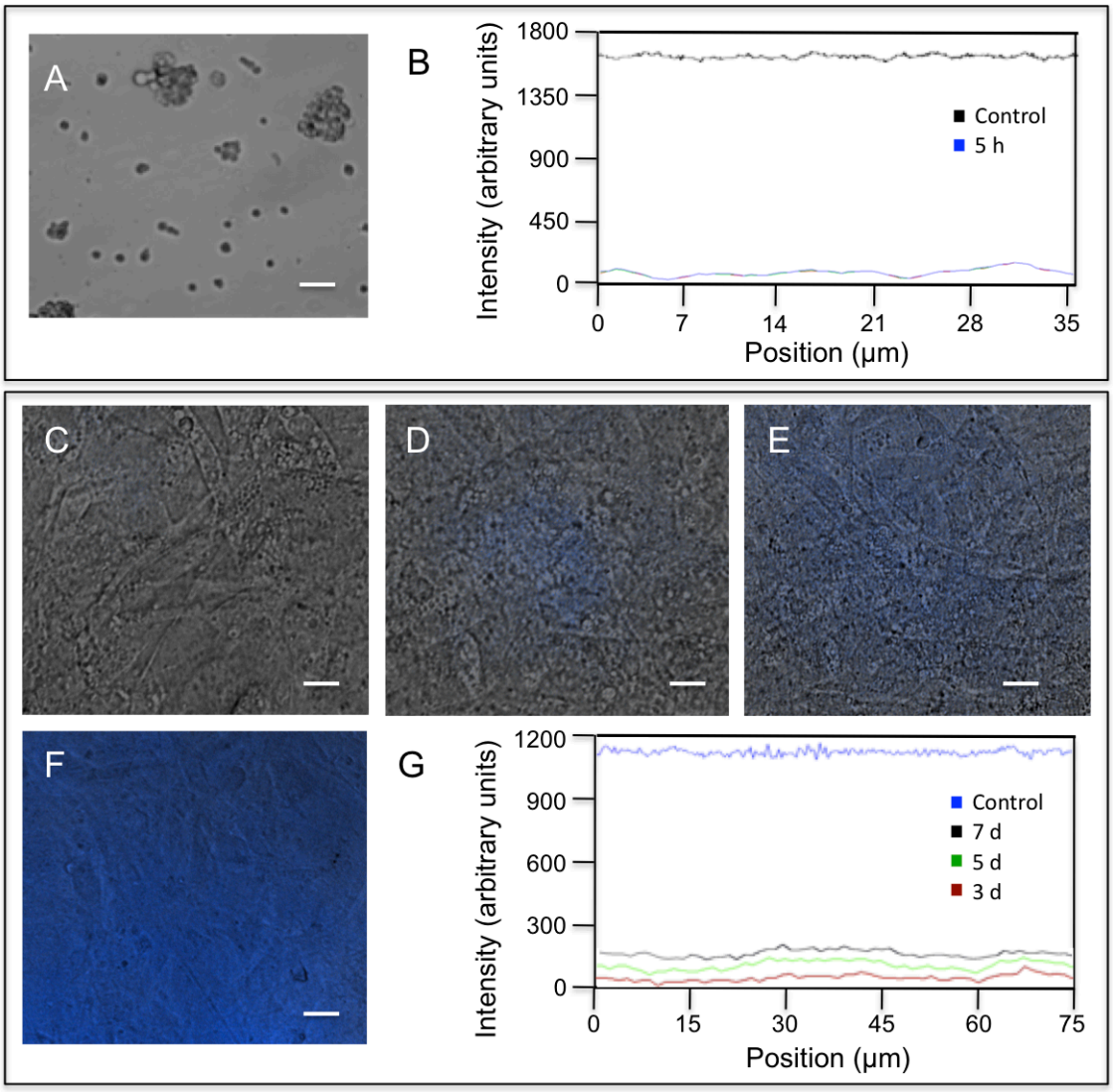

Figure 6.10 3D spheroid and multi-layer structure cell viability, assayed with trypan blue. (A) Ketone- (**10**) and oxyamine-tethered fbs (**9**) were mixed together in solution for 1, 2, 3, and 5 h, resulting in 3D spheroid formation and were then tested for viability using trypan blue dye (0.4 % in PBS, 2 min). (B) Trypan blue linescans (fluorescence false-colored for enhanced visualization) of the spheroids generated after 5 h of culture were compared to a control population in which spheroids were generated for 5 h, fixed with formaldehyde, and stained with trypan blue under the same conditions. Greater than 99 % of cells were determined to be viable. Similarly, 3D multi-layered tissue-like structures were generated and cultured for (C) 3 (D) 5, and (E) 7 days and tested for viability using trypan blue dye. (F) Again as a control, cells were grown in a multilayer for 7 days, then fixed with formaldehyde, and stained with trypan blue, and linescans were constructed for all samples and compared to the control. Cell viability decreased with time and number of cell layers from 3 to 5 to 7 days of culture with approximated viabilities of (C) 98, (D) 91, and (E) 84 %, respectively. The scale bars represent 60 (A) and 30 μm (C-F).

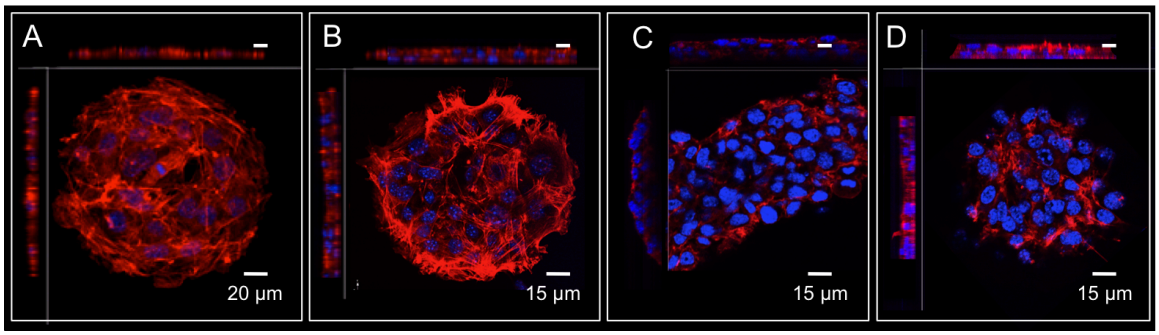

Figure 6.11 Confocal images representing 2D monolayer and 3D multi-layered tissue-like structures of fbs with spatial control. (A) A circular, 2D monolayer of fbs (control) result after ketone-functionalized fbs (**9**) and fbs (not functionalized with oxyamines) are patterned on a circular, microcontact printed region, presenting fibronectin and allowed to grow for 5 days. (B-D) Fbs, functionalized with ketone groups (**9**) were seeded onto microcontact printed regions containing fibronectin and allowed to grow for 2 days. Fbs, functionalized with oxyamine groups (**10**) were then seeded and allowed to grow for 2-3 more days. Confocal images demonstrating 3D tissue formation in (B) circle, (C) bar, and (D) square geometries are depicted. The corresponding z-plane cross-sections that indicate the thickness of the cell layers are shown as an inset; scale bars represent 30 μm. Cells were stained with DAPI (blue, nucleus) and phalloidin (red, actin).

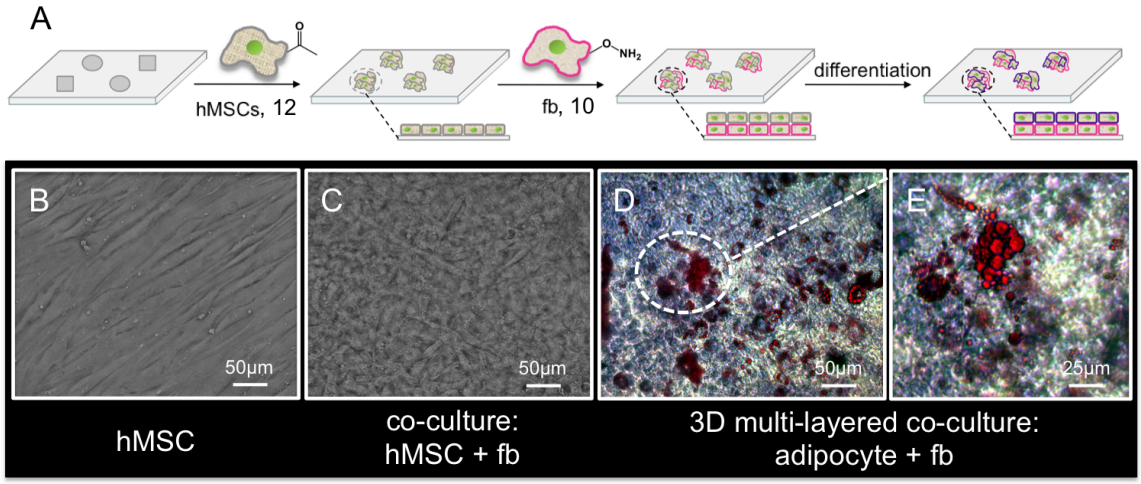

Figure 6.12 General schematic and brightfield images representing oxime-mediated, 3D tissue-like structure formation with hMSC/fb co-cultures and subsequent induced adipocyte differentiation to generate 3D adipocyte/fb co-culture structures. (A) Ketone-tethered hMSCs (**12**) were seeded onto a surface, followed by the addition of oxyamine-functionalized fbs (**10**). The co-culture was allowed to grow and divide for 3 d at which point, adipogenic differentiation was induced with the addition of the appropriate media. This resulted in a 3D multi-layer of adipocytes and fb. (B) A confluent 2D monolayer of ketone-presenting hMSCs is represented. (C) A brightfield image displaying a 3D multi-layer co-culture of hMSCs (**12**) and oxyamine-functionalized fbs (**10**) is shown. (D) Adipogenic differentiation was induced with media resulting in 3D multi-layered adipocyte and fb co-culture structures, represented by low and (E) high-resolution brightfield images (after 10 days in culture). Adipocytes were stained with Oil Red O (lipid vacuoles) and Harris Hemotoxylin (nucleus).

6.3.13 3D stem cell co-cultures with induced adipocyte differentiation. We explored the general use of this liposome fusion method, delivered ketone and oxyamine groups to different cell lines, and demonstrated that 3D spheroid and multi-layer can be generated using co-cultures of hMSCs and fbs (Figures 6.7 and 6.9, respectively). We next extended our methodology toward stem cell differentiation to determine whether 3D multi-layered co-cultures could be induced to generate tissues of differentiated hMSCs and fbs. As shown in figure 6.12A, ketone-functionalized hMSCs (**12**) were first cultured on a substrate for 3 days, producing a 2D monolayer of cells (Figure 6.12B). Oxyamine-tethered fbs (**10**) were then co-cultured with the hMSCs, and the cells were allowed to grow and proliferate for 2 days (Figure 6.12C). Adipogenic induction media was then added, the 3D multi-layered co-culture was stained for nuclei (blue) and lipid vacuoles (red), which are characteristic of adipocytes (fat cells). The phase contrast images in figure 6.12D and 6.12E demonstrate the successful generation of tissue-like structures, comprising induced adipocytes and fbs. The ability to co-culture stem cells with many other cell types and induce differentiation shows great promise in the field of regenerative medicine and stem cell transplantation.

6.4 Conclusion

In this study, we developed a simple liposome delivery and fusion method to display ketone or oxyamine functional groups from cell surfaces for applications in bio-orthogonal ligand conjugation, rewiring cell adhesion, and the generation of stable, 3D spheroid assemblies and multi-layered tissue-like structures. This strategy may have diverse applications in the field of tissue engineering and regenerative medicine, from growing biocompatible tissues and organs *in vitro* to their cellular transplantation *in vivo*.[58,59] For example, assembled tissue patches with geometrically defined shape can be grown in culture and transplanted or grafted to specific locations.[60] Furthermore, this

strategy may allow for time-lapse observation of cell movement *in vivo* by using a pulse (delivery of labeled cells via liposome fusion), followed by a chase (bio-orthogonal reagent to target only the labeled cells). When applied *in vivo*, this method may allow for the monitoring of many spatio-temporal developmental events and tumor metastasis. Since the liposome fusion method is general, many other types of chemistries in a single liposome can be delivered to the membrane surface simultaneously. For example, liposomes containing ketones, alkynes, dienes, azides, hydrazides, or dienophiles in varying combinations may be delivered to a cell surface for iterative or simultaneous post-functionalization via bio-orthogonal ligation reactions.

We have also been able to perform liposome fusion to the same cells several times, which may be important to tailor the membrane with multiple groups or to increase the concentration of a particular surface functional group. By rewiring cell adhesion, a number of materials, surfaces, nanoparticles, and biomedical devices for various biotechnological applications may be decorated with cells. Because no biomolecules are used with this strategy, no long-term stability and degradation issues in complex cell culture media or *in vivo* will affect cell targeting or cell assembly. Combining this strategy with polymer scaffolds, 3D tissues and organs may be generated for paracrine signaling studies, tissue replacement therapies, stem cell plasticity studies, or as a model platform for various high-throughput screening studies.[61-64] Finally, integrating this strategy with traditional liposome delivery, where the interior of the liposome contains small molecules or nanoparticle cargoes, a multiplex system where the delivery of reagents to the interior of cells and simultaneous labeling of the exterior of the cells may be possible for entirely new diagnostic and biomedical applications.

References

(1) Mayer, A. *Annu. Rev. Cell. Develop. Biol*. **2002**, *18*, 289-314.

(2) Rowan, A. *Nat. Rev. Mol. Cell Biol.* **2006**, *7*, 555-561.

(3) Ellens, H.; Bentz, J., Szoka; F. C. *Biochemistry*, **1984**, *24*, 3099-3106.

(4) Dennison, S. M.; Greenfield, N.; Lenard, J.; Lentz, B. R. *Biochemistry*, **2002**, *41*, 14925-14934.

(5) Evans, K. O.; Lentz, B. R. *Biochemistry*, **2002**, *41*, 1241-1249.

(6) Jahn, R.; Lang, T.; Sudhof, T. C. *Cell*, **2003**, *112*, 519-533.

(7) McNew, J. A.; Weber, T.; Parlati, F.; Johnston, R. J.; Melia, T. J.; Sollner, T. H.; Rothman, J. E. *J. Cell Biol.* **2000**, *150*, 105-117.

(8) Soolner, T. H. *Curr. Opin. Biol.* **2004**, *16*, 429- 435.

(9) Parlati, F.; Weber, T.; McNew, J. A.; Westermann, B.; Sollner, T. H.; Rothman, J. E. *Proc. Natl. Acad. Sci. U.S.A.* **1999**, *96*, 12565-12570.

(10) Paumet, F.; Rahimian, V.; Rothman, J. E. *Proc. Natl. Acad. Sci. U.S.A.* **2004**, *101*, 3376-3380.

(11) Richard, A.; Marchi-Artzner, V.; Lalloz, M.-N.; Brienne, M.-J.; Artzner, F.; Gulik-Krzywicki, T.; Guedeau-Boudeville, M.-A.; Lehn, J.-M. *Proc. Natl. Acad. Sci. U.S.A.* **2004**, *101*, 15279-15284.

(12) Marchi-Artzner, V.; Gulik-Krzywicki, T.; Guedeau-Boudeville, M-A.; Gosse, C.; Sanderson, J. M.; Dedieu, J.-C.; Lehn, J.-M. *ChemPhysChem* **2001**, *2*, 367-376.

(13) Marchi-Artzner, V.; Jullien, L.; Gulik-Krzywicki, T.; Lehn, J.-M. *Chem. Commun.* **1997***, 1***,** 117-118.

(14) Paleos, C. M.; Tsiourvas, D. *J. Mol. Recognition*, **2009**,*19*, 60-67.

(15) Chan, Y.-H. M.; Lengerich, B.; Boxer, S. G. *Proc. Nat. Acad. Sci. U.S.A.* **2009***, 106*, 979-984.

(16) Gong, Y.,; Luo, Y.; Bong, D. *J. Am. Chem. Soc.* **2006**, *128*, 14430-14431.

(17) Sarkar, D.; Vemula, P. K.; Zhao, W.; Gupta, A.; Karnik, R.; Karp, J. M. *Biomaterials*, **2010**, *31*, 5266-5274.

(18) Nelson, C. M.; Bissel, M. J. *Annu. Rev. Cell Dev. Biol.* **2006**, 22, 287-309.

(19) Meshel, A. S.; Wei, Q.; Adelstein, R. S.; Sheetz, M. P. *Nat. Cell Biol.* **2005**,

7,157-164.

(20) Isenberg, B. C.; Williams, C.; Tranquillo, R. T. *Annu. Biomed. Eng.,* **2006**, 34, 971-985.

(21) Hollister, S. J. (2005). *Nature Mater.* 4:518-524.

(22) Gillette, B. M.; Jensen, J. A.; Tang, B.; Yang, G. J.; Bazargan-Lari, A.; Zhong, M.; Sia, S. K. *Nat. Mater.* **2008**, 7, 636-640.

(23) Tanaka, H.; Murphy, C. L.; Murphy, C.; Kimura, M.; Kawai, S.; Polak, J. M. *J. Cell Biochem.* **2004**, 93, 454-462.

(24) Gartner, Z. J.; Bertozzi, C. R. *Proc. Natl. Acad. Sci. U.S.A.* **2009**, 106, 4606-4610.

(25) Albrecht, D. R.; Underhill, G. H.; Wassermann, T. B.; Sah, R. L.; Bhatia, S.N. *Nat. Methods* **2006**, 3, 369-375.

(26) Gray, D. S.; Tan, J. L.; Voldman, J.; Chen, C. S. *Biosens. Bioelectron.* **2004**, 19, 1765-1774.

(27) Odde, D. J, Renn, M. J. *Biotechnol. Bioeng.* **2000**, 67, 312-318.

(28) Nahmias, Y.; Odde, D.J. *Nat. Protocol* **2006**, 1, 2288-229626.

(29) Barron, J. A.; Krizman, D. B.; Ringeisen, B. R. *Annu. Biomed. Eng.* **2005**, 33, 121–130.

(30) Inaba, R.; Khademhosseini, A.; Suzuki, H.; Fukuda, J. *Biomaterials* **2009**, 30, 3573-3577.

(31) Ringeisen, B. R.; Othon, C. M.; Barron, J. A.; Young, D.; Spargo, B. *J. Biotechnol.* **2006**, 1, 930-948.

(32) Chiou, P. Y.; Ohta, A.T.; Wu, M. C. *Nature* **2005**, 436, 370-372.

(33) Falconnet, D.; Csucs, G.; Grandin, H. M.; Textor, M. *Biomaterials* **2006**, 27, 3044-3063.

(34) Khademhosseini, A.; Langer, R.; Borenstein, J.; Vacanti, J. P. *Proc. Natl. Acad. Sci. U.S.A.* **2006**, 103, 2480-2487.

(35) Rice, J. *MIT Technol. Rev.* **2009**, March 11.

(36) Mahal, L. K.; Yarema, K. J.; Bertozzi, C. R. *Science* **1997**, *276*, 1125-1128.

(37) Prescher, J. A.; Bertozzi, C. R. *Nat. Chem. Biol.* **2005**, *1*, 13-21.

(38) Chen, I.; Howarth, M.; Lin, W.; Ting, A. Y. *Nat. Methods* **2005**, *2*, 99-104.

(39) Keppler, A.; Pick, H.; Arrivoli, C.; Vogel, H.; Jonhsson, K. *Proc. Natl. Acad. Sci. U.S.A.* **2004**, *101*, 9955-9959.

(40) Miller, L. W.; Sable, J.; Goelet, P.; Sheetz, M. P.; Cornish, V. W. *Angew. Chemie. Int. Ed.* **2004**, *43*, 1672-1675.

(41) Kellam, B.; De Bank, P. A.; Shakesheff, K. M. *Chem. Soc. Rev.* **2003**, *32*, 327-337.

(42) Rabuka, D.; Forstner, M. B.; Grovers, J. T.; Bertozzi, C. R. *J. Am. Chem. Soc.* **2008**, *130*, 5947-5953.

(43) Wilson, J. T.; Krishnamurthy, V. R.; Cui, W.; Qu, Z.; Chaikof, E. L. *J. Am. Chem. Soc.* **2009**, *131*, 18228-18229.

(44) Csiszar, A.; Hersch, N.; Dieluweit, S.; Biehl, R.; Merkel, R.; Hoffmann, B. *Bioconjugate Chem.* **2010**, *21*, 537-543.

(45) Pale-Grosdemange, C.; Simons, E. E.; Prime, K. L.; Whitesides, G. M. *J. Am. Chem. Soc.* **1991**, *113*, 12-20.

(46) Park, S.; Yousaf, M. N. *Langmuir,* **2008**, *24*, 6201-6207.

(47) Westcott, N. P.; Pulsipher, A.; Lamb, B. M.; Yousaf, M. N. *Langmuir,* **2008**, *24*, 9237-9240.

(48) Lamb, B. M.; Barrett, D. G.; Westcott, N. P.; Yousaf, M. N. *Langmuir,* **2008**, *24*, 8885-8889.

(49) Harder, P.; Grunze, M.; Dahint, R.; Whitesides, G. M.; Laibinis, P. E. *J. Phys. Chem. B*, **1998**, *102*, 426-436.

(50) Hsiao, S. C.; Shum, B. J.; Onoe, H.; Douglas, E. S.; Gartner, Z.; Mathies, R. A.; Bertozzi C. R.; Francis, M. B. *Langmuir* **2009**, *25*, 6985-6991.

(51) Dutta, D.; Pulsipher, A.; Yousaf, M. N. *Langmuir*, **2010**, *26*, 9835-9841.

(52) Beigel, M.; Keren-Zur, M.; Laster, Y.; Loyter, A. *Biochemistry* **1988**, *27*, 660-666.

(53) Beck, P.; Liebi, M.; Kohlbrecher, J.; Ishikawa, T.; Ruegger, H.; Fischer, P.; Walde, P.; Windhab, E. *Langmuir*, **2010**, *26*, 5382-5387.

(54) Chang, M.; Prescher, J. A.; Sletten, E. M.; Baskin, J. M.; Miller, I. A.; Agard, N. J.; Lo, A.; Bertozzi, C. R. *Proc. Natl. Acad. Sci. U.S.A.* **2010**, *107*, 1821-1826.

(55) Saxon, E.; Bertozzi, C. R. *Science* **2000**, *287*, 2007-2010.

(56) Rose, K. *J. Am. Chem. Soc.* **1994**, *116*, 30-33.

(57) Love, J. C.; Estroff, L. A.; Kriebel, J. K.; Nuzzo, R. G.; Whitesides, G. M. *Chem. Rev.* **2000**, *105*, 1103-1170.

(58) Mueller-Klieser, W. *Am. J. Physiol.* **1997**, *273*, C1109-C1123.

(59) Khademhosseini, A.; Vacanti, J.; Langer, R. *Sci. Am.* **2009**, *300*, 64-71.

(60) Badylak, S. F.; Nareem, R. M. *Proc. Natl. Acad. Sci. U.S.A.* **2010**, *107*, 3285-3286.

(61) Khetani, S. R.; Bhatia, S. N. *Nat. Biotechnol.* **2008**, *26*, 120-126.

(62) Zeisberg; Yang, C.; Martino, M.; Duncun, M. B.; Rieder, F. Tanjore, H.; Kalluri, R. *J. Biol. Chem.* **2007**, *282*, 23337-23347.

(63) Bhatia, S. N.; Balis, U.; Yarmush, M. L.; Toner, M. *Biotechnol. Prog.* **1998**, *14*, 378-387.

(64) Kunz-Schughart, L. A.; Freyer, J. P.; Hofstaedter, F.; Ebner, R. *J. Biomol. Screen* **2004**, *9*, 273-285.

CHAPTER 7

Bioelectronics: Dynamic Control of Cell Surfaces and Cell Tissue Interactions

7.1 Introduction

Controlling cell-cell interactions and cellular architecture in three-dimensional (3D) space and time is critical for the proper development[1] and survival of higher-order organisms.[2] These dynamic interactions are complex but essential for correct cell behavior and tissue function based on a myriad of physical, mechanical, and hydroynamic forces, as well as autocrine and paracrine signaling cascades.[3,4] However, recapitulating these processes *in vitro* while maintaining these dynamic and discrete cell-cell contacts are difficult and require a multidisciplinary coordinated effort, intersecting several research fields.[5] Thus, the ability to modulate cell-cell interactions in space and time would in turn allow for unprecedented control of cell behavior and enable the design and utility of new dynamic tissue engineering scaffolds, *in vivo* imaging capabilities, high-throughput tissue-based screening assays, and drug delivery therapies.[6,7]

Several recent approaches to generate co-culture tissue structures in two and three dimensions (2D and 3D, respectively) have been developed and employed, including dielectrophoresis[8], microfabrication,[9,10] hydrogel,[11,12] and cell patterning techniques.[13,14] Tailoring cell membranes via cell-surface engineering methods have also proven to be important for the development of co-culture and multicellular micro-tissues.[15] In particular, the integration of bio-orthogonal chemical strategies[16] with cell surfaces might

allow for a range of cell-surface modifications for control of lignd presentation, ligand density, and potentially spatio-temporal control of cell-cell interactions. Bio-orthogonal chemical reactions have been extensively developed and utilized due to their ability to be performed at physiological conditions (i.e., Diels-Alder, Oxime, Huisgen cycloaddition, and Staudinger ligation) without side reactions and in complex protein mixtures, cell lysates, and *in vivo*. Furthermore, these chemistries have been applied in many fundamental cell studies,[17] drug delivery therapies,[18] and diagnostic measuring applications.[19] However, the delivery and incorporation of a range of these chemical groups to a cells surface for a variety of cell types remains challenging and not straightforward.[20]

The development of synthetic liposomes and liposome fusion methods have proven very useful for numerous studies as cell membrane model systems and as microarray platforms to study cell membrane dynamics and for biotechnology applications.[21,22] Additionally, liposome-to-liposome and liposome-to-cell fusion methods have also been developed to deliver therapeutic agents to cells and organelles and study cellular interactions.[23] However, until now, there has been no report utilizing liposome-to-cell fusion to deliver dynamic and bio-orthogonal groups directly to cell surfaces for subsequent chemoselective conjugation and release of ligands or for the temporal programming of controlled cell-cell assembly. A strategy that combines cell-surface modification, without the use of molecular biology techniques or biomolecules, with a stable, dynamic, and switchable bio-orthogonal ligand conjugation and release approach to direct tissue formation and subsequent disassembly, would greatly benefit fundamental cell behavioral studies and tissue engineering research.

In this chapter, we report a novel strategy to rewire cell surfaces for the dynamic control of ligand composition on cell membranes and modulation of cell-cell interactions

to generate 3D tissue structures applied to stem cell, cell-surface tailoring, and tissue engineering. We tailor cell surfaces with bio-orthogonal chemical groups, based on a liposome fusion and delivery method, to create dynamic and switchable cell tissue assemblies through chemoselective conjugation and release chemistry. Cell membranes were decorated with a range of molecules that can be released *in vitro* for subsequent rounds of molecular conjugation and release. Each step to modify the cell surface: activation, conjugation, release, and regeneration, can be monitored and modulated by non-invasive, label-free analytical techniques. Controlled cell assembly is generated by a bottom-up approach and can then be disassembled with an *in situ* dynamic trigger. We demonstrate the utility of this methodology by conjugating and releasing small molecules to and from cell surfaces and by generating 3D co-culture spheroid and multi-layered cell tissues for studies in stem cell differentiation that can be programmed to assemble and disassemble on demand. We show that this strategy is redox responsive and allows for multiple rounds of the controlled conjugation and release of molecules to and from cell surfaces *in situ.* This chemical methodology can simultaneously be used as an analytical probe for monitoring cellular interactions, as well as a trigger to alter cell-surface ligands and cell-cell contacts.

7.2 Materials and Methods

7.2.1 Materials and instrumentation. All chemical reagents were of analytical grade and used without further purification. Lipids egg palmitoyl-oleoyl phosphatidylcholine (POPC), egg 1-palmitoyl-2-oleoyl-phosphatidylglycerol (POPG), 1,2-dioleoyl-3-trimethylammonium-propane (DOTAP), egg 1,2-diphytanoyl-*sn*-glycero-3-phosphoethanolamine-N-(7-nitro-2-1,3-benzoxadiazol-4-yl) (ammonium salt) (NBD-PE), and egg 1,2-dipalmitoyl-*sn*-glycero-3-phosphoethanolamine-N-(lissamine rhodamine B sulfonyl) (ammonium salt) (Rhod-PE) were purchased from Avanti Polar Lipids

(Alabaster, AL). Antibodies and fluorescent dyes were obtained from Invitrogen (Carlsbad, CA). FITC labeled beads were purchased from Spherotech, Inc. (Forest Lake, IL), trypan blue viability dye was obtained from Hyclone (Fisher Sci, Pittsburgh, PA), and all other chemicals were obtained from Sigma-Aldrich or Fisher. Swiss 3T3 albino mouse fibroblasts (Fb) were obtained from the Tissue Culture Facility at the University of North Carolina (UNC). Rat2 Fb transfected with m-cherry were obtained from the Bear Lab (UNC Chapel Hill, NC). Human Mesenchymal stem cells (hMSCs) were purchased from Lonza (Basel, Switzerland).

Transmission electron microscopy images were acquired using a TF30He Polara G2 (FEI company) electron cryo microscope, operating at 300 keV (Figure 7.1B). Images were recorded using a Tietz single port model 415 4k × 4k CCD camera with a 15-μm pixel size. Fourier resonance energy transfer measurements were performed using a SPEX Fluorolog-3 Research T-format Spectrofluorometer with an excitation wavelength of 471 nm (Figure 7.2A). Dynamic light scattering was performed using a Nikomp model 200-laser particle sizer with a 5 mW HeNe laser at an excitation wavelength of 632.8 nm and using a Wyatt DynoPro plate reader (Figure 7.2B). Flow cytometry was performed using a Dako CyAn ADP (Beckman-Coulter, Brea, CA), and the data was analyzed with Summit 4.3 software (Figure 7.7). Phase contrast and fluorescent imaging was performed and processed using a Nikon TE2000-E inverted microscope and Metamorph software, respectively (Figures 7.3, 7.6, and 7.8). All electrochemical measurements were carried out using a Bioanalytical Systems potentiostat and with a Ag/AgCl reference electrode (Bioanalytical Systems), Pt wire as the auxiliary electrode, scan rate of 100 mVs^{-1} (Figure 7.3-6 and 7.8). Scanning electron microscopy images were obtained using a Hitachi S-4700 field emission scanning electron microscope (Hitachi High Technologies America, Inc., Schaumburg, Illinois) (Figure 7.6). Confocal

micrographs were taken and processed in 3D using a Nikon Eclipse TE2000-E inverted microscope (Nikon USA, Inc., Melville, NY) and Volocity software, respectively (Figure 7.6).

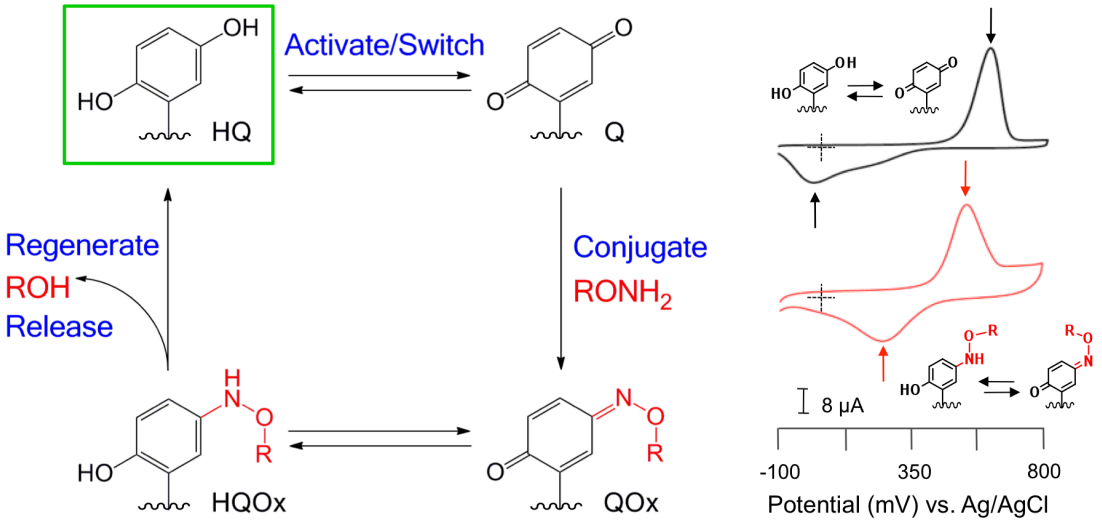

Scheme 7.1 Chemical cycle for redox active, oxime conjugation and release. HQ can be chemically (20 µL, 5 µM $CuSO_4 \cdot 5H_2O$ in PBS at 10 mol %, 5 min) or electrochemically (-100 to 650 mV, pH 0, 100 mVs^{-1}) oxidized to Q for ligation with AO-tethered ligands (R-ONH_2), resulting in a shift of the diagnostic reduction peak associated with the redox species (bottom cyclic voltammogram (CV)). The redox cycle of oxime (QOx to HQOx) is stable at pH < 5 and does not cleave. When this redox cycle is performed at pH > 5, the oxime bond is efficiently cleaved to regenerate HQ. The regenerated HQ can then continue the cycle for subsequent rounds of the conjugation and release of AO-tethered ligands (R-ONH_2).

7.2.2 Syntheses. Tetra(ethylene glycol)-terminated alkanethiol (EG_4)[24] and rhodamine-aminooxy (AO-Rhod) were synthesized as previously reported.[25]

*1,4-bis(tetrahydro-2H-pyran-2-yloxy)benzene (**B**).* To a solution of hydroquinone (6.0 g, 54.5 mmol) in THF (40 mL) was added 2,3-dihydropuran (44.0 mL, 245.3 mmol, 4.5 eq) and 3 drops of concentrated HCl. The mixture was stirred at room temperature for 8h, diluted with EtOAc (40 mL), washed with $NaHCO_3$ (3 x 50 mL) and brine (1 x 25 mL), dried over $MgSO_4$, and concentrated to a white solid. The solid was then dissolved in EtOAc and recrystallized with hexanes to afford a white solid **B** (10.02 g, 66 %), ^{1}H NMR

(400 Hz, $CDCl_3$, δ): 1.67-1.58 (m, 6H, J = 36 Hz; -CH_2-), 1.88-1.85 (m, 4H, J = 12 Hz; -CH_2-), 2.03-2.00 (m, 2H, J = 12 Hz; -CH_2-), 3.62-3.60 (m, 2H, J = 8 Hz; -CH_2-), 3.98-3.96 (m, 2H, J = 8 Hz; -CH_2-), 5.34-5.32 (t, 2H, J = 7 Hz; -CH-), 7.00 (s, 4H; Ar-H).

*2,2'-(2-dodecyl-1,4-phenylene)bis(oxy)bis(tetrahydro-2H-pyran) (**C**)*. To a solution of **B** (2.00 g, 7.0 mmol) in dry THF (40 mL) at 0°C was added tert-butyllithium (4.6 mL of a 1.7 M solution, 9.1 mmol, 1.3 eq) dropwise over 15 min. The mixture was stirred at 0°C for 60 min and then slowly warmed to room temperature over 3h. At this time, 1-bromododecane (5.08 mL, 21.0 mmol, 3 eq) was added and stirred for 12h. The mixture was diluted with DCM (40 mL) and washed with NH_4Cl (3 x 50 mL) and brine (1 x 25 mL), dried over $MgSO_4$, and concentrated to afford a yellow oil. The mixture was purified by flash chromatography 95:5 Hex:EtOAc to elute a yellow oil **C** (2.23 g, 71 %), ^{1}H NMR (400 Hz, $CDCl_3$, δ): 0.91-0.89 (t, 3H, J = 8 Hz; -CH_3), 1.27-1.23 (m, 18H, J = 16 Hz; -CH_2-), 1.72-1.68 (m, 10H, J = 16 Hz; -CH_2-), 2.61-2.58 (t, 2H, J = 12 Hz; -CH_2-), 3.65-3.63 (m, 4H, J = 8 Hz; -CH_2-), 5.80-5.78 (t, 2H, J = 8 Hz; -CH-), 6.68 (s, 1H; Ar-H), 6.81 (s, 1H; Ar-H), 6.84 (s, 1H; Ar-H).

2-dodecylbenzene-1,4-diol (**A**). To a solution of **C** (2.0 g, 4.5 mmol) in 40 mL of a 3:1:1 mixture of AcOH/THF/H_2O was stirred for 16h. The mixture was then concentrated, diluted in EtOAc (20 mL) and washed with 1 mM NaOH (2 x 10 mL), dried over $MgSO_4$, and concentrated to afford a white solid **A** (1.12 g, 90 %), ^{1}H NMR (400 Hz, $CDCl_3$, δ): 0.89-0.87 (t, 3H, J = 8 Hz; -CH_3), 1.30-1.25 (m, 18H, J = 20 Hz; -CH_2-), 1.57-1.55 (m, 2H, J = 7 Hz; -CH_2-), 2.58-2.55 (t, 2H, J = 12 Hz; -CH_2-), 6.57-6.56 (m, 1H, J = 4 Hz; Ar-H), 6.67-6.65 (m, 2H, J = 7 Hz; Ar-H); (ESI) (*m/z*) $[M + Na]^+$: calcd. for $C_{18}H_{30}O_2$, 301.21; found, 301.15.

*2-(dodecyloxy)isoindoline-1,3-dione (**E**).* To a solution of N-hydroxyphthalimide (1.96 g, 12.04 mmol, 1.5 eq) and sodium bicarbonate (10.11 g, 12.04 mmol, 1.5) in DMF (20

mL) at 80°C was added 1-bromododecane (1.93 mL, 8.02 mmol). The mixture was refluxed and stirred for 12 h. The reaction was diluted with DCM and washed with H_2O (6 x 50 mL), 1 M $NaHCO_3$ (3 x 50 mL), and H_2O (2 x 50 mL), dried over $MgSO_4$, and concentrated to afford a white solid (2.66 g, 87 %). ^1H NMR (400 MHz, $CDCl_3$, δ): 1.02 (s, 3H; CH_3), 1.31-1.29 (m, 14H, J = 8 Hz; CH_2), 1.47-1.45 (m, 4H, J = 8 Hz; CH_2), 1.60-1.57 (m, 2H, J = 12 Hz; CH_2), 3.72-3.70 (t, 2H, J = 8 Hz; CH_2), 7.80-7.78, 7.85-7.83 (2 x m, 4H, J = 8 Hz; Ar-H).

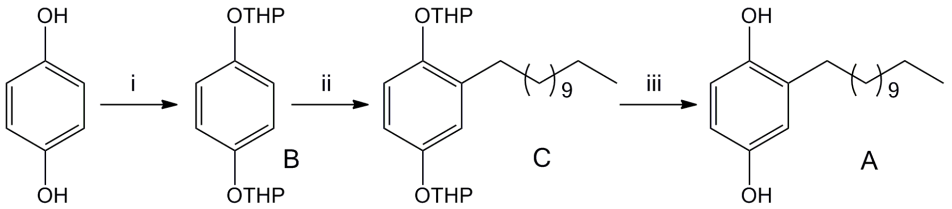

Scheme 7.2 Synthesis of 2-dodecylbenzene-1,4-diol (Hydroquinone Alkane, HQ). Reagents and conditions: (i) 2,3-dihydropuran (4.5 eq), HCl (cat), THF, 8 h; 66 % (ii) tert-butyllithium (1.3 eq), 1-bromododecane (3 eq), THF, 0 °C, 3 h, then 25 °C, 12 h; 71 %; (iii) 3:1:1 AcOH/THF/H_2O, 16 h; 90 %.

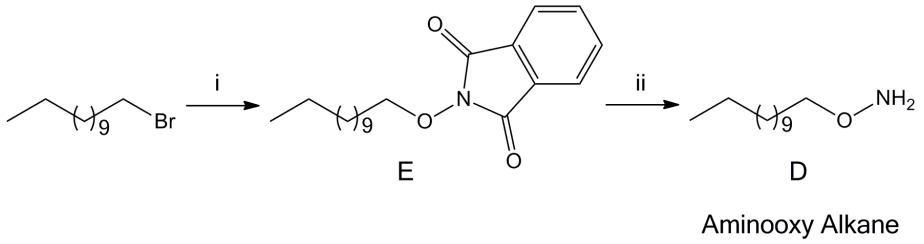

Scheme 7.3 Synthesis of *O*-dodecyloxyamine (Aminooxy Alkane, AO). Reagents and conditions: (i) N-hydroxyphthalimide (1.5 eq), $NaHCO_3$ (1.5 eq), DMF, reflux, 80 °C, 12 h; 87 % (ii) hydrazine (6 eq), dry DCM, N_2, 12 h; 74 %.

*O-dodecyloxyamine (**D**).* To a solution of **E** (2.65 g, 8.00 mmol) in dry DCM (30 mL) under inert atmosphere (Ar) was slowly added hydrazine (1.53 mL, 48.00 mmol, 6 eq). Upon addition, a white precipitate immediately formed. The mixture was stirred for 12 h. The reaction was diluted with DCM and washed with H_2O (6 x 50 mL), dried over $MgSO_4$, and concentrated to afford a pale yellow oil (1.18 g, 74 %). ^1H NMR (400 MHz,

$CDCl_3$, δ): 1.03 (s, 3H; CH_3), 1.33-1.31 (m, 14H, J = 8 Hz; CH_2), 1.43-1.41 (m, 4H, J = 8 Hz; CH_2), 1.50-1.46 (m, 2H, J = 16 Hz; CH_2), 3.64-3.62 (t, 2H, J = 7 Hz; CH_2). (ESI) (*m/z*) [M + H^+]: calcd. for $C_{12}H_{27}NO$, 201.21; found, 201.22.

7.2.3 Lipid vesicle formation for fusion studies. HQ-tethered alkane (160 µL, 10 mM in $CHCl_3$ at 10 mol %, (**A**)) and POPC (410 µL, 10 mg/mL in $CHCl_3$ at 90 mol %) were mixed and then concentrated for 4 hours under high vacuum. Likewise, OA-tethered alkane (60 µL, 10 mM in $CHCl_3$ at 5 mol %, (**D**)), POPG (92 µL, 10 mg/mL in $CHCl_3$ at 20 mol %), and POPC (410 µL, 10 mg/mL in $CHCl_3$ at 75 mol %) were mixed and then concentrated for 4 hours at high vacuum. The dried lipid samples were then reconstituted in 3 mL in PBS buffer, pH 7.4. The contents of the vial were warmed to 50˚C and then sonicated for 15 min with a tip sonicator until the solution became clear, forming small and large and small unilamelar vesicles (LUVs and SUVs, respectively). Vesicle-containing solutions were then centrifuged at 30,000 rpm for 30 min, pelleting out the LUVs and leaving the SUVs in solution. The HQ- or OA-SUVs ((**1)** and (**3)**, respectively) were then used in further vesicle (liposome) fusion studies.

7.2.4 Chemical oxidative activation of HQ-SUVs (4) for liposome fusion studies. HQ-SUVs were prepared as previously described. To a solution of HQ-SUVs (3 mM in PBS, 4 mL) was added $CuSO_4 \cdot 5H_2O$ (20 μL, 5 μM in PBS) for 5 min, producing quinone-tethered vesicles (Q-SUVs, (**2**)).

7.2.5 Transmission electron microscopy (TEM) characterization of liposome fusion. HQ- (**1**) and Q- (**2**) SUVs were prepared and activated, respectively, as previously mentioned OA- (**3**) SUVs were also made as described above. Q- (**2**) and OA- (**3**) SUVs (0.2 mM in PBS) were mixed in a 1:1 ratio at room temperature for 30 min. A 4-μL vesicle suspension mixture was then applied to standard lacey carbon EM grid as prepared according to published methods. The specimens were blotted from behind and

then submerged into aurenyl acetate solution for staining. The hydrated specimens were then placed into a TF30He Polara G2 (FEI company) electron cryo microscope operating at 300 keV. Images were recorded using a Tietz single port model 415 4k × 4k CCD camera with a 15 micron pixel size on the chip. Pixel sizes at the specimen level were used to calculate accurate dimensions for the specimen.

7.2.6 Fourier resonance energy transfer (FRET) characterization of liposome fusion. HQ- (**16**) and OA- (**17**) SUVs were prepared as described above with the addition of NBD-PE (20 μL, 10 mg/mL in $CHCl_3$ at 2 mol %) and Rhod-PE (28 μL, 10 mg/mL in $CHCl_3$ at 2 mol %), respectively. HQ-SUVs were then activated to Q-SUVs as reported. NBD fluorescence was measured at 471 nm (excitation) and 531 nm (emission) maintaining narrow excitation slits to reduce light scattering interference. Q- and OA-SUVs containing NBD-PE and Rhod-PE, respectively, were then mixed (1:1) to obtain FRET measurements. The NBD dye was excited at 471 nm, and the emission was scanned through 600 nm. An emission signal for Rhod-PE was observed at 578 nm. All fluorescence measurements were performed in a SPEX Fluorolog-3 Research T-format Spectrofluorometer. Fluorescence was followed immediately after mixing OA-SUV (**17**) with Q-SUV (**16**) for approximately 2 hours at 2 min intervals. A constant flow of water was passed through the cuvette holder for temperature control. The temperature was maintained at 25 °C.

7.2.7 Dynamic light scattering (DLS) characterization of liposome fusion. Q- (**2**) and OA- (**3**) SUVs were prepared as described and mixed at a 1:1 ratio and were monitored over 80 min. DLS experiments were performed using a Nikomp model 200 laser particle sizer with a 5mW HeNe laser at an excitation wavelength of 632.8 nm. Standard deviation determinations were made using Gaussian analysis. A Wyatt DynoPro dynamic scattering plate reader was used to collect the data.

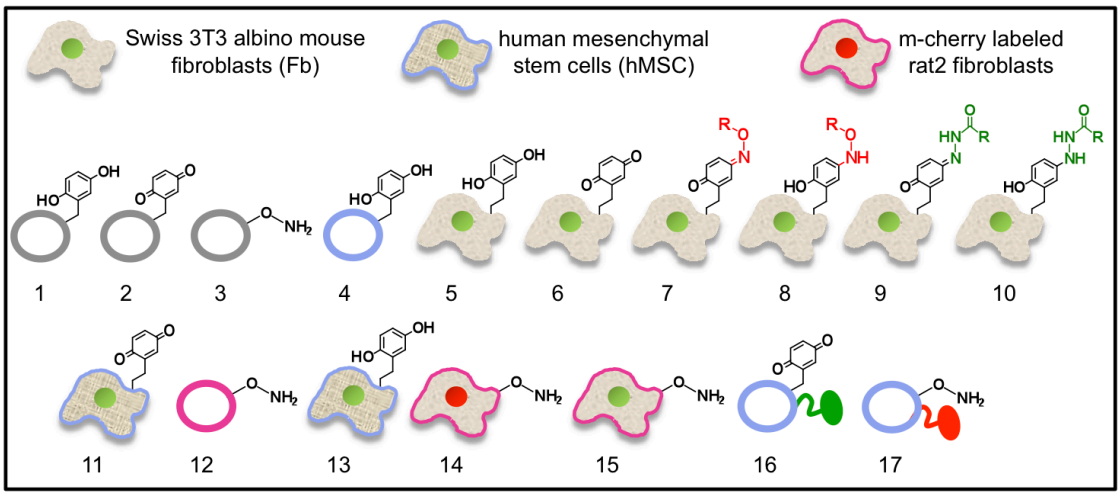

Scheme 7.4 List of molecules, liposomes, and cells used in this study.

7.2.8 Liposome fusion to cells (cell-surface engineering). HQ-tethered alkane (160 µL, 10 mM in $CHCl_3$ at 10 mol %, (**A**)), DOTAP (10 µL, 10 mg/mL in $CHCl_3$ at 2 mol %), and POPC (398 µL, 10 mg/mL in $CHCl_3$ at 88 mol %) were mixed and then concentrated for 4 hours under high vacuum. Similarly, OA-tethered alkane (60 µL, 10 mM solution in $CHCl_3$ at 5 mol %, (**D**)), DOTAP (10 µL, 10 mg/mL in $CHCl_3$ at 2 mol %), and POPC (424 µL, 10 mg/mL in $CHCl_3$ at 93 mol %) were mixed and then concentrated for 4 h under high vacuum. The above-mentioned procedure for forming HQ- (**4**) and Q- (**12**) SUVs was then performed. A 400-*µ*L aliquot of HQ- (**4**) and OA- (**12**) SUVs were then added separate populations of Fbs, m-cherry labeled Fbs, and hMSCs (3 mM in PBS, 400 µL added to 4 mL cells in culture) and were cultured for 16 hours, resulting in vesicle fusion to the cell membrane and subsequent presentation of HQ (**A**) and OA (**D**) groups from the cell surface ((**5**), (**13**), (**14**), and (**15**)) .

7.2.9 Chemical oxidative activation of HQ-presenting cells. HQ-SUVs (**4**) were prepared and fused to cells as previously described. $CuSO_4 \cdot 5H_2O$ (20 *µ*L, 5 *µ*M in PBS) was then added to cells in culture (4 mL of CBS-containing media) for 5 min, producing Q-presenting cells ((**6**) and (**11**)).

7.2.10 Flow cytometry characterization and quantification of HQ (A) and OA (D) on the cell surface. Fluorescence-activated cell sorting (FACS) analysis was performed in order to quantify the approximate number of HQ (**A**) and OA (**D**) groups on the cell surface after membrane fusion. HQ-SUVs were generated as previously mentioned and cultured with Fbs (3 mM in PBS, 400 µL added to 4 mL cells in culture) for 1, 3, 5, and 7 days, resulting in the fusion and display of HQ (**A**) from the cell surface (**5**). HQ (**A**) was activated to Q, as mentioned, before testing. Q-presenting Fbs (**6**) were then reacted with hydrazide-conjugated biotin (3 mM in CBS, 1 mL added to 4 mL CBS in cell culture, 1 h, (**9** and **10**)). Fluorescein- conjugated streptavidin (1 mM in CBS, 0.5 mL added to 4 mL CBS in cell culture, 1 h) was then added. A control cell population (not functionalized with HQ groups) was only incubated with biotin-hydrazide and streptavidin-FITC for 1 h, respectively, under the same conditions as described above. Cells were then centrifuged (5 min, 1000 rpm), re-suspended in RMPI (without phenol red), centrifuged (5 min, 1000 rpm), and re-suspended in RPMI (10^7 cells/2 mL). Fluorescence measurements were calibrated using RCP-5-30 beads (10^7 beads/mL, Spherotech, Inc., Lake Forest, IL) of known fluorescein equivalent molecule density.[26] Fluorescent intensities based on number of cells counted (at least 10^5/sample) were compared to the standard bead and control cells lacking fluorescent molecule conjugation and approximate numbers of fluorescent compound bound to the surface was calculated. Flow cytometry was carried out using a Dako CyAn ADP (Beckman-Coulter, Brea, CA), and data was analyzed with Summit 4.3 software.

*7.2.11 Electrochemical oxidative activation, conjugation, and release of HQ-presenting cells (**5** and **13**).* HQ-SUVs (**4**) were prepared and fused to cells (**5**) as previously described. These cells were then treated with trypsin (1 mL, 2 min, 37 °C) and seeded onto a gold surface (10^5 cells, 2 x 2 cm^2) for 2 h in serum-free-containing media,

and then 16 h in CBS-containing media. Linear sweep voltammetry (LSV) was then performed to oxidize HQ to Q using an Ag/AgCl reference, Pt wire auxiliary, and the gold surface containing the HQ-presenting cells (**5**) as the working electrode (-100 to 650 mV). PBS was used as the electrolyte solution (10 mM, pH 7.4), and the scan rate was 100 mVs^{-1}. OA-tethered ligands were then reacted with Q-presenting cells (**6**) to form an interfacial oxime linkage on the cell surface. This reaction can be monitored using cyclic voltammetry (CV) with a sweeping potential of -100 to 650 mV at 100 mVs^{-1}. To release ligands or cells, the working electrode was subject to a reducing potential (-100 mV, 10 s, PBS, pH = 7.4), resulting in a cleavage of oxime bond. Measurements were performed in a standard electrochemical cell. All electrochemical measurements were performed using a Bioanalytical Systems potentiostat.

7.2.12 Fluorescent characterization of liposome fusion to cells (cell-surface engineering). A solution of HQ-SUV (**4**) (1 mg/mL) was added Fbs in culture to give the desired final HQ concentration of 100 µg/mL in a total volume of 2 mL and were incubated 4 h. The cells (**5**) were then washed with PBS, followed by activation of HQ to Q as mentioned. Rhod-OA (100 μL added to 4 mL cell culture, 7 mM in H_2O) was added to Q-displaying cells (**6**) in culture and was incubated at 37 °C for 30 min, resulting in oxime bond formation and Rhod-presenting Fbs (**7** and **8**). The cells were then washed with PBS buffer and removed with a solution of 0.05 % trypsin 0.53 mM EDTA and re-suspended in serum-free medium (10^5 cells/mL). The cells were then seeded to a fibronectin-coated surface for 2 h and visualized by fluorescence microscopy under the Texas Red channel with an exposure time of 1200 ms. Similarly, a solution containing biotin-hydrazide (1 mg/mL in PBS, 0.5 mL added to 2 mL CBS) was added to Q-presenting Fbs (**6**) for 2 h, followed by addition of FITC-streptavidin for 1 h to produce biotin/streptavidin-presenting Fbs (**9** and **10**). After 1 h, serum-containing media was

added for cell growth and imaged after 3 days under the FITC channel with an exposure time of 600 ms.

7.2.13 Electrochemical characterization of ligand conjugation and release to cell surfaces (cell-surface engineering). Rhod-OA was conjugated to Q-presenting Fbs (**6**) as described above. CV was performed to determine the presence of the oxime bond (**7** and **8**), scanning from -100 to 650 mV, with a scan rate of 100 mVs^{-1}, in PBS (pH = 7.4). To release Rhod-OA, a constant reducing potential (-100 mV, 10 s) was applied, and CV was then used to determine the regeneration of HQ and Q redox peaks (-100 to 650 mV). The cells were then activated to Q by conducting LSV, and biotin-hydrazide was conjugated as reported above (**9** and **10**). CV was again performed after conjugation to determine the presence of the hydrazide bond (-100 to 650 mV, 100 mVs^{-1}).

7.2 14 Fibroblast (Fb) culture. Swiss 3T3 albino mouse Fbs and m-cherry labeled, Rat2 Fbs were cultured in Dulbecco's Modified Eagle Medium (Gibco) containing 10 % calf bovine serum (CBS) and 1 % penicillin/streptomycin at 37 °C in 5 % CO_2. When ready for experimentation, cells are removed from the tissue culture plastic using a solution of 0.05 % trypsin 0.53 mM EDTA and re-suspended in serum-free medium (10^5 cells/mL).

7.2.15 Cell patterning characterization of liposome fusion to cell surfaces. Mixed self-assembled monolayers (SAMs) presenting OA and EG_4 alkanethiolates were patterned using microfluidic lithography.[27] The percentage of OA groups were minimal (1/9 OA:EG_4, 1 mM n EtOH total) to ensure resistance to nonspecific protein and cell adhesion. Fbs were first cultured with HQ-SUVs (**4**) and then activated to Q (**6**) as previously described. Cells were then treated with trypsin (1 mL) and seeded on the OA-patterned surface (10^5 cells/mL) in serum-free medium for 2 h and then CBS-containing medium for 3 days. During this time, cells adhered, spread, and proliferated, filling out

the patterned regions of the surface due to the interfacial oxime reaction and were then stained and imaged. As a control, Fbs were cultured with SUVs, not displaying HQ, and were then seeded to OA-patterned substrates (1:9 OA/EG_4); the cells did not attach. Fbs were then released from the surface by application of a reductive potential (-100 mV, 10 s, PBS, pH = 7.4), which cleaves the interfacial oxime linkage. Substrates were then stained and imaged by fluorescence microscopy.

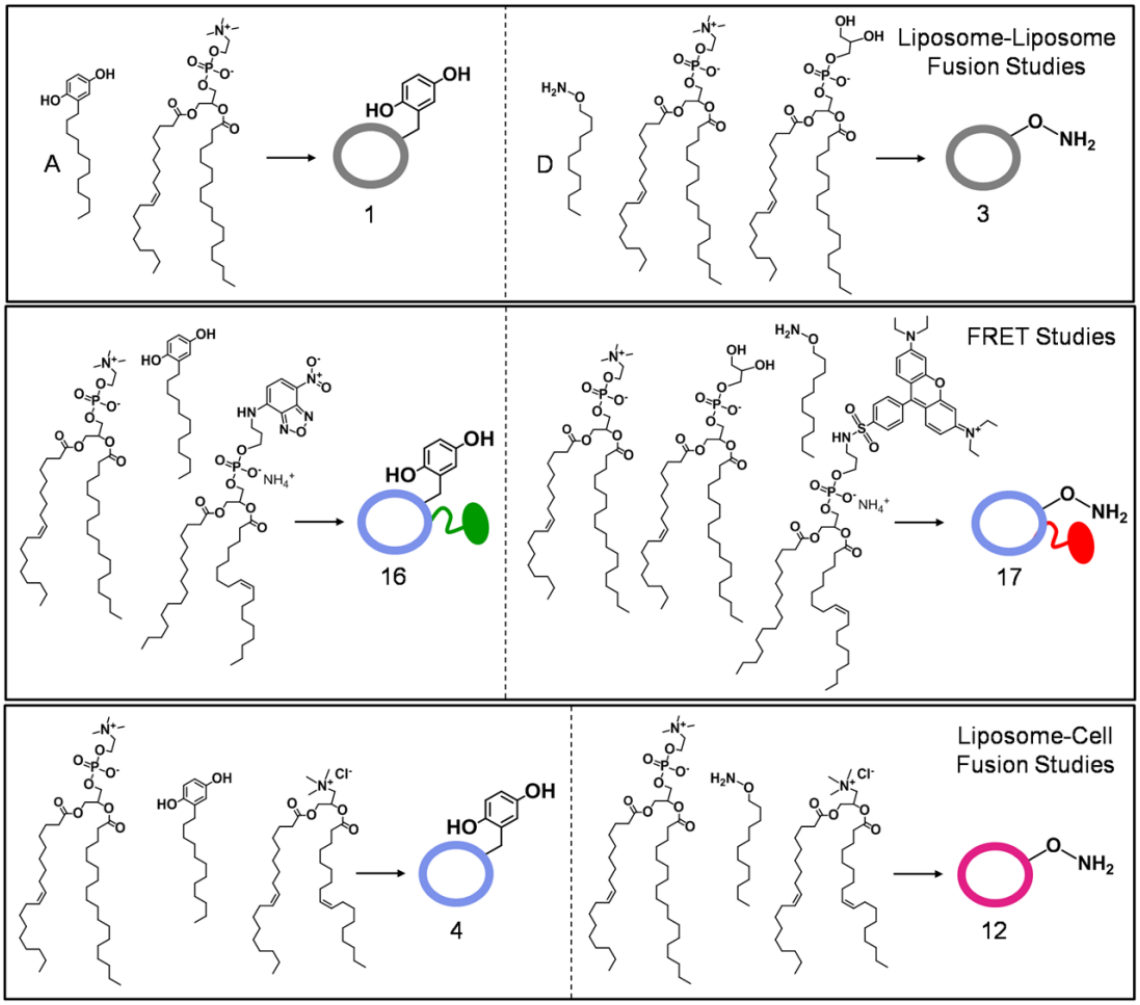

Scheme 7.5 Vesicle generation for liposome-liposome (dynamic light scattering (DLS) and transmission electron microscopy (TEM), Fourier resonance energy transfer (FRET), and liposome-cell fusion studies.

7.2.16 Mass spectrometry (MS) characterization. Preparation of gold-coated MALDI sample plates. Gold-coated MALDI sample plates (123 x 81 mm) (Applied Biosystems,

Foster City, CA) were prepared by electron-beam deposition (Thermionics Laboratory Inc, Hayward, CA) of titanium (5 nm) and then gold (12 nm). In order to form self-assembled monolayers (SAM) of alkanethiolates on the plates, the slides were immersed in a 1-mM solution of aminooxyundecanethiol in EtOH for approximately 1 min, rinsed with EtOH and dried, and then backfilled with a 1-mM solution of mercaptoundecanol in EtOH for 1 h. Once removed from solution, the surfaces were rinsed with EtOH and dried before use. *Liposome preparation.* HQ-containing liposomes (**4**) were generated as previously described, activated to Q (**5**) (10 μL, 5 μM $CuSO_4 \cdot 5H_2O$ in PBS added to 2 mL), and were then delivered to and allowed to react with the AO-terminated MALDI sample plate (90 min). The plates were then washed with water (3 x 3 mL) and EtOH (2 x 3 mL) and dried before use. *Cell preparation.* Swiss 3T3 albino mouse Fbs were incubated with HQ-LUVs (3 mM in tris buffer, 1 mL added to 4 mL culture media, 37 °C in 5 % CO_2, 16 h, **4**). HQ-presenting Fbs (**5**) were then treated with trypsin (1 mL) and seeded (10^7 cells/mL) to the MALDI sample plates in serum-free medium (droplet on the surface). HQ was then oxidized (2 μL, 5 μM $CuSO_4 \cdot 5H_2O$ in PBS) to Q (**5**) and cells were allowed to react with the surface for 3 h. Plates were then rinsed thoroughly with 0.1 % SDS in PBS (2 x 3 mL) and EtOH (2 x 3 mL) and dried before testing to remove the cells and proteins. *MALDI Analyses.* MS analysis was carried out using an AB SCIEX TOF/TOF^{TM} 5800 System (Applied Biosystems, Foster City, CA).

7.2.17 Human Mesenchymal stem cell (hMSC) culture. hMSCs and basic, growth, and differentiation media were obtained from Lonza (Basel, Switzerland). hMSCs were cultured in Dulbecco's Modified Eagle Medium (Gibco) containing 10 % fetal bovine serum (FBS) and 1 % penicillin/streptomycin at 37°C in 5 % CO_2. Culturing with induction medium as described in the Lonza protocol induced Adipogenic differentiation.

7.2.18 3D spheroid co-culture generation. HQ-SUVs (**4**) and OA-SUV (**12**) were added to two separate Fb or hMSC populations in culture for 16 h, resulting in fusion and display of HQ and OA groups from the cell surface (**5**, **13**, **14**, and **15**). The HQ-displaying cells (**5** and **13**) were activated by chemical oxidation as previously described before co-culturing. *Fluorescence imaging.* OA-presenting Rat2 Fbs (**14**) contained an m-cherry label (nucleus) for enhanced visualization, while the Q-presenting Swiss 3T3 albino mouse Fbs (**6**) contained no fluorescent label. These two cell populations were treated with trypsin and mixed together (100 µL, 1:1) in serum-containing (10 % CBS) media in a 10 mL-flask and incubated at 37 °C and 5 % CO_2 for 1, 2, 3, and 5 h. After mixing, the cells were seeded on a glass surface and visualized under a Nikon TE2000-E inverted microscope in the Texas Red channel with an exposure time of 1200 ms. Image acquisition and processing was performed using Metamorph software. *Co-culture spheroids for phase contrast and SEM imaging.* Similarly, activated Q-presenting hMSCs (**11**) were co-cultured with OA-displaying Fbs (**15**) in solution. These two cell populations were treated with trypsin and mixed together (100 µL, 1:1) in serum-containing (10 % FBS) media in a 10 mL-flask and incubated at 37 °C and 5 % CO_2 for 1, 2, 3, and 5 h. After mixing, the cells were seeded on a glass surface and visualized under a Nikon TE2000-E inverted microscope (Brightfield channel, 75 ms) or by scanning electron microscopy (described below). Control experiments were also performed in which Q-hMSCs (**11**) were mixed and co-cultured with Fbs (not functionalized with OA groups) under the same conditions as described above, and images were taken. Image acquisition and processing was performed using Metamorph software.

7.2.19 Scanning electron microscopy (SEM) of 3D spheroids. After spheroids co-cultures of Fbs (**15**) and hMSCs (**11**) were generated in solution as described above, cells were delivered to a glass slide (0.8 x 0.8 cm^2) and then fixed with 10 % formalin in

PBS for 15 min. The substrate was then washed with water (15 min), and cells were then dehydrated stepwise in 30, 50, 70, 90, and 100 % ethanolic solutions for 15 min each. After critical point drying and sputtering 2 nm of gold, the sample was ready for imaging using a Hitachi S-4700 field emission scanning electron microscope (Hitachi High Technologies America, Inc., Schaumburg, Illinois).

7.2.20 3D multi-layered co-culture cell tissue generation. HQ-SUVs (**4**) were cultured with hMSCs (3 mM in PBS, 400 µL added to 4 mL cells in culture, 16 h), resulting in membrane fusion and display of HQ from the cell surface (**13**). HQ-hMSCs (**13**) were then treated with trypsin (1 mL), seeded on a gold surface as mentioned above (10^5 cells/mL), and were allowed to grow and proliferate for 3 days. The HQ groups were then activated to Q by performing LSV (-100 to 650 mV) and were incubated for 4 hours before adding OA-functionalized Fbs (10^5 cells/mL) (**15**) that had been treated with trypsin (1 mL). The Fbs (**15**) were seeded to Q-presenting hMSCs (**11**) for 2 h in serum-free medium, followed by the addition of serum-containing media (4 mL) to promote cell growth. The cells were cultured for 3, 5, and 7 days before staining and confocal imaging. Controls showed no multi-layer formation when OA or Q groups were not presented on the cell surfaces or when two Q- or OA-displaying cells interacted with one another. Only when the correct oxime pair is combined do multi-layered co-cultures. After generation, substrates were fixed, stained, and imaged by confocal microscopy as described below.

7.2.21 3D spheroid and multi-layered co-culture generation and release. Spheroids. HQ- (**4**) and OA- (**12**) SUVs were generated as previously reported, added to hMSCs and Fbs (3 mM in PBS, 400 µL added to 4 mL cells in culture), respectively, and cultured for 16 h. After activation, these two cell populations (**11** and **15**) were then treated with trypsin (1 mL) and mixed together (100 µL, 1:1) in serum containing (10 % FCS) media

in a 10 mL flask and incubated at 37 °C and 5 % CO_2 for 1, 2, 3, and 5 h. After mixing for the allotted time, cells were seeded onto a gold surface and visualized under a Nikon TE2000-E inverted microscope under the brightfield setting (75 ms). Image acquisition and processing was performed using Metamorph software. *Multi-layers*. HQ- (**4**) and OA- (**12**) SUVs were added to hMSC and Fb (3 mM in PBS, 400 µL added to 4 mL cells in culture), respectively, and were cultured for 16 h. hMSCs displaying HQ (**13**) groups were treated with trypsin (1 mL) and cultured on gold slides (10^5 cells/mL) and allowed to grow for 2 days and then activated by conducting LSV (-100 to 650 mV). OA-presenting Fbs (**15**) were then treated with trypsin (1 mL) and added (10^5 cells/mL) to Q-hMSCs (**11**). These cells were co-cultured for 3, 5, and 7 d, resulting in the formation of 3D multi-layered co-cultured structures of hMSC and Fb. To selectively release cells in either spheroid or multi-layered tissue structures, a reduction potential of -100 mV was applied for 1 min in serum-free medium and cells were imaged by phase contrast or confocal microscopy as described.

7.2.22 Cell staining for imaging. Cells were fixed with formaldehyde (4 % in PBS, 10 min), permeated (PBS containing 0.1 % Triton X–100, 10 min), and rinsed in PBS (2 x 5 min). *Fluorescence imaging.* A fluorescent dye mixture containing phalloidin-TRITC (red, actin) and anti-vinculin (green, focal adhesions) was made in PBS with 5 % normal goat serum and 0.1 % Triton X –100. Cells were incubated with the dye solution for 1 h and were then rinsed in PBS for 5 min. A second fluorescent dye mixture consisting of phalloidin-TRITC (red, actin), DAPI (blue, nucleus), and Cy-2 (green, focal adhesions) was then made in PBS with 5 % normal goat serum and 0.1 % Triton X –100. Cells were incubated with the dye solution for 1 h and were then rinsed in PBS for 5 min. The substrates were secured in fluorescence mounting medium (Dako, Carpinteria, CA, USA), which enhances the visualization of cells when viewed under a fluorescent

microscope on a glass cover slip. Exposure times for imaging DAPI, actin, and focal adhesions were 400, 1200, and 600 ms, respectively. *Confocal imaging.* A fluorescent dye mixture containing phalloidin-TRITC (red, actin) and DAPI (blue, nucleus) was then made in PBS containing 5% normal goat serum and 0.1% Triton X –100. Cells were incubated with the dye solution for 2 h. The substrates were then secured in fluorescence mounting medium (Dako, Carpinteria, CA, USA), which enhances the visualization of cells when viewed under a fluorescent microscope on a glass cover slip. An average of 84 scans were taken to generate 3D reconstruction images.

7.2.23 HMSC differentiation and immunohistochemistry. Adipogenic differentiation of Q-hMSCs (**11**) was induced after the growth of 3D tissue-like structures and co-culture with AO-Fb (**15**) by culturing substrates with induction medium as described in the Lonza protocol. Surfaces were then fixed with formaldehyde (4 % in PBS, 30 min), immersed in a solution containing water and 60 % isopropyl alcohol (3-5 min) and stained with Oil Red O (red, lipid vacuoles, 5 min) and Harris Hemotoxylin (blue, nucleus, 1 min). Substrates were visualized by phase contrast microscopy using a Nikon TE2000-E inverted microscope. Image acquisition and processing was performed using Metamorph software.

7.2.24 Confocal microscopy. Cell clusters and tissue formation were generated, stained, and secured on a glass slide as previously described above and were visualized with a Nikon Eclipse TE2000-E inverted microscope (Nikon USA, Inc., Melville, NY). Data was analyzed by Metamorph software and a spectral confocal microscope (LeicaMicrosystems, Bannockburn, IL). 3D reconstructions of fluorescent images were generated using Volocity software with an average of 84 scans/image.

7.2.25 Cell viability assay of 3D spheroid and multi-layered co-culture structures. Cell viability of 3D spheroid and multi-layered tissue-like structures was assessed by

performing a trypan blue viability assay (Hyclone, Fisher Sci, Pittsburgh, PA). Fb (**15**) and hMSC (**11**) spheroid and multi-layer co-culture structures were prepared as previously described. A solution of 0.4 % trypan blue in PBS was made and diluted in CBS (1:1) containing the spheroids (1, 2, 3, and 5 h after mixing) in solution and multi-layer cell sheets (3, 5, and 7 d after a second cell population was added) on a glass slide. Trypan blue was allowed to react with the cells for 2 min, at which time spheroids and surfaces were imaged for blue fluorescence using a Nikon TE2000-E inverted microscope. A control experiment was performed in which 3D multilayered hMSC and Fb co-cultures were generated for 7 days and then fixed with paraformaldehyde and stained with trypan blue as described above. Images were compared to the control to approximate the % viability of cells in multilayers.

7.2.26 Cell viability assay of cells after potential application. HMSCs and Fbs were cultured with HQ-functionalized liposomes for 1, 3, 5, and 7 d as mentioned (**5** and **13**) and tested for viability after being subject to varying potentials. All cell populations maintained viability > 95 %. Measurements were performed in PBS, pH = 7.4. Each potential was held for 10 s, ranging from -100 to 650 mV, in ~185 mV increments. Cell viability was approximated by conducting a trypan blue assay after being subject to different potentials.

7.3 Results and Discussion

To deliver and tailor cell surfaces with dynamic and bio-orthogonal chemical groups for cell membrane manipulation and control of cell-cell interactions, we first developed a liposome fusion-based model system. Hydroquinone (**1**, HQ) and aminooxy alkanes (**3**, AO) were synthesized and incorporated into liposomes (Schemes 7.2, 7.3, and 7.5). We have previously shown in solution and on conducting substrates how HQ is in the ‘off state’ and can be activated to the ‘on state’ quinone (Q) by mild chemical or

electrochemical oxidation. Q can then chemoselectively react with AO-tethered ligands to form stable oxime linkages at physiological conditions (Figure 7.1).[28-30] The oxime linkage can then be selectively cleaved under reductive conditions to regenerate HQ with simultaneous release of the AO-tethered groups. This redox-active, oxime-based conjugation and release chemistry is bio-orthogonal and can be performed in complex protein mixtures, cell lysates, and in cell culture.[30] Thus, our rationale was to combine this dynamic, switchable, and bio-orthogonal conjugation and release strategy with liposome fusion to tailor cell surfaces *in vitro* for studies in cell-surface manipulation and tissue engineering.

To evaluate if liposome-to-liposome fusion can occur via oxime chemistry, we activated HQ- (**1**) to Q-containing liposomes (**2**) and then mixed them with AO-containing liposomes (**3**) (Figure 7.1A). We observed rapid liposome aggregation and fusion (Figure 7.1B), as shown by transimission electron microscopy (TEM) image analyses. It was demonstrated that over time, an oxime-driven process directed liposomes to first aggregate and then fuse, forming larger assemblies. Fluorescence resonance energy transfer (FRET) characterization of liposome fusion displays a clear FRET signal, only when the complimentary oxime pair is present in the liposomes (Figure 7.2A). Furthermore, dynamic light scattering (DLS) analysis shows the spontaneous liposomal growth due to this oxime-driven liposomal fusion (Figure 7.2B). Aggregated or fused liposomal structures were not observed in control experiments where HQ-containing liposomes were not activated or when either oxime pair was missing.

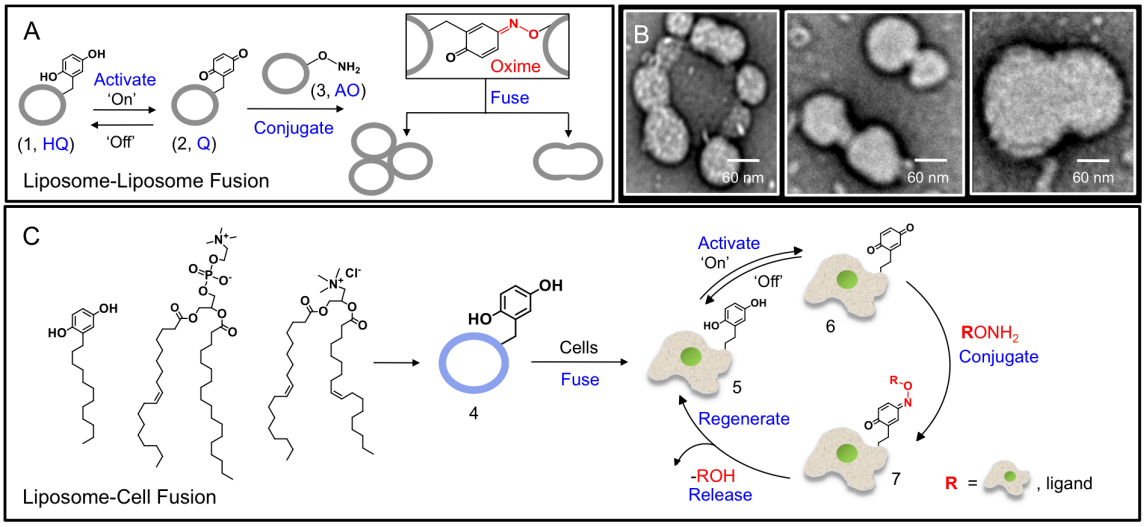

Figure 7.1 Schematic and transmission electron micrographs (TEM) demonstrating dynamic liposome-liposome fusion and liposome-cell fusion for tailoring cell surfaces. (A) Hydroquinone (HQ)-containing liposomes (**1**) (3 mM in tris buffer, pH 7.4) are in the 'off state' and are thus, activated to the 'on state' quinone (Q) (**2**) by mild chemical oxidation (20 μL, 5 μM $CuSO_4 \cdot 5H_2O$ in PBS at 10 mol %, 5 min) and mixed with aminooxy (AO)-containing liposomes (**3**). Mixing these two populations (0.2 mM total in PBS, 1:1) over 2 hours results in the formation of (B) multi-adherent, partially fused, and completely fused liposomal structures driven by oxime bond formation. Over time, the liposomes grow in size due to fusion. (C) General schematic representing the dynamic control of cell surfaces based on liposome-cell fusion for the delivery and tailoring of bio-orthogonal groups. POPC (398 μL, 10 mg/mL in $CHCl_3$ at 88 mol %), DOTAP (10 μL, 10 mg/mL in $CHCl_3$ at 2 mol %), and HQ-functionalized alkane (160 μL, 10 mM in $CHCl_3$ at 10 mol %) are mixed to form liposomes (3 mM in tris buffer, pH 7.4). The HQ-tethered liposomes (**4**) are then added to cells in culture (400 μL to 4 mL, 16 h), resulting in fusion and subsequent presentation of HQ groups from the cell surface (**5**). HQ is then activated to Q (**6**), which reacts chemoselectively with a range of AO (or $RONH_2$)-tethered ligands or cells via a covalent and stable oxime linkage (**7**). Upon a mild change in redox environment, the oxime bond is cleaved (-100 mV, 10 s, pH 7.4) to release the ligand or cell, followed by regeneration of the HQ-presenting cell (**5**) for subsequent rounds of dynamic and controlled conjugation and release.

After the successful characterization of liposome-to-liposome fusion, we aimed to employ a similar strategy to generate electroactive, dynamic, and switchable cell surfaces. Therefore, we applied our liposome fusion method to deliver the bio-orthogonal HQ (**4**) and AO (**12**) groups for subsequent fusion and presentation from cell membranes. For these studies, HQ alkane was mixed with neutral POPC, and cationic DOTAP in a 10:88:2 ratio, and AO alkane with POPC, and DOTAP (5:93:2) (Scheme 7.5D). After addition to cells (Swiss 3T3 fibroblasts (Fbs)) in culture, the liposomes first fuse, delivering the chemical groups to cell surfaces (Figure 7.1C). HQ can then be

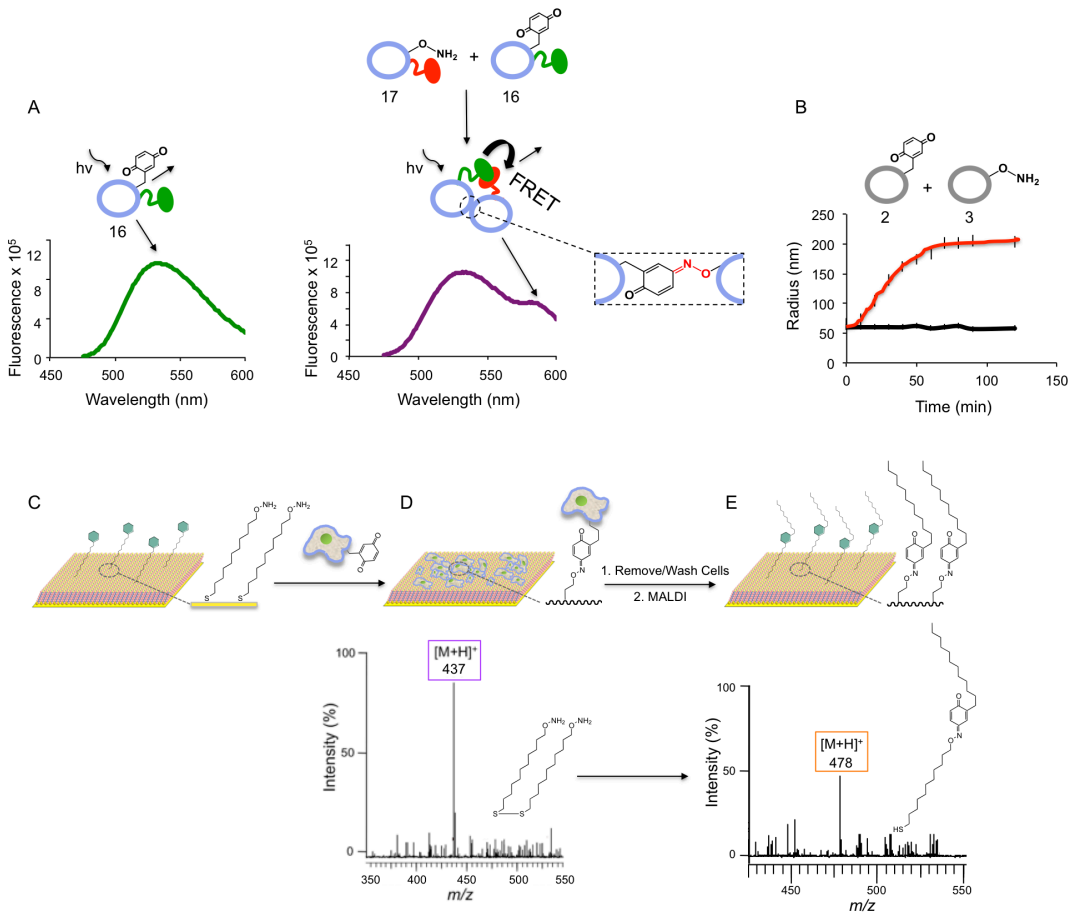

Figure 7.2 Characterization of liposome adhesion and fusion based on chemoselective oxime formation between Q- and AO-containing liposomes. (A) Q- (160 μL, 10 mM in $CHCl_3$ at 10 mol %) and NBD-PE- (20 μL, 10 mg/mL in $CHCl_3$ at 2 mol %) containing liposomes (**16**) were excited at 471 nm, producing light emission at 531 nm (green trace). When these liposomes (200 μL, 1:1) were mixed with AO- (60 μL, 10 mM in $CHCl_3$ at 5 mol %) and rhodamine-PE/POPG- (28 μL, 10 mM in $CHCl_3$ at 2 mol %) functionalized liposomes (**17**), a FRET emission peak is observed at 578 nm indicating oxime-mediated liposomal adhesion and fusion. No FRET signal is observed with non-activated HQ liposomes or when liposomes without AO groups are mixed. Fluorescence was monitored for 2 h at 2 min intervals, and the temperature was maintained at 25 °C. (B) Q- and AO-containing liposomes (**2** and **3**, respectively) were mixed (0.2 mM in PBS, 100 μL, 1:1) and monitored by DLS to observe the changes in liposome size over reaction time. Over a period of 80 min of mixing, liposomes grew in size due to adhesion, partial, or complete fusion (red trace). As a control, liposome size remained constant when Q-containing liposomes (**2**) were added to liposomes not functionalized with AO groups or un-activated, HQ liposomes (**1**) with AO liposomes (**3**) (black trace). (C) Self-assembled monolayers (SAMs) of AO-terminated alkanethiol (1 mM in EtOH, 1 min, and backfilled with 1 mM mercaptoundecanol in EtOH, 1 h) were formed on gold-coated (12 nm) MALDI sample plates (123 x 81 mm). MALDI analysis was performed directly on the surface to display mass $[M + H]^+$ of 437 corresponding to the AO-terminated alkanethiol connected by disulfide linkage. (D) Q-displaying Fbs (**6**) were seeded (10^7 cells/mL, 3 h in serum-free conditions) on gold-coated MALDI sample plates presenting AO-terminated alkanethiol. The cells were then washed several times (0.1% SDS in PBS, 2 x 3 mL and EtOH, 2 x 3 mL) and dried before testing to result in (E) oxime conjugation on the surface. MALDI was again performed, and a mass $[M + H]^+$ of 478 corresponding to the product of Q and AO conjugation was observed.

activated to generate Q, which will conjugate chemoselectively with AO-tethered ligands or cells to form a stable, interfacial oxime linkage. The oxime bond at the cell membrane can then be selectively cleaved with the simultaneous release of the ligand or cell and regenerate the HQ-presenting cell. This dynamic cycle is non-cytotoxic (Figure 7.4), redox triggered and switchable (Scheme 7.1 and Figure 7.1C), performed *in situ* and under physiological conditions, and provides unprecedented control of cell-cell and cell membrane interactions through the conjugation and release of ligands and cells.

Figure 7.3 demonstrates the dynamic and switchable conjugation and release of ligands to and from the cell membrane. After HQ-containing liposomes (**4**) were fused with Fbs (**5**) on a conductive substrate, cyclic voltammetry (CV) was performed, and distinct HQ to Q redox peaks were observed (Figure 7.3A).[30] Upon activation to Q (**6**) (400 mV, 10 s) and conjugation of AO-tethered rhodamine (**7** and **8**) to cells, a shift in CV peaks, characterisitic of oxime formation,[30] was observed. The rhodamine-labeled Fbs were also imaged, and red fluorescence was observed (Figure 7.3B). After application of a non-cytotoxic, reductive potential (-100 mV, 10 s, Figure 7.4), rhodamine was released from the cells, and HQ was regenerated on the cell surface as indicated by CV and fluorescence microscopy (Figure 7.3C). We then re-activated the HQ-presenting Fbs to Q and conjugated biotin-hydrazide, followed by FITC-streptavidin. Cells could once again conjugate and release molecules from the cell surface shown by CV and fluorescence microscopy (Figure 7.3D). The oxime linkage is stable, and only upon application of a mild reductive potential does the oxime cleave and release ligands.[30] In general, this dynamic strategy can be used for controlling the chemical structure of cell surfaces in 3D space and time with micro- or nanoelectrode arrays, where the cell surface ligands can be replaced with any biomolecule of interest, creating a new tool for the modulation of cell interactions.

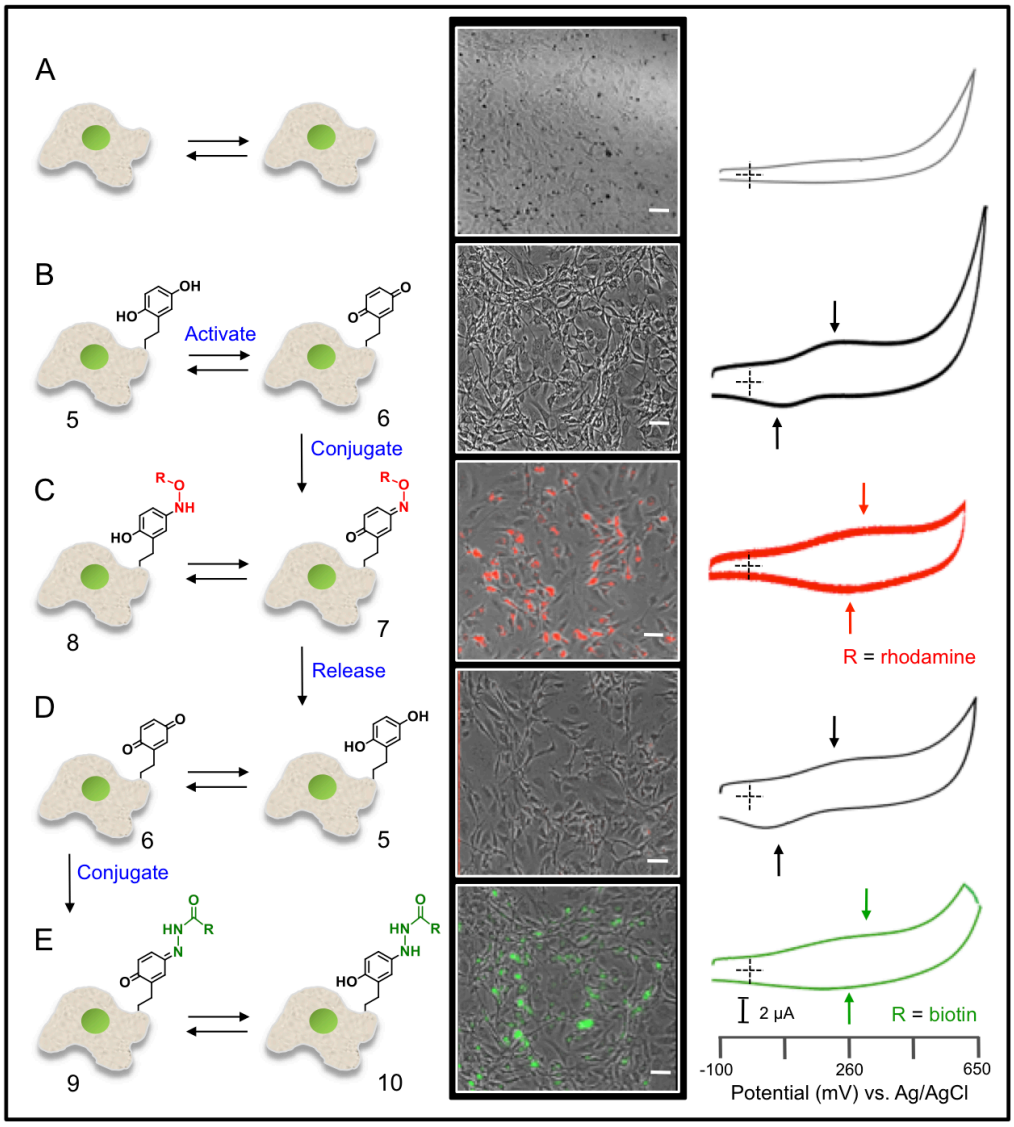

Figure 7.3 (Top) Electrochemical characterization of cyclical cell-surface tailoring and the release of ligands based on redox responsive chemoselective chemistry. (**a**) Fibroblasts (Fb), not fused with liposomes presenting HQ groups show no redox signal or fluorescence. (**b**) HQ-containing liposomes (**4**) are added to Fbs (3 mM in tris buffer, 400 μL to 4 mL, 16 h), resulting in membrane fusion and presentation of HQ from the surface (**5**). The stable HQ (**5**) to Q (**6**) interconversion can be monitored by cyclic voltammetry (CV) (-100 to 650 mV, pH 0, 100 mVs^{-1}) due to its diagnostic redox peaks (black trace, HQ = 130 mV, Q = 258 mV). (**c**) Activated Q-presenting Fbs (**6**) can be chemoselectively reacted with rhodamine-AO (7 mM in H_2O, 100 μL to 4 mL, 30 min) for cell-surface tailoring (**7** and **8**). This results in stable, fluorescently labeled cells (red) and a diagnostic shift in redox signal (red trace, 252 mv, 284 mV). (**d**) In a reductive environment (-100 mV, 10 s, pH 7.4), the oxime bond is cleaved with the release of rhodamine and the regeneration of HQ-presenting Fbs (**5**) as indicated by a loss in fluorescence and the redox peaks of the HQ to Q cycle (black trace). (**e**) Cell surfaces can once again be conjugated for a second time with hydrazide-tethered biotin (**9** and **10**) and fluorescein-presenting streptavidin (1 mg/mL in PBS, 0.5 mL to 2 mL, 1 h each), resulting in fluorescently labeled cells (green) and a shift in redox peaks (green trace). (Bottom) A general schematic and corresponding fluorescent images demonstrating dynamic control of cell adhesion and release from patterned substrates.

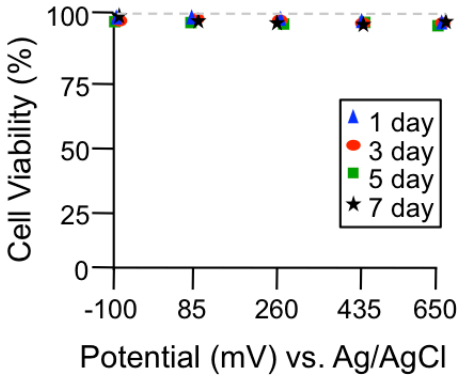

Figure 7.4 Cell viability assay of hMSCs and Fbs when subjected to mild redox potentials. HMSCs and Fbs were cultured with HQ-functionalized liposomes (**4**) (3 mM in tris buffer, 400 μL to 4 mL) for 1 (blue triangle), 3 (red circle), 5 (green square), and 7 (black star) days and tested for viability after being subject to varying redox potentials (-100 to 650 mV, 10 s, ~185 mV increments, PBS, pH 7.4). All cell populations (**13** and **15**) maintained viability >95% (trypan blue viability assay, 0.4 % in PBS, 2 min) and were indistinguishable from control populations not exposed to redox potentials.

Several assays were performed to evaluate cell viability as a function of applied redox potential (Figure 7.4). As a result, no change in cell viability was observed after applying different electrochemical potentials (-100 to 650 mV, 10 s) on cells cultured with HQ for up to 7 days. Other control experiments concluded that removing either HQ or AO from the fusion liposomes resulted in no ligand conjugation at the cell surface. When AO-alkane or HQ-alkane was added directly to cells in culture but not in liposome form no incorporation of AO or HQ groups in cell surfaces were observed. Additionally, when chemical or electrochemical activation does not occur, conjugation and release of ligands was not observed. Furthermore, we determined the amount of HQ molecules at the cell membrane upon initial liposome fusion by FACS analysis. FACS analysis also demonstrated that HQ remains incorporated in the membrane after several rounds of cell growth and division and that HQ can still be actived for conjugation and release of ligands (Figure 7.5). These results may lead to new ways to tailor and monitor *in vitro*

and *in vivo* events that occur at cell membranes and allow for new types of pulse and chase type experiments for cell imaging and for tracking cell movement.[31,32]

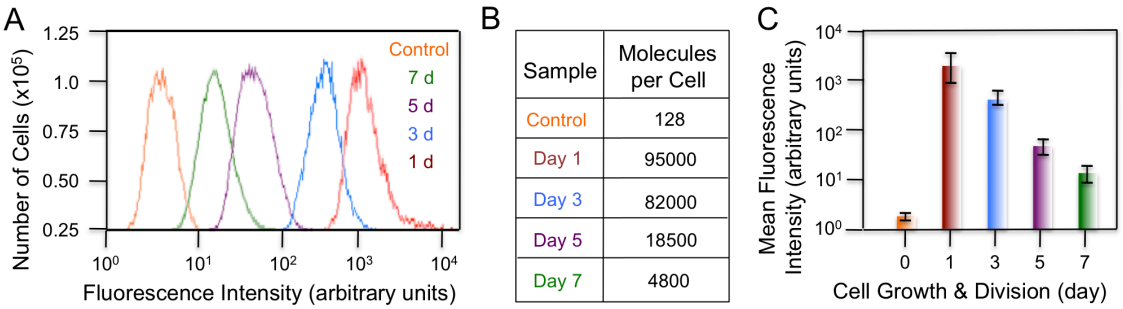

Sample	Molecules per Cell
Control	128
Day 1	95000
Day 3	82000
Day 5	18500
Day 7	4800

Figure 7.5 Fluorescence activated cell-sorting (FACS) analysis to determine the number of HQ molecules per cell. HQ-containing liposomes (**4**) were added to Fbs in culture (3 mM in tris buffer, 400 μL to 4 mL, 1, 3, 5, and 7 d). The amount of HQ on cell surfaces as delivered by membrane fusion was determined after 1, 3, 5, and 7 days. Before conducting FACs, cells were chemically (20 μL, 5 μM $CuSO_4 \cdot 5H_2O$ in PBS at 10 mol %, 5 min) activated to Q (**6**), followed by conjugation of biotin-hydrazide (**9**) (3 mM in CBS, 1 mL added to 4 mL CBS in cell culture, 37ºC in 5% CO_2, 1 h) and fluorescein-streptavidin (1 mM in CBS, 0.5 mL added to 4 mL CBS in cell culture, 37ºC in 5% CO_2, 1 h). A control population in which Fbs (not functionalized with HQ groups) were reacted with biotin-hydrazide and FITC-streptavidin under the same conditions was also tested. All sample populations were centrifuged (5 min, 1000 rpm), resuspended in RPMI (10^7 cells/mL), centrifuged, and resuspended in RPMI. 1-mL samples were tested against a standard bead (10^7 beads/mL) with known fluorescein molecule density. (**A**) The relationship between the number of cells scanned (~10^5) and fluorescence intensity of control population and cells incubated with HQ-functionalized liposomes for 1, 3, 5, and 7 days as determined by flow cytometry analysis is reported. The fluorescence intensities decrease over time, indicating that cells are able to carry the HQ moiety through division and growth. The control cells show little to no fluorescence. (**B**) The number of fluorescein molecules was calculated by comparing the relative mean intensity to a standard bead with known FITC equivalent molecule density. The numbers of HQ molecules per cell are listed, showing a decrease in density on the cell surface over time. (**C**) The relationship between the mean fluorescence intensity (3 trials per day, error bars) and liposome incubation day is shown as a linear decrease from 1 to 7 days.

The incorporation and utility of HQ on the cell surface was further investigated by attaching and releasing cells from an OA-patterned substrate (Figure 7.6D). HQ-presenting Fbs (**5**) were activated to Q (**6**) and then seeded onto an inert substrate, presenting AO groups.[33] The Q groups on the cell surface (**6**) reacted biospecifically with the patterned OA ligands to form an interfacial oxime linkage. The cells attached and then proliferated, filling out the patterned regions. An electrochemcial trigger was then applied to cleave the oxime linkage, and cells released from the substrate. Furthermore, a novel MALDI mass spectrometry analysis of cell membrane incorporation shows oxime

conjugation between Q presenting cells and OA terminated surfaces (Figure 7.2C-E).[34] This strategy allows for spatial and temporal control of cell interactions in 2D and may be extended to other materials and nanoparticles for designing new cell-based assays and renewable microarray platforms.[35,36]

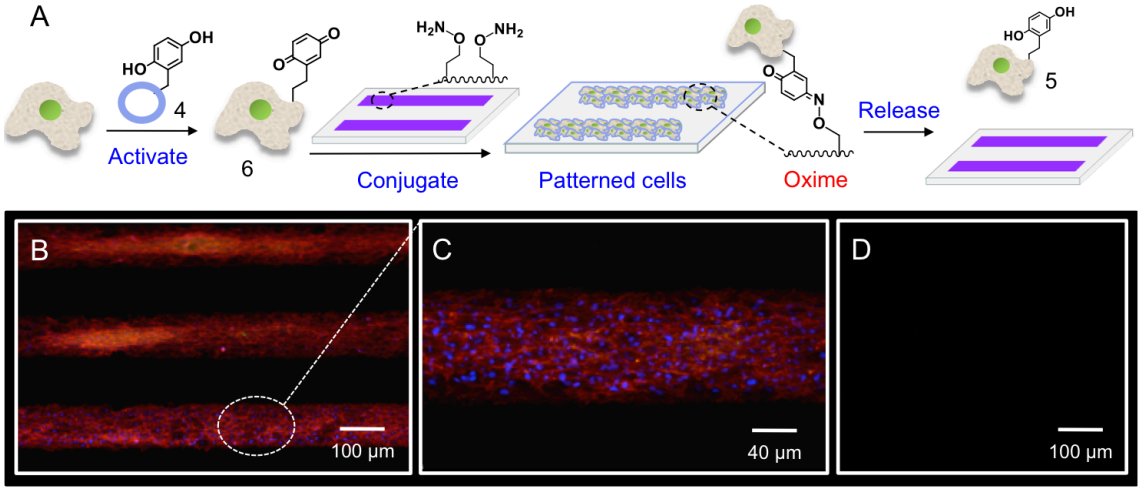

Figure 7.6 Fluorescent characterization of cyclical cell-surface tailoring and the release of ligands based on redox responsive chemoselective chemistry. (**a**) Fbs were cultured with HQ-containing liposomes (**4**), resulting in membrane fusion and subsequent display of HQ from cell surfaces (**5**). Mild chemical oxidation (20 μL, 5 μM $CuSO_4 \cdot 5H_2O$ in PBS at 10 mol %, 5 min) converts the HQ to Q groups on the cell surface (**6**). Q-presenting Fbs (**6**) (10^4 cells/mL, 2 h) were then added to a substrate patterned with AO-terminated ligands (1 mM in EtOH, 1:9 AO/EG_4). Cells adhered to the substrate due to a biospecific interfacial oxime ligation and then proliferated (4 d) within the patterned region as shown in lower (**b**) and higher (**c**) magnified fluorescent micrographs. Upon electrochemical reduction, the interfacial oxime is cleaved and the cells are released from the substrate (**d**). Cells were stained for actin (red, phalloidin), nucleus (blue, DAPI), and anti-vinculin (green, Cy-2).

We extended this methodology to demonstrate the dynamic control over cell-cell interactions by co-culturing HQ-presenting human mesenchymal stem cells (hMSC) (**13**) with AO-displaying Fbs (**15**) to form 3D tissue structures. Upon chemical activation and mixing in solution, 3D spheroid assemblies were able to be rapidly generated (Figure 7.7A-C and 7.7E). By increasing the mixing duration, control of the spheroid size could be achieved. The interconnected cells that make up the spheroids could then be disassembled, back to individual cells by mild electrochemical reduction (-100 mV, 10 s) (Figure 7.7D). Additionally, spheroids were formed when Swiss 3T3 albino mouse Fbs

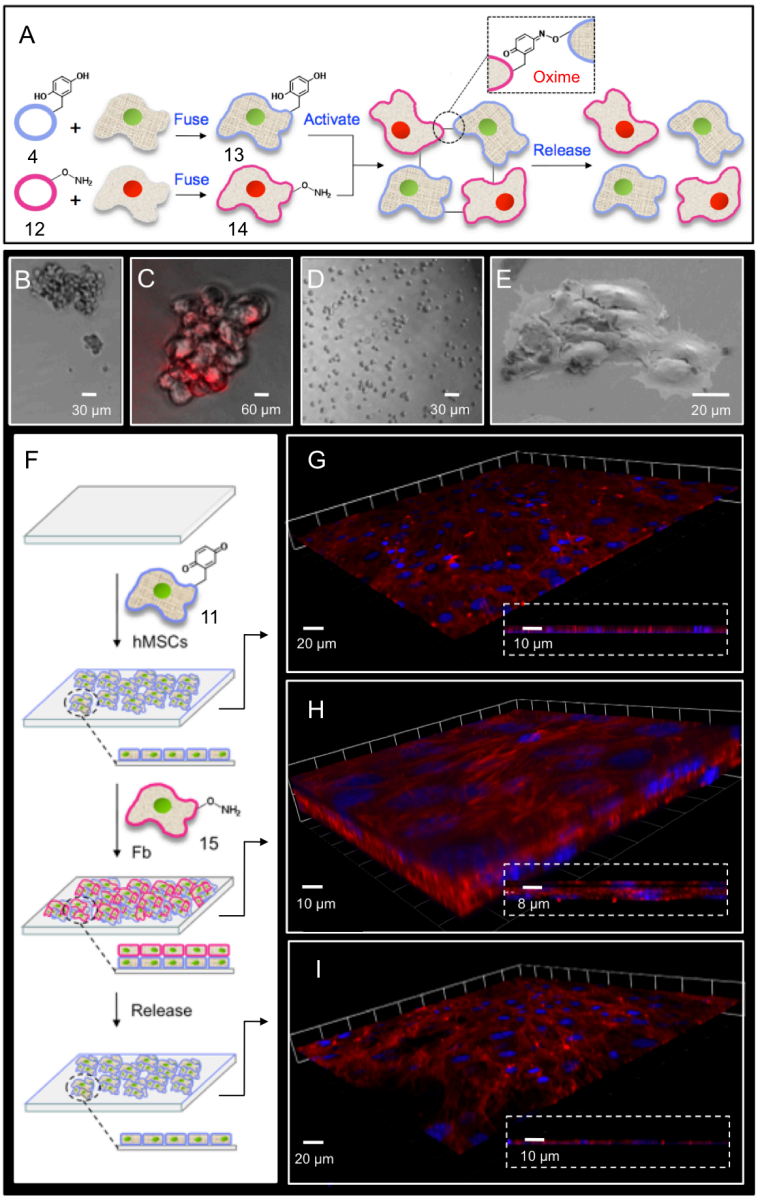

Figure 7.7 Schematic and corresponding images of 3D dynamic spheroid and multi-layered tissue assembly and disassembly via liposome fusion and chemoselective cell-surface tailoring. (A) Human mesenchymal stem cells (hMSCs) are functionalized with HQ groups (**13**) (3 mM in tris buffer, 400 µL to 4 mL, 16 h) after liposome fusion and are then activated to Q (**11**). Fbs presenting AO groups (**14**) are then co-cultured (1 mL, 1:1, 3 h) with Q-displaying hMSCs (**11**), producing (B, C, and E) 3D spheroid assemblies, interconnected through chemoselective oxime chemistry. Mild electrochemical reduction (-100 mV, 10 s, pH 7.4) causes oxime cleavage and the dynamic disassembly of cells as shown in (D). (F) Activated, Q-tethered hMSCs (**11**) are cultured on a substrate (10^5 cells/mL, 3 d), resulting in a 2D cell monolayer (G). AO-presenting Fbs (**15**) are added (10^5 cells/mL, 2 d) to the hMSCs (**11**), and a 3D interconnected multi-layered structures (H). A reductive potential applied to the substrate cleaves the oxime bond and induces the dynamic release of Fbs from the multi-layer, regenerating the 2D monolayer of hMSCs (**i**). The nuclei of OA-tethered Fbs (**14**) shown in C are stained with m-cherry for enhanced visualization. HMSCs (**11**) and Fbs (**15**) displayed in G-I are stained for actin (red, phalloidin) and nucleus (blue, DAPI).

presenting HQ groups were activated (**6**) and co-cultured with nuclear m-cherry-labeled Rat2 Fbs displaying AO groups (**14**) (Figure 7.7C). Figure 3D exhibits a cryo scanning electron micrograph (SEM) of an oxime ligated, spheroid assembly of hMSC (**15**) and Fbs (**13**) attached to a substrate. Viability for the cells in the spheroids was analyzed over time (1 to 5 hours, trypan blue assay, blue false colored) and found to be > 99%. Control experiments when no activation occurs or when one of the oxime compliments is not present in a cell type showed no spheroid formation. These results indicate that 3D co-culture assemblies in solution can be generated in a straightforward manner with the ability to control both the size, compostion, and the duration of cell-cell interactions. This strategy is general and may be used for numerous studies, including autocrine and paracrine signaling events and when combined with microfabricated scaffolds as a tissue engineering platform.

In addition to forming spheroid assemblies, we demonstrate that 3D multi-layered co-culture tissue structures are able to be generated on a solid support. We cultured activated, Q-presenting hMSCs (**11**) on a substrate to form a 2D monolayer (Figure 7.7F and 7.7G) and then added AO-displaying Fbs (**15**). Chemoselective ligation occurs between the two cell populations followed by 3D multi-layer tissue growth after 3 days (Figure 3H). When the proper oxime pair is not present, only a single monolayer of hMSC is observed with no Fbs adhering. We found that cells were viable for many days (> 7 days) and that the HQ and AO could be carried forward on the cell surface (FACS analysis over time, Figure 7.5) even through cell growth and proliferation. The multi-layers were able to be disassembled by applying a mild reductive potential to the substrate (-100 mV, 10 s, pH = 7.4), which cleaved the oxime linkage and released the interactions between cells. Overall, this dynamic method to generate 3D multi-layer

tissue structures may be used to control cell-cell interactions for many co-culture-based cell behavioral and cell tissue applications.[37]

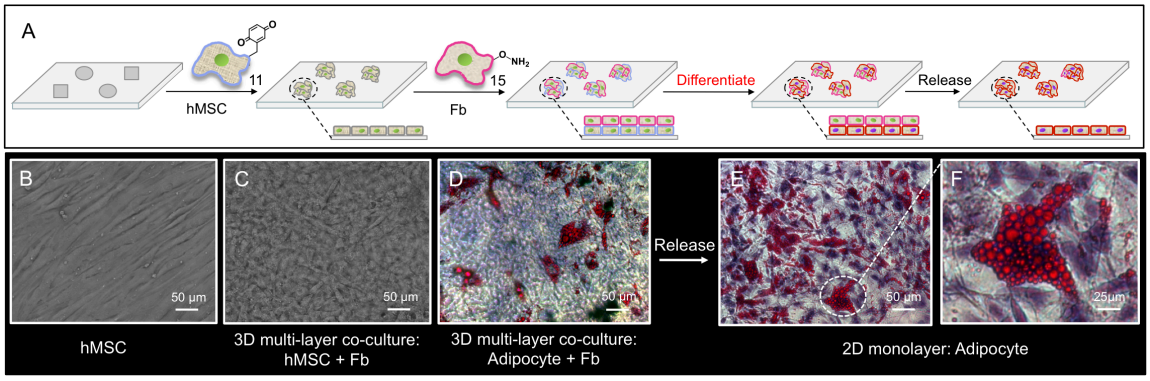

Figure 7.8 Schematic and corresponding phase contrast images displaying the formation, differentiation, and release of 3D dynamic tissues using an Fb/hMSC co-culture. (**a**) Activated, Q-tethered hMSCs (**11**) are cultured on a substrate (10^5 cells/mL, 3 d) and form a 2D monolayer as shown by the image in (**b**). AO-presenting Fbs (**15**) are then added (10^5 cells/mL, 2 d), producing a 3D multi-layered, interconnected co-culture (**c**). When the appropriate induction media is delivered to the co-culture, hMSCs differentiate into adipocytes, resulting in a 3D multi-layered co-culture of Fbs and adipocytes (**d** dynamic release of Fbs, leaving only the adhered adipocytes on the surface as a 2D monolayer shown by lower (**e**) and higher (**f**) magnified images. Adipocytes were stained for lipid vacuoles (red, Oil Red O) and nucleus (purple, Harris Hemotoxylin).

We further employed this dynamic strategy to study stem cell differentiation by applying our liposome fusion-based delivery of activatable bio-orthogonal groups to cell surfaces to generate 3D multi-layered cell tissues and induce adipocyte differentiation (Figure 7.8). HQ-presenting hMSCs were activated and co-cultured with Fbs as described previously. This tissue was grown in media that induced adipocyte differentiation after 10 days, resulting in 3D multi-layered co-culture tissues of adipocytes and Fbs (Figure 7.8D). Application of a mild reductive potential disassembled the 3D tissue, leaving a relatively pure, 2D adipocyte monolayer (Figure 7.8E and 7.8F). The dynamic and controlled 3D multi-layer cell disassembly indicates that cell-cell interactions, even for complex stem cell differentiation processes over long time periods, can be precisely manipulated. By assembling and disassembling the co-cultures on

demand, a time course of cell behavior, due to length of cell-cell interactions, is able to be determined for a range of cell lines and co-culture-based applications.[38,39]

In summary, we have developed a new general and straightforward liposome fusion based methodology to deliver dynamic and switchable bio-orthogonal chemistries to tailor cell membranes and direct the formation of 3D co-culture tissue structures. We demonstrated and extensively characterized the conjugation and release of molecules to and from cell surfaces *in situ*, as well as the triggered assembly and disassembly of 3D spheroid and multi-layered tissues. Additionally, dynamic co-cultures of hMSCs and Fbs were able to be generated and differentiated with this redox oxime strategy.

7.4 Conclusions

The dynamic and bio-orthogonal oxime chemistry reported has several key advantages to serve as a cell-surface engineering and cell-tissue generating system. First, the oxime complimentary pair is synthetically straightforward, and ketone-, hydrazide, and AO-tethered ligands are commericially available. Second, oxime reactivity can be switched 'on' and 'off' with a change in the redox environment and therefore, can be used to monitor cell-surface incorporation of moleucles and cell-surface interactions. Third, the oxime bond forms rapidly and is stable under physiological conditions until subject to a chemical or electrochemical reducing potential. Fourth, the redox manipulation is non-cytotoxic. Fifth, this liposome fusion-based method is general and can be used to deliver the oxime pair to a range of cell lines for a variety of applications. Lastly, this methodology can be used to deliver a variety of other bio-orthogonal 'click' chemistries to cell surfaces.

Future applications of this strategy may be extended to study and manipulate stem cell fate of 3D multi-layered co-culture tissues and for controlling stem cell plasticity. Integration of this approach with 3D polymer scaffolds may lead to the design of new

tissue enginering and regenerative medical therapies, devices, and applications. Theranostic applications, where simultaneous delivery of therapies and diagnostic monitoring, may also be possible for a variety of *in vitro* and *in vivo* imaging and cell tracking studies. With the introduction of an electroactive cell surface, it may be possible to track dynamic biophysical events, such as lipid diffusion and endo- and exocytosis. By generating a photo-inducible linker within the bio-orthogonal pair lipids a light sensitive cleavable system may also be generated for spatial and temporal control of cell-cell interactions.[11,40] By altering the lipid composition and mix of bio-orthogonal groups in cell membranes via liposome fusion and delivery, potential cell to cell fusion experiments and the generation of tailored giant unilamellar vesicles may be possible. Finally, by tailoring and controlling cell surfaces and cell-cell interactions, new types of autocrine and paracrine signaling studies for fundamental cell behavior and tissue regeneration applications may be explored.[41,42]

References

(1) Nelson, C. M.; Bissell, M. J. *Annu. Rev. Cell and Dev. Biol.* **2006***, 22*, 287-291.

(2) Li, L.; Xie, T. *Annu. Rev. Cell and Dev. Biol.* **2005**, *21*, 605-612.

(3) Meshel, A. S.; Wei, Q.; Adelstein, R. S.; Sheetz, M. P. *Nat. Cell Biol.* **2005**, *7*, 157-160.

(4) Engler, A.; Sen, S., Sweeney, H. L.; Discher, D. E. *Cell*, **2006**, *126*, 677-683.

(5) Badylak, S. F.; Nareem, R. M. *Proc. Nat. Acad. Sci. U.S.A.* **2010**, *107*, 3285-3288.

(6) Ibold, Y.; Frauenschuh, S.; Kaps, C.; Sittinger, M.; Ringe, J.; Goetz P. M. *J. Biomol. Screen.* **2007**, *12*, 956-960.

(7) Geng, Y.; Dalhaimer, P.; Cai, S.; Tsai, R.; Tewari, M.; Discher, D. E. *Nat. Nanotech.* **2007**, *2*, 249-255.

(8) Albrecht, D. R.; Underhill, G. H.; Wassermann, T. B.; Sah, R. L.; Bhatia, S. N. *Nat. Methods* **2006**, *3*, 369-374.

(9) Legant, W. R.; Pathak, A.; Yang, M. T.; Deshpande, V. S.; MacMeeking, R. M.; Chen, C. S. *Proc. Nat. Acad. Sci. U.S.A.* **2009**, *106*, 10097-10103.

(10) Raghavan, S.; Nelson, C. M.; Baranski, J. D.; Lim, E.; Chen, C. S. *Tissue Eng. Part A* **2010**, *16*, 2255-2263.

(11) Kloxin, A. M.; Kasko, A. M.; Salinas, C. N.; Anseth, K. S. *Science* **2009**, *324*, 59-63.

(12) Lutolf, M. P.; Hubbell, J. A. *Nat. Biotechnol.* **2005**, *23*, 47-55.

(13) Falconnet, D.; Csues, G.; Grandin, H. M.; Textor, M. *Biomaterials* **2006**, *27*, 3044-3063.

(14) Khademhosseini, A.; Langer, R.; Borenstein, J.; Vacanti, J. P. *Proc. Nat. Acad. Sci. U.S.A.* **2006**, *103*, 2480-2487.

(15) Gartner, Z. J.; Bertozzi, C. R. *Proc. Nat. Acad. Sci. U.S.A.* **2009**, *106*, 4606-4610.

(16) Mahal, L. K.; Yarema, K. J.; Bertozzi, C. R. *Science* **1997**, *276*, 1125-1128.

(17) Yoder, N. C.; Yuksel, D.; Dafik, L.; Kumar, K. *Curr. Opin. Chem. Biol.* **2006**, *10*, 576-583.

(18) Raghavan, R. S.; Hang, H. C. *Drug Discov. Today* **2009**, *14*, 178-184.

(19) Best, M. D. *Biochemistry* **2009**, *48*, 6571-6584.

(20) Saxon, E.; Bertozzi, C. R. *Science* **2000**, *287*, 2007-2010.

(21) Gong, Y.; Luo, Y.; Bong, D. *J. Am. Chem. Soc.* **2006**, *128*, 14430-14431.

(22) Lee, J.; Jun, H.; Kim, J. *Adv. Mater.* **2009**, *21*, 3674-3678.

(23) Sarkar, D.; Vemula, P. K.; Zhao, W.; Gupta, A.; Karnik, R.; Karp, J. M. *Biomaterials*, **2010**, *31*, 5266-5274.

(24) Pale-Grosdemange, C.; Simon, E. S.; Prime, K. L.; Whitesides, G. M. *J. Am. Chem. Soc.* **1991**, *113*, 12-20.

(25) Chan, E. W. L.; Yousaf, M. N. *J. Am. Chem. Soc.* **2006**, *128*, 15542-15546.

(26) Hsiao, S. C.; Shum, B. J.; Onoe, H.; Douglas, E. S.; Gartner, Z. J.; Mathies, R. A.; Bertozzi, C. R.; Francis, M. B. *Langmuir* **2009**, *25*, 6985-6991.

(27) Lamb, B. M.; Barrett, D. B.; Westcott, N. P.; Yousaf, M. N. *Langmuir* **2008**, *24*, 8885-8889.

(28) Yousaf, M. N.; Houseman, B. T.; Mrksich, M. *Proc. Nat. Acad. Sci. U.S.A.* **2001**, *98*, 5992-5996.

(29) Dutta, D.; Pulsipher, A.; Yousaf, M. N. *Langmuir* **2010**, *26*, 9835-9841.

(30) Chan, E. W. L.; Park, S.; Yousaf, M. N. *Angew. Chem. Int. Ed.* **2008**, *47*, 6267-6271.

(31) Fuchs, J.; Bohme, S.; Oswald, F.; Hedde, P. N.; Krause, M.; Wiedenmann, J.; Nienhaus, G. U. *Nat. Methods* **2010**, *7*, 627-630.

(32) Larsen, M.; Wei, C.; Yamada, K. M. *J. Cell. Sci.* **2006**, *119*, 3376-3384.

(33) Park, S.; Yousaf, M. N. *Langmuir* **2008**, *24*, 6201-6207.

(34) Mrksich, M. *ACS Nano* **2008**, *2*, 7-18.

(35) Karnik, R.; Hong, S.; Zhang, H.; Mei, Y.; Anderson, D.; Karp, J.; Langer, R. *Nano Letters* **2008**, *8*, 1153-1158.

(36) Khetani, S. R.; Bhatia, S. N. *Nat. Biotech.* **2008**, *26*, 120-126.

(37) Inaba, R.; Khademhosseini, A.; Suzuki, H.; Fukuda, J. *Biomaterials* **2009**, *30*, 3573-3579.

(38) Gan, L.; Kandel, R. A. *Tissue Eng.* **2007**, *13*, 831-842.

(39) Kidambi, S.; Sheng, L.; Yarmush, M. L.,; Toner, M.; Lee, I.; Chan, C. *Macromolecular Biosci.* **2007**, *7*, 344-353.

(40) Chan, E. W. L.; Yousaf, M. N. *Mol. BioSyst.* **2008**, *4*, 746-753.

(41) Langer, R. *Adv. Mater.* **2009**, *21*, 3235-3236.

(42) Discher, D. E.; Janmey, P.; Wang, Y. L. *Science* **2005**, *310*, 1139-1143.

CHAPTER 8

Conclusions and Future Directions

8.1 Conclusions

In this work, several material and cell surface technologies were developed to control and study cell behavior. In combining μFL and microfluidic oxidative activation, selective SAM regions were patterned and chemically altered for subsequent biospecific, chemoselective, and bioorthogonal ligand immobilization and cell adhesion studies.[1-4] Using a number of different ligands and characterization tools, the generation of cell and ligand microarray patterning strategies, were established.[5,6] Furthermore, this oxidation methodology was extended to activate two orthogonal chemistries for selective ligand immobilization with spatial control on ITO.[2,3] A renewable, chemoselective, and quantitative ligand density microarray for the analyses of biological interactions was also developed.[5] Through the use of electroactive SAMs, the extent of molecule immobilization, release, and amount bound was monitored and quantified. All these technologies focused on combining SAMs of alkanethiols or alkane phosphonates with chemoselective oxime chemistry and microfluidic, microcontact, or microarray patterning strategies to investigate peptide-cell, protein-carbohydrate, and lipid-cell interactions.

In Chapters 7 and 8, a liposome delivery and fusion method to display ketone and oxyamine functional groups from cell surfaces for applications in bio-orthogonal ligand conjugation, cell-surface engineering, cell adhesion rewiring, and the generation of

stable, 3D spheroid assemblies, and multi-layered tissue-like structures was established.[7,8] This liposome fusion and cell-surface engineering strategy was further extended to the assembly and disassembly of tissue structures, demonstrating complete control over cell surfaces and cell tissue interactions

8.2 Future Directions

Regarding the work in Chapters 2-4, future studies include utilizing these microfluidic and microarray techniques for the precise delivery of various biomolecules, such as peptides, carbohydrates, DNA, or metabolites to surface arrays for high-throughput biotechnological applications in proteomics, glycomics, and transcriptomics. These methods can be also extended to incorporate a number of functionalized alkanethiols or alkane phosphonates for multiple chemoselective coupling strategies. In combination with oxime conjugation, a differently functionalized SAM (e.g., Click chemistry with azide or alkyne presenting SAMs) would enable access to two orthogonal immobilization methods, widening the range of commercially available bioligands for study. Ongoing research includes exploring multiple ligand immobilizations for co-culture studies, cell migration studies, high-throughput ligand microarrays on nickel and other metal-oxide surfaces, and biosensors.

Future research following the work in Chapters 7 and 8 include generating 3D tissues and organs for paracrine signaling studies, tissue replacement therapies, stem cell plasticity studies, or as a model platform for various high-throughput screening studies. Integrating this strategy with traditional liposome delivery, where the interior of the liposome contains small molecules or nanoparticle cargoes, a multiplex system where the delivery of reagents to the interior of cells and simultaneous labeling of the exterior of the cells may be possible for entirely new diagnostic and biomedical applications. Assembled tissue patches with geometrically defined shape can be grown in culture and

transplanted or grafted to specific locations. These strategies may allow for the time-lapse observation of cell movement *in vivo* by using a pulse, delivery of labeled cells via liposome fusion, followed by a chase, bio-orthogonal reagent to target only the labeled cells. When applied *in vivo*, this method may allow for the monitoring of many spatio-temporal developmental events and tumor metastasis. Because the liposome fusion method is general, many other types of chemistries in a single liposome can be delivered to the membrane surface simultaneously. For example, liposomes containing ketones, alkynes, dienes, azides, hydrazides, or dienophiles in varying combinations may be delivered to a cell surface for iterative or simultaneous post-functionalization via bio-orthogonal ligation reactions.

With the introduction of an electroactive cell surface, it may be possible to track dynamic biophysical events, such as lipid diffusion and endo- and exocytosis. By generating a photo-inducible linker within the bio-orthogonal pair lipids a light sensitive cleavable system may also be generated for spatial and temporal control of cell-cell interactions. By altering the lipid composition and mix of bio-orthogonal groups in cell membranes via liposome fusion and delivery, potential cell to cell fusion experiments and the generation of tailored giant unilamellar vesicles may be possible. Finally, by tailoring and controlling cell surfaces and cell-cell interactions, new types of autocrine and paracrine signaling studies for fundamental cell behavior and tissue regeneration applications may be explored. Lastly, the generation of 3D tissues can be integrated with magnetic micro- and nanoparticles for the directed *in vivo* delivery of tissue patches during surgery or transplanation.

References

(1) Westcott, N. P.; Pulsipher, A.; Lamb, B. M.; Yousaf, M. N. *Langmuir* **2008**, *24*, 9237-9240.

(2) Pulsipher, A.; Yousaf, M. N. *Langmuir* **2010**, *26*, 4130-5.

(3) Pulsipher, A.; Westcott, N. P.; Luo, W.; Yousaf, M. N. *J. Am. Chem. Soc.* **2009**, *131*, 7626-7632.

(4) Pulsipher, A., Westcott, N. P.; Luo, W.; Yousaf, M. N. *Adv. Mater.* **2009**, *21*, 3082-6.

(5) Pulsipher, A.; Yousaf, M. N. *ChemComm* **2011**, *47*, 523-525.

(6) Dutta, D.; Pulsipher, A.; Yousaf, M. N. *Langmuir* **2010**, *26*, 9835.

(7) Dutta, D.; Pulsipher, A.; Luo, W.; Yousaf, M. N. *J. Am. Chem. Soc.* **2011**, *133*, 8704-8713.

(8) Dutta, D.; Pulsipher, A.; Luo, W.; Yousaf, M. N. *Editors' Choice, Science* **2011**, *332*, 1011.